

Dynamics in groundwater and surface water quality

From field-scale processes to catchment-scale models

Ype van der Velde

Thesis committee

Thesis supervisors

Prof. dr. ir. S.E.A.T.M. van der Zee,
Professor of Soil Physics, Ecohydrology and Groundwater Management,
Wageningen University

Prof. dr. ir. F.C. van Geer,
Professor of Methods of Soil and Groundwater monitoring,
Utrecht University &
Senior researcher Soil and Groundwater,
TNO Geological survey of the Netherlands, Utrecht

Thesis co-supervisor

Dr. ir. G.H. de Rooij,
Deputy Head Soil Physics Department,
Helmholtz Centre for Environmental Research – UFZ, Halle, Germany

Other members

Prof. dr. P. Grathwohl, Universität Tübingen, Germany
Prof. dr. A. Rinaldo, EPFL, Lausanne, Switzerland
Prof. dr. S. Uhlenbrook, UNESCO-IHE, Delft
Prof. dr. ir. R. Uijlenhoet, Wageningen University

This research was conducted under the auspices of the Graduate School of ‘SENSE’.

Dynamics in groundwater and surface water quality

From field-scale processes to catchment-scale models

Ype van der Velde

Thesis

submitted in fulfilment of the requirements for the degree of doctor
at Wageningen University
by the authority of the Rector Magnificus
Prof. dr. M.J. Kropff,
in the presence of the
Thesis Committee appointed by the Academic Board
to be defended in public
on Friday 14 January 2011
at 4 p.m. in the Aula.

Ype van der Velde
Dynamics in groundwater and surface water quality
From field-scale processes to catchment-scale models
176 pages

Thesis Wageningen University, Wageningen, NL (2011)
With references, with summaries in Dutch and English

ISBN 978-90-8585-824-9

Contents

1	Introduction	7
1.1	Improving surface water quality of lowland catchments	7
1.2	Lowland hydrology	8
1.3	Measuring water quality dynamics	11
1.4	Model concepts for water quality	11
1.5	DYNAQUAL-project	14
1.6	Thesis objectives and research question	15
1.7	Thesis outline	16
2	Field-scale measurements for separation of catchment discharge into flow route contributions	17
2.1	Introduction	18
2.2	Materials and methods	20
2.3	Results and discussion	24
2.4	Conclusions	36
3	Catchment-scale non-linear groundwater-surface water interactions in densely drained lowland catchments	37
3.1	Introduction	38
3.2	Theory: model formulation	39
3.3	Materials and methods	54
3.4	Results and discussion	58
3.5	Conclusions	67
4	Nested-scale discharge and groundwater level monitoring to improve predictions of flow route discharges and nitrate loads	69
4.1	Notation	70
4.2	Introduction	71
4.3	Materials and methods	73
4.4	Results and discussion	81

4.5 Conclusions	90
Appendix 4A	92
Appendix 4B	95
5 Improving load estimates for NO₃ and P in surface waters by characterizing the concentration response to rainfall events	97
5.1 Introduction	98
5.2 Methods	99
5.3 Results	104
5.4 Discussion and conclusions	108
5.5 Supporting information	111
6 The nitrate response of a lowland catchment: on the relation between stream concentration and travel time distribution dynamics	115
6.1 Introduction	116
6.2 Materials and methods	118
6.3 Results and discussion	128
6.4 Conclusions	140
Appendix 6A: Average absolute Difference Plot (ADP)	141
Appendix 6B: Calibration specifications	141
7 Synthesis and discussion	143
7.1 Questions and answers	143
7.2 Outlook	151
References	155
Summary	165
Samenvatting	167
Dankwoord	169
Curriculum vitae	171

Chapter 1

Introduction

1.1 Improving surface water quality of lowland catchments

High nutrient loads of surface waters are a widespread environmental issue in lowland catchments in countries with developed or rapidly growing economies (Vitousek et al., 2009). Commonly, lowland catchments have fertile soils, are easily accessible, and have high water availability, making these catchments very attractive for intensive agriculture. High inputs of nutrients via fertilizers and cattle fodder to stimulate agricultural production have led to extensive leaching of nutrients from agricultural fields into small surface waters (Tiemeyer et al., 2010) and the groundwater (Visser, 2009; Broers, 2002). High nutrient concentrations stimulate plant and algal growth that reduce the ecological and recreational functioning of small headwaters. Major problems also arise in large down-stream (marine) surface water bodies, where high concentrations of nutrients lead to algal blooms (Van der Molen, 1998) and hypoxia. Large-scale examples of hypoxia can be found in the Gulf of Mexico (Petrolia and Gowda, 2006; Alexander et al., 2000) and the Baltic Sea (Conley et al., 2009; Behrendt and Bachor, 1998).

In the European Union, the European Water Framework Directive (WFD; EU, 2000) pressures member states to achieve or maintain “good water quality status” in groundwater bodies and surface waters. Especially in lowland areas with intensive agriculture, nutrient concentrations in surface waters frequently exceed the water quality targets set in the WFD (Oenema et al., 2007) and many measures are required to reduce nutrient leaching into surface waters. These measures can roughly be subdivided into four categories: 1) reducing agricultural and other human inputs, 2) increasing nutrient uptake by crops, 3) changing the flow routes of water to optimize the cleaning capacity of micro-organisms in the soil or prevent soil erosion and 4) actively cleaning polluted waters and soils (Cherry et al., 2008). However, an effective implementation of these measures is frustrated by the current lack in understanding of the transport mechanisms of water and nutrients within lowland catchments. Firstly, because we do not know how and when nutrients move from the moment of application at the soil surface to surface waters, a knowledge-based choice between different types of measures can hardly be made. Secondly, monitoring of surface water quality yields datasets with a large natural variability in nutrient concentrations. This

variability is likely to be larger than the potential effects of measures. Since we do not understand the transport mechanisms that created this variability, it often is impossible to quantify the effects of measures on the water quality. For these reasons, improving the surface water quality of lowland catchments requires new types of measurements, model concepts, and strategies to integrate measurements and models that explicitly account for dynamics in surface water quality.

This thesis aims to increase our understanding of the movement of water and nutrients within lowland catchments. By an innovative nested-scale measurement setup that quantifies the flow routes of water and nutrients and new model concepts that describe water and nutrient transport dynamics, this thesis contributes to the knowledge needed for a sustainable management of the groundwater and surface water resources of lowland catchments.

1.2 Lowland hydrology

In freely draining lowland agricultural catchments water enters the surface water network via four major flow routes: groundwater flow towards ditches and streams, overland flow, artificial drainage by tube-drains (plastic tubes) or tile drains (short pipes of baked clay), and natural drainage by animal burrows (Fig. 1.1). Waters discharging by each of these flow routes experience distinctly different contact times with the soil, resulting in distinct ionic compositions. Many studies reported high nitrate concentrations in tube-drain flow (e.g. Skaggs et al., 1994; Tiemeyer et al., 2006; Nangia et al., 2010) and high phosphorus concentrations for overland flow (Heathwaite and Dils, 2000). The water quality of groundwater flow is strongly dependent on the reactivity and the thickness of the soil and hence is strongly catchment-specific (Visser, 2009).

Installing tube drains to improve subsurface drainage is a common agricultural measure to improve aeration of soils with shallow groundwater tables and increase their accessibility for heavy machines (Lennartz et al., 2010). The impacts of tube drainage on discharge and surface water pollution are twofold. On the one hand, tube drains shorten the flow paths to surface waters leading to increased discharges during and shortly after rainfall events. In combination with preferential flow routes created by excavating and refilling trenches around tube drains, tube drains accelerate transport towards surface waters of highly mobile pollutants such as nitrate (Kamra et al., 1999; Fig 1.2). On the other hand, tube drains lower the groundwater table and thus enhance the soil storage capacity, which leads to a decrease in overland flow and discharge peaks (Skaggs et al., 1994). Strongly sorbing solutes such as phosphorus and heavy metals are mainly mobilized by the erosion caused by overland flow. Hence, surface water pollution with these sorbing solutes is reduced by installing tube drains. The actual impact of artificial drainage strongly depends on the individual site with its unique topography, drainage system, and soil characteristics.



Figure 1.1. The major flow routes in a lowland catchment. **A:** Groundwater seepage into surface water, as indicated by the oily sheen floating on the stream. This sheen consists of bacteria that thrive on reduced iron and manganese in seepage, **B:** Ponding and overland flow, **C:** Tube drain flow, and **D:** Natural drainage by animal burrows.

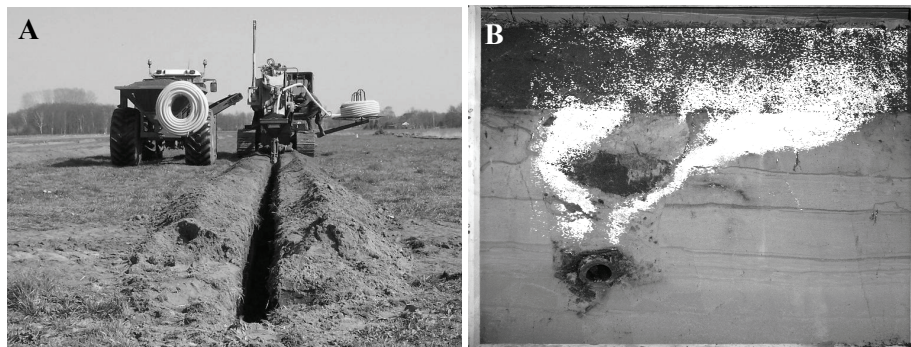


Figure 1.2. **A)** Installation of subsurface tube drains (plastic) by excavation and refilling, **B)** Cross section of a dye tracer experiment. Blue dye was applied at the soil surface above a tile drain (80 cm below soil surface). Infiltration occurred by natural rainfall. The preferential downward flow through the excavated and refilled soil is apparent (in white), even for this tile drain installed 30 years ago.

Subsurface water fluxes toward the surface water network in lowland catchments (groundwater flow and tube-drain flow) are driven by local gradients of the groundwater table. These local gradients change continuously as the groundwater table moves up and down. During high groundwater tables (wet conditions) all ditches, streams, and tube drains in a catchment drain water, creating a pattern of groundwater table gradients dominated by field-scale features. Under dry conditions only the main stream drains water, creating a catchment-scale pattern of groundwater table gradients. This strongly ephemeral character of the drainage system and groundwater gradients typifies lowland catchments and has been recognized as a main mechanism governing solute transport and water quality dynamics (Ernst, 1978; Raats, 1978; Wriedt et al., 2007; Rozemeijer and Broers, 2007; this thesis).

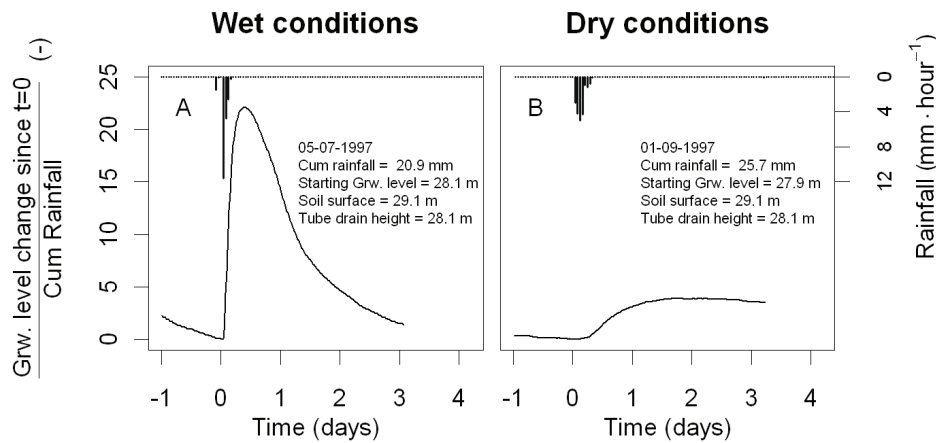


Figure 1.3. Observed groundwater level change during two similar rainfall events. Event **A** has wet initial conditions with high average soil moisture content and Event **B** has dry initial conditions with low average soil moisture content.

Another mechanism that directly affects surface water quality dynamics of lowland catchments is the interaction between soil moisture in the unsaturated zone and groundwater in the saturated zone (Brooks et al, 2010; Seibert et al., 2003). Soil moisture in the unsaturated zone acts as an amplifier of the precipitation signal towards the saturated zone. Under wet conditions far less air-filled porosity in the unsaturated zone is available than under dry conditions, which results in stronger reactions of the groundwater table on rainfall events during wet conditions than under dry conditions. Figure 1.3 shows that under wet conditions (high average soil moisture content), we observed an increase in groundwater level of 22 times the amount of rainfall, while under dry conditions an increase of only 5 times the amount of rainfall was observed. These sudden high groundwater levels during rainfall events rapidly mobilize waters that were previously stored in the unsaturated and saturated soil and lead to a fast release of “old” water (Kirchner, 2003).

Ponding (Fig 1.1B) and high surface water levels (Fig 1.4) reduce discharge by reducing the groundwater table gradient towards the draining ditches and surface elevations depressions. Reduced gradients lead to lower fluxes and consequently ponding and high surface water levels dampen discharge. However, animal burrows in the shallow subsoil were observed to form highly permeable root zones that can accelerate lateral transport of water and solutes under extremely wet conditions with substantial ponding.

The processes mentioned above are all part of the complicated relations between groundwater and surface water quality. Monitoring and modeling of lowland hydrology and solute transport often focus on groundwater, the unsaturated zone or surface waters. However, an accurate understanding of water quality dynamics at the catchment scale requires a natural integration of these zones.



Figure 1.4. The Hupsel Brook during dry (A), wet (B) and wettest (C) conditions. Note that picture C (by A.J. Teuling) was taken after widening and re-meandering of the Hupsel Brook.

1.3 Measuring water quality dynamics

Recent developments in water quality monitoring equipment have hugely increased measurement frequencies. Jordan et al. (2009) used an automatic bank site analyzer to measure phosphate concentrations with a 15-minute frequency in Irish streams and Kirchner et al. (2004) presented hourly measurements of pH and electrical conductivity. These new types of high-frequency concentration datasets spanning several years revealed large solute concentration dynamics with clear but incompletely understood implications for solute loads of surface waters. The cost of such measurements will limit them to a few locations in operational monitoring networks. Therefore, new methods are needed to deploy the information in these continuous records to better interpret the commonly collected monthly grab samples (Chapter 5).

An alternative emerging technology for water quality monitoring networks are passive samplers that measure discharge-weighted time-averaged concentrations for long periods (for example SorbiSense technology, De Jonge and Rothenberg, 2005; Rozemeijer et al., 2010b). Because of their easy installation and low maintenance efforts, passive samplers can effectively provide information on the spatial variation and patterns of concentrations of individual flow routes (Rozemeijer et al., 2010b).

As we do not only want to quantify dynamics of water quality, but also want to understand its drivers, we need to understand how contributions of specific flow routes to discharge and solute transport change with time (McDonnell, 2003; Kirchner, 2006). While many studies measured tube drain discharges and concentrations (De Vos et al., 2000; Jaynes et al., 2001a; Stamm et al., 2002; Gächter et al., 2004; Tiemeyer et al., 2006) or discharges from small catchments (Tomer et al., 2003; Tiemeyer et al., 2007), surprisingly few studies reported measurements of overland flow and groundwater flow fluxes within lowland catchments. For a better understanding of lowland hydrology and the resulting water quality dynamics, new simultaneous measurements of all flow route fluxes, as will be introduced in this thesis (Chapter 2), are paramount.

1.4 Model concepts for water quality

In this thesis models are used for two reasons. Firstly, we use models to identify processes that can explain the observed behavior of discharge and water quality. Secondly, models are used to extrapolate observed behavior of discharge and water quality to other time

periods, locations and scales. Here, we briefly introduce the concepts and model codes that are relevant for this thesis.

1.4.1 Flow route mixing models

Flow route mixing models assume that solute concentrations in a stream are the result of the mixing of flow routes with different concentrations. This concept is often used for hydrograph separation into contributions of individual flow routes (e.g. Tiemeyer et al., 2008; Soulsby et al., 2003). A major limitation of flow route mixing models is that the discharge and concentration of each of the flow routes needs to be known a priori from measurements or other models. Although it is difficult to determine the discharge and concentration of flow routes exactly, separation of discharge into contributions of individual flow routes hugely increases our understanding of the origin of surface water quality dynamics (e.g. Tiemeyer et al, 2008; Soulsby, 2003.; Chapter 2). It often provides the first indication of the potential success of a measure in reducing concentrations. Flow route mixing models will be used in Chapters 2 and 4, to relate observed nitrate concentrations to mixing ratios of the four dominant flow routes shown in Fig. 1.1.

1.4.2 Process models for coupled flow and transport

Process models describe the processes and fluxes within a system (soil volume or catchment) that eventually lead to discharge and surface water concentrations. The scale at which the equations describe flow and transport can range from small soil blocks to entire catchments.

Among the most frequently used process models that describe both water flow and solute transport at the scale of elementary soil blocks are MODFLOW (McDonald and Harbough, 1988) combined with MT3D, HydroGeoSphere (Therrien et al., 2009) and Hydrus-1D/2D/3D (Šimunek et al., 1998). The strength of these models is that discharge and the transport of solutes are directly related to spatially distributed soil properties and topography, which allows relating the catchment-scale behavior of discharge and solute concentrations to spatial patterns of process occurrence. In this thesis the groundwater model MODFLOW in combination with a particle tracking approach is frequently used to characterize the shape of the groundwater table and the distribution of travel times of water within a catchment.

These process models, however, require many spatially distributed input parameters, with the obvious burdens of data acquisition, large model building time, and computational demand. Especially when we are interested in rainfall-induced water quality dynamics, detailed spatial and temporal resolutions are required, which makes these models tedious to calibrate or operate in a Monte Carlo uncertainty estimation approach. Another point of attention is that many studies have shown that preferential flow routes caused by soil heterogeneity, preferential flow towards tube drains, and preferential fluxes through animal burrows may dominate the dynamics in groundwater and surface water quality (e.g. De Louw, 2010; Van Schaik, 2010; Beven, 2010). These preferential fluxes are difficult to incorporate in a process model that calculates fluxes at a scale of representative soil blocks,

because the exact locations and processes underlying the preferential flow phenomena are unknown (Rode et al, 2010).

Models that are built to predict discharges of entire catchments, such as HBV (Lindström et al., 1997) and TOPMODEL (Kirkby and Beven, 1978), are based on concepts that describe flow directly at the catchment scale. These models are able to accurately calculate discharge with small time steps (hours to minutes) and with very short calculation times. This allows these models to make detailed temporal flood forecasts and because of the short calculation times, these models can easily be applied in a Monte Carlo uncertainty estimation setting. The disadvantage of these models is that the effective parameters needed to describe the water fluxes can often not be measured directly and have to be calibrated against measured data. In Chapter 3 we will develop a process model with catchment-scale concepts for the individual flow routes of lowland catchments (the Lowland Groundwater Surface water Interaction, LGSI, model). The concepts are based on results of a MODFLOW simulation with a great spatial detail. In this way, we combine the descriptive power of a catchment-scale process model with the explanatory strength of a highly detailed MODFLOW model.

1.4.3 Transfer function models

Transfer function models (Jury and Roth, 1990) describe complex flow systems in a simple way by characterizing the output flux as a function of the input flux, without including the processes within the system. Transfer function models describe the water and solute fluxes through a control volume (soil column or entire catchment) by Travel Time Distributions (TTD) of water parcels or solute particles: if all travel times of water parcels or solute particles that enter a system are known, the amount and timing of outflow can be derived entirely from the inputs. This approach implicitly includes the effects of all soil heterogeneities and animal burrows and therefore can give accurate results, even when the flow routes and flow processes are unknown. However, transfer function models can only be applied for systems where the ingoing and outgoing fluxes have both been measured and hence the possibilities to predict the effectiveness of nutrient reducing measures are limited.

Rinaldo and Marani (1987) combined a transfer function model with a process model to describe solute transport of entire catchments and called it the Mass Response Function (MRF) approach. They coupled TTDs of water parcels within a catchment (transfer function model) to a catchment-scale solute mass balance and defined exchange processes between water parcels and solutes (process model). It was shown that the MRF approach could effectively describe solute concentration responses to rainfall events (Rinaldo et al., 2007; Botter et al., 2008). Major disadvantages of the MRF approach, however, are that in its original set-up TTDs are considered constant with time and that subsurface water in a catchment is assumed completely mixed. Both assumptions are rarely valid for the highly dynamic flow systems of lowland catchments with clear concentration gradients with depth below the soil. In Chapter 6 we will show that both assumptions can be relaxed to make the

MRF approach suitable to calculate 26 years of nitrate and chloride mass balances for a lowland catchment.

1.5 DYNAQUAL-project

This thesis is part of the DYNAQUAL-project (DYNAmics in ground- and surface water QUALity) launched in 2006 by Joachim Rozemeijer and Ype van der Velde. The DYNAQUAL-project aims to understand, quantify and predict nutrient concentration dynamics of groundwater and surface waters in lowland catchments. This project resulted in this PhD-thesis, a companion thesis by Rozemeijer (2010), and a series of papers. The thesis you are now reading reports on innovative measurements of field-scale water and solute fluxes that quantify nutrient leaching into surface water. Based on these observations new model concepts that describe dynamics in surface water quality at the catchment scale were developed and tested.

The companion thesis of Rozemeijer (2010) entitled “Dynamics in ground- and surface water quality: from field-scale processes to catchment-scale monitoring” describes the implications of field-scale processes knowledge for effective catchment-scale water quality monitoring. Figure 1.5 gives an outline the DYNAQUAL-project and the relations between both PhD-theses. In addition, both Joachim Rozemeijer and Ype van der Velde can be considered first author of chapters 2 and 5 of this thesis.

All fieldwork reported in this thesis is entirely situated in the Hupsel Brook catchment and was carried out in full cooperation between Joachim Rozemeijer and Ype van der Velde. The Hupsel Brook catchment serves as an example catchment for freely draining lowland catchments. The Hupsel Brook catchment was selected for its well-defined shallow phreatic aquifer and high nutrient inputs from agriculture. This combination was expected to yield rapid reactions and hence measurable reactions on practical time scales of both discharge and water quality on rainfall events. This experimental bias should be taken into account when comparing Hupsel Brook results to other catchments. Care should also be taken to extrapolate the findings of the Hupsel Brook to lowland catchments with substantial water admission from a regional surface water system, a regional groundwater-flow system, or from urban areas. These external influxes of water complicate the relation between catchment characteristics and surface water quality and therefore are out of the scope of this study.

	Monitoring	Model concepts	Objective	Ch. + Paper
Field Point	Continuous groundwater quality (Marken)	Hydrus-1D	Groundwater quality dynamics	Rozemeijer et al., 2009
	Groundwater heads, groundwater quality, flow route discharge, and flow route solute conc. at field site (Hupsel)	Hydro-Geosphere	Field-scale groundwater surface water interaction	Rozemeijer et al., 2010c
Catchment	Continuous discharge at 2 nested catchment scales (Hupsel)	Linear flow route-response model	Separation of catchment-scale discharge into flow route contributions and resulting nutrient conc. dynamics	Ch. 2 Van der Velde et al., 2010a.
	1 year of continuous NO ₃ and P conc. (Hupsel)	LGSI-model		Ch. 3 Van der Velde et al., 2009.
	26 years of NO ₃ and Cl conc. by grab-samples and continuous discharge at catchment outlet (Hupsel)	Flow route mixing model	Ch. 4 Van der Velde et al., 2010c.	
Catchment	Sorbisense: Spatially distributed temporally averaged conc. (Hupsel)	Conc. Response characteristics	Nutrient conc. dynamics at catchment scale and estimation of yearly nutrient loads	Ch. 5 Rozemeijer et al., 2010a.
		Transient Travel time distr. & Mass-response functions		Ch. 6 Van der Velde et al., 2010b.
Region	Regional surface water quality and discharge monitoring (Brabant)	Hydrograph separation	Spatial pattern of flow route concentration	Rozemeijer et al., 2010b
			Spatial pattern of gr.water contribution to surface water contamination	Rozemeijer and Broers, 2007

Approach 1
Approach 2

Figure 1.5. DYNAQUAL-project overview. The right-hand side column shows the papers that were written (details are found in the reference list) and the corresponding chapter within this thesis. Approach 1 and 2 refer to the approaches followed in this thesis explained in section 1.6.

1.6 Thesis objectives and research questions

The main objectives of this thesis are to identify the origins of surface water concentration dynamics of a lowland catchment and develop and test new model concepts that can describe the observed surface water concentration dynamics. Figure 1.5 shows the two approaches pursued to quantify the dynamics of surface water concentrations. The first approach aims to separate the catchment-scale discharge into contributions of individual flow routes with distinct ionic compositions. Many of the currently widely applied hydrological models are well capable of reproducing measured surface water discharges or measured groundwater heads. However, for accurate water quality simulations a model should be able to describe the fluxes of individual flow routes correctly (Kirchner, 2006). To create new model concepts that explicitly account for flow route fluxes we formulated the following research questions:

- What are the dominant flow routes that contribute to the surface water discharge at both the field scale and the catchment scale of the Hupsel Brook catchment and how do these flow routes affect surface water nitrate concentrations? (Chapter 2)
- How can the dominant hydrological mechanisms that drive the individual flow route fluxes be captured in catchment-scale model concepts? (Chapter 3)

- How can the information derived from a nested-scale experimental setup be utilized to constrain uncertainty in catchment-scale flow route contributions to discharge? (Chapter 4)

The second approach tries to quantify the concentration dynamics at the catchment-scale directly. This approach gave rise to two more research questions:

- How do rainfall-induced dynamics in nitrate and phosphorus concentrations affect load estimates for the Hupsel Brook catchment? (Chapter 5)
- To what extent can surface water quality dynamics be explained from dynamics in contact times between water parcels and the soil matrix within the catchment? (Chapter 6)

New field observations of flow routes and their fluxes, and long term datasets (26 years) of catchment-scale discharge and nutrient concentrations were used for answering these research questions.

1.7 Thesis outline

The five research questions are addressed in subsequent chapters. Each chapter is based on a paper that has been published or submitted to an international peer reviewed journal. The chapters, therefore, have their own introduction and conclusions and the notation of variables is redefined in each Chapter. In Chapter 2 the results of unique measurements of flow route fluxes at a field site and their relation to discharge measurements at two larger scales are presented (nested-scale measurements). Chapter 3 introduces a new model concept that relates the spatial pattern of the groundwater table to fluxes of individual flow routes (Lowland Groundwater Surface water Interaction, LGSI-model). In Chapter 4 the LGSI-model is applied to the nested-scale discharge measurements introduced in Chapter 2. The information from field-site discharges is used to constrain the modeled flow route contributions at the catchment outlet.

Chapter 5 presents concentration response models that relate the reaction of nitrate and phosphorus concentrations during discharge events to the behavior of rainfall, discharge and groundwater levels. In Chapter 6 catchment-scale mass response functions combined with transient travel time distributions are used to construct catchment-scale nutrient budgets for a period of 26 years. Finally in Chapter 7, the results of the individual chapters are summarized and discussed in a broader perspective. This introduction together with Chapter 7 should provide the reader with the main results of this thesis and can be read independently.

Field-scale measurements for separation of catchment discharge into flow route contributions

Abstract

Agricultural pollutants in catchments are transported towards the discharging stream through various flow routes such as tube drain flow, groundwater flow, interflow and overland flow. Direct measurements of flow route contributions are difficult and often impossible. We developed a field-scale setup that can measure the contribution of the tube drain flow route to the total discharge towards the surface water system. We then embedded these field-scale measurements in a nested measurement setup to assess the value of field-scale measurements for interpretation of catchment-scale discharge and nitrate concentrations using a linear flow route mixing model. In a lowland catchment, we physically separated the tube drain effluent from the discharge of all other flow routes. Upscaling the field-scale flow route discharge contributions to the sub-catchment and the catchment-scale with a linear flow route mixing model gave a good prediction of the catchment discharge. Catchment-scale nitrate concentrations were simulated well for a heavy rainfall event but poorly for a small rainfall event. The nested measurement setup revealed that the fluxes at a single field site cannot be representative for the entire catchment at all times. However, the distinctly different hydrograph reaction of the individual flow routes on rainfall events at the field site made it possible to interpret the catchment-scale hydrograph and nitrate concentrations. This study shows that physical separation of flow route contributions at the field scale is feasible and essential for understanding catchment scale discharge generation and solute transport processes.

This chapter is adapted from: Van der Velde, Y., J.C. Rozemeijer, G.H. De Rooij, F.C. Van Geer, H.P. Broers (2010). Field-scale measurements for separation of catchment discharge into flow route contributions. Vadose Zone J. 9, 25-35.

2.1 Introduction

Precipitation water leaves catchments by evapotranspiration, regional groundwater flow, and surface water discharge. Particularly the generation of discharge is complicated and involves a myriad of routes along which a water drop can travel to the stream (e.g. Beven and Kirkby, 1979, Ward and Robinson, 1990). In agricultural catchments, these routes and their relative contributions to stream discharge have often been manipulated to increase agricultural productivity. In relatively humid climates this typically involved the construction of an artificial drainage network of ditches and subsurface tube drains to improve the discharge of excess precipitation water. Many studies have described the importance of artificially constructed drainage networks for local and regional solute and water transport: Carluer and De Marsily (2004) looked at the impact of man-made drainage networks on regional hydrology, Hirt et al. (2005) tried to estimate tube drainage area percentages in Germany and Van den Eertwegh et al. (2006) estimated the contribution of tube drain discharge and solute transport for a Dutch polder (reclaimed area). Subsurface tube drains reduce the importance of overland flow as a route towards the surface water. In addition, ditches and drains shorten the residence times in the shallow groundwater by tapping the phreatic aquifer. The observed acceleration of the transfer of nutrients and other agrochemicals through the hydrologic system has been attributed to these shorter residence times: Stamm et al. (1998) and Heathwaite and Dils (2000) investigated transport of phosphorus; Van Ommen et al. (1989) used a bromide tracer and Jaynes et al., (2001a) worked with pesticides and bromide. The quantification of the relative contributions of different flow routes and the temporal variations of these contributions are important to understand discharge characteristics and solute loading mechanisms of surface waters. Wriedt et al. (2007) showed that the temporal variations in groundwater heads and subsequent variations in groundwater flow route contributions can explain much of the observed dynamics in surface water nitrate concentrations.

Flow route contributions to stream water discharge can be estimated indirectly by different methods like process-based hydrological modeling, regional mass balance studies, and hydrograph separation techniques. Many physically based hydrological model codes include different routes that generate surface water discharge. The calibration of model parameters and the validation of the model results are usually based on stream discharge or groundwater level measurements. Often, the wide range of possible parameter sets that provide satisfactory results for discharge and groundwater level predictions result in large uncertainties in the predictions of flow route contributions (Gallart et al., 2007).

Regional mass balancing based on measurements is another frequently used indirect method for estimating flow route contributions. If an adequate monitoring network is available for precipitation, evapotranspiration, groundwater levels, groundwater quality, tube drain and surface water discharge and quality, water and solute fluxes along the various routes to the stream can be deduced. For example, Van den Eertwegh et al. (2006) attempted to determine the balances of water, chloride, nitrate and phosphate for a catchment within an area of reclaimed land (polder). However, not all balance terms could

be derived directly from their measurements; the contribution of overland flow was estimated using an unsaturated flow model and regional groundwater flow directly discharging into the ditches and canals was estimated using a groundwater flow model. Mulla et al. (2003) demonstrated that regional mass balancing approaches become more appropriate relative to physically based spatially distributed modeling approaches as the scale of the studied area increases. A major limitation of regional mass balance approaches is that they are difficult to operate in a predictive mode.

Hydrograph separation during rainfall and subsequent discharge events using the signatures of chemical tracers is another widely used indirect method to estimate the contributions of two or three different flow routes to the stream discharge (Ladouche et al., 2001; Soulsby et al., 2003). A limitation of chemically based hydrograph separation is the assumption that the tracer concentrations of the individual flow routes are constant in time and should therefore be verified. Different studies showed variable solute concentrations for example in upper groundwater (Bjerg and Christensen, 1992; Boumans et al., 2005), tube drain effluent (De Vos et al., 2000; Jaynes et al., 2001a, Stamm et al., 2002; Gächter et al., 2004, Tiemeyer et al., 2006) and overland flow (Langlois and Mehuys, 2003).

Direct measurements of the contributions of different flow routes to surface water runoff would contribute to the validation and optimization of the different indirect methods described above. However, the processes that lead to discharge of water and solutes are in general dynamic, operate on various scales in space and time and have many and complex interactions. Setting up an observation network that quantifies all relevant fluxes within a catchment is not realistic. Fluxes such as groundwater recharge and overland flow are notoriously difficult to observe directly even at the field-scale and therefore datasets are scarce. Nevertheless, the tube drain flow route can be measured at the field scale (De Vos et al., 2001; Van Ommen et al., 1989). To explain observed catchment-scale discharges and solute concentrations Tiemeyer et al. (2008) suggested linear mixing of tile drainage and groundwater flow, Rozemeijer and Broers (2007) suggested a continuum of drainage levels from baseflow to overland flow and Wriedt et al. (2007) suggested a dynamic active draining channel network. These suggestions, however, have never been verified by a multi-scale measurement approach that also captures water and solute transport routes at a field site. Previous multi-scale experiments by Tiemeyer et al. (2007) and Tomer et al. (2003) combined measurements of discharge and nitrate concentrations from tile drainage and surface water discharge and nitrate concentrations at larger scales, but could not conclusively relate the different scales because at field scale the groundwater flow route and the overland flow route had not been measured. Still, these studies showed that nitrate is the most interesting water quality parameter in tube drained catchments, because of the large differences in nitrate concentration between the tube drain flow route (high concentrations), ground water flow route (low concentrations) and overland flow route (low concentrations).

The objectives of this study were (1) to quantify the contribution of the tube drain flow route to the total discharge from an experimental field site towards the surface water system

and (2) to embed these field-scale measurements in a nested measurement setup to assess the value of field-scale measurements for interpretation of catchment-scale discharge and nitrate concentrations using a linear flow route mixing model.

We attempted to measure both outflow from tube drains and the combined flux of all other flow routes towards a ditch. At the same time discharge and nitrate concentrations were monitored at the catchment outlet and at selected locations within the tributaries to the main stream. This paper presents this nested-scale observation approach and an exploratory mixing model analysis that connects the observations at the various scales.

2.2 Materials and methods

2.2.1 Setting, Geology and Climate

The experiments of this study were performed in the Hupsel brook catchment in the eastern part of The Netherlands (Fig. 2.1) (52°06' N; 6°65' E). The size of the catchment is 6.64 km², with surface elevations ranging from 22 to 36 m above sea level. At depths ranging from 0.5 to 20 m a 20-30 m thick impermeable marine clay layer of Miocene age is found of which the top is carved by glacial erosion. This clay layer forms a natural lower boundary for the unconfined groundwater flow (Van Ommen *et al.*, 1989). The unconfined aquifer consists of Pleistocene aeolian sands with occasional layers of clay, peat and gravel of which the spatial extension is only marginally known. Wösten *et al.* (1985) classified the main soil type of the catchment as sandy, siliceous, mesic Typic Haplaquads (See Wösten *et al.* (1985) for more details).

The Hupsel catchment is drained by the straightened and deepened main brook and by a dense artificial drainage network of ditches and tube drains. The spacing between the ditches averages 300 m (Fig. 2.1). Tube drains were installed into approximately 50% of the catchment's fields. A natural or reference situation is almost impossible to identify, because the Hupsel catchment has been under continuous anthropogenic change (reclamation, canalization, tube draining, leveling, re-meandering, land use change) for the last hundred years. The land use during the last decades has predominantly been agricultural with maize and grass land. A few small patches of forest are located in the catchment. Residential areas are absent, but individual houses and farms are scattered through the area. None of these houses is allowed to discharge waste water into the surface water network.

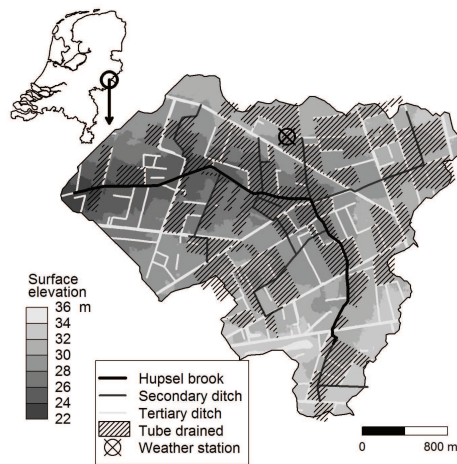


Figure 2.1. Location, surface elevation, tube drained area and surface water network of the Hupsel brook catchment.

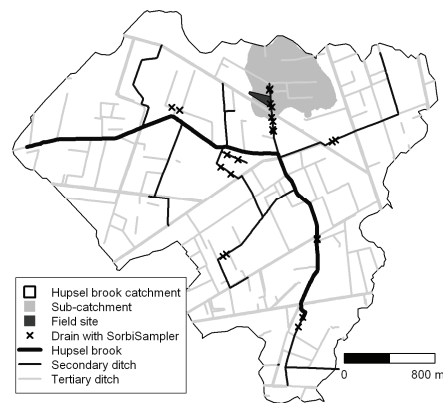


Figure 2.2. Nested setup of the experiment with the field site, the sub-catchment the total catchment and the tube drains for which nitrate concentrations have been monitored.

The Hupsel brook catchment has a semi-humid sea climate with a yearly precipitation of 500 to 1100 mm and a yearly estimated evaporation of 300 to 600 mm, resulting in an estimated recharge of 200 to 800 mm per year. A weather station of the Royal Dutch Meteorological Institute (KNMI, De Bilt, The Netherlands) is located within the catchment (Fig. 2.1). This station hourly measures rainfall, wind speed, solar radiance, temperature and humidity.

2.2.2 Nested experimental setup of discharge and nitrate concentration measurements

Within the Hupsel brook catchment discharge and nitrate concentrations were measured at three nested spatial scales (Fig. 2.2): (1) the entire catchment of 6.64 km², (2) a sub-catchment of 0.38 km² and (3) a 0.041 km² field with a 0.009 km² field site within the sub-catchment. From August 2007 through May 2008, discharge was measured every 15 minutes by a calibrated weir for the total catchment and by a calibrated V-notch for the sub-catchment. The setup of the discharge measurements at the field site is addressed in the next section.

Water samples were collected weekly from August 2007 through May 2008 at the three scale levels. The samples were taken using a peristaltic pump and filtered in situ (0.45 μm). Electrical conductivity and the pH of the samples were measured directly in the field. The samples were analyzed within 48 hours with IC (Ion Chromatography) for nitrate.

Continuous surface water nitrate concentrations were measured at the outlet of the 6.64 km² catchment with a Hydrion-10 multi-parameter probe (Hydrion BV Wageningen, the Netherlands). Water from the brook was pumped in a flow-through cell, in which the probe

was placed. Nitrate concentrations, temperature, EC and pH were stored every 10 minutes. The probe was cleaned and calibrated weekly.

Average monthly nitrate concentrations of tube drain effluent were measured at 20 locations in the catchment using SorbiSamplers (De Jonge and Rothenberg, 2005; Fig. 2.2). A SorbiSampler is a passive accumulating collector (PAC) that is in continuous capillary contact with its surroundings. The samplers function as a quasi-infinite adsorptive sink for nitrate. The volume of water that has passed during the installation period is estimated from the weight reduction of a salt tracer in the sampler (De Jonge and Rothenberg, 2005).

2.2.3 Experimental setup at the field site

For the field-scale observations a 4.1 ha pasture field was selected with surface elevations ranging between 27.5 m above mean sea level in the Southeast and 31 m in the North (Fig. 2.3). There were tertiary ditches bordering the field to the South and North that discharged into a secondary ditch at the eastern side that in turn discharged into the main brook. The average depths of the ditches were 60 cm (South), 80 cm (North) and 120 cm (East). A 1.5 m strip bordering the eastern ditch was separated by a fence from the rest of the field to allow for ditch maintenance. The field was tube drained with PVC tube drains with a diameter of 60 mm. Tube drain spacing was 14.5 m and the tubes discharged into the eastern ditch at 90 cm depth. Over their 200 m length the tubes sloped upward by 20 to 60 cm away from the ditch, depending on the local topography.

This study focuses on the field-scale observations on drains 1, 2 and 3 (Fig. 2.3). These tube drains were spaced 14.5 m apart and drained a combined catchment area of 0.9 ha, termed the “field site” from hereon. To separate the fluxes towards the eastern ditch via different routes, three adjacent sheet pile reservoirs were built in the eastern ditch. Each in-stream reservoir was constructed around a single drainage outlet and together stretching along 43.5 m of the field (Fig. 2.4). The wooden sheet piles were driven into the impermeable Miocene clay layer at 3 to 4 m depth to capture all groundwater flow from the field into the ditch. The sides of the reservoir stretched from half way the ditch sideways till the top of the reservoir touched the ditch bank (about 1.2 m). The in-stream reservoirs captured overland flow, interflow, direct precipitation and groundwater inflow. Water levels in the in-stream reservoirs and in the adjacent ditch were measured using pressure sensors. The water levels inside the in-stream reservoirs were maintained at the ditch water level by pumps (+ 1 cm when pumps start and -1 cm when pumps stop). Excess water was pumped from the in-stream reservoirs into the ditch and the pumped volumes were recorded with digital flux meters.

We did not install separate collectors for overland flow because of the abundant burrowing macrofauna (moles and mice). These animals tend to burrow under the overland flow collector thereby creating large numbers of bypass channels (P. Groenendijk, personal communication, 2006). We observed that these holes are especially abundant close to the ditch. They created bypass channels for overland flow up to several meters length and discharged from the ditch bank at depths up to 80 cm.

The discharge of the tube drains was separated from the other flow routes by connecting each drain outlet to a 500 liter vessel using a flexible tube (Fig. 2.5). The vessels were partly dug into the ditch bottom and they were allowed to fill up to the tube drain outlet height, which led to an effective storage capacity of about 200 liter. When this water level was reached, the water was pumped into the ditch and the flux was measured with digital water flux meters (Fig. 2.5). When tube drain outlets were below the ditch water level, the surface water pressure affected the flow rate. To imitate this effect, floaters were attached to the flexible tubes that connected the drains to the collection vessels. Thus, water leaving the drain had to flow up to the ditch level before being discharged into the vessel.

In addition to the discharge measurements, we manually measured phreatic groundwater levels at 31 locations within the field every week. Pressure sensors in 15 piezometers along drain 1 (Fig. 2.3) recorded phreatic levels every 10 minutes.

Water quality samples at the field site were taken weekly from the three in-stream reservoirs and from the three drain effluent vessels. The sampling and processing procedure is the same as described above.

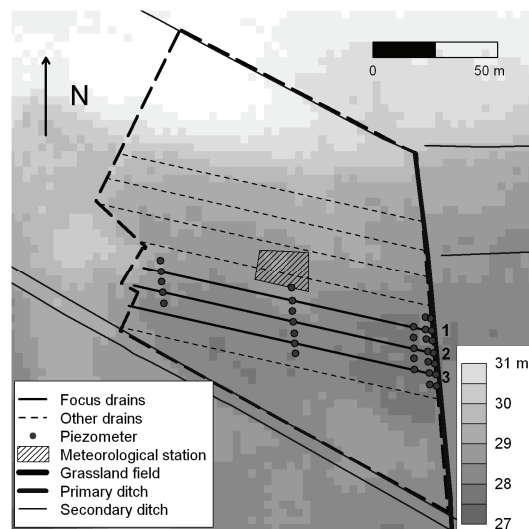


Figure 2.3. Overview of the experimental field site. The numbers 1-3 next to the tube drains correspond to the numbers used in the text for identifying tube drains 1-3 and in-stream reservoirs 1-3.

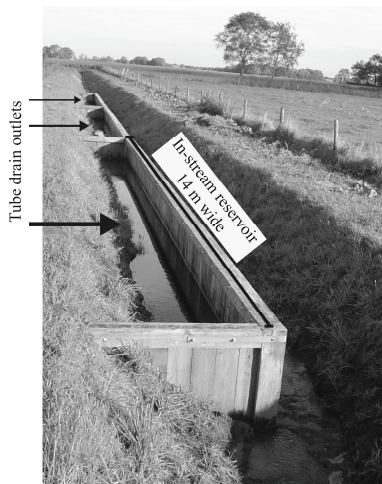


Figure 2.4. In-stream reservoirs. Reservoir number 1 is the reservoir in the back, number 3 is the reservoir in the front.

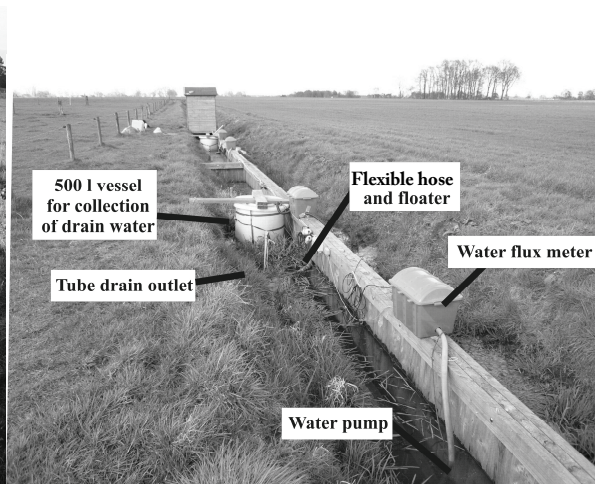


Figure 2.5. Measurement setup with collector vessels for drain discharge, pumps and water flux meters. The shed in the back houses the data acquisition and control equipment. The fence on the left separates the farmland from the ditch maintenance strip.

2.3 Results and discussion

2.3.1 Field site discharges

Tube drains

The measured tube drain discharge varied between no flow and 0.31 L s^{-1} (Fig. 2.6A), which corresponds with 8.9 mm d^{-1} . The sudden stop of the measured discharge of drain 1 in December was caused by a defect pump. The tube drains were pressure washed on November 1st, 2007. This washing is common agricultural practice in The Netherlands and is performed once every two years at this field. During the first weeks after this cleaning, the discharge response to precipitation events was similar for the three drains. From January on drain 2 was showing considerably higher discharge rates than the other drains, possibly reflecting re-clogging up of drains 1 and 3 by silt and iron oxide particles. This lowered the overall tube drain discharge (Fig. 2.6C). An increase of the drain entrance resistance and the resulting decrease of drain flow rates with time have also been observed in a laboratory experiment reported by Bentley and Skaggs (1993). The conditions of these laboratory experiments, however, can only be compared indicatively with our site specific iron rich anaerobic conditions as was also one of the main conclusions of a review on clogging processes of Stuyt and Dierickx (2006).

In-stream reservoirs

The in-stream reservoir discharges, resembling the combined discharges of overland flow, interflow, direct precipitation and groundwater inflow towards the ditch, varied between no flow and 0.90 L s^{-1} (Fig. 2.6B) This corresponds with $6.0 \cdot 10^{-5} \text{ m}^3 \text{ s}^{-1}$ discharge for a meter of ditch bank. The average discharge from the in-stream reservoirs is generally lower than

the average tube drain discharge (Fig. 2.6C). From these observations we may conclude that during normal flow conditions, the tube drain contribution to surface water discharge at the field site is more important than the groundwater contribution.

During several periods with high precipitation intensities, however, the reservoir discharges showed high peaks, especially in in-stream reservoir 3. During the January event, overland flow and interflow through macrofauna burrows towards in-stream reservoir 3 was observed. To a lesser extent, overland flow was observed towards in-stream reservoir 2. This explains the discharge peaks in both reservoirs. The overland flow mainly originated from a ponded area near the ditch. The likely causes of ponding in our field site are a combination of compaction by tractor traffic, shallow organic layers with a large vertical flow resistance and local depressions in the surface elevation. Flow through biopores contributed significant amounts of discharge that would not have been collected by a surface construction for capturing overland flow. Biopore flow presumably constituted a mixture of groundwater and water from ponded areas. Consequently, the water entering the ditch through the biopores will have a wider travel time distribution than would be expected from overland flow alone.

From Fig. 2.6B it appears that all in-stream reservoirs had elevated discharges simultaneously, but with very different magnitudes. We did not observe overland or biopore flow into reservoir 1. Therefore, the contribution of overland flow and biopore flow into reservoir 2 and 3 can be estimated when we assume that (1) all discharge into reservoir 1 originates from groundwater inflow and direct precipitation and (2) the contributions of groundwater and direct precipitation do not vary much between the reservoirs. The second assumption is likely to result in an overestimation of the tube drain contribution because the discharge of in-stream reservoir 1 is relatively low during normal flow conditions (Fig. 2.6B). However, this overestimation is small due to the magnitude of the discharge peaks from in-stream reservoirs 2 and 3. We estimated the maximum and overall contributions of overland and biopore flow routes to peak discharges accordingly for reservoirs 2 and 3 for four heavy rainfall events. The fraction of the precipitation that was drained from the field by overland and biopore flow has also been estimated (Table 2.1).

Table 2.1 shows that in reservoir 3 up to 58% of the total amount of precipitation water was drained by overland flow and biopore flow. During the March 21-25 event, the maximum relative contribution of overland flow to the surface water discharge was 92%. For the three in-stream reservoirs together, resembling a 45 meter ditch transect, the maximum relative overland flow contribution was 67% (Table 2.1). The differences between the storm events and between the in-stream reservoirs were large. Reservoir 2 received much smaller contributions from these flow routes. For the three reservoirs together up to 22% of the total precipitation was discharged by overland and biopore flow. The large variability of the overland and biopore flow contributions in reservoirs 2 and 3 could be an effect of the instability of large short-cut flow routes through mouse and mole holes. Other factors that can cause the observed temporal variability are differences in storm duration and intensity

and differences in the storage capability of the field at the onset of the storm event. Besides, infiltration capacity at the field site can vary over the seasons, for example due to tillage, seasonal crop cycles and foraging birds perforating the upper soil.

The average fluxes in Fig. 2.6C show drainage outflow displaying the type of behavior consistent with drainage theory (De Zeeuw and Hellinga, 1958; Kraijenhoff van der Leur, 1958 and 1962) that predicts tailing after a peak. The other flow routes generate a more spiked response to rainfall. Particularly, these spiked responses are extremely variable in this field (Compare Fig. 2.6A and Fig. 2.6B). This also shows from the maximum contributions of these other flow routes to the total discharge during a storm event (Table 2.1), which have been measured to be up to 67 % for the total field site, but vary greatly between reservoir and storm event.

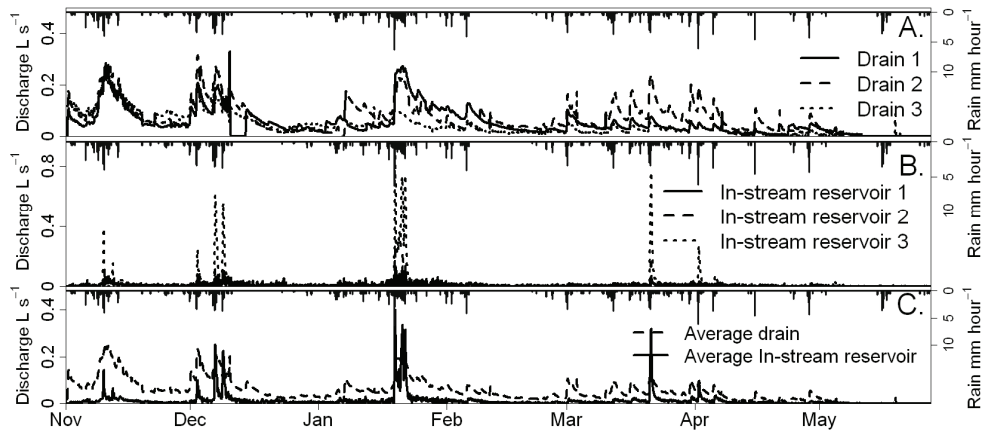


Figure 2.6. Measured precipitation and water fluxes at the field site in discharge volume per tube drain catchment: **A** Drain discharge for the three tube drains; **B** Measured in-stream reservoir discharge; **C** Average tube drain flux and in-stream reservoir flux from the field site.

Table 2.1. The contribution of overland and biopore flow (OBflow) to the fieldsite discharge during several rainfall events. OBflow is given in total fluxes (m^3) and as a percentage of the total rainfall. OBflow fluxes were estimated by subtracting the discharge of reservoir 1, representing the groundwater flow, from the results of reservoirs 2 and 3. Volumes of water were divided by the width of the reservoirs. The maximum contribution of the OBflow during the rainfall event is given by MaxC (%)

Rainfall event	Dec 1 – 22, 2007	Jan 19- Feb 1, 2008	Mar 21 – 25, 2008	Mar 30 – Apr 9, 2008
Cumulative rainfall per m ditch (m^3)	15.6	14.8	6.60	8.10
Reservoir 2				
OBflow	0.16, 1.1%	1.07, 7.2 %	0.37, 5.6%	0.33, 4.1%
MaxC	51%	54%	34%	22%
Reservoir 3				
OBflow	4.75, 31%	8.56, 58%	2.52, 38%	1.35, 17%
MaxC	75%	89%	92%	84%
Reservoir 1,2 and 3				
OBflow	1.64, 1.1%	3.21, 22%	0.96, 15%	0.56, 6.9%
MaxC	51%	64%	67%	47%

Table 2.2. Water balance for the unsaturated zone and the shallow groundwater of the 0.9 ha field site between November 1st, 2007 and May 28th, 2008 (208 days).

Balance Term	Volume (m^3)	Volume (mm)
Precipitation	4660	536
Potential evapotranspiration	2007	231
Tube drain discharge	2985	343
Rapid discharge	752	86
Influx from groundwater or overland flow across the site boundary	545	63
Storage change	-538	-62

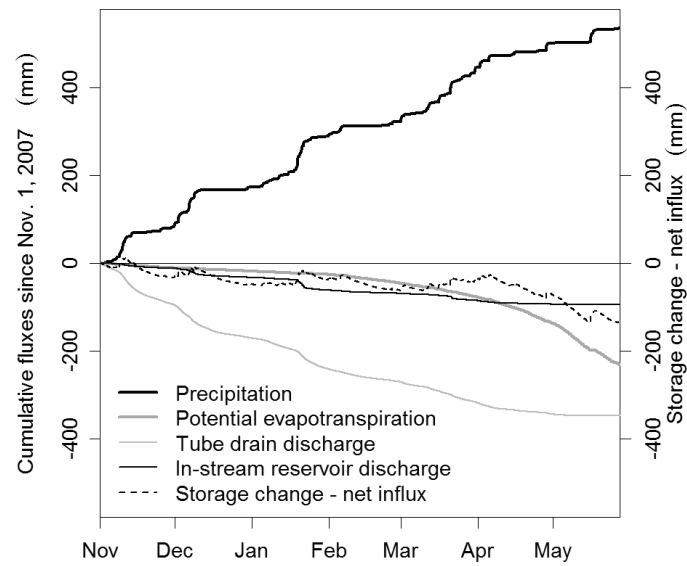


Figure 2.7. Waterbalance of cumulative fluxes observed at the 0.9 ha field site (solid lines). The dashed line combines storage change (negative when storage decreases) and net water influx. It is derived from the observed fluxes by requiring the balance to close.

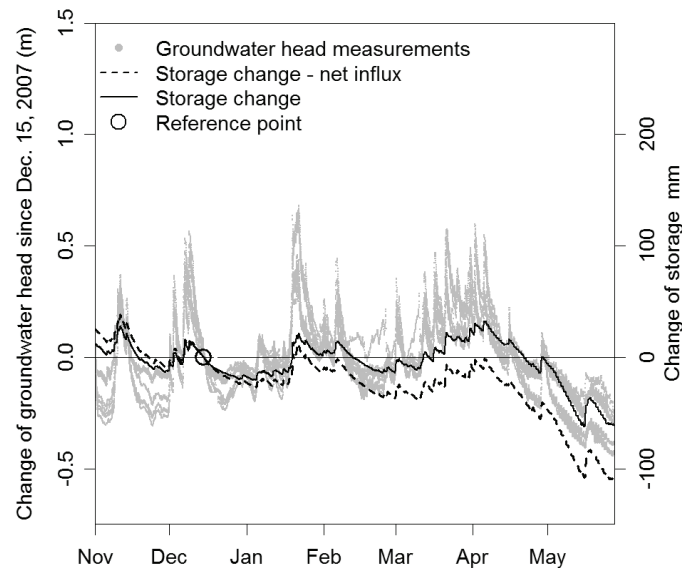


Figure 2.8. Observed groundwater levels in the 15 monitoring wells around tube drain 1 (see Fig. 2.3). On the second Y-axis the change of total storage within the saturated, the unsaturated and the ponded part of the field site is displayed. A net influx of 0.3 mm d^{-1} is needed to keep a zero change of calculated storage whenever there is a zero change in groundwater levels with respect to the reference level on December 15th.

Water balance

Figure 2.7 presents the cumulative fluxes of the field site (0.9 ha) since November 1st, 2007. The spiky behavior of the rapid flow routes resulted in a nearly horizontal cumulative reservoir discharge with sharp jumps during heavy rainfall. The more gradual drain discharge led to a more continuous slope that only approximated zero during the relatively dry period in April and May (Fig. 2.6A).

Over the seven month period there was an overall water balance deficit. The deficit has several causes: (1) the actual evapotranspiration is overestimated by assuming it equal to the potential evapotranspiration, (2) additional water enters the field site by groundwater flow or overland flow which we did not measure, (3) storage decreased between the beginning and the end of the water balance period, (4) flux measurement errors and (5) an inaccurate estimation of the contributing area or even a non-stationary contributing area. Closing the water balance would need a measuring period of several years. However, it is expected that even the long term water balance will give a deficit.

At the end of the observation period the phreatic water level dropped by 0.3-0.4 m (Fig. 2.8) since the November 1st, which partially explains the deficit. Reduced evapotranspiration because of dry weather and a deep groundwater table contributed to the deficit during the last month of measurements, because only then evapotranspiration was substantial compared to the rainfall. To close the water balance, we used a simple procedure to estimate an additional net influx. First, we selected a representative reference date. We chose December 15th, because the groundwater levels at this date approximate the average groundwater levels during the experimental period in a groundwater level recession period. Selecting the reference in a recession period is important because the timing of groundwater rise can differ between locations, but all locations will be halfway in the recession around the same time. Whenever the groundwater levels equaled that of December 15th, we assumed that the amount of water storage in the field also should equal the storage on December 15th. An additional influx of 0.3 mm d⁻¹ was required to maintain a storage that corresponds to the measured groundwater heads (Fig. 2.8) (i.e. zero storage change on all dates with groundwater levels equal to the December 15th groundwater level). This additional water may have been supplied by regional scale groundwater flow, but may also have originated from overland flow from adjacent fields that infiltrated on our field site or flowed directly into our reservoirs. The water balance is summarized in Table 2.2.

The groundwater inflow and overland flow into the reservoirs did not necessarily have the same contributing area as the tube drain effluent. At the field site, the main groundwater flow direction was NNW-SSE, following the topography (Fig. 2.3). Therefore, the source area of the groundwater flow towards the reservoirs was probably situated NNW of the reservoirs, while the tube drains were directed WNW. The contributing area for overland and biopore flow towards the reservoirs is limited to a nearby frequently ponded part of the field. Overland flow from another frequently ponded part is directed towards the southern ditch. This uncertainty in the contributing surface area might also explain the water deficit in the water balance.

From Table 2.2 it can be concluded that tube drainage accounted for 80% of the total discharge, confirming the relevance of the tube drainage system for agricultural land use in the area. Still, 20% of the total discharge is discharged by other flow routes, predominantly in episodic events with high fluxes. These flow routes may be of particular importance for the fate of sediment bound agricultural pollutants like heavy metals and phosphate.

2.3.2 Catchment and sub-catchment discharges

Figure 2.9A presents the hydrograph (in mm day^{-1}) of the sub-catchment and Fig. 2.9B shows the hydrograph of the entire catchment. The data gap at the end of January in Fig. 2.9B was caused by an electrical power failure. The field site hydrograph could be separated into drain discharge and reservoir discharge with contrasting responses to rainfall and dry periods. We therefore attempted to fit the sub-catchment and catchment-scale hydrographs by a linear combination of the field-scale route contributions to the hydrograph according to:

$$q_i(t + \Delta t_i) = a_i \cdot q_d(t) + b_i \cdot q_r(t) \quad [2.1]$$

where q_i is the area specific stream discharge [$\text{L}^3\text{L}^{-2}\text{T}^{-1}$] of the sub-catchment ($i = s$) or the catchment ($i = c$), t is the time [T], a_i and b_i are dimensionless fitting parameters that weigh the contributions of the area specific drain discharge q_d [$\text{L}^3\text{L}^{-2}\text{T}^{-1}$] and the area specific reservoir discharge q_r [$\text{L}^3\text{L}^{-2}\text{T}^{-1}$] measured at the field site; Δt_i [T] is a parameter (assumed constant) representing the time lag caused by the travel time in the surface water system. In reality Δt_i may depend on the discharge. The parameters a_i , b_i , and Δt_i were fitted by linear regression. Table 2.3 gives the fitted values.

Figures 2.9A and 2.9B show the estimated contributions of drain discharge and alternative flow routes (derived from the in-stream reservoir discharge) to the fitted total discharge, based on the parameter values in Table 2.3. In our tube-drained field site, 80% of the total discharge originated from the drains. The tube drain contribution decreased with increasing scale from 67% in the sub-catchment to 59% in the entire catchment (Table 2.3). The effectiveness of tube drains at the field site cannot be extrapolated to other scales because the ratio of ditch bank length per area changes from field site to sub-catchment to catchment-scale. The higher this ratio the larger the contribution of groundwater and overland flow and consequently the smaller the contribution of tube drain water to surface water discharge. This ditch bank length per area ratio is 5.0 km^{-1} (0.045/0.009) for the field site, 8.1 km^{-1} (3.06/0.38) for the sub-catchment and 15.6 km^{-1} (106/6.64) for the entire catchment. The increase of this ratio corresponds to the decrease in the relative contribution of tube drain flow routes from 80% at the field site to 67% in the sub-catchment and 59% in the catchment.

If we speculate that the reaction of the tube drains on rainfall events are unique to tube drains, a_i is an estimate of the fraction tube drained area. This simple estimate gives 83% for the sub-catchment and 54% for the total catchment. These estimates lie well within the range of expected values (70-90 % for the sub-catchment and 50-70 % for the entire catchment). Together with a decreasing area being tube drained at increasing spatial scales,

the increasing ditch bank length per area at increasing spatial scales causes a decreasing contribution of tube drain discharge with larger spatial scales.

The consistency of the results of this relatively elementary procedure for scaling up the flow route contributions measured at the field-scale is remarkable. Within the catchment there are many variables that may affect the discharge routes of water towards the surface water system. Variables like the heterogeneity of the subsurface, surface water storage behind weirs and the geometry of the drainage network were not taken into account. In addition, setup and maintenance level of the subsurface tube drain systems within the catchment were not known. Nevertheless, these results show that the field-scale flux measurements of individual flow routes are useful for understanding the discharge and water quality behavior of surface water at catchment-scales.

Table 2.3. Fitting parameters of Eq. [2.1] for the sub-catchment and the catchment. The correlation coefficient R^2 indicates the goodness of fit between observed and fitted (sub)catchment discharges. The relative contribution of drain discharge to surface water discharge is also given, with the remaining fraction attributed to all other flow routes.

	Sub-catchment	Catchment
a_i	0.83	0.54
b_i	1.61	1.50
Δt_i (hour)	1.7	3.1
R^2	0.83	0.90
Fraction drain discharge during observation period	0.67	0.59

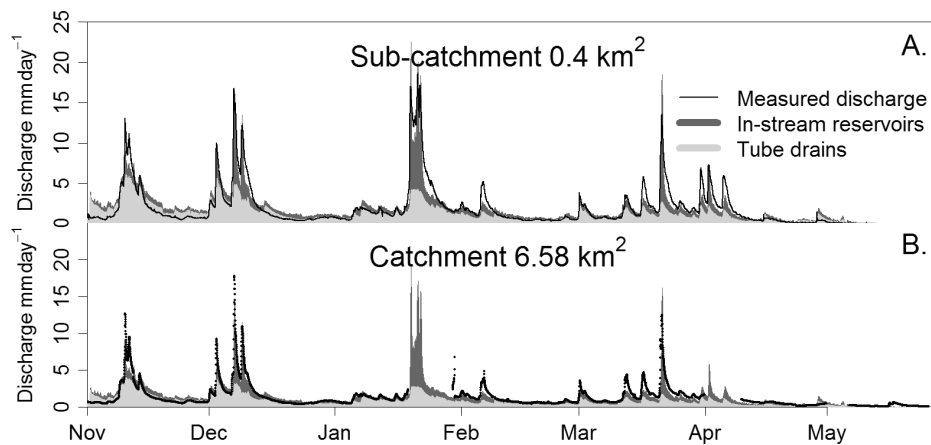


Figure 2.9. Measured normalized hydrographs of the sub-catchment (A) and the entire catchment (B). The fitted hydrographs of the sub-catchment and the entire catchments and the estimated contributions of tube drain discharge and other flow routes according to Eq. [2.1] are given shades of grey.

2.3.3 Catchment-scale nitrate concentrations

The results of the nitrate measurements from the sampling at the field site and from the entire catchment during March and April of 2008 are summarized in Fig. 2.10. The mean nitrate concentration was 9.1 mg L^{-1} in the in-stream reservoirs, 18.6 mg L^{-1} in the drainage outflow at the field site and 71.2 mg L^{-1} in the drains within the catchment.

The low nitrate concentrations in the in-stream reservoirs can be explained by the low nitrate concentrations in the contributing deeper groundwater, direct precipitation and overland and biopore flow. The tube drains tap the upper groundwater with relatively high nitrate concentrations. The nitrate concentrations in the field site tube drains are in the lower range of the nitrate concentrations measured in the catchment.

At the field site, the measured nitrate concentrations varied more in the drainage outflow than in the in-stream reservoirs. The variation in the drains distributed over the catchment was much larger, with an asymmetric distribution (Fig. 2.10). The extremes in the distribution of catchment values (> 3 times the mean, > 6 times the median) significantly affected the total nitrate loading at the catchment-scale.

The field-scale discharge measurements revealed the important contribution of the overland and biopore flow route contributions collected by the reservoirs during heavy precipitation events. Fig. 2.10 suggests that this could lead to a reduction in nitrate concentrations during these events. This was examined for two rainfall events between March 15th and 21th, 2008 using the nitrate measurements at 10-minute intervals at the catchment outlet. The measured discharge and nitrate concentration patterns during the event are shown in Fig. 2.11. The measured nitrate concentrations indeed showed the expected behavior.

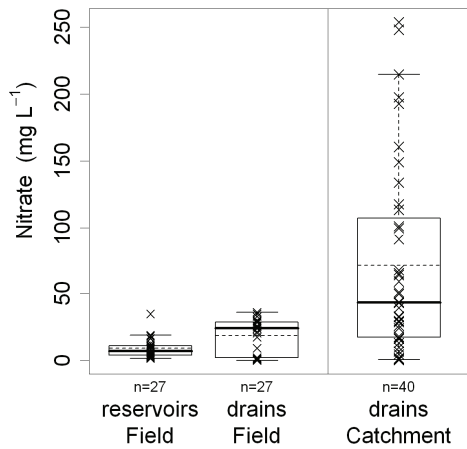


Figure 2.10. Boxplots of nitrate concentration measurements. The left side boxes represent the field site. The right side boxplot is based on measurements from drains throughout the catchment. The solid line within each box plot is the median concentration; the dotted line is the mean concentration. The lower and upper side of the box represent the 0.25 and the 0.75 quantile. The whiskers extend to the maximum and minimum value unless these values are larger or smaller than 1.5 times the box length. The number of data points is indicated by n .

To verify if the relative contributions of the overland and biopore flow route to the total discharge observed at the field site could explain the observations, the nitrate concentrations in the stream at the catchments outlet were calculated by:

$$c(t + \Delta t) = (\bar{c}_d \cdot a_c \cdot q_d(t) + \bar{c}_r \cdot b_c \cdot q_r(t)) \cdot (a_c \cdot q_d(t) + b_c \cdot q_r(t))^{-1} \quad [2.2]$$

where c is the nitrate concentration [ML^{-3}] at the catchment outlet, \bar{c}_d and \bar{c}_r are the average nitrate concentrations [ML^{-3}] for the tube drain flow route and for all other flow routes. The water fluxes were calculated from Eq [2.1], with the parameters a_c and b_c from Table 2.3. The value of \bar{c}_d was set to 71.2 mg L^{-1} and \bar{c}_r to 9.1 mg L^{-1} , equal to the catchment-scale average for the tube drain nitrate concentrations and the field-scale average for the in-stream reservoirs, respectively. It is assumed that these concentrations were constant in time during two subsequent rainfall events. To conclusively validate this assumption, high-frequency nitrate concentration observations of tube drain flow and in-stream reservoir flow at the field site would have been needed. However, this assumption is supported by weekly measurements that show little response to precipitation events. The calculated nitrate concentrations for the catchment outlet are shown together with the measured concentrations in Fig. 2.11B. The calculated nitrate concentrations for the large rainfall event on March 21th are close to the measured concentrations. However, the decrease in nitrate concentrations that is observed during the small rainfall event on March 16th is completely missed by the mixing model. Instead, the linear flow route mixing model gave increased nitrate concentrations. At the field site tube drain discharge had increased while no increase in in-stream reservoir flux was observed. Based on the measured decrease in nitrate concentrations this increase in in-stream flux was expected. For this discharge event the measurements at the field site were not representative for the entire catchment.

During the larger discharge events the large discharge peaks of the catchment were caused by the flux that was measured with the in-stream reservoirs (Fig. 2.9B). Comparing these large discharge events with the small discharge events between March and April, it appears that the measurements at our field site underestimated the catchment-representative flux to the in-stream reservoirs. By postulating that the difference between measured and modeled flux during this small discharge peak mainly originated from overland and biopore flow from locations that react faster than our field site, we can construct a new prediction of nitrate concentrations. This corrected prediction of catchment-scale nitrate concentrations is shown in Fig 2.11B and is defined by:

$$c_{cor}(t + \Delta t) = (\bar{c}_d \cdot a_c \cdot q_d(t) + \bar{c}_r \cdot (q_{tot}(t) - a_c \cdot q_d(t))) \cdot q_{tot}(t)^{-1} \quad [2.3]$$

with $q_{tot} [\text{L}^3 \text{L}^{-2} \text{T}^{-1}]$ the measured catchment-scale discharge. A much better prediction of the nitrate concentrations during the small discharge event of March 16th was obtained after this correction. During the low flow periods, the fluxes from the groundwater towards the in-stream reservoirs were low. Because these fluxes were derived from pumping intervals, we did not measure a continuous flux, but rather a stepwise cumulative flux. Smoothing

this stepwise cumulative flux resulted in a fluctuating groundwater flux causing the fluctuating behavior of the nitrate concentration in Fig. 2.11B. Also the exact timing of the onset of the fluxes is partly filtered out by the pumps. This caused the high nitrate concentrations at the onset of the large rainfall event (March 21st) when the increase in in-stream flux occurred later than the increase in the drainage flux (Fig. 2.11B).

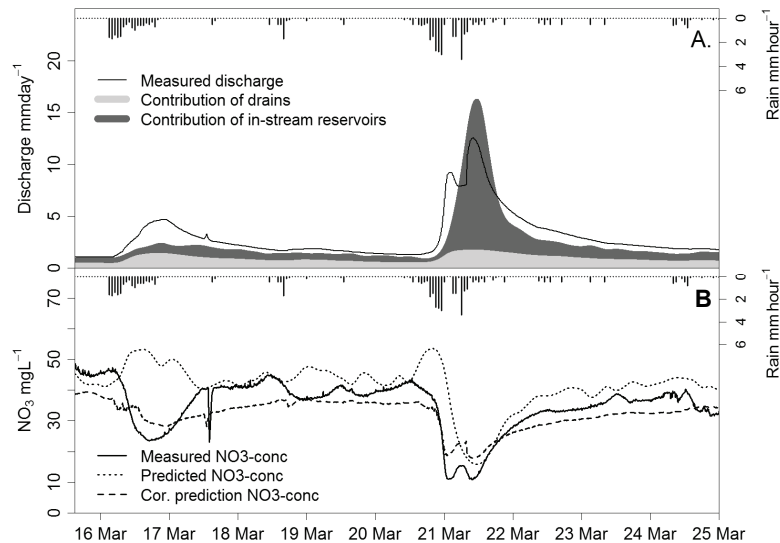


Figure 2.11. Observed precipitation, discharge and nitrate concentrations during a selected rainfall event. Drain discharge and discharge from other flow routes were separated according to Eq. [2.1] and Table 2.3. From these contributing fluxes, the nitrate concentrations were calculated with Eq. [2.2] (B dotted). A corrected nitrate concentration based on the difference between the measured catchment discharge and the simulated discharge is also given (dashed).

2.3.4 Field-scale versus catchment-scale responses to rainfall

In setting up an observation network to monitor fluxes at nested spatial scales within a catchment, the smaller scale observations should not be considered representative for the catchment; a field is not a miniature catchment, but one individual of a large population of units constituting the catchment. This is illustrated during the small discharge event on March 16th. The field site had no increased flux towards the in-stream reservoirs but other locations had, as can be deduced from the observed decrease in nitrate concentrations.

The value of the nested-scale monitoring lies in the increased understanding of the ways in which field-scale processes influence catchment scale discharge and water quality. In our catchment we needed the field site to reveal how the fast flow routes dominated by overland and biopore flow caused a decrease in nitrate concentration during rainfall events. Because the recession behavior of the groundwater flow route, overland and biopore flow route and tube drain flow route after rainfall events are distinctly different, it enabled us to

upscale the flow route contributions from the field site to the total catchment. Even for events when the field site measurements were not representative for the total catchment, like the March 16th-event, the typical recession behavior of the fast flow route during larger discharge events allowed us to estimate the contribution of the fast flow routes to the catchment discharge.

Based on the field site measurements, it is now also possible to explain differences with results from other studies on seemingly comparable sites. Tiemeyer et al. (2008) used a similar mixing model approach to model surface water nitrate concentrations in a lowland catchment in Northeast Germany. They separated the discharge into a base flow and a fast flow route with constant concentrations and they used Eq. [2.2] to calculate the surface water concentrations. However, their fast flow route was assigned the highest concentration, producing higher nitrate concentrations during discharge peaks. In addition, Rozemeijer and Broers (2007) and Wriedt et al. (2007) also found higher nitrate concentrations during wet periods for lowland catchments in the Netherlands and Germany.

These results seem to contradict the low nitrate values for the rapid flow route found in this study. This contradiction arises from the differences in hydrology between the Hupsel catchment and the catchments studied by Tiemeyer et al. (2008), Rozemeijer and Broers (2007) and Wriedt et al. (2007).

The Hupsel brook catchment has a shallow unconfined aquifer with an average thickness of only four meters and a dense artificial drainage system. This results in relatively short residence times and a relatively small groundwater flow (base flow) route contribution towards the surface water system compared to tube drain flow and overland flow. This is shown by the flatness of the cumulative in-stream reservoir discharge during dry periods in Fig. 2.7. The rapid response to precipitation events in the Hupsel catchment consists of overland flow, interflow and direct precipitation with low nitrate concentrations. Similar decreasing nitrate concentrations during rainfall events in agricultural catchments have been observed by Borah et al. (2003), Chang and Carlson (2004) and Poor and McDonnell (2007).

The catchments studied by Tiemeyer et al. (2008), Rozemeijer and Broers (2007) and Wriedt et al. (2007) on the other hand, have much thicker unconfined aquifers and longer residence times. The more important base flow contribution in these catchments consists of deep groundwater with low nitrate concentrations. During precipitation events, shallow groundwater and drain effluent with high nitrate concentrations start to contribute, resulting in an increase of nitrate concentrations in the main streams. This comparison between the Hupsel catchment and the catchments studied by Tiemeyer et al. (2008), Rozemeijer and Broers (2007) and Wriedt et al. (2007) shows the value of the process-based field-scale measurements.

2.4 Conclusions

To reduce catchment discharge model uncertainty and equifinality of parameterizations, measurements of the flow route contributions to the total discharge are essential. Our field-scale results for the Hupsel brook catchment showed that various rapid flow routes towards the surface water system exist. The method of decoupling the drainage effluent and constructing a reservoir in the ditch that collects groundwater inflow, interflow and overland flow, offers a feasible way to capture these various fluxes.

In spite of the large differences between individual tube drains and in-stream reservoirs, the signals of their average discharges proved to be characteristic for the larger scale levels. The main features of the hydrographs (particularly the spikes caused by rapid flow routes) were conserved over all observation scales in this study. Therefore we conclude that the field-scale flux measurements of individual flow routes are very useful to understand and to interpret quantitatively the discharge and water quality behavior of surface water at catchment-scale.

The nested experimental setup enabled us to understand the discharge and nitrate transport mechanisms of the Hupsel Brook catchment. The presented linear flow route mixing model to describe catchment discharge and nitrate transport from field-scale flow route measurements is a first step towards a better understanding of the complexity of transport mechanisms at the catchment-scale. The dataset of discharge and nitrate fluxes from field-scale to catchment-scale will prove highly valuable for development and validation of more complex models that include nested-scale hydrologic processes. More high-frequency concentration observations at the field and catchment scale are desirable to increase insight in the behavior of solute concentrations of individual flow routes during rainfall and discharge events.

The study reported here is the first in which all major flow routes were observed simultaneously at the field site. A comparison with the results of other studies revealed that quantifying field-scale flow routes is the key to a successful separation of the total catchment discharge into flow route contributions.

Catchment-scale non-linear groundwater-surface water interactions in densely drained lowland catchments

Abstract

Freely discharging lowland catchments are characterized by a strongly seasonally contracting and expanding system of discharging streams and ditches. Due to this rapidly changing active channel network, discharge and solute transport cannot be modeled by a single characteristic travel path, travel time distribution, unit hydrograph, or linear reservoir. We propose a systematic spatial averaging approach to derive catchment-scale storage and discharge from point-scale water balances. The effects of spatial heterogeneity in soil properties, vegetation, and drainage network are lumped and described by a relation between groundwater storage and the spatial probability distribution of groundwater depths with measurable parameters. The model describes how, in lowland catchments, the catchment-scale flux from groundwater to surface water via various flow routes is affected by a changing active channel network, the unsaturated zone and surface ponding. We used observations of groundwater levels and catchment discharge of a 6.6 km² Dutch watershed in combination with a high-resolution spatially distributed hydrological model to test the model approach. Good results were obtained when modeling hourly discharges for a period of eight years. The validity of the underlying assumptions still needs to be tested under different conditions and for catchments of various sizes. Nevertheless, at this stage the model can already improve monitoring efficiency of groundwater-surface water interactions.

This chapter is adapted from: Van der Velde, Y., G.H. de Rooij and P.J.J.F. Torfs (2009). Catchment-scale non-linear groundwater-surface water interactions in densely drained lowland catchments. Hydrol. Earth Syst. Sci. 13, 1867-1885.

3.1 Introduction

Catchments without real hillslopes, with an unconsolidated soil, a dense artificial drainage system, and with high inputs of nutrients due to intensive agriculture can be found in lowland landscapes all over the world. Polluted surface waters are an important environmental issue in all these catchments, with nutrient loads far exceeding loads in most mountainous catchments. Recent research on catchment scale discharge and transport modeling, however, was mainly oriented towards sloped catchments, creating concepts and models that are inappropriate for lowland catchments (e.g. TOPMODEL by Beven and Kirkby (1979); ARNO by Todini (1996); Representative Elementary Watershed (REW) approach as implemented by Zhang et al. (2006); HBV by Lindström et al. (1997)).

Typically, lowland catchments have a soil with sand, clay, and peat layers, sometimes interspersed with gravelly layers, with a shallow groundwater table. The absence of significant slopes makes groundwater the dominant contributor to stream discharge, either via direct inflow through the stream bed or through man-made drainage systems (De Vries, 1994; Wriedt et al., 2007; Tiemeyer et al., 2007). This groundwater flux is driven by continuously changing groundwater level gradients towards draining ditches and streams rather than by a fixed regional bedrock or surface elevation slope as is a common assumption for sloped catchments. Direct runoff occurs only when the infiltration capacity of the soil is exceeded by heavy rainfall or when the phreatic level rises to the soil surface. Freely discharging lowland catchments are characterized by a strongly seasonally contracting and expanding system of discharging ditches and streams (Ernst, 1978; De Vries, 1995). In hillslope hydrology this changing active channel network is reflected in the hydrological connectivity (Ocampo et al., 2006; Molenat et al., 2008) between the riparian and upland zones. Due to this rapidly changing active channel network, discharge and solute transport cannot be modeled by a single characteristic travel path, travel time distribution, unit hydrograph, or linear reservoir. This highly non-linear, transient behavior is well recognized (Beven and Kirkby, 1979; Van de Griend et al., 2002). Many approaches incorporated a variable contributing area concept for the description of stream discharge, but most of them focused on hillslopes (TOPMODEL based on a kinematic wave approach, Beven and Kirkby, 1979), direct runoff (PDM rainfall-runoff model based on spatial distribution of soil moisture, Moore, 1985), or characteristic soil-segments (Lazzarotto et al., 2006), making them over-parameterized and needlessly complicated for applications to large catchments, or even irrelevant for relatively flat lowland areas. Moore (1985) and Moore (2007) proposed a probability distribution for soil moisture storage to include the spatial variability of discharge generation, but did not relate this to a distribution in groundwater levels. Discharge generation in lowland catchments, however, is driven to a far greater extent by the distribution of groundwater levels than it is by the soil moisture content of the top layer. Seibert et al. (2003) explored this interaction between groundwater level and unsaturated soil moisture and concluded that runoff models for catchments with shallow groundwater levels should explicitly include unsaturated zone storage coupled to groundwater levels.

Wriedt et al. (2007), Ocampo et al. (2006) and Molenat et al. (2008) showed that hydrological connectivity through channel activity or high groundwater tables can be one of the major controls of nitrate transport within a catchment. A spatially distributed hydrological model can in principle calculate these spatial and temporal groundwater dynamics but has a huge data demand and to model correct contributions of specific flow routes (overland flow, tube drain flow, or groundwater flow) to the total discharge, very small spatial and temporal resolutions would be needed. This causes long building and calculation times and makes such models tedious to operate and calibrate. Rainfall-runoff models with variable source area concepts, on the other hand, can effectively calculate fluxes of individual flow routes when measurements are available, but their storage volumes are often inaccurate. Both aspects, an accurate separation in flow route contributions and accurate storage volumes are essential for catchment-scale solute transport modeling. Molenat et al. (2007), Ocampo et al. (2006) and McDonnell (2003) reached a similar conclusion and suggested that for an accurate description of nitrate transport a classic “variable source area” model is not the way forward.

The objectives of this paper are to formulate expressions for catchment-scale water fluxes from the unsaturated zone to the groundwater and from groundwater to the stream network. The expressions need to incorporate spatial and temporal groundwater variations and should calculate realistic storage changes within the catchment. We apply these equations to a lowland agricultural catchment in The Netherlands (Hupsel Brook catchment, 6.6 km²) and evaluate their performance.

3.2 Theory: model formulation

3.2.1 The basics

We seek to develop a water flux model for densely drained lowland catchments without snow cover. The model should be able to describe the dynamic saturated groundwater-surface water contact interface. The interaction between the saturated and unsaturated zone is expected to help generate peak discharges during wet periods by amplifying the precipitation signal toward the saturated zone (Seibert et al., 2003). Surface ponding and water storage by filling dry ditches and stream branches, on the other hand, is expected to dampen peak discharges during wet periods. Both types of interactions are included in the model description.

In lowland catchments groundwater discharge from the saturated zone to the surface water system is the most important discharge generating process. It can occur as flow into tube drains (q_{dr} [LT⁻¹]), flow into ditch and stream beds, and as overland flow from groundwater seepage when the phreatic level is above the soil surface. Both overland flow and groundwater seepage into ditches and streams occur because groundwater levels rise above the level of the water layer on the soil surface (which may also be the stream/ditch bed) and therefore they both received the notation: q_{ex} [LT⁻¹]. Discharge generation is generally described by a linear reservoir with a threshold, driven by groundwater heads, $H(x,y,t)$:

$$q_i(x, y, t) = \frac{H(x, y, t) - H_{thres,i}(x, y, t)}{r_i(x, y, t)} \text{ for } H(x, y, t) > H_{thres,i}(x, y, t) \quad [3.1]$$

$$q_i(x, y, t) = 0 \quad \text{for } H(x, y, t) \leq H_{thres,i}(x, y, t) \quad [3.2]$$

A location x, y [L] at time t [T] starts to generate discharge, $q_i(x, y, t)$ [LT^{-1}], when the groundwater head, $H(x, y, t)$ [L], is larger than a threshold groundwater head, $H_{thres,i}(x, y, t)$ [L]. The resistance that this water flux has to overcome is denoted by $r_i(x, y, t)$ [T]. The subscript i denotes the type of flux (groundwater flow towards surface water and surface ponds: $i = ex$ and tube drain flow: $i = dr$). Since we limit ourselves to groundwater discharging directly into the surface water, the discharge flux can only be non-zero along the wet perimeters of stream beds, along the tube drains below groundwater level and at the soil surface when the phreatic level reaches the surface and overland flow occurs. For stream/ditch and overland flow (q_{ex}), $H_{thres,ex}$ is the surface water level, or the soil surface elevation when there is no water storage on the soil surface. For tube drain discharge (q_{dr}), $H_{thres,dr}$ is the elevation of the drain tube. A catchment can be viewed as a population of such point-scale linear reservoirs with individual values for H , $H_{thres,i}$ and r_i . The draining area $A_{q,i}$ [L^2], i.e. the area of the catchment where groundwater and surface water are in direct contact, is then defined by:

$$A_{q,i}(t) = \int_A \mathbf{1}_{\{H(x,y,t) > H_{thres,i}(x,y,t)\}} \, dA \quad [3.3]$$

with $\mathbf{1}_{\{var\}}$ an indicator function that is 1 when variable var is true and 0 when var is false and A [L^2] the catchment area. The values of $H(x, y, t)$, the groundwater level, and $H_{thres,i}(x, y, t)$, the surface water level, are strongly time dependent and may cause the drainage area $A_{q,i}$ to vary strongly in time. In relatively flat lowland catchments with dynamic and shallow groundwater levels, $A_{q,i}$ has been observed to change considerably over time (Ernst, 1978; Wriedt et al., 2007; De Vries, 1995). This is a combined effect of groundwater tables that lose contact with surface water or tube drains during dry periods (compare the wet and dry state in Fig. 3.1) and of high surface water levels during wet periods, raising the threshold groundwater head. Consequently, models that use one linear reservoir to calculate groundwater flow towards the surface water network, which rely on the assumption that $A_{q,i}$ is constant with time, fail to describe groundwater discharge in lowland catchments or need multiple reservoirs to model discharge. Often, a fast- and slow-response reservoir arranged in parallel are used. Although conceptually straightforward, this modeling strategy does not fully recognize the system dynamics and its parameters cannot be directly linked to observable catchment properties.

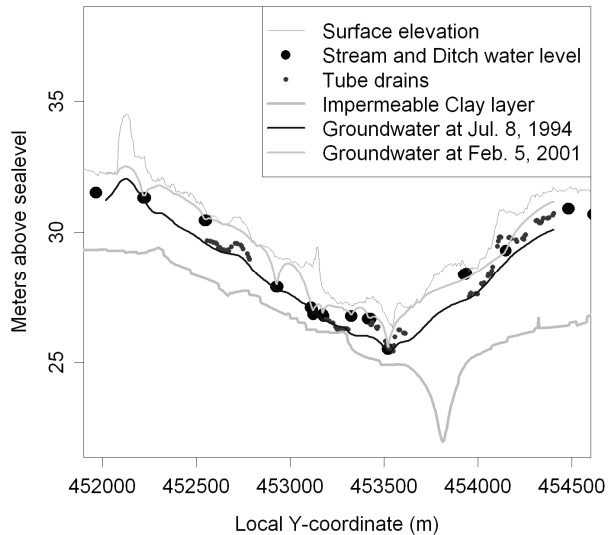


Figure 3.1. Vertical cross-section of the Hupsel brook catchment in The Netherlands (see the main text for details). The surface elevation and the elevation of the impermeable thick clay layer are indicated, as well as the water levels of the brook that drains the catchment and of the ditches that discharge into the streams. Many of the fields in the catchment have tube drains, which are also indicated. Calculated groundwater levels on a wet day (Feb. 5, 2001) and a dry day (Jul. 8, 1994) are also given.

In lowland catchments a huge simplification can be made in upscaling Eqs. [3.1] and [3.2] when the change in saturated groundwater storage related to a change in groundwater level is expressed by a change in the thickness of the unsaturated zone, u [L]. It is important to realize that from here on, we will use the change in unsaturated zone thickness to express the change in saturated storage. In lowland catchments with a shallow phreatic groundwater system, the spatial variation of $u(x,y,t)$ is heavily affected by the distance between draining ditches or tube drains (See how the groundwater level during a wet day is affected by ditches and drains in Fig. 3.1). This yields a spatial distribution between draining ditches or drains of point-scale values of $u(x,y,t)$ that is mainly influenced by soil type, drainage depth and distance, and recharge flux. A lowland catchment typically has a dense network of ditches and drains with many different drainage depths and distances between ditches and drains. Thus the spatial distribution of $u(x,y,t)$ at any given time over the entire catchment is the sum of the spatial distributions of $u(x,y,t)$ at that time between actively draining ditches and drains. According to the central limit theorem, summing n distributions of weakly correlated random variables with finite means and variances, will yield a normal overall distribution for sufficiently large n (Feller, 1971). The key characteristic of our model is that the distribution of point-scale $u(x,y,t)$ for the entire catchment is described by a Normal distribution function, $f_u(u(t), \langle u(t) \rangle, \sigma_u(t))$ with mean unsaturated zone thickness, $\langle u \rangle$ [L], and standard deviation, σ_u [L]. From here on the Normal distribution will be denoted by $f_u(t)$, reflecting that each time has a unique spatial distribution of unsaturated zone thicknesses. The validity of this Normality assumption will be assessed in the Results and Discussion section. The locations with negative values for $u(x,y,t)$ described by $f_u(t)$ indicate locations with a seepage face (i.e. groundwater is higher than the soil surface). This negative fraction of the distribution will be used to calculate the exfiltration fluxes of groundwater to the surface water (q_{ex}). The spatial structure of u within the catchment is lost, but the mean and

variance of the values of u are preserved. Hence, no information on the location of a flux is available and consequently water cannot be routed downstream within the catchment. The model requires that the catchment characteristics are statistically homogeneous so that all local distributions of u have a mean and variance within the same order of magnitude and that the local distributions are to some degree independent. Therefore, it is not possible to choose a catchment size larger than typical rainfall and potential evaporation patterns, or to have significant trends or discontinuities in stream network densities or soil properties within the catchment. However, it is possible to couple multiple models to account for these spatial discontinuities. These are the preliminaries from which the model is developed below.

3.2.2 Mass balance equation

The basis of the model is the mass balance equation for the saturated zone, the unsaturated zone and surface storage for each vertical column in the landscape (no changes in water density are assumed):

$$\frac{\partial s_{surf}(x, y, t)}{\partial t} + \frac{\partial s_{unsat}(x, y, t)}{\partial t} + \frac{\partial s_{sat}(x, y, t)}{\partial t} = p(x, y, t) - e_{act}(x, y, t) - l_{sat}(x, y, t) - l_{surf}(x, y, t) - o(x, y, t) \quad [3.4]$$

with s [L] reflecting storage within a vertical column located at horizontal coordinates x, y , at time t . The subscripts *surf*, *unsat* and *sat* refer to storage of surface water/ponds, unsaturated soil water and saturated groundwater respectively. Rainfall is denoted by p [LT^{-1}] and evapotranspiration by e_{act} [LT^{-1}]. The net lateral outward flux density through the subsurface is denoted by l_{sat} [LT^{-1}], and the net lateral outward flux density over the soil surface by overland flow, stream flow, and tube drain discharge by l_{surf} [LT^{-1}]. No lateral fluxes in the unsaturated zone are assumed. Any sources and sinks are reflected by o [LT^{-1}]. The water balance of each of the storage compartments of Eq. [3.4] requires the fluxes between these compartments. The fluxes between the unsaturated and the saturated soil are denoted by j [LT^{-1}] while q [LT^{-1}] denotes the fluxes from soil to the surface storage and vice versa:

$$\frac{\partial s_{surf}(x, y, t)}{\partial t} = 1_{\{s_{surf}(x, y, t) > 0\}} (p(x, y, t) - e_{act}(x, y, t) - q_{inf}(x, y, t) + q_{ex}(x, y, t) + q_{dr}(x, y, t) - l_{surf}(x, y, t)) \quad [3.5]$$

$$\frac{\partial s_{unsat}(x, y, t)}{\partial t} = 1_{\{s_{unsat}(x, y, t) > 0\}} (p(x, y, t) - e_{act}(x, y, t) + j_{cap}(x, y, t) - j_{rch}(x, y, t)) \quad [3.6]$$

$$\frac{\partial s_{sat}(x, y, t)}{\partial t} = j_{rch}(x, y, t) - j_{cap}(x, y, t) + q_{inf}(x, y, t) - q_{ex}(x, y, t) - q_{dr}(x, y, t) - l_{sat}(x, y, t) - o(x, y, t) \quad [3.7]$$

Subscripts of q denote the infiltration from surface storage into the unsaturated zone, inf , exfiltration of groundwater to the surface water and surface ponds, ex , and groundwater flow towards tube drains, dr . Subscripts of j denote capillary up rise of groundwater to the unsaturated zone, cap , and the recharge of the saturated zone by unsaturated soil water, rch . Note that the flux into the drains appears in the surface water budget (Eq. [3.5]). Although counterintuitive, it signals that tube drain discharge no longer flows through the porous medium. Similarly, l_{surf} comprises lateral fluxes of water both over the land surface, and through drain tubes. Both q_{dr} and the tube drain contribution to l_{surf} can only be non-zero for (x,y) located directly above a drain tube. Note that we assume that perched water tables do not occur. Therefore, one of the storages s_{surf} or s_{unsat} is necessarily zero and consequently the atmospheric forcings, p and e_{act} , act on the active reservoir ($s_{surf} > 0$ or $s_{unsat} > 0$). All subsurface flows towards drains and surface water bodies are incorporated in l_{sat} and all overland flows towards the surface water and flow from adjacent streams, ditches, and drains are incorporated in l_{surf} . Figure 3.2 summarizes all fluxes that are described by this model.

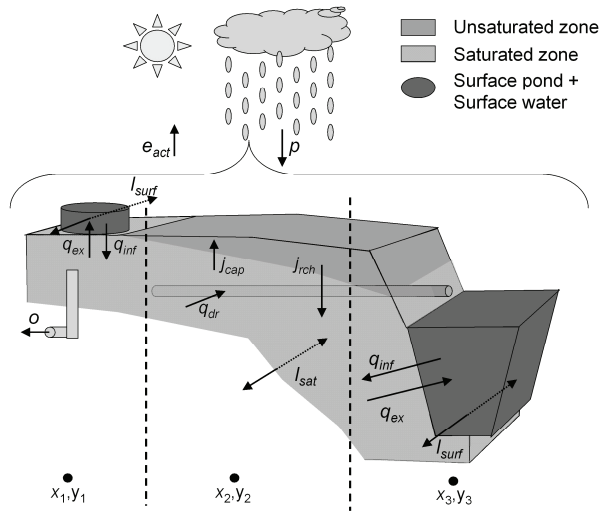


Figure 3.2. The water balance model describes fluxes at the point-scale. This figure illustrates three locations (x_1, y_1) , (x_2, y_2) and (x_3, y_3) within a cross section of a typical lowland field. The groundwater level at location (x_1, y_1) is above soil surface, which leads to ponding. Note that when the groundwater level is above soil surface there is no unsaturated zone. Infiltrating water from the pond into the saturated zone is denoted q_{inf} . Exfiltrating water from the saturated groundwater into the pond is denoted q_{ex} . A sink

is denoted o and the lateral overland flow l_{surf} . Location (x_2, y_2) has an unsaturated zone and consequently no surface storage. The flux from the unsaturated zone to the saturated zone is denoted j_{rch} and the capillary flux from saturated to unsaturated zone j_{cap} . This location is also tube-drained with a tube drain flux q_{dr} . Note that surface storage and tube drainage can occur at the same location. Point (x_3, y_3) is located at a stream. Above the stream bed surface storage occurs. The exfiltrating, infiltrating, and lateral surface fluxes are treated the same way for a ponded location (x_1, y_1) and a stream/ditch location (x_3, y_3) . Rainfall, p , evapotranspiration, e_{act} , and lateral saturated groundwater fluxes, l_{sat} , occur in all three locations.

Equation [3.4] represents a point-scale mass balance. By integrating over the catchment area A [L^2], a catchment-scale mass balance can be obtained. In doing so, lateral flow components within A cancel out, and only the lateral flow over the boundary of A affects the mass balance. Thus we obtain:

$$\int_A \left(\frac{\partial s_{sat}}{\partial t} + \frac{\partial s_{unsat}}{\partial t} + \frac{\partial s_{surf}}{\partial t} \right) dA = \int_A (p - e_{act} - o) dA - \int_S \mathbf{l}_{sat} \cdot \mathbf{n} dS - \int_S \mathbf{l}_{surf} \cdot \mathbf{n} dS \quad [3.8]$$

where $S[L]$ represents the boundary of A at soil surface, \mathbf{l}_{sat} is the vertically integrated lateral flux density vector of the saturated zone [L^2T^{-1}], \mathbf{l}_{surf} is the vertically integrated lateral flux density of surface storage [L^2T^{-1}] and \mathbf{n} is the outward normal vector of unit length [-] of S . The integrations convert flux densities [LT^{-1}] to fluxes [L^3T^{-1}]. We dropped the reference to the spatial and temporal coordinates for clarity. Of particular interest is the last term of Eq. [3.8] because this term represents the total catchment discharge by surface water at any given time.

3.2.3 Dimension reduction of the catchment scale mass balance equation

The integral formulation of the mass balance, Eq. [3.8], has two spatial dimensions and one time dimension, and generally will be impossible to evaluate in a practical way. We therefore seek a dimensional reduction approach in which we lump spatially distributed processes where possible while maintaining the characteristic behavior of a typical lowland catchment with realistic water storage changes inside the catchment. The characteristic behavior we focus on is defined by:

- A continuously changing active drainage system defined by the contact zone between saturated groundwater and surface water, due to varying groundwater and surface water levels (Fig. 3.3a, b, c, and d).
- The unsaturated zone as an amplifier of rainfall and evapotranspiration fluxes towards and from the groundwater.
- Ponding of parts of the soil during prolonged periods of rain (Fig. 3.3e and f).

As a first step, we eliminate the spatial dimensions in Eq. [3.8] by spatial averaging. Spatial averaging is simply obtained by carrying out the integration over A for that variable and dividing by A . Thus we obtain:

$$\left\langle \frac{\partial s_{sat}}{\partial t} \right\rangle + \left\langle \frac{\partial s_{unsat}}{\partial t} \right\rangle + \left\langle \frac{\partial s_{surf}}{\partial t} \right\rangle = \langle p(t) \rangle - \langle e_{act}(t) \rangle - \langle o(t) \rangle - \frac{1}{A} \int_S \mathbf{l}_{sat}(t) \cdot \mathbf{n} dS - \frac{1}{A} \int_S \mathbf{l}_{surf}(t) \cdot \mathbf{n} dS \quad [3.9]$$

where $\langle \rangle$ denotes the spatial averaging operation over any A . Note that the dimensional reduction changed the dimensions of all terms from [L^3T^{-1}] in Eq. [3.8] to [LT^{-1}] in Eq. [3.9]. When we choose the catchment such that its boundaries are zero-flux boundaries for the shallow groundwater, the boundary integral of the saturated lateral flux can be

neglected. Even in the case of a large-scale background flow of groundwater passing through the catchment the net flux over S will be close to zero if no significant groundwater exfiltration or recharge of the aquifer occurs. The boundary integral of lateral fluxes of surface storage on the other hand, represents the total stream discharge from the catchment. This is of course the key flux that can be compared with discharge measurements.

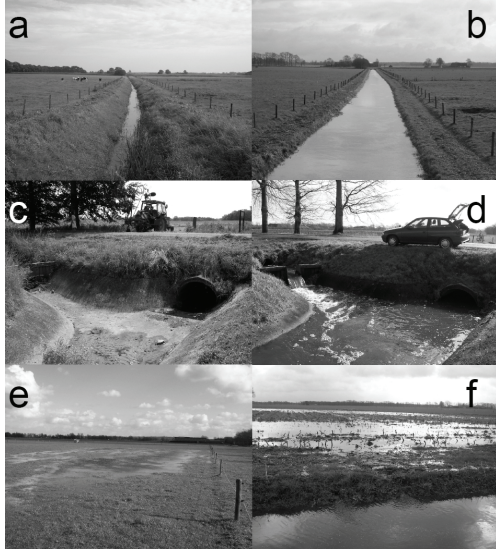


Figure 3.3. Pictures of the Hupsel brook catchment. Figures **a** and **b**, and **c** and **d** show the typical change in surface water level during a dry and a wet period resulting in changes in unsaturated zone thickness variation. Picture **e** shows the large scale ponding that occurs during wet periods, and the resulting overland flow is shown in picture **f**.

The storage and flux terms in Eq. [3.9], are functionally dependent on the thickness of the unsaturated zone $u(x,y,t)$: Low phreatic levels lower $e_{act}(x,y,t)$, $q_{ex}(x,y,t)$ and $q_{di}(x,y,t)$. In soils with a high infiltration capacity, overland flow, $l_{surf}(x,y,t)$, will be zero if $u(x,y,t)$ is significantly larger than zero. We formalize this by declaring all local flux densities dependent upon $u(x,y,t)$:

$$\langle J(t) \rangle - J(x, y, t) = g_J(\langle u(t) \rangle - u(x, y, t)) \quad [3.10]$$

where J [LT^{-1}] denotes a flux density or change in storage in Eq. [3.9], and $g_J()$ denotes a non-linear functional dependence on the variables in parentheses. The spatial average of J is:

$$\langle J(t) \rangle = \int_{-\infty}^{+\infty} f_u(t) \cdot J(u) du \quad [3.11]$$

Note that the spatial dependence is replaced by a dependence of J on u through the probability density function (PDF) of u at the time of interest, which describes the spatial variation of u . Equations [3.10] and [3.11] reduce the problem of the spatial variation of the many terms in Eq. [3.9] to that of the variation in u and identifying $g_J()$ for the various J 's.

If we assume $f_u(t)$ to be Normal as discussed above, $f_u(t)$ is completely characterized by its mean $\langle u(t) \rangle$ and standard deviation $\sigma_u(t)$.

By noting that during dry periods $e_{act}(x,y,t)$ tends to be large for small $u(x,y,t)$, we can deduce that $\sigma_u(t)$ is relatively small during prolonged dry periods: shallow groundwater levels are lowered more than deep groundwater tables, reducing the variation of $u(x,y,t)$ for large $\langle u(t) \rangle$. During and shortly after rainfall, with ditches and drains discharging, u varies strongly within fields, increasing σ_u (see also the cross section of Fig. 3.1). For prolonged rainfall, $\langle u(t) \rangle$ will reduce further, and the occurrence of ponding creates negative values of u . Eventually, when nearly the entire catchment is flooded, the water level above the soil surface will run approximately parallel to the groundwater level under dry conditions. Consequently, it is expected that σ_u will tend towards the same relatively low value under very wet and very dry conditions. Based on these arguments and in the spirit of dimension reduction we will assume $\sigma_u(t)$ to be a function of $\langle u(t) \rangle$ that peaks at an intermediate value and tails off at the extremes. The exact functional dependence is a characteristic of the catchment topography, soil, and climate. A simple empirical four-parameter expression to approximate this relation is given by:

$$\sigma_u = (\sigma_{\max} - \sigma_{\min}) \cdot e^{-\left(\frac{\langle u(t) \rangle - u_{sd\max}}{b}\right)^2} + \sigma_{\min} \quad [3.12]$$

where σ_{\max} [L] is the maximum standard deviation of u , occurring at $\langle u(t) \rangle = u_{sd\max}$ [L]. The minimum standard deviation, σ_{\min} [L], occurs for large and very small (negative) $\langle u(t) \rangle$ values. The shape parameter b [L] determines the steepness of the curve. The ability of this empirical function to describe the complex shape of the catchment-scale groundwater table will be assessed in the Results and Discussion section.

3.2.4 Storage and flux expressions

In this section the terms of the water balance, Eq. [3.9], are one by one expressed as functions of u and f_u . Section 3.2.5 gives the final water balance equation, which is used to calculate catchment-scale fluxes and storages.

3.2.4.1 Temporal variations of average saturated storage

The point-scale saturated storage, s_{sat} , is defined as:

$$s_{sat}(x, y, t) = \int_{z_0(x,y)}^{z_s(x,y)-u(x,y,t)} \theta_s(x, y, z) dz \quad \text{for } u(x,y,t) > 0 \quad [3.13]$$

$$s_{sat}(x, y, t) = \int_{z_0(x,y)}^{z_s(x,y)} \theta_s(x, y, z) dz \quad \text{for } u(x,y,t) \leq 0 \quad [3.14]$$

where z [L] is the vertical coordinate, z_0 [L] is the elevation of the impermeable base or another suitable lower boundary, z_s [L] is the elevation of the soil surface, and θ_s is the saturated volumetric water content. Since we are interested in storage of water at a given

horizontal location, the exact vertical location is of limited value. By noting that $z_s(x,y) - z_\theta(x,y)$ is the local thickness $T[L]$ of the subsurface affecting the catchment hydrological behavior, Eqs. [3.13] and [3.14] can be simplified to:

$$s_{sat}(x, y, t) = \int_0^{T(x,y)} \theta_s(x, y, z^*) dz^* - 1_{\{u(x,y,t)>0\}} \int_{T(x,y)-u(x,y,t)}^{T(x,y)} \theta_s(x, y, z^*) dz^* \quad [3.15]$$

where z^* is a transformed coordinate defined as $z^* = z - z_\theta(x,y)$. The first term on the right-hand-side of Eq. [3.15] is a location-specific constant, if temporal variations in θ_s caused by soil tillage, biological activity etc. are neglected. It reflects the total pore space $[L]$ in the column at (x,y) . Likewise, the second term represents the total pore space in the unsaturated zone at (x,y) . Spatially averaging Eq. [3.15] gives the average groundwater storage of the catchment as the difference between the total and the unsaturated volumes of pores in the catchment:

$$\langle s_{sat}(t) \rangle = \left\langle \int_0^T \theta_s dz^* \right\rangle - \left\langle 1_{\{u(t)>0\}} \int_{T-u(t)}^T \theta_s dz^* \right\rangle \quad [3.16]$$

where we dropped the references to the spatial coordinates for clarity. The change of the average saturated storage is:

$$\frac{\partial}{\partial t} \langle s_{sat}(t) \rangle = - \left\langle 1_{\{u(t)>0\}} \frac{\partial}{\partial t} \int_{T-u(t)}^T \theta_s dz^* \right\rangle \quad [3.17]$$

The time derivative of $\int_{T-u(t)}^T \theta_s dz^*$ is determined by the depth interval in the soil between the maximum and the minimum value of $u(x,y,t)$. If θ_s varies little within that interval, Eq. [3.17] simplifies to:

$$\frac{\partial}{\partial t} \langle s_{sat}(t) \rangle = - \left\langle 1_{\{u(t)>0\}} \theta_s \frac{\partial}{\partial t} u(t) \right\rangle \quad [3.18]$$

If θ_s and $\frac{\partial}{\partial t} u(t)$ are uncorrelated random variables distributed over A , the average of their product equals the product of their averages:

$$\frac{\partial}{\partial t} \langle s_{sat}(t) \rangle = - \langle \theta_s \rangle \left\langle 1_{\{u(t)>0\}} \frac{\partial}{\partial t} u(t) \right\rangle \quad [3.19]$$

where θ_s is evaluated between the highest and the lowest groundwater level. Applying Eq. [3.11] for positive values of u yields:

$$\frac{\partial}{\partial t} \langle s_{sat}(t) \rangle = - \langle \theta_s \rangle \frac{\partial}{\partial t} \int_0^\infty f_u(t) u du \quad [3.20]$$

3.2.4.2 Temporal variations of average unsaturated storage

The unsaturated zone is assumed to be in hydrostatic equilibrium with the groundwater table at all times, making the volume of stored water in the unsaturated zone a function of the soil type and the water table. This assumption is only valid for shallow ground water tables, but has proven to be very useful in estimating the total amount of water in the unsaturated zone and its effect on groundwater table fluctuations (Kim *et al.*, 1996; Bierkens, 1998). The equilibrium assumption implies that any water added to the soil (e.g. by precipitation) is transferred immediately to the groundwater. Similarly, any water removed from the unsaturated zone (e.g. by evapotranspiration) is immediately withdrawn from the groundwater.

The assumption of instantaneous equilibrium throughout the unsaturated zone implies that the soils will always be on the wet end of the soil water characteristic. We therefore use van Genuchten's (1980) expression with the dry-end residual water content equal to zero:

$$\theta(x, y, z, t) = \theta_s(x, y, z) \left(1 + [\alpha h(t)]^n \right)^{\frac{1}{n}-1} \text{ for } u > 0 \quad [3.21]$$

where $\alpha[\text{L}^{-1}]$ and $n[-]$ are location-specific shape parameters and $h(t) = z - z_s(x, y) + u(x, y, t)$ is the height above the phreatic water level [L]. The point-scale unsaturated zone storage, s_{unsat} , can be obtained by integrating Eq. [3.21] for z ranging from $z_s - u$ to z_s . Similarly to Eq. [3.11], the spatial average can be obtained by integrating across all positive values of u , where $\langle \theta_s \rangle$ represents the spatial average of the local vertically integrated θ_s of the unsaturated zone, already introduced in Eq. [3.20]. At catchment-scale, however, we do not define spatial average Van Genuchten parameters, α , and n , but we view them as effective parameters describing the storage behavior of the unsaturated zone of the catchment incorporating the effects of unsaturated zone heterogeneities.

$$\langle s_{unsat}(t) \rangle = \langle \theta_s \rangle \int_0^\infty f_u(t) \int_0^u \left[1 + (\alpha h)^n \right]^{\frac{1}{n}-1} dh du \quad [3.22]$$

The temporal derivative follows directly. Note that the assumption of instantaneous hydrostatic equilibrium of the unsaturated zone implies that $\left\langle \frac{\partial s_{sat}(t)}{\partial t} \right\rangle$ and $\left\langle \frac{\partial s_{unsat}(t)}{\partial t} \right\rangle$ in Eq. [3.9] have opposite signs and the absolute value of $\left\langle \frac{\partial s_{sat}(t)}{\partial t} \right\rangle$ is always the largest (if the average thickness of the unsaturated zone increases, the saturated storage decreases, and the storage of the unsaturated zone increases). Effectively, the unsaturated zone amplifies the effects of the atmospheric fluxes on the groundwater table.

3.2.4.3 Temporal variations of average surface storage

Storage on the soil surface is assumed to occur only when groundwater levels rise above the soil surface. Ponding due to high rainfall intensities is assumed not to occur, which is valid for permeable soils in climates without long high-intensity rainfalls. A linear relation is assumed between the surface storage depth, $s_{surf}[L]$, and the height of the groundwater level above soil surface at location (x,y) (i.e. negative values of u):

$$s_{surf}(x, y, t) = -m(x, y, t) \cdot u(x, y, t) \text{ for } u(x, y, t) < 0 \quad [3.23]$$

where $m[-]$ is a location-specific empirical constant with a value between 0 and 1 that gives the fraction of the excess water stored on the soil. If $m = 1$, the negative u is entirely accounted for by the depth of the water layer on the soil surface. Consequently, no water is removed from the location by overland flow. For $m < 1$, a water layer of thickness $-m \cdot u$ is stored on the soil surface, and the pressure head difference $(m - 1) \cdot u$ generates overland flow. For $m = 0$, no ponding occurs and all excess water is discharged. This relation underestimates the complexity of the generation of overland flow and groundwater flow towards surface water at the point-scale but it is expected that the averaging operation over the catchment, with its wide range of negative u values, gives a reasonable approximation of increased surface storage with decreasing average unsaturated zone thickness. Assuming independence between the factor m and u and applying Eq. [3.11] gives:

$$\langle s_{surf}(t) \rangle = -\langle m \rangle \int_{-\infty}^0 f_u(t) u \, du \quad [3.24]$$

The temporal derivative follows directly. Note that the time derivative, $\left\langle \frac{\partial s_{surf}(t)}{\partial t} \right\rangle$, has the same sign as, and is always smaller than $\left\langle \frac{\partial s_{sat}(t)}{\partial t} \right\rangle$ in Eq. [3.9]: when the thickness of the unsaturated zone decreases, the saturated storage and the surface storage increase (with a thinner average unsaturated zone, there will be more ponding and therefore a higher surface storage). This term dampens the fluctuations in groundwater levels needed to maintain the water balance (Eq. [3.9]) and consequently dampens peak discharges.

Each negative thickness of the unsaturated zone translates into a fixed volume of stored water on the surface. This assumption implies that lateral surface fluxes cannot be stored elsewhere in the catchment (all available surface storage is always occupied) and that consequently surface water discharge over the catchment boundary is equal to the catchment average discharge:

$$\frac{1}{A} \int_S \mathbf{l}_{surf}(t) \cdot \mathbf{n} \, dS = \langle l_{surf}(t) \rangle \quad [3.25]$$

The catchment scale discharge can be calculated from the mass balance equation of the surface storage reservoir, Eq. [3.5]:

$$\begin{aligned} \langle l_{surf}(t) \rangle = & \langle q_{ex}(t) \rangle + \langle q_{dr}(t) \rangle - \langle q_{inf}(t) \rangle + \\ & \int_{-\infty}^0 f_u(t) du \cdot (\langle p(t) \rangle - \langle e_{act}(t) \rangle) - \left\langle \frac{\partial s_{surf}(t)}{\partial t} \right\rangle \end{aligned} \quad [3.26]$$

From the assumptions of instantaneous equilibrium of the surface storage reservoir, we can define $\langle q_{grw}(t) \rangle$, the groundwater exfiltration additional to the water needed to fill the surface storage, as:

$$\langle q_{grw}(t) \rangle = \langle q_{ex}(t) \rangle - \langle q_{inf}(t) \rangle - \left\langle \frac{\partial s_{surf}(t)}{\partial t} \right\rangle \quad [3.27]$$

Note that the average infiltration flux density, $\langle q_{inf}(t) \rangle$, is zero when surface storage increases, i.e., $\left\langle \frac{\partial s_{surf}(t)}{\partial t} \right\rangle > 0$, and equal to $-\left\langle \frac{\partial s_{surf}(t)}{\partial t} \right\rangle$ when surface storage decreases (the excess surface storage re-infiltrates for $\left\langle \frac{\partial s_{surf}(t)}{\partial t} \right\rangle < 0$). The total catchment discharge becomes:

$$\langle l_{surf}(t) \rangle = \langle q_{grw}(t) \rangle + \langle q_{dr}(t) \rangle + \int_{-\infty}^0 f_u(t) du \cdot (\langle p(t) \rangle - \langle e_{act}(t) \rangle) \quad [3.28]$$

3.2.4.4 Groundwater exfiltration

Exfiltration of groundwater, $q_{grw}(x,y,t)$ [LT^{-1}], defined by Eq. [3.27], is assumed to occur only when a groundwater head is higher than the level of the water layer stored on the soil surface. We also assume that groundwater exfiltration is proportional to the magnitude of the difference between the groundwater level $u(x,y,t)$ and the surface storage level, $s_{surf}(x,y,t)$, yielding:

$$q_{grw}(x,y,t) = 1_{\{u(x,y,t) > s_{surf}(x,y,t)\}} \frac{-u(x,y,t) - s_{surf}(x,y,t)}{r_{grw}(x,y,t)} \quad [3.29]$$

with $r_{grw}(x,y,t)$ [T] the resistance that the water flux from soil to surface water must overcome.

Replacing $r_{grw}(x,y,t)$ by its catchment scale average $\langle r_{grw} \rangle$, invoking Eq. [3.11] and introducing Eq. [3.23] gives the catchment-scale average groundwater exfiltration rate:

$$\langle q_{grw}(t) \rangle = - \int_{-\infty}^0 f_u(t) \frac{u + s_{surf}(u)}{\langle r_{grw} \rangle} du = \frac{\langle m \rangle - 1}{\langle r_{grw} \rangle} \int_{-\infty}^0 f_u(t) u du \quad [3.30]$$

3.2.4.5 Tube drain discharge

Tube drain discharge occurs when the drainage depth, $d_{dr}(x,y)[L]$, is larger than $u(x,y,t)$:

$$q_{dr}(x,y,t) = g(x,y) \cdot 1_{\{d_{dr}(x,y) > u(x,y,t)\}} \cdot \frac{d_{dr}(x,y) - u(x,y,t)}{r_{dr}(x,y,t)} \quad [3.31]$$

with the function $g(x,y)$ [-] equal to one above a drain tube and equal to zero elsewhere, and $r_{dr}(x,y,t)$ [T] denoting the resistance that the water flux from soil to tube drain has to overcome. However, drainage fluxes derived only at the exact location of drain tubes are of little practical value. We therefore introduce q_{dr}^* [LT^{-1}] as the rate at which saturated flow towards nearby drain tubes removes water from a location (x,y) at time t . Consequently, this fraction of the total flow should be subtracted from the value of $I_{sat}(x,y,t)$ to maintain mass conservation. We then have:

$$q_{dr}^*(x,y,t) = g^*(x,y) \cdot 1_{\{d_{dr}^*(x,y) > u(x,y,t)\}} \cdot \frac{d_{dr}^*(x,y) - u(x,y,t)}{r_{dr}^*(x,y,t)} \quad [3.32]$$

where $g^*(x,y)$ equals one whenever (x,y) is in a tube drained field and is zero elsewhere. The drainage depth d_{dr}^* [L] gives the average drainage depth of the field in which (x,y) is located. Similarly r_{dr}^* [T] denotes the resistance to the flow towards and into the drain tube. When $g^* = 0$, d_{dr}^* and r_{dr}^* are undefined.

In order to express q_{dr}^* as a function of $u(t)$, we assume $u(t)$ and d_{dr}^* to be independent. For the drained area of the catchment we may then write:

$$q_{dr}^*(t) = 1_{\{d_{dr}^* > u(t)\}} \cdot \frac{\langle d_{dr}^* \rangle - u(t)}{\langle r_{dr}^* \rangle} \quad [3.33]$$

where the averaging operations have been carried out over the region within A where $g^* = 1$. Some of the very wet locations within a catchment (small u) are likely not to be drained. For example there are no drains under ditches and streams which are obviously the wettest locations in the catchment. For an accurate contribution of tube drain discharge to the total discharge under dry conditions it is important to define this fraction of the catchment (wet and undrained). When we would ignore this and assume drainage to be more or less uniformly distributed over the full range of u , the model will generate substantial tube drain discharge even under dry conditions. We therefore assume that a fixed fraction of the catchment area ($A_{nd,wet}$ [L^2]) has the lowest values of u all the time and is not tube drained. Since $f_u(t)$ describes the distribution of u over A , the wet and undrained fraction of A equals the value of the cumulative probability distribution function, $F_u(u(t), \langle u(t) \rangle, \sigma_u(t))$, for the largest values of u still in wet but non-drained land ($u_{nd,max}$ [L]):

$$\frac{A_{nd,wet}}{A} = F_u(u_{nd,max}(t), \langle u(t) \rangle, \sigma_u(t)) \quad [3.34]$$

Hence:

$$u_{nd,max}(t) = F_u^{-1}\left(\frac{A_{nd,wet}}{A}, \langle u(t) \rangle, \sigma_u(t)\right) \quad [3.35]$$

Note that of course many of the undrained fields simply are dry enough without drain tubes. Therefore $A_{nd,wet}$ is smaller than the total undrained area. Equation [3.35] constitutes an additional condition that must be satisfied for q_{dr}^* to be non-zero. Extending Eq. [3.33] accordingly yields:

$$\begin{aligned} q_{dr}^*(u(t)) &= 1_{\{\langle d_{dr}^* \rangle > u(t)\}} \cdot 1_{\{u(t) > u_{nd,max}(t)\}} \cdot \frac{\langle d_{dr}^* \rangle - u(t)}{\langle r_{dr}^* \rangle} \\ &= 1_{\{\langle d_{dr}^* \rangle > u(t)\}} \cdot 1_{\left\{u(t) > F_u^{-1}\left(\frac{A_{nd,wet}}{A}\right)\right\}} \cdot \frac{\langle d_{dr}^* \rangle - u(t)}{\langle r_{dr}^* \rangle} \end{aligned} \quad [3.36]$$

Again, we determine the catchment average drainage discharge flux density by applying Eq. [3.11], taking into account that only the drained area $\int_A g^* dA$ generates discharge:

$$\begin{aligned} \langle q_{dr}^*(t) \rangle &= \frac{\langle d_{dr}^* \rangle}{F_u^{-1}\left(\frac{A_{nd,wet}}{A}\right)} \int_{F_u^{-1}\left(\frac{A_{nd,wet}}{A}\right)}^{\langle d_{dr}^* \rangle} f_u(t) \cdot \frac{\langle d_{dr}^* \rangle - u}{\langle r_{dr}^* \rangle} du \cdot \frac{1}{A} \int_A g^* dA \\ &= \frac{\langle g^* \rangle}{\langle r_{dr}^* \rangle} \frac{\langle d_{dr}^* \rangle}{F_u^{-1}\left(\frac{A_{nd,wet}}{A}\right)} \int_{F_u^{-1}\left(\frac{A_{nd,wet}}{A}\right)}^{\langle d_{dr}^* \rangle} f_u(t) \cdot (\langle d_{dr}^* \rangle - u) du \end{aligned} \quad [3.37]$$

3.2.4.6 Rainfall and evapotranspiration

Rainfall does not depend on u . We assume the catchment small enough for the rainfall rate $p(x,y,t)$ to be uniform: $p(t)$. Thus, $\langle p(t) \rangle = p(t)$.

In soils with shallow groundwater and a humid climate, transpiration by far exceeds evaporation when the plant cover is complete. In autumn and winter, cropped soils are bare, but the evapotranspiration rate in this period is low. The transpiration is assumed equal to the potential evapotranspiration, $e_{pot}[\text{LT}^{-1}]$, as long as $u(x,y,t)$ is smaller than some threshold. When $u(x,y,t)$ exceeds that threshold, $e_{act}(x,y,t)$ drops to zero. It is expected that the averaging operation over the catchment with its wide range of local values of u produces a smoothly decreasing $\langle e_{act}(t) \rangle$ as the catchment becomes drier. For a threshold $u_{et}(x,y,t)$ [L] we have:

$$e_{act}(x, y, t) = 1_{\{u(x,y,t) < u_{et}(x,y,t)\}} \cdot e_{pot}(x, y, t) \quad [3.38]$$

Applying Eq. [3.11] with $u_{et}(x,y,t)$ constant in time and space gives the average transpiration rate over the catchment:

$$\langle e_{act}(t) \rangle = \int_{-\infty}^{\infty} f_u(t) 1_{\{u(x,y,t) < \langle u_{et} \rangle\}} \langle e_{pot}(t) \rangle du = \langle e_{pot}(t) \rangle \int_{-\infty}^{\langle u_{et} \rangle} f_u(t) du \quad [3.39]$$

A more elaborate function such as a linear or exponential decline between two groundwater depths or a linear decline with unsaturated water content will only improve the results when the standard deviation of groundwater depth is small (<0.2). The averaging effect of the catchment will then be less, and only then the effect of the extra parameters of a more elaborate function will not be overruled by the averaging effect. For the entire Hupsel brook catchment we have chosen the most basic formulation as presented above.

3.2.5 The water balance as function of groundwater table fluctuations.

In the previous sections all terms of the water balance, Eq. [3.9], have been made solely dependent on $\langle u(t) \rangle$ and $f_u(t)$. We now take Eq. [3.9] and substitute Eqs. [3.20], [3.22], and [3.24] for the three storage terms, maintain the precipitation term $\langle p(t) \rangle$, and set the source/sink term $\langle o(t) \rangle$ to zero, and assume the net subsurface flux l_{sat} across S to be negligible. Finally we insert Eq. [3.39] for the evapotranspiration, and Eq. [3.25] for the net surface water flux across S to obtain the water balance of the catchment:

$$\begin{aligned} -\langle \theta_s \rangle \frac{\partial}{\partial t} \left(\int_0^{\infty} f_u(t) u du \right) + \langle \theta_s \rangle \frac{\partial}{\partial t} \left(\int_0^{\infty} f_u(t) \int_0^u [1 + (\alpha h)^n]^{1/n-1} dh du \right) \\ - \langle m \rangle \frac{\partial}{\partial t} \left(\int_{-\infty}^0 f_u(t) u du \right) = \langle p(t) \rangle - \langle e_{pot}(t) \rangle \int_{-\infty}^{\langle u_{et} \rangle} f_u(t) du - \langle l_{surf}(t) \rangle \end{aligned} \quad [3.40]$$

with the total discharge from the catchment, $\langle l_{surf}(t) \rangle$, derived from Eq. [3.28] combined with expressions for the individual flux terms, Eqs [3.30], [3.37] and [3.39]:

$$\begin{aligned} \langle l_{surf}(t) \rangle = \frac{\langle m \rangle - 1}{\langle r_{grw} \rangle} \int_{-\infty}^0 f_u(t) u du + \frac{\langle g^* \rangle}{\langle r_{dr}^* \rangle} \frac{\langle d_{dr}^* \rangle}{F_u^{-1} \left(\frac{A_{nd,wet}}{A} \right)} \int_{-\infty}^{\langle d_{dr}^* \rangle} f_u(t) (\langle d_{dr}^* \rangle - u) du \\ + \langle p \rangle \int_{-\infty}^0 f_u(t) du - \langle e_{pot}(t) \rangle \int_{-\infty}^0 f_u(t) du \end{aligned} \quad [3.41]$$

where we assume zero travel time in the surface water. Note that e_{act} is equal to e_{pot} for negative values of u . Hence, e_{act} in Eq. [3.28] is replaced by e_{pot} . When we combine these two equations with a relation between $\langle u(t) \rangle$ and $\sigma_u(t)$ as given by Eq. [3.12], the model is

complete. The advantage of the presented probability distribution function approach is that all point-scale threshold values for which a flux generating process is (de)activated have been translated into gradual changes and smooth transitions between fluxes at the catchment-scale, without introducing many new parameters. Therefore this model is stable in backwards iterations and during automatic calibration.

In this model, changes in saturated storage drive all catchment fluxes. The saturated storage change is dictated by the relation between mean and standard deviation of a Normally distributed thickness of the unsaturated zone. However, this relation cannot be derived by measuring catchment discharge only. When we want to apply this model, we need to derive this relation separately. Fortunately, it is possible to measure the spatial distribution of groundwater depth (= thickness of unsaturated zone) by measuring many randomly located groundwater depths or to use a spatially distributed groundwater model to derive the spatial distribution of groundwater depths. The latter method is less accurate because errors in the groundwater model propagate to the water balance model.

Other models such as TOPMODEL (Beven and Kirkby, 1979), the soil routine in HBV (Lindström et al., 1997) and the PDM rainfall runoff model (Moore, 1985) also use spatial distributions. These models have chosen slope type, soil type or soil moisture storage, of which the distributions remain constant in time, as the primary source of spatial variation. Because we deal with lowland catchments, the spatial distribution of groundwater levels drives discharge generation. This spatial distribution of groundwater depth, however, is not a constant in time but a function of storage. We defined relations between the distribution parameters and the storage. This resulted in a much more dynamical model driven by continuously changing groundwater head gradients.

3.3 Materials and methods

3.3.1 Case study: The Hupsel Brook catchment

Catchment characteristics

The Hupsel Brook catchment is located in the eastern part of The Netherlands (Fig. 3.4). The size of the catchment is about 6.6 km², with the surface elevation ranging from 22 to 30 m above sea level. The soil texture class is mostly loamy sand with occasional layers of clay, peat and gravel of which the spatial extension is only marginally known (Wösten et al., 1985). A Miocene clay layer (20-30 m thick, starting at 0.5 to 20 m below the soil surface) forms an impermeable boundary for the unconfined water flow. The surface of this clay layer is carved by Pleistocene glacier erosion.

The entire catchment is densely drained with 68 km of ditches and many tube drains. The main brook is canalized (Fig. 3.4). A natural or reference situation is impossible to identify, because this catchment has been under continuous antropogenic change (canalization, re-meandering, land use change) for the last hundred years. The land use during the last ten years is mainly agricultural (maize and grass), with isolated farms and a few patches of forest.

The Hupsel brook catchment has a semi-humid sea climate with an annual precipitation of 500 to 1100 mm and an annual estimated evaporation of 300 to 600 mm, leaving an estimated sum of runoff and recharge of 200 to 800 mm·year⁻¹.

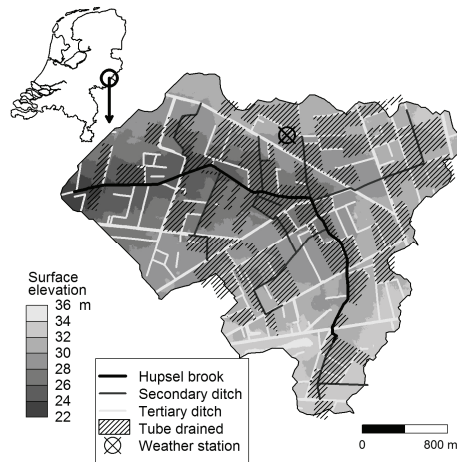


Figure 3.4. Hupsel Brook catchment with the main hydrologically relevant features.

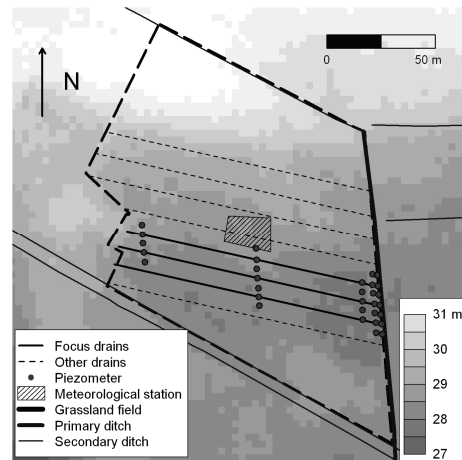


Figure 3.5 Field site with wells (piezometers) to measure groundwater levels.

Measured data

For the period 1994 through 2001 hourly weather data are available from a measurement station within the catchment operated by the KNMI (Royal Dutch Meteorological Institute) (Fig. 3.4). For the same period, discharges of the Hupsel brook were measured at the catchment outlet by the local waterboard with a 15 min. interval using a calibrated weir. Groundwater levels were also recorded every 20 min. in a monitoring well located at the meteorological station. For the period May 2007 through October 2008 weekly groundwater levels at 31 locations at a tube drained field site of 0.9 ha, located next to the meteorological station, were manually collected (Fig. 3.5). Within the catchment more than a 100 drilling logs were available to estimate the depth of the impermeable clay layer and the transmissivity. A Digital Elevation Model (DEM) was developed from radar data with a 5 m resolution. An estimate of the surface water levels in ditches and tributary brooks was obtained from this detailed DEM.

3.3.2 Groundwater model

The catchment water balance model requires the distribution of u , which obviously depends on the phreatic surface and the topography within the catchment. Since the former is not well-known and certainly not available with a high temporal resolution we resorted to modeling the phreatic aquifer of the Hupsel Brook catchment. We used a spatially distributed groundwater model with a 5 m resolution to test two major assumptions in the Theory section:

- The Normality of the distribution of the thickness of the unsaturated zone within the catchment
- The validity of Eq. [3.12] to describe the relation between the standard deviation of the thickness of the unsaturated zone at any given time and the average thickness of the unsaturated zone at that time.

The goal of this groundwater model, therefore, is not to represent the Hupsel Brook discharges and groundwater heads as accurately as possible, but to capture the most important flow processes like the wetting and drying of ditches and streams, tube drain drainage, and the effect of spatially distributed evapotranspiration so that we can establish the relation between the standard deviation of the thickness of the unsaturated zone and the average thickness of the unsaturated zone for the catchment. We therefore refrained from a detailed calibration of the model, since this was not expected to significantly change the relationship sought.

The groundwater model Modflow (McDonald and Harbaugh, 1988) was used to calculate the Darcian groundwater flow with daily time steps for the period of 1994 through 2001. The model consisted of one unconfined layer of 740 by 800 cells. Transmissivity values were corrected for incisions of the brook and ditches and for the groundwater head, only taking into account the thickness of the wet cross-section (an unconfined simulation). Surface water levels were fixed to their annual average, with no flow of water from surface water to the soil allowed. Potential evapotranspiration was determined using the Makkink relation (Makkink, 1957) with temperature and global radiation measurements of the Hupsel meteorological station. To determine the actual transpiration for each cell, a relation with u was adopted. For $0 < u \leq 0.7$ m, $e_{act} = e_{pot}$. For $0.7 < u < 1.5$ m, $e_{act} = e_{pot} \cdot (1.5 - u) / 0.8$. For $u \geq 1.5$ m, $e_{act} = 0$. The effect of the unsaturated zone is modeled with an effective storage expressing the water layer needed for one meter of groundwater level rise. The value depends on soil type and the average local u , and varies between 0.08 for wet clayey soils and 0.26 for dry sandy soils. Because the main goal of this groundwater model was to mimic and not to exactly reproduce the natural groundwater flow these value were indicative and were not experimentally based.

3.3.3 Calibration and validation of the storage and flux model

The model developed in the Theory section (Eqs. [3.12], [3.40] and [3.41]) was calibrated on hourly measured catchment discharges for the period of Jan 1, 1994 to Jan 1, 1996, hourly measured groundwater depths at the meteorological station for the same period and an estimated yearly 59% contribution of tube drains to the total catchment discharge (estimation originates from Van der Velde et al., 2009). We selected an hourly time step because the time to peak of the catchment discharge after rainfall typically is a few hours. We adopted the fitted parameter values for Eq. [3.12] that relate σ_u to $\langle u(t) \rangle$ from the groundwater model results and added 5 cm to σ_{min} and σ_{max} to account for additional soil surface elevation variation within 5 x 5m model cells (this is an intuitive value and has not been validated by measurements). Table 3.1 shows which model parameters were kept

constant during calibration at their estimated value and which parameters were calibrated. Validation of the model was performed on similar data for the period 1996 through 2001. Within this period we have chosen the periods Feb. 1997 through Feb. 2000 and April 2001 through Dec. 2001 (32570 hours) for the validation, because the quality of the catchment discharge data was good for these periods. Note that, for calibration and validation purposes, we had groundwater levels available for only a single location during this period. We considered those observations suitable, since the monitoring well was in the middle of a tube drained pasture field, approximately 100 m away from the nearest ditch. Therefore, we were confident that the values of u observed there were within the 20 percent (U_{20}) and 80 percent quantile (U_{80}) of all u within the catchment at all times. Including measured groundwater heads in the calibration (even at a single point) reduces the problem of model equifinality. The parameter estimation code PEST (Doherty, 2002) was used to optimize the model parameters for the objective function:

$$Obj = EQ_{tot} + EMq_{str} + EMQ_{tot} + EH \quad [3.42]$$

$$EQ_{tot} = \sum_{t=T_{start}}^{T_{end}} \left[1.0 \cdot (Q_{meas}(t) - \langle l_{surf}(t) \rangle \cdot A) \right]^2 \quad [3.43]$$

$$EMq_{dr} = \left\{ 2000 \cdot \left[0.59 - \sum_{t=T_{start}}^{T_{end}} \langle q_{dr}(t) \rangle \cdot \left(\sum_{t=T_{start}}^{T_{end}} \langle l_{surf}(t) \rangle \right)^{-1} \right] \right\}^2 \quad [3.44]$$

$$EMQ_{tot} = \left(2.0 \cdot \left[\sum_{t=T_{start}}^{T_{end}} \langle l_{surf}(t) \rangle \cdot A - \sum_{t=T_{start}}^{T_{end}} Q_{meas}(t) \right] \right)^2 \quad [3.45]$$

$$EH = \sum_{t=T_{start}}^{T_{end}} (5.0 \cdot EU(t))^2 \quad [3.46]$$

$$\text{with } EU(t) = u_{meas}(t) - U_{80}(t) \quad \text{if } u_{meas}(t) > U_{80}(t)$$

$$EU(t) = U_{20}(t) - u_{meas}(t) \quad \text{if } u_{meas}(t) < U_{20}(t)$$

$$EU(t) = 0 \quad \text{if } U_{20}(t) < u_{meas}(t) < U_{80}(t)$$

$Q_{meas}(t)$ is the measured discharge and $\langle l_{surf}(t) \rangle \cdot A$ is the modeled discharge at time step t . Variable EQ_{tot} represents the error between measured and modeled fluxes, and EMQ_{tot} accounts for the error in the cumulative mass flux during the simulation period between measured and modeled fluxes. The variable, EMq_{dr} , accounts for the deviation in tube drainage contribution to the total discharge from the estimated 59%, and EH assures that the optimal parameter set gives a solution for which the measured groundwater head lies within the 20th to 80th percentile of the modeled distribution of groundwater depths. The

weighting factors, 1.0, 2000, 2.0 and 5.0, for the respective components of the objective function were determined iteratively by running several optimization runs. These values ensure that each of the errors, Eq. [3.43], Eq. [3.44], Eq. [3.45] and Eq. [3.46], contributed in the same order of magnitude to the final objective function, Eq. [3.42]. Evaluation of the objective function starts at time T_{start} [T] (40 days), allowing for uncertainty in the starting value of $\langle u(0) \rangle$, and runs until the time, T_{end} [T].

3.4 Results and discussion

3.4.1 Groundwater modeling

Figures 3.6 and 3.7 show the results of the distributed groundwater model for simulating measured discharges and groundwater heads. High groundwater heads and low discharges are overestimated and high discharges are underestimated. A sensitivity analysis showed that the phreatic storage coefficient was the most sensitive parameter to improve high flow or low flow model results. However, because we used a single coefficient for both flow conditions no significant improvements could be made. This also underlines the importance of the unsaturated-saturated zone interaction as implemented in our model in the Theory section.

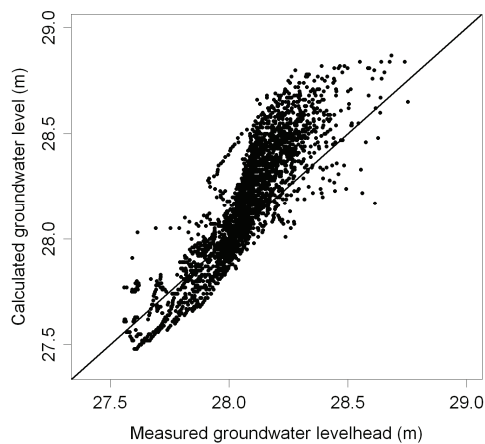


Figure 3.6. Observed daily groundwater levels at the weather station against Modflow calculations for the same location (2922 days).

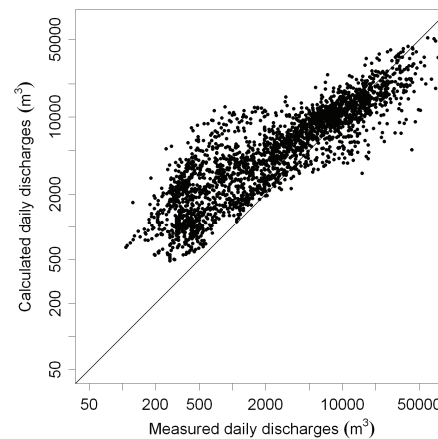


Figure 3.7. Observed daily totals of catchment discharge against daily Modflow calculations (2922 days).

For each time step, u was calculated from the Modflow results at all discretisation nodes. From this, the extent of water-filled drains, ditches and soil surface could also be found, thus allowing us to establish the extent of the active drainage network with time. Figure 3.8 illustrates the analysis for a dry and a wet day. The discharge was peaked, reflecting the efficiency of the drainage system during wet periods. The total spatial extent of the active drainage network differed dramatically between the dry and the wet situation. The

necessity of the variable contributing area concept for groundwater flow to surface water is evident. The average u is much smaller during the wet period, as expected. For both events, the Normal distribution provides a good fit of the spatial distribution of u except for the hump around $u = 0$. For the dry period this hump is caused by a few very deep incisions of ditches. Because there are only few deep incisions in the catchment the central limit theorem is not valid to describe their effect on u . During the wet period this hump is caused because the groundwater model removes all water above the average soil surface elevation in a grid cell not taking into account the possibility of ponding.

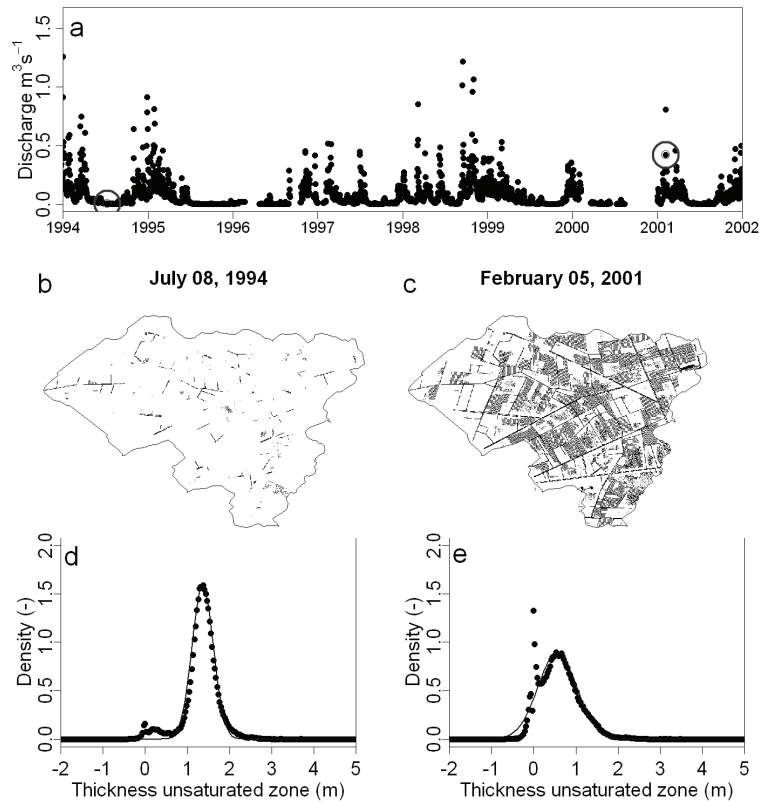


Figure 3.8 a) Measured daily discharge, with a wet and a dry day highlighted. The active (water draining) portion of the drainage network for the indicated dates is shown in b and c. Figures d and e give the corresponding simulated distributions over the catchment of the thickness of the unsaturated zone (dots), and the fitted normal distribution (solid line).

The points in Fig. 3.9 represent the relation between the standard deviation, σ_u , and the average calculated thickness of the unsaturated zone, $\langle u \rangle$, for the fitted Normal distributions for every simulated time step. Figure 3.9 corroborates the relationship between $\langle u \rangle$ and σ_u hypothesized in the Theory section. Only one part (the string of outliers for $0.9 < \langle u \rangle <$

1.5m) did not match the general trend. Figure 3.9 also shows that Eq. [3.12] fits the data generated with the groundwater model well.

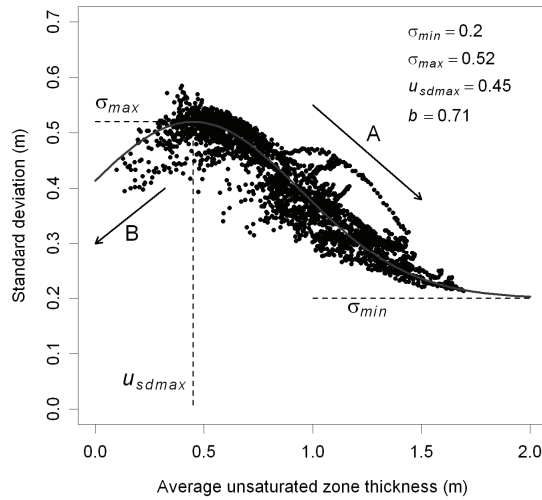


Figure 3.9. Relation between daily values of the average thickness of the unsaturated zone, $\langle u(t) \rangle$, and the standard deviation σ_u of the spatial distribution of u , derived from the results of the groundwater model. The line represents a fit of Eq. 12. Arrow A shows the decline in variation when the catchment becomes drier (larger value of $\langle u(t) \rangle$). Arrow B shows the decline in variation when the catchment becomes wet.

3.4.2 Field site results

Figure 3.10 shows the depth of the groundwater levels relative to the local surface elevation observed in the 31 monitoring wells installed in the 0.9 ha field. This graph quantitatively confirms that the spatial variation is large during wet periods and small during dry periods. The measured groundwater levels are spatially interpolated to obtain a groundwater table for the entire field site. Figure 3.11 shows the relation between $\langle u(t) \rangle$ and σ_u within this field, together with a fit of Eq. [3.12]. Within the range of groundwater depths measured at the field site Eq. [3.12] gave a good fit.

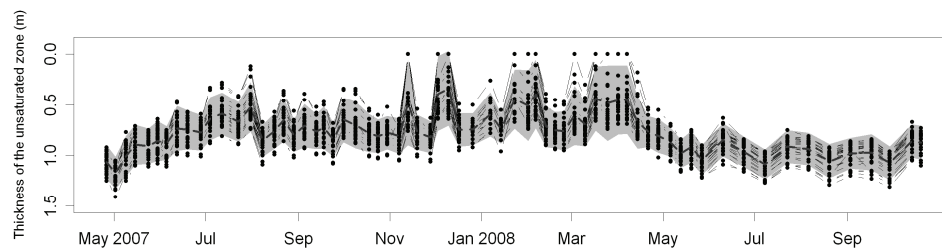


Figure 3.10. Depth of groundwater levels relative to the local surface elevation (thickness of the unsaturated zone) for 31 wells at the field site within the Hupsel catchment (Fig. 3.4). The dashed line shows the field average thickness of the unsaturated zone. The gray area represents the ranges between the 0.05 and 0.95 quantiles of a normal distribution around the mean.

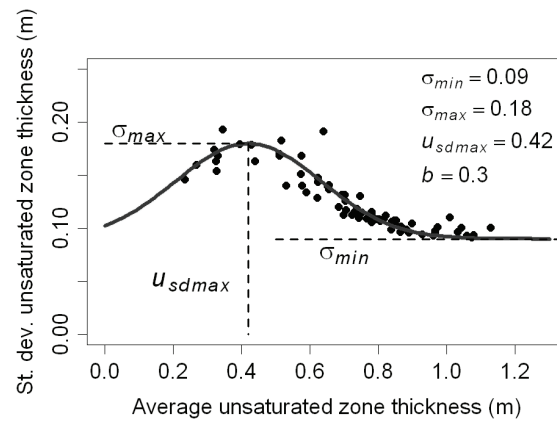


Figure 3.11. Relation between measured average and standard deviation of thickness of the unsaturated zone. The line is a fit of Eq. [3.12].

Table 3.1. Calibration ranges and calibrated values for the model parameters (symbols explained in the main text).

Parameter	Min value	Max value	Calibrated value	Constant
α	0.0 m ⁻¹	20.0 m ⁻¹	0.88 m ⁻¹	-
N	0.0	20.0	4.17	-
$\langle \theta_s \rangle$	0.22	0.55	0.45	-
$\langle r_{grv} \rangle$	0.01 d	100 d	0.49 d	-
$\langle r_{dr}^* \rangle$	0.1 d	1000 d	35 d	-
$\langle u_{et} \rangle$	0.1 m	2 m	1.57 m	-
$\langle m \rangle$	0.0	1.0	0.47	-
$\langle g^* \rangle$	-	-	-	0.6
σ_{max}	-	-	-	0.57 m
σ_{min}	-	-	-	0.25 m
B	-	-	-	0.71 m
u_{sdmax}	$\langle u \rangle$ with max variance	-	-	0.45 m
$\langle d_{dr}^* \rangle$	-	-	-	0.80 m
A	-	-	-	6.64 km ²
$\frac{A_{nd,wet}}{A}$	-	-	-	0.008

3.4.3. Calibration results

Table 3.1 gives the fifteen parameters of the model. During the automatic calibration the eight parameters in the last column were kept constant, while the remaining parameters were allowed to vary between the maximum and minimum values of Table 3.1. We found significant non-uniqueness of the optimal dataset, which originates from the large correlation between storage and fluxes. Therefore, storage and fluxes should be determined separately (storage should not be derived from fluxes or fluxes from storages) by independently determining the parameters of Eq. [3.12] (that relate $\langle u(t) \rangle$ to σ_u), the parameters describing the unsaturated zone storage (Eq. [3.22]), and the surface storage $\langle s_{surf}(t) \rangle$. Since measurements of $u(x,y,t)$ are only available at the field site, we added prior information to the PEST optimization to ensure that the optimal solution has:

- Values for $\langle \theta_s \rangle$, α and n close to the ranges for Dutch sandy soils reported by Wösten et al. (2001).
- An estimated average value for $\langle s_{surf}(t) \rangle$ between 0.1 and 1 mm.

We visualized the model by means of eight characteristic curves: one representing σ_u as function of $\langle u \rangle$ (Eq. [3.12]), three curves representing saturated, unsaturated and surface storage as a function of $\langle u \rangle$ (Eq. [3.16], Eq. [3.22] and Eq. [3.24]), and four curves giving the fluxes as a function of $\langle u \rangle$. Figure 3.12 presents all eight curves. Figure 3.12b shows the relations between storage and $\langle u \rangle$. The solid line represents the total pore space in the unsaturated zone, denoted by $\langle s_{sat,max} \rangle - \langle s_{sat} \rangle$, with $\langle s_{sat,max} \rangle$ the total soil pore space. The difference between the curves for $\langle s_{sat,max} \rangle - \langle s_{sat} \rangle$ and $\langle s_{unsat} \rangle$ gives the catchment average air-filled pore space. Figure 3.12c shows the delicate balance between tube drain discharge $\langle q_{dr} \rangle$ and discharge by streams, ditches, and overland flow $\langle q_{grw} \rangle$ given by Eqs. [3.31] and [3.38]: for $\langle u \rangle < 0.9$ m $\langle q_{grw} \rangle$ is larger than $\langle q_{dr} \rangle$, for $\langle u \rangle > 0.9$ m $\langle q_{dr} \rangle$ is larger than $\langle q_{grw} \rangle$. Figure 3.12d gives the fraction of precipitation that reaches and the fraction of potential evaporation that stems from the unsaturated zone. For small $\langle u \rangle$, relatively large areas have surface storage (i.e. no unsaturated zone, see also $\langle s_{surf} \rangle$ as a function of $\langle u \rangle$ in Fig. 3.12b). On locations with surface storage, precipitation is converted to discharge and evapotranspiration is subtracted from discharge (appears in the last term of Eq. [3.41]). For large $\langle u \rangle$ evapotranspiration is reduced (Eq. [3.40]). Both effects create the shape of the curves of Fig. 3.12d.

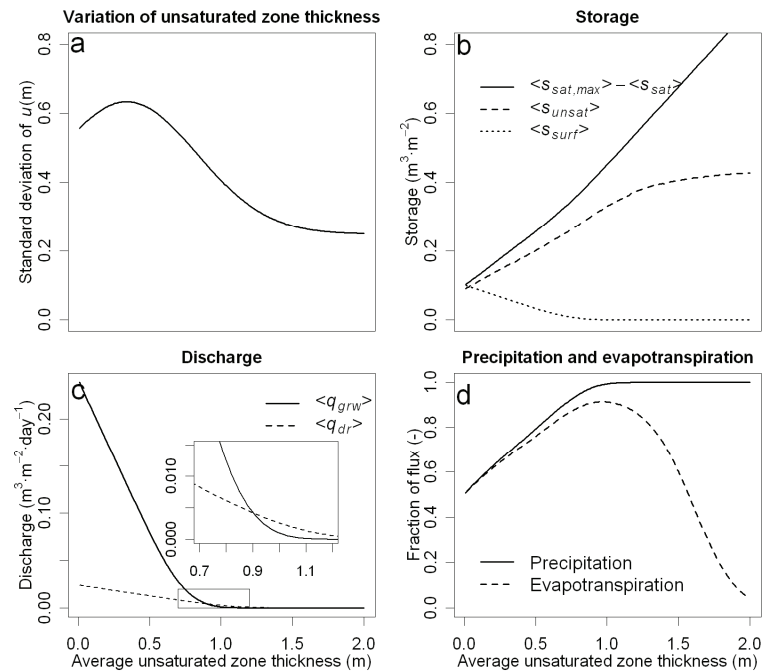


Figure 3.12. Characteristic curves for the catchment scale: variation of the unsaturated zone thickness (a); unsaturated zone pore space $\langle s_{sat,max} \rangle - \langle s_{sat} \rangle$, unsaturated zone storage and surface storage (b); stream, ditch and overland flow discharge ($\langle q_{grw} \rangle$), and tube drain discharge (c); and the fraction of precipitation that reaches and evapotranspiration that stems from the unsaturated zone (d). Reduction of precipitation that reaches the unsaturated zone occurs because part of the rain falls on locations with surface storage. Reduction of evapotranspiration is partly caused by surface storage (small $\langle u(t) \rangle$) and partly by and deep groundwater tables (large $\langle u(t) \rangle$).

Most of the discharge peaks were slightly underestimated, except for the discharge peak just after the summer dry period of 1994 which was simulated too high (Fig. 3.13). This resulted in an underestimation of the mean discharge by 3% (Table 3.2). Overall the hourly discharge was reproduced well ($R^2 = 0.88$; Nash-Sutcliffe (NS) coefficient = 0.87 (Nash and Sutcliffe, 1970)). In contrast the root mean squared error (RMSE) was high compared to the average discharge. However the RMSE was dominated by errors during peak flow events between 0.1 and 1.5 $m^3 s^{-1}$, i.e. up to an order of magnitude larger than the average flux.

The model performed not so well for discharge events during dry conditions (the smaller discharge events around July, 1994 and July, 1995 in Fig. 3.13). We attribute this to the fact that under dry conditions only a small portion of the catchment generates discharge. Consequently, the number of fields involved in the discharge-generating process is too limited for the central limit theorem to apply. The assumption of a Normal distribution of u therefore becomes untenable. Figure 3.8d shows the distribution of u during a dry period.

Overall, the normality of the PDF is convincing, but the generation of discharge in this situation is dominated by the few fields close to the sparsely distributed active drainage channels (including tube drains, Fig. 3.8b). These locations are represented by the small hump for $u \approx 0$ of the distribution of u . This hump is not described by the overall Normal distribution.

Table 3.2. Calibration and validation results of the catchment model. *RMSE* is the Root Mean Squared Error. *NS* is the Nash-Sutcliffe coefficient (Nash and Sutcliffe, 1970). R^2 is the squared Pearson correlation coefficient.

	Calibration	Validation
Percentage tube drainage	52%	57%
Percentage drainage by streams and ditches	46%	41%
Percentage direct rainfall	1.5%	1.4%
Observed mean discharge ($\overline{Q_{meas}}$)	0.074 m ³ s ⁻¹	0.075 m ³ s ⁻¹
Calculated mean discharge ($\langle I_{surf} \rangle$)	0.072 m ³ s ⁻¹	0.079 m ³ s ⁻¹
Number of hours with measurements (grw + disch)	16560	32570
$RMSE = \sqrt{\frac{\sum (Q_{tot}(t) - Q_{meas}(t))^2}{N}}$ With N the number of measurements	0.042 m ³ s ⁻¹	0.053 m ³ s ⁻¹
$R^2 = \left[\frac{\sum (Q_{tot}(t) - \overline{Q_{tot}})(Q_{meas}(t) - \overline{Q_{meas}})}{\sqrt{\sum (Q_{tot}(t) - \overline{Q_{tot}})^2 \sum (Q_{meas}(t) - \overline{Q_{meas}})^2}} \right]^2$	0.88	0.85
$NS = 1 - \frac{\sum (Q_{tot}(t) - Q_{meas}(t))^2}{(\overline{Q_{meas}} - \overline{Q_{meas}})^2}$	0.87	0.78

The groundwater levels measured at a single point at the field site were assumed to be within the 20% and the 80% quantile envelope of the spatial distribution of u , during calibration. This is visualized by Fig. 3.14. The measured data points lay within the dark gray area (the 20% to 80% quantile), but it is clear that the measured groundwater depths were smaller than the modeled average groundwater depth, $\langle u \rangle$. The measured location should therefore be relatively wet. The fact that the measurement field is tube-drained is consistent with this.

The total contribution of tube drains was somewhat lower than the 59% estimated by Van der Velde et al. (2010a). This estimation, however, was based on the winter 2007-2008. Rainfall differences between years are likely to cause differences in the tube drain contribution. The sharp drops in tube drain contribution to total discharge in Fig. 3.13b during low discharge periods indicate a shift from tube drain discharge dominated to groundwater discharge dominated surface water. Only with surface water concentration measurements and a clear contrast between concentrations of tube drain flux and

groundwater flux it is possible to calibrate $\frac{A_{nd,wet}}{A}$ and to align these shifts with measured shifts in surface water concentrations.

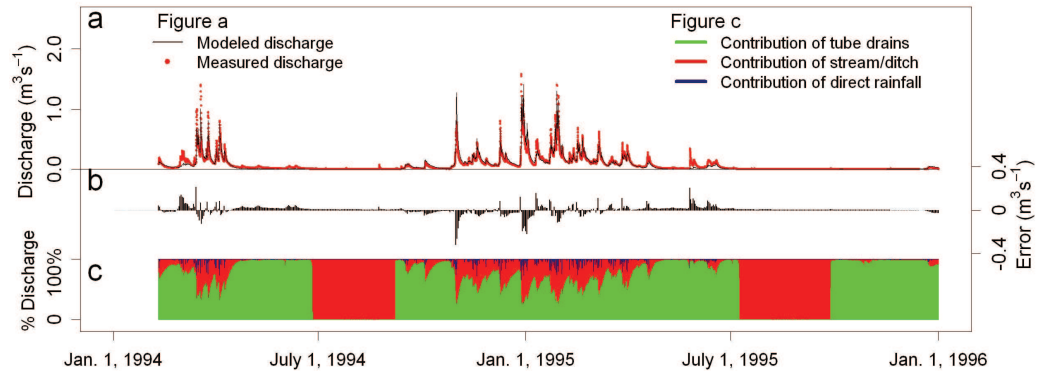


Figure 3.13. Figure a shows modeled discharge and measured discharge for the calibration period. Figure b shows the daily average error between measured and modeled discharge (measured – modeled) and figure c shows the modeled discharge subdivided into the contribution of tube drains, the contribution of stream, ditches, and land surface, and the contribution of direct rainfall in increasingly dark tones.

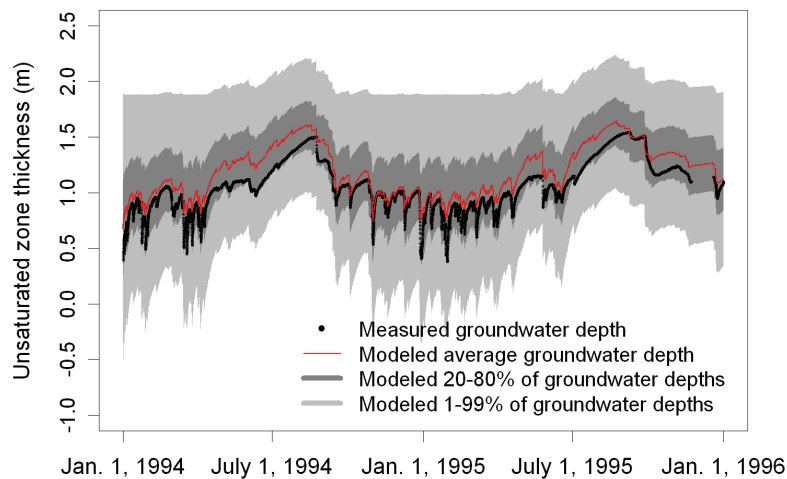


Figure 3.14. The modeled spatial distribution of unsaturated zone thicknesses. The black dots are the measured groundwater depths at the meteorological station. Whenever the light gray area is below zero, more than 1% of the catchment soil surface contributes actively to discharge. Whenever the dark gray area is below 0.8 m, more than 20% of the catchment area has a groundwater level above the tube drainage level. Of this area a fraction of 0.6 (i.e. $\langle g^* \rangle$) is tube drained and generates tube drain discharge.

3.4.4 Validation results

Table 3.2 shows that the average measured and calculated discharge for the validation period were close to those of the calibration period. The *RMSE*, however, increases to 53 L s^{-1} but also the extreme discharges during the validation period are much higher than during the calibration period. The R^2 and the *NS* coefficients of the validation decrease slightly to 0.85 and 0.78, respectively. The model performed well for the validation period, even for the high flows that were a factor two higher than the high flows of the calibration period (Fig. 3.15).

The model regularly overestimated discharge during autumn after a dry summer period (October, November and December 1994, 1997, 1999 and 2001) and underestimated discharge during spring after a wet winter (March through June 1994, 1995, 1997, 1999 and 2001). Possible sources of these errors are:

- A slightly different relation between $\langle u(t) \rangle$ and $\sigma_u(t)$ when the groundwater table evolves from relatively parallel to the soil surface (low $\sigma_u(t)$ during summer) to a groundwater table with many large curvatures (high $\sigma_u(t)$) between draining elements during autumn and winter than vice versa (from winter and spring to summer).
- The equilibrium assumption for the unsaturated zone storage overestimates unsaturated storage during evapotranspiration periods and underestimates unsaturated zone storage during infiltration periods. This reduces the precipitation amplifying nature of the unsaturated zone.
- Vegetation growth inside ditches and streams during summer and early autumn increases surface storage. After ditch cleaning in late autumn water is discharged more effectively with consequently higher peak discharges.
- Systematic measurement and up-scaling errors in precipitation and evapotranspiration also contribute to the calculated errors in discharge.

Figure 3.16 shows distinct underestimations of the low flows as was already observed during calibration. Another difficulty with low flows is that they are far less accurate to measure because of the large dimensions of the weir and the abundant vegetation growth in and around the weir during summer. Particularly the latter leads to measurement errors that overestimate the true discharge, which would exaggerate the deviation from the 1:1 line in Fig. 3.16.

Infiltration excess overland flow is not incorporated in the model. Therefore, high discharge events due to high rainfall intensities, which occur mainly in summer, cannot be simulated accurately with the current model. This is shown in Fig. 3.16, where six discharge events that were measured were not simulated (the horizontal strands of data points under the 1:1 line). The modeled values of $\langle u \rangle$ deviated from the single-location values of u at the field site during the validation period (Fig. 3.17). Still, the deviations were nearly all contained within the envelope defined by U_{20} and U_{80} .

3.5 Conclusions

In lowland catchments without significant hillslopes, the depth to groundwater (thickness of the unsaturated zone) governs the various storage and flux terms in the water balance. We developed a model in which catchment-scale terms of the water balance are all expressed in terms of the PDF of the unsaturated zone thickness. By assuming this PDF to be Normal, a considerable reduction in the model complexity could be achieved. We demonstrated the ability of this parsimonious and uncomplicated model in a full calibration-validation cycle. While the potential of this novel approach to catchment modeling has been demonstrated, it is still unclear over which range of spatial scales the distribution of the unsaturated zone thickness remains Normal; small areas in particular are likely to have deviating distributions. Furthermore, the relation between the shape of the distribution and properties of the drainage network and the transmissivity of the phreatic aquifer are still poorly understood.

This model offers great opportunities to improve our understanding of the interactions between groundwater and surface water. The model integrates subsurface and surface processes giving catchment-scale information about the interaction between groundwater and surface water, between groundwater and evapotranspiration, and the importance of the unsaturated zone and surface ponding during high-discharge events.

The model relies heavily on the relation between the average thickness of the unsaturated zone and its standard deviation. This relation cannot be derived from discharge data only, and needs to be derived from other data sources such as groundwater head measurements or a spatially distributed groundwater model to prevent large equifinality problems common to models of groundwater-surface water interactions (Beven, 2001). At the moment, measuring the average and standard deviation of the unsaturated zone thickness appears to be quite feasible in many catchments, possibly helped by remote sensing to quantify wet and dry fractions of a catchment. A well chosen nested-scales setup of discharge and groundwater head measurements could reduce the number of measurement needed. Monitoring programs in catchments aimed at determining the interactions between the groundwater and the surface water (which is relevant if the quality of the discharged water is of interest) should therefore be designed for quantifying the distribution of groundwater depths throughout the catchment in time.

Reggiani *et al.* (1998) formulated a unifying framework for watershed thermodynamics, with conservation equations for mass, momentum, energy, and entropy, but leaving hydrologists struggling with the search for appropriate expressions for the interfaces between the different reservoirs (saturated zone, unsaturated zone, surface water) for their specific problems. In this paper we developed expressions for the interfaces between saturated zone, unsaturated zone, and surface water for typical lowland catchments based on the Normality assumption of the thickness of the unsaturated zone.

So far, the model has only been applied to one catchment and applications to new catchments will have to reveal the general applicability of the model concepts. The model

results can be further improved by adding measurements of concentrations of selected compounds in various locations in the surface water, the soil, and the groundwater. Equally helpful are measurements that help quantify the contributions of individual flow routes, possibly leading to a water balance model that can accurately estimate the average travel time within the various reservoirs comprising the catchment.

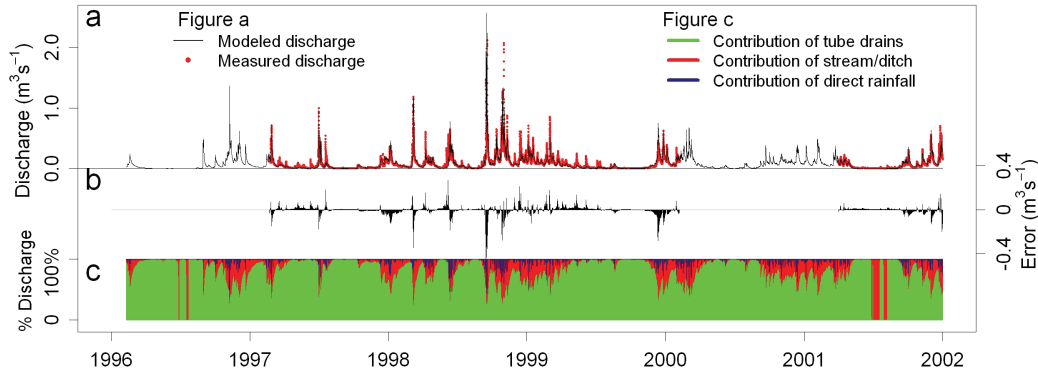


Figure 3.15. Figure a. shows modeled and measured discharges for the validation period. Only for the periods Feb. 1997 – Feb. 2000 and April 2001 – Dec. 2001 we had good quality discharge data. Figure b shows the daily average model error (measured – modeled discharge). Figure c shows the contribution of individual flow routes to the total discharge.

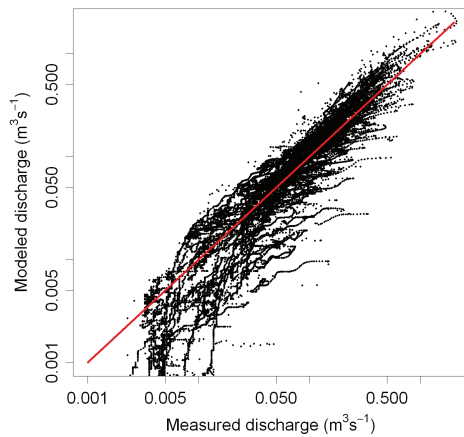


Figure 3.16 Modeled versus measured hourly discharges for the validation period. The horizontally oriented strands of data points are observed high-discharge events which were not modeled.

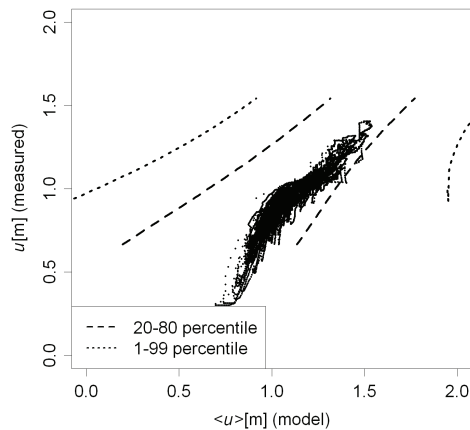


Figure 3.17 Modeled versus measured hourly groundwater heads for the validation period in the monitoring well at the meteorological station.

Nested-scale discharge and groundwater level monitoring to improve predictions of flow route discharges and nitrate loads

Abstract

Identifying effective measures to reduce nutrient loads of headwaters in lowland catchments requires a thorough understanding of flow routes of water and nutrients. In this paper we assess the value of nested-scale discharge and groundwater level measurements for predictions of catchment-scale discharge and nitrate loads. In order to relate field-site measurements to the catchment scale, an upscaling approach is introduced that assumes that scale differences in flow route fluxes originate from differences in the relationship between groundwater storage and the shape of the groundwater table. This relationship is characterized by the Groundwater Depth Distribution (GDD) curve. The GDD-curve was measured for a single field site (0.009 km²) and simple process descriptions were applied to relate the shape of the groundwater table to the flow route discharges. This parsimonious model could accurately describe observed storage, tube drain discharge, overland flow, and groundwater flow simultaneously with Nash-Sutcliffe coefficients exceeding 0.8. A probabilistic Monte Carlo approach was applied to upscale field-site measurements to catchment scales by inferring scale-specific GDD-curves from hydrographs of two nested-scale catchments (0.4 and 6.5 km²). The estimated contribution of tube drain effluent (a dominant source for nitrates) decreased with increasing scale from 76-79% at the field site to 34-61% and 25-50% for both nested catchment scales. These results were validated by demonstrating that a model conditioned on nested-scale measurements simulates better nitrate loads and gives better predictions of extreme discharges during validation periods compared to a model that was conditioned on catchment discharge only.

This chapter is adapted from: Van der Velde, Y., J.C. Rozemeijer, G.H. de Rooij, F.C. van Geer, P.J.J.F. Torfs, and P.G.B. de Louw (Submitted). Nested-scale discharge and groundwater level monitoring to improve predictions of flow route discharges and nitrate loads. Hydrol. Earth Syst. Sci.

4.1 Notation

4.1.1 Abbreviations

LGSI-model	Lowland Groundwater-Surface water Interaction model developed by Van der Velde et al. (2009).
GDD-curve	Groundwater Depth Distribution curve. Curve that relates the spatial standard deviation of the groundwater depth to its spatial average.
Ponding-curve	The relation between spatially averaged groundwater depth and the volume of ponds and surface waters.
BPS	Ensemble of 500 Behavioral Parameter Sets
BPS-FS, BPS-C, BPS-N:	BPS for each of the three models: field-site, catchment and nested-scales model respectively.

4.1.2 Symbols

A_{dr} [L^2]	Area within the catchment that is drained by subsurface tubes
A_s [L^2]	Area within the catchment covered with surface water
A_{tot} [L^2]	Catchment area
a_{dr} [-]	Rate with which r_{dr} increases during wet periods
b_{dr} [T^{-1}]	Fractional rate with which r_{dr} decreases during dry periods
c_{dr} [L^3T^{-1}]	Threshold tube drain discharge: below this discharge r_{dr} decreases, above this discharge r_{dr} increases
CDE [-]	Cumulative discharge error, difference between cumulative measured and modeled discharge
CE [-]	Curve error, difference between measured data and the modeled GDD-curve or ponding-curve
D_{dr} [L]	Tube drain depth
e_{pot} [$L T^{-1}$]	Potential evapotranspiration
ET_{act} [LT^{-1}]	Actual evapotranspiration
E_Q [LT^{-1}]	Evaporation from ponded surface and surface waters
fu [L^{-1}]	Normal distribution function of groundwater depths
Fu [-]	Cumulative distribution function of groundwater depths
$Fu-1$ [-]	Inverse cumulative distribution function of groundwater depths
GE [L]	Average groundwater depth error between measured and modeled groundwater time series.
h [L]	Height above the groundwater table
L_f [LT^{-1}]	The constant lateral inflow of groundwater at the field site
m [-]	Fraction of groundwater levels above the soil surface that remain on the soil surface to constitute surface storage.
NS [-]	Nash-Sutcliffe (Nash and Sutcliffe, 1970) coefficient for time series.
P [LT^{-1}]	Rainfall
P_Q [LT^{-1}]	Rainfall on ponded surface or surface waters

Q [LT^{-1}]	Discharge at catchment outlet
Q_{grw} [LT^{-1}]	Groundwater flow for sub-catchment and entire catchment
$Q_{grw,field}$ [LT^{-1}]	Groundwater flow towards ditch at field site
Q_{ov} [LT^{-1}]	Overland flow
Q_{res} [LT^{-1}]	Discharge as measured by the in-stream reservoirs
r_{ditch} [T]	Resistance of the field site to groundwater flow towards the ditch.
r_{dr} [T]	Tube drain resistance
r_{ex} [T]	Groundwater exfiltration resistance
S_{sat} [L]	Storage in saturated zone normalized by area
S_{surf} [L]	Storage in ponds and surface water normalized by area
S_{unsat} [L]	Storage in unsaturated zone normalized by area
u [L]	Groundwater depth
$\langle u \rangle$ [L]	Spatial average of the groundwater depth
u_{ditch} [L]	Depth of the field-site ditch relative to the mean surface elevation of the field site
u_{ET} [L]	Groundwater depth at which the actual evapotranspiration drops from e_{pot} to reduction depth
u_{smax} [L]	Average groundwater depth at which the standard deviation of the groundwater depths is at its maximum
α [L], n [-]	Van Genuchten (1980) parameters that describe the soil water retention curve
σ_{diff} [L]	Maximum increase in the standard deviation of the groundwater depth
σ_{min} [L]	Minimal groundwater depth standard deviation
σ_u [L]	Groundwater depth standard deviation corresponding to a certain $\langle u \rangle$
θ_s [-]	Average porosity between highest and lowest groundwater table [-]

4.2 Introduction

Intensive agriculture in lowland catchments often leads to high nitrate losses and eutrophication of downstream waters (Oenema, 2007; Van der Molen, 1998; Vitousek et al., 2009). To identify effective measures to reduce these nitrate loads, the flow routes of water that enter a stream and their nutrient concentrations need to be quantified (Tiemeyer et al., 2010). In densely drained lowland catchments, surface water discharge is fed by groundwater flow toward streams and ditches, tile drain effluent, and overland flow. Many field-scale studies identified tube drain effluent as the major source of nitrate (Tiemeyer et al., 2006; Nangia et al., 2010). However, the field scale at which these contributions can be directly measured (De Vos et al., 2000; Van der Velde et al., 2010a) often is not the scale of interest to water management authorities. Extrapolation of fields site results to entire catchments can easily lead to wrong conclusions as field sites can prove non-representative of the patterns and processes that emerge at larger scales (Sivapalan, 2003; Soulsby et al., 2006; Didszun and Uhlenbrook 2008). Therefore, our challenge is to effectively integrate

information from field-scale measurements into the prediction of catchment-scale flow route contributions.

In Van der Velde et al. (2010a), we presented the results of a field-scale measurement setup that separated tile drain flow from overland flow and groundwater flow. We also measured discharges at two larger nested scales and showed that, rather than the actual measured volumes at the field site, the characteristic response of individual flow routes can be used to upscale the field-site flow routes to the catchment scale. This elementary upscaling approach was purely based on measured data. A model framework was needed to upscale the measured field-scale fluxes to catchment-scale contributions of flow routes for periods without complete sets of measurements.

To develop such a model upscaling approach, Sivapalan (2003) advocated the search for concepts that “easily connect scales, and that can also be easily scaled”. This should lead to “a watershed-scale representation that is clearly tied to process descriptions at a lower level of scale, and which is not overly complex”. In sloped terrain, scaling research has focused on the way in which hillslopes connect to headwaters (Uchida et al., 2005, Jensco et al., 2009; Tetzlaff et al., 2008; Clark et al. (2009) and headwaters to entire basins (Shaman et al., 2004). Rodgers et al. (2005), Tetzlaff et al. (2007), and Didszun and Uhlenbrook (2008) studied the scaling behavior of both discharge and tracers across nested-scale catchments and found that scaling effects in discharge and solutes could largely be attributed to scale-related morphologic, topographic and land-use features. In contrast to sloped catchments, lowland catchments generally have little morphological heterogeneity and the main flow routes occur at all scales. Therefore, the scale effects in discharge of lowland catchments are primarily driven by scale-differences in drainage density of ditches and tube drains, micro-topography, and soil type.

In Van der Velde et al. (2009) we proposed an upscaling approach for hydrology in lowland catchments (from here on called the Lowland Groundwater-Surface water Interaction model, LGSI-model). We assumed there that each flow route (i.e., ditch and stream drainage, overland flow, and tube drain flow) starts to discharge if the groundwater level exceeds a flow route-specific threshold groundwater level at that location, and that the magnitude of the flux depends on the groundwater level. The contribution of a flow route to the total catchment discharge is calculated by integration over all groundwater levels in the catchment, described by a groundwater depth distribution. Van der Velde et al. (2009) showed that each storage volume of groundwater in the saturated zone corresponds to a unique groundwater depth distribution. They also showed that the relation between storage and groundwater depth distribution can be defined at any spatial scale and has the same basic shape at any scale and thus satisfies Sivapalan’s (2003) criterion: it “easily connects scales, and can also be easily scaled”.

However, in order to measure this relationship between storage and the groundwater depth distribution at catchment scales relevant to water management authorities, many groundwater depth time series are needed throughout the catchment. This makes this approach laborious and in our previous paper (Van der Velde et al., 2009) we had to resort

to spatially distributed transient groundwater modeling to derive this relationship. A workable alternative would be to have a dense network of groundwater monitoring wells on a small area within the catchment, and observe the groundwater levels frequently for a limited time period. Obviously some sort of upscaling is then needed to use this data to characterize the behavior of the entire catchment. We introduce here a nested-scale model setup combined with a probabilistic Monte Carlo approach to achieve this.

The objectives of this paper are twofold. Firstly, we test whether the LGSI-model can accurately describe all individual flow route fluxes at the field scale. This would increase our confidence in the ability of the LGSI-model to simulate flow route fluxes accurately at the catchment scale where these fluxes cannot be measured directly. Secondly, we want to assess the value of nested-scale monitoring as presented in Van der Velde et al. (2010a) for reducing uncertainty in predictions of catchment-scale flow route discharges.

4.3 Materials and methods

This paper combines the nested-scale measurements introduced by Van der Velde et al. (2010a) and the upscaling approach described in Van der Velde et al. (2009). Therefore, we offer a brief summary of the relevant information (sections 4.3.1, and 4.3.2), and refer to both papers for detailed background information. The LGSI- model is first applied to the field-site discharge and groundwater level measurements, which are described in section 4.3.3. Section 4.3.4 introduces a catchment model (C) conditioned on catchment discharge and a groundwater level time series and in section 4.3.5 the field-site model (FS) and the catchment model are combined into a nested-scales model (N). Section 4.3.6 introduces validation strategies for both the catchment model and the nested-scales model to assess the value of nested scale monitoring.

4.3.1 Nested experimental setup

The measurements for this study were performed in the Hupsel Brook catchment in the eastern part of The Netherlands (Fig. 4.1A; 52°06' N; 6°65' E). The size of the catchment is 6.5 km², with surface elevations ranging from 22 to 36 m above sea level. At depths ranging from 0.5 to 20 m an impermeable marine clay layer is found (Van Ommen et al., 1989). The unconfined aquifer consists of Pleistocene aeolian sands with occasional layers of clay, peat, and gravel (see Wösten et al. (1985) for more details).

The Hupsel Brook catchment is drained by a straightened and deepened main brook and by a dense artificial drainage network of ditches and tube drains. The spacing between the ditches averages 300 m (Fig. 4.1A) and approximately 50% of the area has tube drains (plastic perforated flexible tubes). The Hupsel Brook catchment has a semi-humid sea climate with a yearly precipitation of 500 to 1100 mm and a yearly estimated evaporation of 300 to 600 mm, resulting in an estimated recharge of 200 to 800 mm per year.

Within the Hupsel Brook catchment, discharge was measured at three nested spatial scales: (1) the entire catchment of approximately 6.5 km², (2) a sub-catchment of 0.4 km² and (3) a 0.009 km² field site located within the sub-catchment (Fig. 4.1B). From August 2007 through December 2008, discharge was measured every 15 minutes for both catchment

scales. Continuous surface water nitrate concentrations were measured at the outlet of the entire catchment with a Hydrion-10 multi-parameter probe (Hydrion BV Wageningen, the Netherlands). Monthly average nitrate concentrations of tube drain effluent were measured at 20 locations in the catchment with Sorbi-Samplers (Rozemeijer et al., 2010b).

The tube drained field site of 0.9 ha had a drain spacing of 14.5 m. Along a 43.5 m stretch inside the deep easterly ditch (Fig. 4.1C), we built in-stream reservoirs with separate vessels to capture tube drain discharge. The in-stream reservoirs collected overland flow and groundwater influx through the stream bed. Thus we separated the tube drain flow from the combined flux of overland flow and groundwater flow. The discharge of both flow routes was measured with 5 minute intervals for November 2007 through December 2008. During that period we also manually measured phreatic groundwater levels at 31 locations within the field-site every week. Pressure sensors in 15 piezometers along drain 1 (Fig. 4.1C) recorded phreatic levels every 10 minutes. A meteorological station of the KNMI (Royal Dutch Meteorological Institute) bordering the field-site measured hourly rainfall and potential evapotranspiration derived with the Makkink relation (Makkink, 1957).

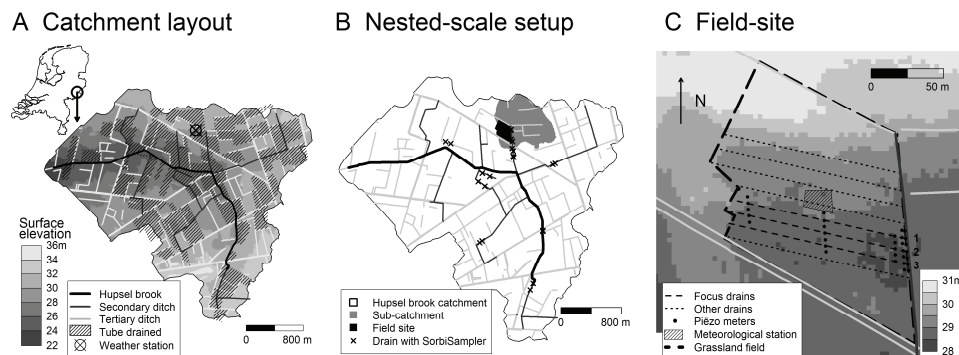


Figure 4.1 Hupsel Brook catchment and nested-scale measurement setup

4.3.2 Lowland Groundwater-surface water interaction (LGSI) model

4.3.2.1 Basic model equations

The LGSI-model (Van der Velde et al., 2009) essentially consists of point-scale expressions of flow route fluxes (tube drain flow, overland flow, groundwater flow, direct rainfall, and evapotranspiration) and storages (saturated storage, unsaturated storage, and surface storage). A point in the catchment starts to generate a flux for a certain flow route when its groundwater level exceeds a threshold specific to that flow route. The magnitude of this flux (except for evapotranspiration) is directly proportional to the difference between the groundwater level and the threshold level. Upscaling of fluxes and storages is achieved by integrating the point-scale expressions over all groundwater depths within a model area. This distribution of groundwater depths was found to approximate a normal

distribution with a mean and standard deviation that are a unique function of the total water storage. We formalized this function by the Groundwater Depth Distribution curve (GDD-curve) that describes the relationship between the spatial average groundwater depth and the spatial groundwater depth standard deviation.

Table 4.1. LGSI-Model basics and parameters. The process formulations are point-scale model equations. The catchment-scale equations are obtained by integration over the groundwater depth distribution within appropriate integration bounds (see Appendix 4A).

Process	Formulation	Process-specific parameters
Unsaturated zone storage (s_{unsat})	$s_{unsat} = \theta_s \int_0^u \left[1 + (\alpha h)^n \right]^{1-n} dh \text{ for } u > 0$ $s_{unsat} = 0 \text{ for } u < 0$	u : Groundwater depth [L] θ_s : Porosity [-] α, n : Van Genuchten parameters [L], [-] h : Height above water table [L]
Saturated zone storage (s_{surf})	$s_{surf} = -m \cdot u \text{ for } u < 0$ $s_{surf} = 0 \text{ for } u > 0$	m : Fraction of ponding [-]
Evapo-transpiration (e_{act})	$e_{act} = e_{pot} \text{ for } u < u_{ET}$ $e_{act} = 0 \text{ for } u > u_{ET}$	e_{pot} : Potential evapotranpiration [$L \cdot T^{-1}$] u_{ET} : Evapotranpiration reduction depth [L]
Overland (q_{ov}), Groundwater flow (q_{grw})	$q_{grw,ov} = \frac{(m-1) \cdot u}{r_{ex}} \text{ for } u < 0$ $q_{grw,ov} = 0 \text{ for } u > 0$	r_{ex} : Exfiltration resistance [T]
Tube drain flow (q_{dr})	$q_{dr} = \frac{D_{dr} - u}{r_{dr}} \text{ for } u < D_{dr}$ $q_{dr} = 0 \text{ for } u > D_{dr}$	D_{dr} : Tube drain depth [L] r_{dr} : Tube drain resistance [T]
Scale	Formulation	Scale-specific parameters
GDD-curve	$\sigma_u = \sigma_{diff} \cdot e^{-\left(\frac{\langle u \rangle - u_{s,max}}{b}\right)^2} + \sigma_{min}$	σ_u : Spatial groundwater depth st. dev. [L] $\langle u \rangle$: Spatial average grw. depth [L] σ_{min} : Minimal grw. depth st. dev. [L] σ_{diff} : Maximum increase in grw. depth st. dev. [L] $u_{s,max}$: Average grw. depth with maximum grw. depth st. dev. [L]
Surfaces	-	A_{tot} : Catchment area [L^2] A_{drain} : Area with tube drainage [-] A_s : Area with surface water [-]

The model parameters can be subdivided into process-specific parameters that describe fluxes and storages as a function of the local groundwater level and scale-specific parameters that describe the spatial distribution of groundwater depths, the total catchment area, the tube-drained area, and the area occupied by the surface water network. In Table 4.1 all point-scale process formulations, the GDD-curve, and their parameters are introduced. The complete set of LGSI-model equations is summarized in Appendix 4A. The LGSI-model is a fast calculating process model that calculates flow route discharges for a decade on hourly basis within a few seconds. This is a huge advantage over fully distributed models (e.g. Rozemeijer et al, 2010c), and allows for extensive parameter estimation by Monte Carlo simulation as will be demonstrated in this paper. However, the model is less suited to evaluate the effects of measures that affect the shape of the groundwater table, since this shape is derived from measurements and not calculated from physical principles.

4.3.2.2 Model extensions for the field site

To apply the LGSI-model to the field site, the basic setup needed to be extended to explicitly include groundwater flow out of the field into the deep ditch, lateral groundwater flow into the field from adjacent fields, and a time-variant flow resistance of the tube drains.

The single deep ditch to the east of the field is an anomaly in the surface elevation and is not well represented by the assumption of a normal distribution of groundwater depths (at larger scales with many different drainage depths a normal distribution is more appropriate). To account for groundwater flow towards this ditch, we introduce a new discharge term that approximates the groundwater flux to the deep ditch as a function of the average groundwater depth in the field, $\langle u(t) \rangle$ [L]:

$$Q_{grw,field}(t) = \frac{u_{ditch} - \langle u(t) \rangle}{r_{ditch}} \quad \text{for } u_{ditch} > \langle u(t) \rangle \quad [4.1]$$

with u_{ditch} [L] the depth of the ditch relative to the mean surface elevation of the field site area and r_{ditch} [T], the resistance of the field-site to groundwater flow towards the ditch. The lateral groundwater inflow, L_f [LT^{-1}], was assumed constant throughout the simulation period.

The total discharge measured by the in-stream reservoirs of the field experiment, Q_{res} [LT^{-1}], can now be calculated by all the water that enters the surface water except for the tube drain flux:

$$Q_{res}(t) = Q_{grw,field}(t) + Q_{ov}(t) + P_Q(t) - E_Q(t) \quad [4.2]$$

with Q_{ov} the flux by overland flow, P_Q rainfall on ponded surfaces (including the ditch) and E_Q evaporation from ponded surfaces (all LT^{-1}).

During the experimental period, we observed a strong decline in the drainage effectiveness of the tube drains. At the beginning of the experiment the tube drains were cleaned by pressure flushing as is common practice in the Hupsel Brook catchment. This pressure flushing is repeated every two years. We hypothesize that the tube drains slowly get clogged in periods with substantial discharge and that in dry periods without discharge, aeration and oxidation of the clogging material inside the tube drains reduces the resistance. Similar behavior was also observed by Bentley and Skaggs (1993). The following simple empirical relation was adopted to account for the tube drain resistance change as a function of cumulative discharge:

$$\frac{dr_{dr}}{dt} = 1_{\{Q_{dr} > c_{dr}\}} a_{dr} - 1_{\{Q_{dr} < c_{dr}\}} b_{dr} r_{dr} \quad [4.3]$$

with a_{dr} [-] the rate with which the drainage resistance, r_{dr} [T], increases when the tube drain discharge is larger than threshold discharge c_{dr} [L^3T^{-1}]. The resistance decreases with fractional rate b_{dr} [T^{-1}] for discharges smaller than c_{dr} .

4.3.2.3 Probabilistic parameter estimation

A parsimonious process model as the LGSI-model necessarily suffers from equifinality (parameter non-uniqueness; Beven and Freer, 2001) stemming from parameter uncertainty, the lumped nature of the parameters, the subjectivity introduced by including and excluding processes, the chosen process formulations, and the many different types of measurements that the model needs to describe. We dealt with equifinality by generating many combinations of parameters in a Monte Carlo procedure (GLUE methodology; Beven and Freer, 2001).

In this study we introduce three LGSI-models: a field-site model, a catchment model, and a nested-scales model. For each model, random parameter values were generated from prior uniform and independent distributions between predetermined parameter ranges. All parameter ranges are listed in Table 4.2 and were determined from literature data, field observations, topographic maps, and surface elevation maps. Parameter sets were qualified behavioral when the model satisfactorily described the measured data and all behavioral parameter sets were considered equally probable. The criteria that divide the parameter space in behavioral and non-behavioral parameter sets are listed in Table 4.3, which will be further explained in the next three sections. This procedure was continued for each model until an ensemble of 500 behavioral parameter sets was found. This Monte Carlo multi-criteria model conditioning procedure is a simple but partly subjective and computationally inefficient procedure to generate ensembles of parameter sets. Many (mostly more complicated) variations of this procedure are possible and the subjectivity of the criteria that divide parameter sets in behavioral and non-behavioral may influence the uncertainty in model results. However, the proposed procedure is deemed accurate enough for the objectives of this study: to model field-site flow routes and to assess the value of nested-scale discharge and groundwater level monitoring for discharge and nitrate load predictions.

Table 4.2. Estimated Process-specific and Scale-specific parameter ranges.

Process-specific parameters		Scale-specific parameters			
		Field site	Sub-catchment	Catchment	
α	1 – 2 m ^{&}	σ_{min}	0.06 – 0.13 m ⁺	0.14 – 0.22 m ⁺	0.2 – 0.30 m ⁺
n	1 – 6 ^{&}	σ_{diff}	0.1 – 0.6 m %	0.1 – 0.6 m %	0.1 – 0.6 m %
θ_s	0.35 – 0.45 ^{&}	u_{smax}	0.1 – 0.6 m %	0.1 – 0.6 m %	0.1 – 0.6 m %
M	0.05 – 0.7 [%]	B	0.1 – 0.6 m %	0.1 – 0.6 m %	0.1 – 0.6 m %
u_{ET}	1 – 2 m [%]	A_{dr}/A_{tot}	1.0	0.7 – 0.9 [!]	0.4 – 0.6 [!]
r_{ex}	0.1 – 10 d [%]	A_s/A_{tot}	0	0.0054 – 0.0066 [!]	0.009 – 0.011 [!]
r_{ditch}	500-4000 d [%]	A_{tot}	7700-9000 m ²	0.36 – 0.48 Km ² [!]	6.0–7.3 Km ² [!]
u_{ditch}	1.05 m [*]	* Field-site measurements			
D_{dr}	0.75 – 0.95 m [*]	+ DEM			
r_{dr}	100 – 300 d [%]	! Topographic maps and field survey			
a_{dr}	0 – 2.2 [%]	& Soil parameter estimates from Wösten et al. (2001)			
b_{dr}	0 – 0.14 d ⁻¹ %	% Rough estimates			
c_{dr}	0 – 0.8 mmday ⁻¹ %				
L_f	0 – 0.8 mmday ⁻¹ %				
Mp	0.95 – 1.05 %				
Me	0.95 – 1.05 %				

Table 4.3. The cutoff criteria for behavioral model runs. Model runs are assigned behavioral when they meet to all ‘goodness of fit’ criteria. Expressions for the error terms are given in Appendix 4B

	Field site (storage)			Field site (fluxes)		Sub-catchment	Catchment
	GDD-curve	Ponding curve	Grw. depth	Tube drain	Reservoir		
Curve Error: CE	< 0.07	< 0.2	-	-	-	-	-
Cumulative discharge error: CDE	-	-	-	< 5%	< 10%	< 8%	< 8%
Nash-Sutcliffe coeff. for time series: NS	-	-	> 0.9	> 0.8	> 0.8	> 0.85	> 0.75
Average Groundwater depth error: GE	-	-	-	-	-	< 1 cm (0.2-0.8p)*	< 1 cm (0.1-0.9p)*

*The lower and upper quantile of the modeled groundwater depth distribution that is assumed to envelope the measured groundwater depth at the field site. The GE gives the maximum average difference between the measured groundwater depth and the modeled envelope.

4.3.3 Field-site model of flow route fluxes

4.3.3.1 Interpretation of field site data

The field-site groundwater level measurements were converted to field-site average groundwater depths, standard deviations of groundwater depths, and volumes of ponds on the soil surface to comply with the variables of the LGSI-model. The measured absolute groundwater levels at 31 locations within the field (Fig. 4.1C) were interpolated to arrive at

a groundwater table for the entire field (essentially, the interpolation weighs the individual measured groundwater depths with their representative area). Subsequently, this groundwater table was subtracted from a detailed DEM (5×5 m resolution) and all groundwater depths were grouped into a groundwater depth distribution. The volume of negative groundwater depths of this distribution quantifies the volume of ponds on the field. A mean and standard deviation of the groundwater depth distribution and the volume of ponds were calculated for all 57 weekly field-site groundwater depth surveys. Continuous groundwater level measurements in the 15 groundwater wells around the tube drain 1 (Fig. 4.1C) were used to interpolate between the weekly field average groundwater depths in order to create a continuous field average groundwater depth time series.

4.3.3.2 Parameter estimation of field-site LGSI-model.

The field-site model is conditioned on 5 sources of measured data:

- The measured relation between the average groundwater depth and the standard deviation of groundwater depth (GDD-data),
- The measured relation between the average groundwater depth and the volume of surface storage (Ponding-data),
- Time series of the spatial average groundwater depth,
- Time series of tube drain discharge,
- Time series of discharge measured by the in-stream reservoirs.

Figure 4.2 shows the five sequential steps that were followed to generate an ensemble of Behavioral Parameter Sets (BPS-FS). The specific order of these steps is determined by the relation between model equations and measured data. In the first step, the parameters for the GDD-curve (Eq. A4.7) are conditioned on the measured GDD-data. Secondly, the single parameter of the ponding-curve (Eq. A4.4), which also depends on the GDD-curve, is conditioned on the measured ponding-data. In the third step, storage (Eqs. A4.1, A4.2, A4.3, A4.5, and A4.6), which depends on both the GDD-curve and the ponding-curve, is conditioned on the observed time series of the average groundwater depth. The measured tube drain and reservoir fluxes were used as input variables, which allowed the storage parameters to be estimated independently from the flux parameters. In the fourth step, the flow route fluxes (Eqs. A4.9 and A4.10) were conditioned on the measured tube drain and reservoir fluxes. The measured average groundwater depth was an input variable and hence was not calculated by the model. In the last step, a complete LGSI-model run allowed to check if the combination of the parameters still yielded an accurate model. These 5 steps were repeated until 500 behavioral parameter sets (BPS-FS) were found. The parameter distributions of BPS-FS were analyzed to determine parameter sensitivity and the model results were analyzed to quantify the uncertainty in flow route contributions to the total discharge owing to equifinality.

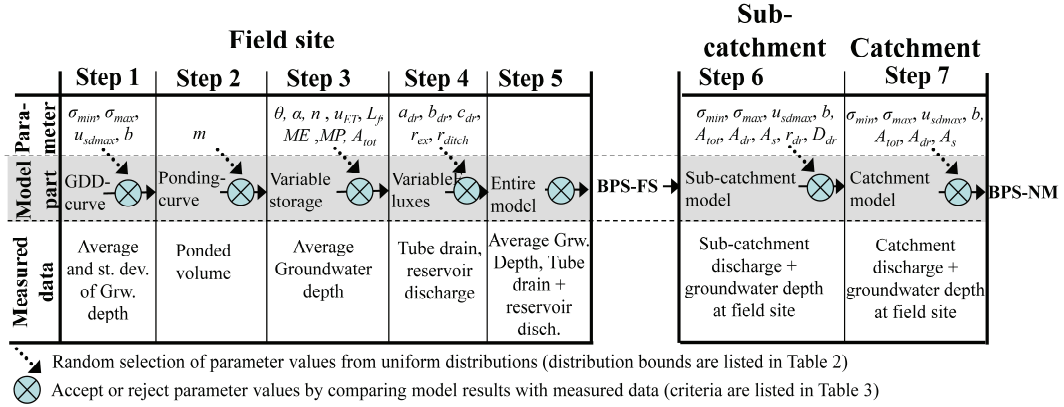


Figure 4.2. Procedure for derivation of behavioral parameter sets for fields-site and nested-scales model. The first five steps yield behavioral parameter set for the field site (BPS-FS). All seven steps yield behavioral parameter sets for the nested scale model setup (BPS-N). The parameters are explained in Table 4.1.

4.3.4 Catchment model

The parameters of the catchment model were conditioned on catchment discharge and a single groundwater level time series only. The resulting ensemble of Behavioral Parameter Sets is referred to by BPS-C. Table 4.2 lists the parameter ranges from which the parameter sets were generated. The ranges for the process-specific parameters were equal to those used for the field-site model. Only the ranges for the scale-specific parameters that described areas (i.e. the catchment area, the tube drained area, and the area of the surface water network), which could be estimated from maps, were different.

The single groundwater level time series was not considered representative for the dynamics of the groundwater storage of the entire catchment. From experience, we estimated that at any one time, at least 10% of the catchment area had shallower groundwater and another 10% had deeper groundwater than the single observed level: the observed groundwater level thus was assumed to be within the 0.10 and 0.90 percentile but allowing for an average exceedence of 1.0 cm (*GE*, Table 4.3).

4.3.5 Nested-scales model setup

We attempted to constrain the uncertainty in flow route contributions of the catchment model by combining information from measurements from the field site, discharge measurements of a small sub-catchment, and discharge measurements at the catchment outlet in a nested-scales model setup. This nested-scales model consists of three sub-LGSI-models representing each of the scales: field-site, sub-catchment, and catchment. These models are connected by assuming that the parameters that describe the discharge response to groundwater depth are scale invariant (process-specific parameters, see Table 4.1), while the parameters that describe the spatial distribution of groundwater depths are assumed scale-specific (Table 4.1). The underlying hypothesis is that the differences between the

observed hydrographs at the three scales are primarily an effect of a different spatial distribution of groundwater depths and resulting different active drainage areas.

All seven steps shown in Fig. 4.2 were followed to derive an ensemble of Behavioral Parameter Sets for the nested-scale model setup (BPS-N). First, a behavioral parameter set for the field site was created (first five steps of Fig. 4.2). Subsequently, we randomly generated new scale-specific parameter values for the sub-catchment until the model results for discharge and groundwater depth were satisfactory (criteria in Table 4.3). We also estimated a new constant drainage depth and drainage resistance, because the drainage depth and the time variant drainage resistance of the field site were specifically estimated for the three drains of the field site. Three drains probably do not represent the drain populations at larger scales. For the sub-catchment and catchment scale, we assumed that the many different pressure flushing (cleaning) dates of the tube drains and different drainage spacings led to a constant spatially averaged drainage resistance. Next, we re-estimated the scale-specific parameters for the entire catchment, and assumed the drainage depth and drainage resistance of the sub-catchment representative for the entire catchment. These seven steps were continued until 500 behavioral parameter sets were found. (BPS-N). The flow route contributions to discharge during the entire field-site monitoring period and the parameter distributions for BPS-C and BPS-N were compared to assess the added value of introducing nested-scale measurements.

4.3.6 Model validation

The BPS-C and the BPS-N were both validated for their ability to predict the catchment-scale discharge. For the validation we chose the period 1994-1995 for its high quality discharge data without data gaps and obvious measurement errors, and 1996-2001 for its episodes of extremely high discharges that are outside the discharge range of the calibration period.

A second model verification was performed by comparing nitrate loads calculated by BPS-C and BPS-N with measured nitrate loads. For this comparison, constant flow route concentrations were adapted from Van der Velde et al. (2010a) for tube drain flow (72 mg L^{-1}), overland flow (9 mg L^{-1}) and direct rainfall (9 mg L^{-1}). The groundwater flow concentration was estimated to be 50 mg L^{-1} , which corresponds to results of Rozemeijer et al. (2010d). Uncertainty in these concentrations are significant but are not accounted for in this comparison. Hence, we do not claim a real validation, but want to evaluate if the model is able to predict nitrate concentration behavior and to assess uncertainty propagation of flow route discharge uncertainty to nitrate load estimates.

4.4 Results and discussion

4.4.1 Nested-scale measurements

Figure 4.3 shows the results of the nested-scale discharge measurements. At the field site, tube drain discharge was by far the most important flow route. Over the entire period this flow route contributed 78% of the total discharge. The remaining 22% is a mixture of overland flow during rainfall events (the sharp peaks in reservoir discharge of Fig. 4.3) and

groundwater flow. The discharges of the sub-catchment and the entire catchment reflect the characteristic behavior of both the peaks measured by the in-stream reservoirs (overland flow) and the long recession tails of the tube drain discharge at the field scale.

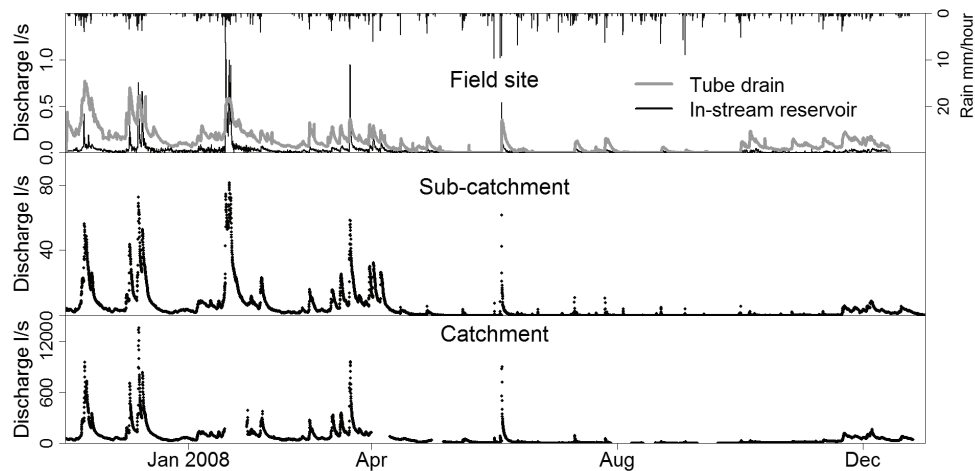


Figure 4.3. Measured nested-scale discharges in response to rainfall measured at the field site.

4.4.2 Field-site model

Van der Velde et al. (2009) reported a decrease in the simulated groundwater depth variance as the groundwater depth increased in their catchment-scale groundwater model. For the field site this finding is corroborated by observations for a wet and a dry day (Fig. 4.4). Approximating these distributions by normal distributions introduced only small errors (Fig. 4.4). Fig. 4.5A shows the measured groundwater depths means and standard deviations for the 57 weekly groundwater depth surveys. The grey band in Fig. 4.5A represents the results of all behavioral parameter sets (BPS-FS) for the GDD-curve. This grey band is particularly narrow between average groundwater depths of 0.5 and 0.8 m (some of the data points are even outside it), indicating that the model results for storage and discharge are very sensitive to the GDD-curve in this range of average groundwater depths. GDD-curves outside the grey band, although they closely fit the observed GDD-data, did not yield behavioral models for some of the other criteria such as storage or discharge. In Fig. 4.5B we plotted the measured ponding volumes and the ponding curves of all BPS-FS. Because the measured ponding volumes are relatively uncertain (they are difficult to measure and we have only a few measurements) we allowed for a larger curve error (*CE*, Table 4.3). This resulted in the grey band in Fig 4.5B.

Figure 4.6A shows the measured and modeled spatially averaged groundwater depth. The model results are accurate, but some of the moderate groundwater level peaks are underestimated. This also caused an underestimation of the tube drain discharge (Fig. 4.6B) during these moderate groundwater level peaks. Overall, Fig. 6 shows that the LGSI-model is able to accurately describe the average groundwater depth, tube drain flow, and reservoir

discharge (Eq. 4.2) simultaneously. All three time series were simulated with a Nash-Sutcliffe (*NS*) coefficient (Nash and Sutcliffe, 1970) exceeding 0.8.

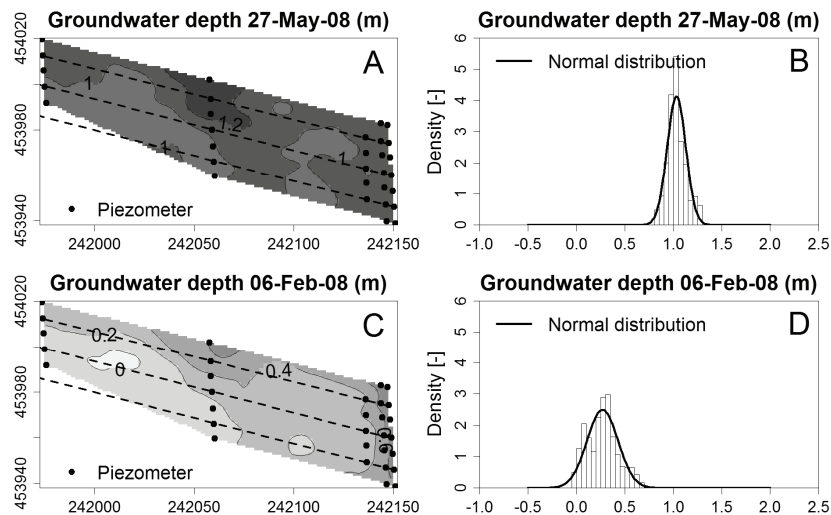


Figure 4.4. Map of field-site groundwater depth for a dry (A) and a wet (C) day and the corresponding groundwater depth distributions (B and D).

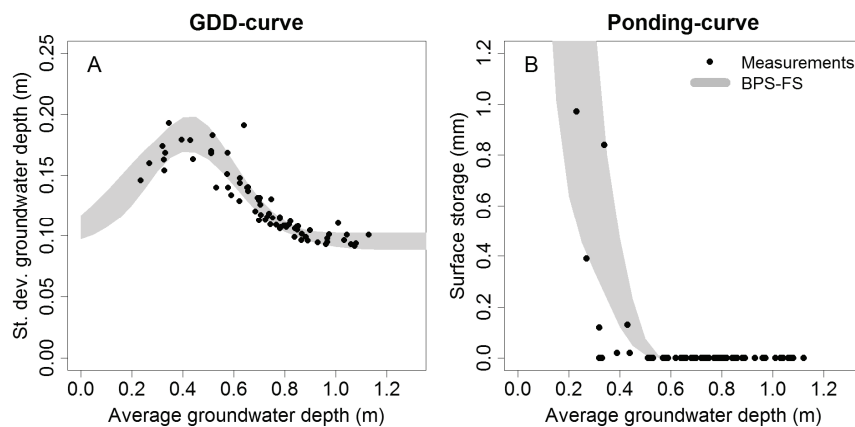


Figure 4.5. Measured and simulated groundwater depth distribution curve (GDD-curve) (A) and Ponding curve (B) of the field-site. The grey area represents the ensemble of behavioral parameter sets of the field-site model (BPS-FS).

A comparison of the LGSI-model results with the results of Rozemeijer et al. (2010c), who used the same dataset and a fully distributed HydroGeosphere (Therrien et al, 2009) model to simulate flow routes during a single discharge event, demonstrate that the relatively simple LGSI-model concepts can simulate the discharges of individual flow routes equally well as the sophisticated HydroGeosphere model and hence constitute a very powerful tool

for simulation and prediction of flow routes at a field site. Like Rozemeijer et al. (2010c), we found that measurements of both the storage of groundwater within the field and the corresponding discharge of flow routes are indispensable for an accurate model representation of the groundwater-surface water interaction.

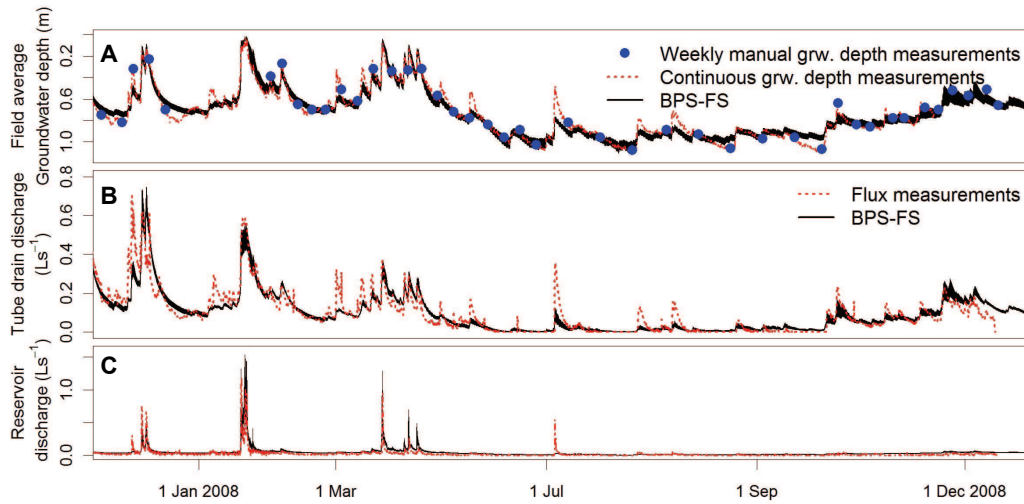


Figure 4.6. Measurements and simulation results of the field site model (BPS-FS) for the spatially averaged groundwater depth (A), tube drain discharge (B), and reservoir discharge (combined flux of overland flow and groundwater flow, C) of the field-site. The black band gives the results of all behavioral parameter sets (BPS-FS).

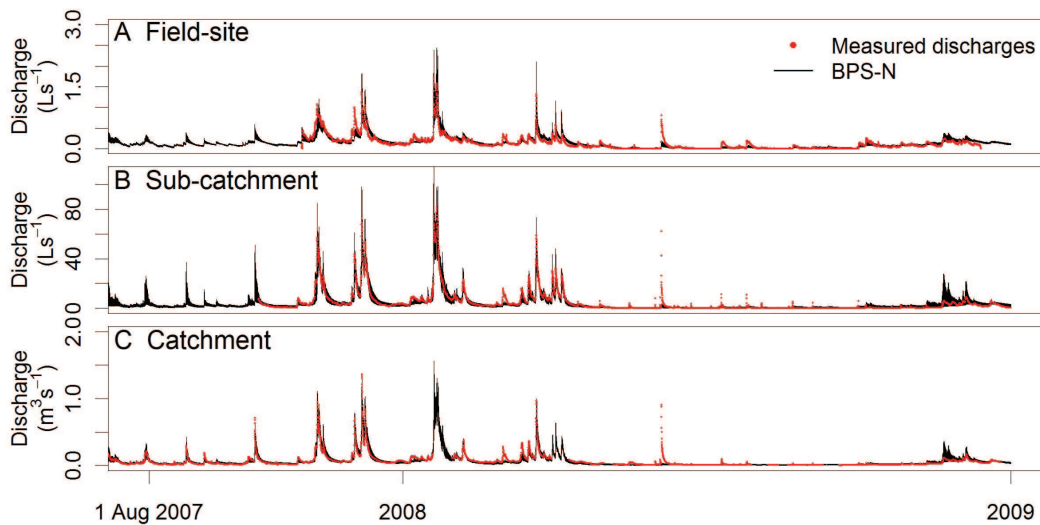


Figure 4.7. Measurements and simulation results of the nested-scales model for total discharges of the field-site (A), sub-catchment (B) and entire catchment (C). The black band gives the results of all behavioral parameter sets (BPS-N).

4.4.3 Nested-scales model and model uncertainty

The discharges at all three nested-scales could be accurately described by parameter sets that share the same values for the process-specific parameters and differ only in scale-specific parameter values (Fig. 4.7). This result supports our hypothesis that scale effects in lowland hydrology can be attributed to scale differences in the shape of the groundwater table. These scale differences were quantified by the GDD-curves of the individual scales. Figure 4.8 shows the inferred ensemble of GDD-curves for the three nested scales. The differences between the field-site GDD-curve and the GDD-curve of the two catchment scales are much larger than those between the GDD-curves of both catchment scales. This is consistent with the small differences in the shape of the hydrographs between both catchment scales (Fig. 4.3).

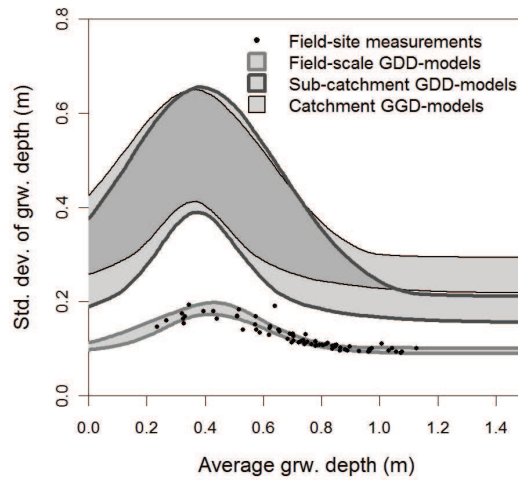


Figure 4.8. Bandwidth of behavioral GDD-curves for the three scales of the nested-scales model (BPS-N). The dark grey area indicates overlap between ensembles of GDD-curves.

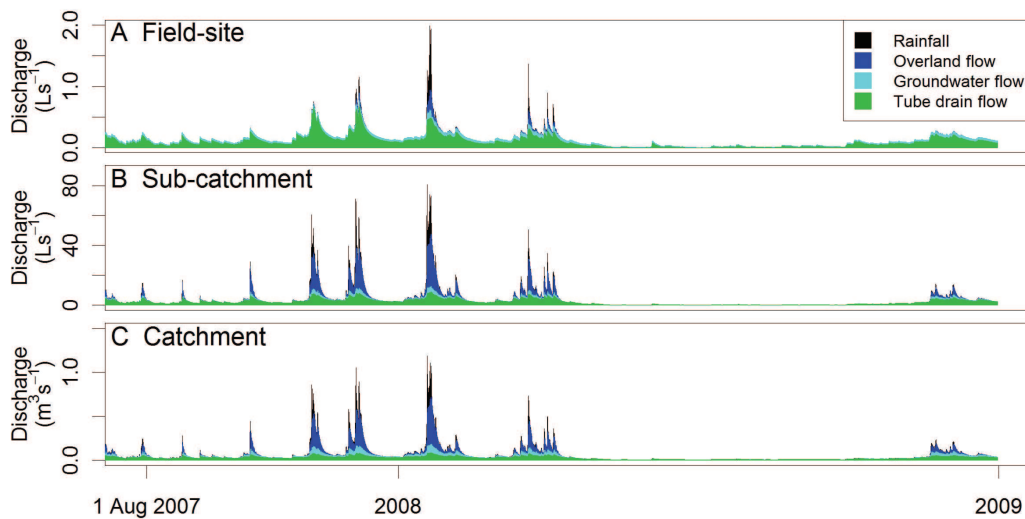


Figure 4.9. Contributions of flow routes to total discharge. The displayed contribution is the median of contribution of all behavioral parameter sets (BPS-N).

The individual flow route contributions (the median contribution of BPS-N) to discharge are shown in Fig. 4.9. The relative overland flow and groundwater flow contributions to discharge increase with increasing scale, at the expense of tube drain discharge. Table 4.4 gives the 10-90 percentile estimates of flow route contributions for the entire simulation period (this period equals the field-site measurement period). The uncertainty in the flow route contributions at the field site is constrained by many different types of measurements (see also Fig. 4.6), but is much larger for the large scales, where less measurements were available. In Table 4.4 we also compared the uncertainty of the flow route contributions calculated by BPS-N and BPS-C. The uncertainty in groundwater flow, overland flow, and direct rainfall is significantly reduced by introducing nested scale measurements. In contrast, the uncertainty of the tube drain discharge could hardly be reduced because the field-site tube drain depth and tube drain resistance could not be transferred to larger scales. We re-estimated the tube drain-specific parameters for the sub-catchment and catchment-scale by assuming them to be equal for both scales, but even this assumption did not reduce the uncertainty.

Table 4.4. Calculated flow route contribution (0.1-0.9 quantiles) of BPS-N and BPS-C. The contribution is calculated over the period Nov 2008 through Dec 2009.

	BPS-N			BPS-C
	Field-site	Sub-catchment	Catchment	Catchment
Tube drain flow	0.76 - 0.79	0.34 - 0.61	0.25 - 0.50	0.21 - 0.51
Groundwater flow	0.10 - 0.15	0.06 - 0.16	0.12 - 0.27	0.14 - 0.50
Overland flow	0.04 - 0.07	0.24 - 0.42	0.27 - 0.41	0.18 - 0.37
Direct rainfall	0.03 - 0.05	0.07 - 0.11	0.08 - 0.11	0.03 - 0.10

4.4.4 Parameter distributions

Figure 4.10 shows the distribution of the behavioral parameter sets of all process-specific parameters. Since the prior distributions were uniform, sensitive parameters are identified by markedly non-uniform distributions. For the field site model (BPS-FS) the most sensitive parameters are α , D_{dr} , a_{dr} , L_f , and r_{ditch} . The sensitivity of a_{dr} signals that the tube drain resistance increases after tube drain cleaning. However, the insensitivity of b_{dr} and c_{dr} might indicate that the reduction in tube drain resistance during dry periods is of minor importance. The lateral inflow of groundwater, L_f , which is the closing term for the water balance, could be determined accurately around 0.6 mm day^{-1} . Surprisingly insensitive parameters are θ_s and u_{ET} . The insensitivity of u_{ET} signals that evapotranspiration reduction at our relatively wet (high groundwater tables) field site might not be very important. As long as the value of u_{ET} is less than two standard deviations (20 cm) below the lowest average groundwater water table, the modeled evapotranspiration reduction is small and u_{ET} does not affect the model results.

At the catchment scale (BPS-C) on the other hand, u_{ET} is the most sensitive parameter. At this scale this parameters closes the overall mass balance by increasing or reducing

evapotranspiration (at the catchment scale there is not net lateral groundwater flow). Also m and r_{ex} are relatively sensitive as they directly control the discharge, which is the only calibration objective. All other parameters are insensitive and the uncertainty in flow route contribution is largely determined by the boundaries of the prior distributions.

For the nested-scales model (BPS-N) we sought process-specific parameter sets that can describe all three scales simultaneously. Figure 4.10 shows that the parameter distributions of BPS-N combine the constraints of the distribution of both BPS-FS and BPS-C. The added value of including nested-scale measurements to reduce parameter uncertainty is apparent for almost all process-specific parameters.

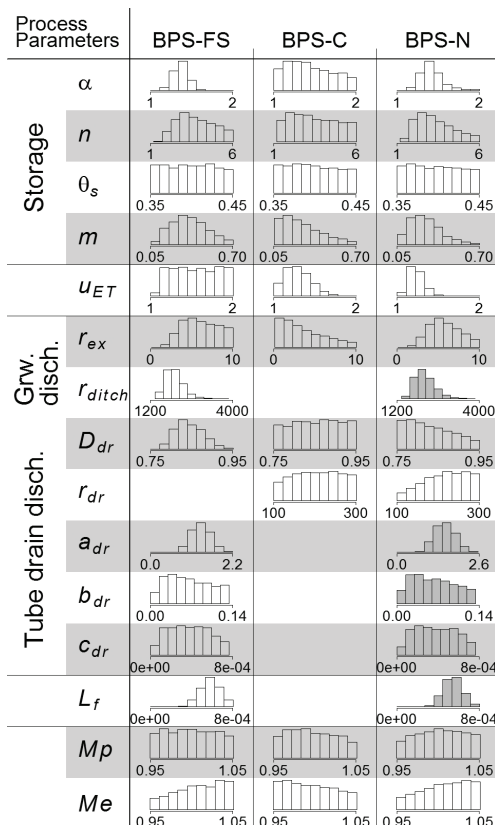


Figure 4.10. Process-specific parameter distributions for the three behavioral parameter sets: BPS-FS, BPS-C, and BPS-N. The grey-filled distributions were only used for the field-site sub-model within the nested-scales model.

Figure 4.11 shows the distributions of the scale-specific parameters and again the reduction in parameter uncertainty by introducing nested-scale measurements is clear. Note that the distribution of σ_{min} tends to high values exceeding the preset boundaries in Table 4.2 that were determined from a detailed DEM. Under dry conditions, the groundwater level is almost parallel to the soil surface at the resolution of the DEM (5 m). Variations in the groundwater depth under such conditions emanate largely from local variations in the soil surface elevation that are too small to appear in the phreatic level. However, under dry conditions a few very deep incisions of the stream produce most discharge. Around these

incisions, the groundwater depth necessarily decreases sharply to zero at the stream bank, and these deviating groundwater depths produce outliers from the normal distribution valid for the rest of the catchment. As a consequence, the calibration tried to increase the groundwater depth variation (and thereby the range of σ_{min}) under dry conditions to be able to generate low discharges. Because these discharges are low, the effect of underestimating discharges during dry conditions on the entire water balance of the catchment is small.

In general, both Figs. 4.10 and 4.11 suggest that the LGSI-model is highly overparameterized when the model is only calibrated on discharge, because almost all parameters of BPS-C are insensitive (uniform distributions). However, nested-scale measurements and the assumption that scale differences are driven only by the groundwater table increases the parameter sensitivity and allows most parameters to be conditioned.

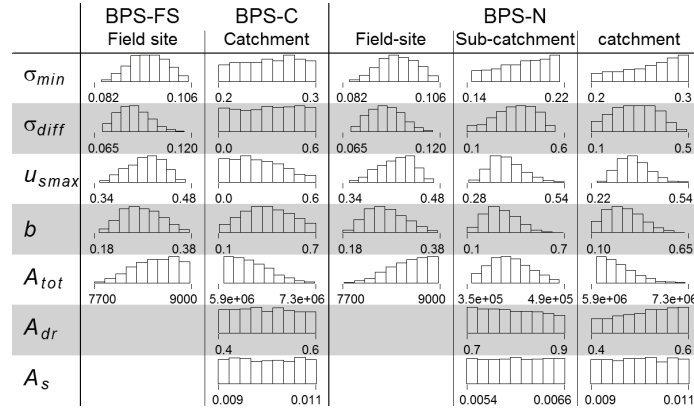


Figure 4.11. Scale-specific parameter distributions for the three behavioral parameter sets: BPS-FS, BPS-C, and BPS-N

4.4.5 Model validation

The BPS-N performed slightly better than BPS-C for both validation periods. For the period 1994-1995 the BPS-N yielded an average *NS*-coefficient of 0.90, against 0.85 for the BPS-C. For the validation period 1996-2001 the average *NS*-coefficients were 0.79 for BPS-N and 0.73 for BPS-C. Although these may seem minor improvements in model performance when weighted against the efforts involved in the nested-scale monitoring, these model improvements are especially apparent in extreme discharges beyond the range of the calibration dataset. Figure 4.12 shows the validation results of the four most extreme discharge events during the period 1996-2001. From all events it is clear that the BPS-N much better predicted discharge than BPS-C (particularly the magnitude of the peaks), with far smaller uncertainty ranges. During the discharge events in Fig. 4.12C, which are the highest discharges measured in the past 20 years, the measured maximum discharge was more than twice the maximum discharge of the calibration period. During this period some of the BPS-C overestimated the discharge by a factor 3, while the BPS-N predicted all discharges close to the measured discharge.

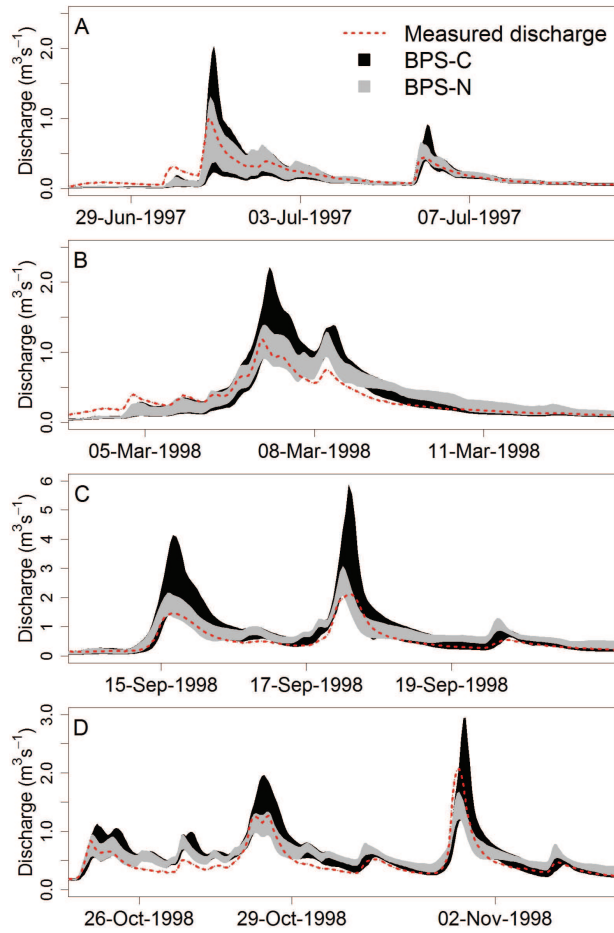


Figure 4.12. Model validation results for extreme discharge events at the catchment outlet

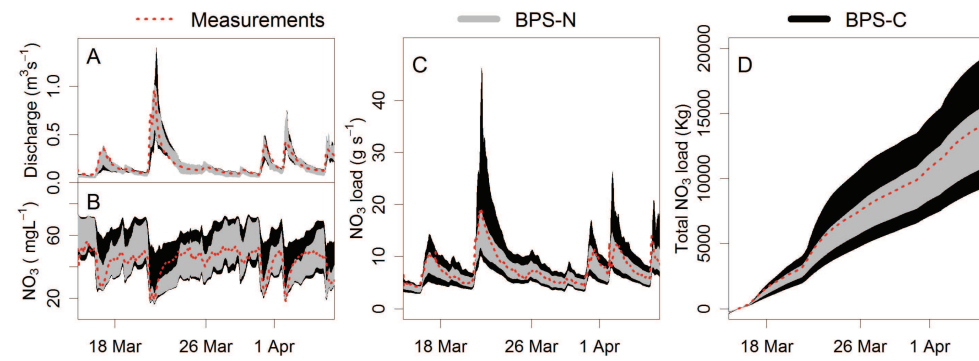


Figure 4.13. Simulation results of BPS-N and BPS-C for discharge (A), nitrate concentration via a flow route mixing analysis (B), nitrate load (C) and cumulative nitrate load (D).

The model improvement achieved by conditioning the model on nested-scale measurements is also apparent from the comparison between simulated and measured nitrate concentrations and nitrate loads (Fig. 4.13). Assuming constant flow route concentrations yielded good descriptions of the nitrate concentration fluctuations at the catchment outlet for both models (BPS-C and BPS-N). But conditioning on nested-scale data reduced the uncertainty in cumulative load estimates by 50%. This shows how vital accurate estimations of flow route discharges are for estimating solute loads towards downstream surface water bodies.

We argue that, because the nested scale measurements combined with the nested-scale model could partly constrain the uncertainty in flow route discharges (Table 4.4), the BPS-N have a better chance of describing ‘the right discharge for the right reason’ (Kirchner, 2006), i.e., the correct combination of flow routes. This was demonstrated by the better peak discharge predictions during the validation period and reduced uncertainty in nitrate load estimates of the nested-scales model (BPS-N).

4.5 Conclusions

Detailed and unique flux measurements at a pasture field site allowed us to formulate and calibrate our parsimonious LGSI-model. Even the very non-linear process of saturated overland flow was adequately simulated by the field-site model. An exceptional feature of this model is that the model concepts were designed around the available measurements (Van der Velde et al., 2009). Consequently, the parameters that describe the discharge and storage processes could all be conditioned on measurements. This yielded a field-site model that accurately described both storage and fluxes simultaneously.

The combined nested-scale measurement and model setup made it possible to combine discharge information of the field scale, a small sub-catchment, and the entire catchment. We demonstrated that the differences between hydrographs at the three scales could all be described by only changing the Groundwater Depth Distribution (GDD) curve, even though the hydrographs were markedly different. This result supports our hypothesis that scale effects on discharge in lowland catchments are primarily an effect of differences in the spatial distributions of groundwater depths between different scales. Still, the range of GDD-curves that yielded good model results for the catchment scales was wide. This emphasizes the importance of spatially distributed groundwater depth monitoring to further condition these GDD-curves. This should lead to an even more solid foundation supporting the physical representation of the catchment’s hydrology, and hence to more reliable results.

Tube drain effluent is the most important route for nitrate towards the surface water network in lowland catchments. We were able to measure tube drain discharge at the field site and we concluded that almost 80% of the water (Van der Velde et al., 2010a) and 92% of the nitrate (Rozemeijer et al., 2010d) was transported by tube drains. It is by no means trivial to extrapolate these field-scale findings to the entire catchment. Our combined

nested-scales observation and modeling approach could narrow down the contribution of tube drain discharge to the discharge of a sub-catchment of 0.4 km² to 34-61% of the total discharge. For the entire catchment of 6.5 km² 25-50% of the discharge originated from tube drains. These results not only demonstrate that we need to be careful extrapolating field experiment results to entire catchments but also show that nested-scale measurements are essential to understand and quantify the flow route contributions to the discharge of a catchment.

In this paper we demonstrated the potential of combined nested-scale monitoring and modeling for the Hupsel Brook catchment. However, many of our findings can be generalized. First of all, we showed that detailed field-site measurements of storage and flow routes provide the process-understanding that is needed to develop a model structure that adequately describes the catchment-specific flow routes. Secondly, we demonstrated that the combination of a relatively short period of nested-scale measurements with nested-scale models significantly constrains uncertainty in the contributions of groundwater flow, overland flow, and direct rainfall into surface waters, which in turn significantly reduces uncertainty in nitrate load estimates. Finally, we showed that conditioning parameter sets on nested-scale measurements considerably improves discharge predictions compared to parameter sets constrained on discharge only. Model calibration on nested-scale measurements may not yield models with better calibration-statistics than models that are calibrated on catchment discharge alone, but the nested-scales model approach yields models that are able to predict (peak) discharges during validation periods more accurately. Improved quantifications and predictions of nitrate loads and peak discharges make the efforts involved in nested-scale monitoring worthwhile.

Appendix 4A

The overall water balance of the model normalized by area and zero lateral influx is given by:

$$\frac{\partial S_{sat}(t)}{\partial t} + \frac{\partial S_{unsat}(t)}{\partial t} + \frac{\partial S_{surf}(t)}{\partial t} = P(t) - ET_{act}(t) - Q(t) \quad [A4.1]$$

with saturated zone storage, S_{sat} [L], unsaturated zone storage, S_{unsat} [L], surface storage in streams, ditches and ponds, S_{surf} [L], the rainfall flux, P [LT^{-1}], actual evapotranspiration, ET_{act} [LT^{-1}], and discharge, Q [LT^{-1}]. The storage terms on the left-hand side of Eq. (A4.1) are described as a function of the distribution of groundwater depths, f_u [L^{-1}]. The change in saturated storage is expressed by the inverse of the change in unsaturated zone volume:

$$\frac{\partial S_{sat}(t)}{\partial t} = -\theta_s \frac{\partial}{\partial t} \left(\int_0^{\infty} f_u(t) u du \right) \quad [A4.2]$$

with the groundwater depth, u [L], the spatially averaged soil porosity, θ_s [-], the distribution in groundwater depths, f_u [L^{-1}], and the total unsaturated zone volume normalized by the catchment area $\int_0^{\infty} f_u(t) u du$. Note that the positive integration bounds imply that the unsaturated zone does not exist for negative groundwater depths (ponding).

The volume of water stored in the unsaturated zone is described with a Van Genuchten (1980) relationship for soil moisture in an unsaturated zone at hydrostatic equilibrium. The change in unsaturated zone storage is described by:

$$\frac{\partial S_{unsat}(t)}{\partial t} = \theta_s \frac{\partial}{\partial t} \left(\int_0^{\infty} f_u(t) \int_0^u \left[1 + (\alpha h)^n \right]^{\frac{1}{n}-1} dh du \right) \quad [A4.3]$$

The height above the groundwater level is denoted by h [L], and α [L^{-1}] and n [-] are the Van Genuchten parameters, with the residual volumetric water content equal to zero.

Water stored on the soil surface in ditches and ponds is described by a fixed fraction, m [-], of the total volume of groundwater heads above the soil surface:

$$S_{surf}(t) = -m \int_{-\infty}^0 f_u(t) u du \quad [A4.4]$$

The change in surface storage is given by:

$$\frac{\partial S_{surf}(t)}{\partial t} = -m \frac{\partial}{\partial t} \left(\int_{-\infty}^0 f_u(t) u du \right) \quad [A4.5]$$

Deep groundwater levels reduce the potential evapotranspiration. We chose a single cutoff level, u_{et} , below which no evapotranspiration is possible and above which potential

evapotranspiration, e_{pot} , occurs. This leads to the following expression for evapotranspiration:

$$ET_{act}(t) = e_{pot}(t) \int_{-\infty}^{u_{et}} f_u(t) du \quad [A4.6]$$

Furthermore, we assumed that a specific volume of groundwater is always stored in the same way (i.e., the moments of the distribution of groundwater depths only depend on the amount of storage and are not hysteretic). We are not interested in the exact configuration of storage within the catchment, and therefore assumed a normally distributed groundwater depth with an empirical relationship relating the standard deviation of groundwater depths σ_u [L] to the spatial average of the groundwater depth $\langle u(t) \rangle$:

$$\sigma_u = \sigma_{diff} \cdot e^{-\left(\frac{\langle u(t) \rangle - u_{sd \max}}{b}\right)^2} + \sigma_{\min} \quad [A4.7]$$

Van der Velde et al. (2009) showed that this relation holds for field- and catchment-scales.

Storage-discharge relationships

The contribution of specific flow routes to overall discharge largely determines the discharge quality. Therefore we subdivided the total discharge, Q , into four flow routes with distinctly different water chemistry:

$$Q(t) = Q_{drain}(t) + Q_{grw}(t) + Q_{ov}(t) + P_Q(t) - E_Q(t) \quad [A4.8]$$

with Q_{drain} [LT^{-1}] groundwater discharge by tube drains, Q_{ov} [LT^{-1}], discharge by overland flow, and Q_{grw} [LT^{-1}], discharge of phreatic groundwater flow by ditch and stream drainage. Rain falling directly on the surface water network is denoted by P_Q [LT^{-1}] and evaporation from the surface water network is denoted by E_Q [LT^{-1}].

The tube drain discharge is calculated from the groundwater depth distribution by:

$$Q_{drain}(t) = \frac{A_{dr}}{r_{dr} A_{tot}} \int_{F_u^{-1}\left(\frac{A_s}{A_{tot}}\right)}^{D_{dr}} f_u(t) \cdot (D_{dr} - u) du \quad [A4.9]$$

with A_{dr} [L^2] the surface area occupied by tube drains, A_{tot} the catchment surface area, r_{dr} [T] the resistance of the soil to tube drain discharge and D_{dr} [T] the average depth of the tube drains. The fraction of catchment surface that is wet but has no tube drains, such as the surface area of ditches and streams, is denoted by A_s . This fraction is important under dry conditions when tube drainage stops and groundwater drainage by ditches and the stream takes over.

Van der Velde et al. (2009) made no distinction between overland flow and groundwater flow towards ditches and streams. They reasoned that the physical principles driving both

fluxes are equal: groundwater level gradients driving water from the soil into surface waters or ponds. In this study we follow the same line of reasoning but we want to separate both fluxes, because the two fluxes have distinctly different effects on the water quality. We hypothesize that under wet conditions, first all ditches start draining and only when the catchment becomes so wet that the drainage area, $F_u(0) = \int_{-\infty}^0 f_u(t) du$, exceeds the surface area occupied by ditches, A_s , overland flow starts to occur. Now we can subdivide the groundwater flux into groundwater flow towards ditches and overland flow by the corresponding drainage area:

$$\begin{aligned}
 Q_{grw}(t) + Q_{ov}(t) &= \frac{m-1}{r_{ex}} \int_{-\infty}^0 f_u(t) \cdot u \, du \\
 Q_{grw}(t) &= \frac{m-1}{r_{ex}} \int_{-\infty}^{\min\left(F_u^{-1}\left(\frac{A_s}{A}\right), 0\right)} f_u(t) \cdot u \, du \\
 Q_{ov}(t) &= \frac{m-1}{r_{ex}} \int_{\min\left(F_u^{-1}\left(\frac{A_s}{A}\right), 0\right)}^0 f_u(t) \cdot u \, du
 \end{aligned} \tag{A4.10}$$

with r_{ex} [T] the resistance of the soil to groundwater flow towards surface water and ponds. The term $\min\left(F_u^{-1}\left(\frac{A_s}{A}\right), 0\right)$ divides the negative part of the distribution of groundwater depth f_u (i.e. areas with ponding) in two areas: an area with groundwater flow and an area with overland flow, where $F_u^{-1}\left(\frac{A_s}{A}\right) < 0$.

The amount of rain that falls on the active drainage area and is discharged immediately is:

$$P_Q(t) = p(t) \int_{-\infty}^0 f_u(t) \, du \tag{A4.11}$$

The evaporation of surface water is:

$$E_Q(t) = e_{pot}(t) \int_{-\infty}^0 f_u(t) \, du \tag{A4.12}$$

Appendix 4B

Four error-terms divide the parameter space in behavioral and non-behavioral parameter sets. The Curve Error term quantifies the average normalized distance between the measurements and the modeled GDD-curve or Ponding curve:

$$CE = \frac{1}{n} \sum_{i=1}^n \min \left(\sqrt{\left(\frac{\langle u \rangle_i - \langle u \rangle_c}{\langle u \rangle} \right)^2 + \left(\frac{y_i - y_c}{\bar{y}} \right)^2} \right), \text{ with } y_c = f(\langle u \rangle_c) \quad [\text{B4.1}]$$

The minimum function identifies the minimum normalized distance between the measurements and the model-curve. The number of measurements is denoted by n ; $\langle u \rangle_i$ is the spatially averaged groundwater depth at the time measurement i was obtained; $\langle u \rangle_c$ is an spatially averaged groundwater depth defined by the GDD-curve or the Ponding-curve; $\langle u \rangle$ is the temporal average of the measured spatially averaged groundwater depth (i.e., the groundwater depth averaged over space and time); y_i is the measured variable (the standard deviation of the groundwater depth for the GDD-curve, and the ponding volume for the Ponding-curve); y_c is the same variable defined by the model curve, and \bar{y} the temporal average of the measured values of this variable.

The second error term quantifies the error in the total water balance:

$$CDE = \left| 1 - \frac{\sum_{i=1}^n Q_{mod,i}}{\sum_{i=1}^n Q_{meas,i}} \right| \quad [\text{B4.2}]$$

With $Q_{mod,i}$ [L^3T^{-1}], the modeled discharge corresponding to measured discharge $Q_{meas,i}$ [L^3T^{-1}]. The dynamics of groundwater depth and discharge time series (both are defined by the variable V in the following equation) are evaluated by the Nash-Sutcliffe statistic (Nash and Sutcliffe, 1970)

$$NS = 1 - \frac{\sum_{i=1}^n (V_{meas,i} - V_{mod,i})^2}{\sum_{i=1}^n (V_{meas,i} - \overline{V_{meas}})^2} \quad [\text{B4.3}]$$

with $\overline{V_{meas}}$ [L^3T^{-1}] the average measured discharge or groundwater depth.

The simulated groundwater dynamics for both catchment scales are compared with a single measured groundwater level time series. This comparison is evaluated by:

$$GE = \frac{1}{n} \sum_{i=1}^n fGE_i \quad [\text{B4.4}]$$

with fGE [-] a measure of the degree to which a measured groundwater depth, $u_{meas,i}$ [L], is outside the acceptable bounds ($Ul_{min,i}$ [L] and $Ul_{max,i}$ [L]) of the modeled groundwater depth distribution:

$$\begin{aligned} fGE_i &= u_{meas,i} - Ul_{max,i} && \text{if } u_{meas,i} > Ul_{max,i} \\ fGE_i &= Ul_{min,i} - u_{meas,i} && \text{if } u_{meas,i} < Ul_{min,i} \\ fGE_i &= 0 && \text{if } Ul_{min,i} < u_{meas,i} < Ul_{max,i} \end{aligned}$$

The acceptable bounds, Ul_{min} and Ul_{max} , are a fixed quantile of the modeled distribution and are recalculated for each time step, i , based on an estimate of the representativity of a location where groundwater depths are measured for a certain area. We estimated that the measured average groundwater depth at the field site should always be within the 0.20-0.80 percentile of all groundwater depths in the sub-catchment and within 0.1-0.90 of the groundwater depths of the entire catchment.

Improving load estimates for NO₃ and P in surface waters by characterizing the concentration response to rainfall events

Abstract

The loss of nutrients from agricultural fields threatens the ecological, recreational, and industrial functioning of many surface waters. For the evaluation of action programs to reduce surface water pollution, water authorities invest heavily in the monitoring of NO₃ and P loads from upstream catchments. However, sampling frequencies in regional monitoring networks are generally insufficient to capture the concentration dynamics in surface water, which leads to large uncertainties in estimates of loads and average concentrations. For this study, we used on-site equipment that performed semi-continuous (15 minute interval) NO₃ and P concentration measurements from June 2007 to July 2008. Our measurements recorded the concentration responses to rainfall events with a wide range in antecedent conditions and rainfall durations and intensities. Through sequential linear multiple regression analysis, we successfully related the NO₃ and P event responses to high frequency records of precipitation, discharge, and groundwater levels. We applied the explanatory strength of these quantitative hydrological variables to reconstruct concentration patterns between low-frequency water quality measurements. This new approach significantly improved load estimates from a 20% to a 1% bias for NO₃ and from a 63% to a 5% bias for P.

This chapter is adapted from: Van der Velde, Y., J.C. Rozemeijer F.C. Van Geer, G.H. De Rooij, P.J.J.F. Torfs, and H.P. Broers (2010). Improving load estimates for NO₃ and P in surface waters by characterizing the concentration response to rainfall events. Environ. Sci. Technol, 44, 6305-6312.

5.1 Introduction

Surface water pollution is a serious problem in areas with intensive agriculture such as the Netherlands (Oenema et al., 2007). Policy makers of the European Union and elsewhere in the world aim at improving water quality in receiving surface water bodies (e.g. EU, 2000). For the evaluation of action programs and pilot studies, water authorities invest heavily in the monitoring of NO_3 and P loads from upstream catchments. However, the interpretation of the data from their monitoring networks is often problematic. Grab samples only provide ‘snapshots’ of solute concentrations and sampling frequencies are generally not sufficient to capture the dynamic behavior of surface water quality (Kirchner et al., 2004; Johnes, 2007; Rozemeijer et al., 2010). Together with the uncertainties in the concentration measurements themselves (e.g. Harmel et al., 2006), this results in large uncertainties in the estimates of loads and average concentrations.

The uncertainties in estimates of loads and average concentrations can be reduced by increasing the sampling frequencies. However, the field sampling, sample transport, and laboratory procedures are laborious and expensive. Another option is to apply on-site automatic samplers and analyzers, which can produce continuous concentration time series of many chemicals (e.g. Jordan et al., 2007; Rozemeijer et al., 2010). Major drawbacks of this equipment are the expensive purchase, maintenance and field installation in a sheltered environment with electrical power supply. Furthermore, the complex automatic analyzers are vulnerable to technical problems and power supply failures. As a consequence, regional surface water quality monitoring will continue to rely predominantly on low-frequency grab sampling data. Therefore, improving load estimates from low-frequency concentration measurements is still an important research topic.

A favorable approach for improving load estimates from low-frequency concentration data is to make use of the explanatory strength of commonly available continuous measurements of quantitative hydrological data like precipitation, discharge, and groundwater levels. These measurements are relatively inexpensive and often already available near surface water quality monitoring locations to facilitate quantitative water management such as flood control and groundwater level management.

Previous studies focused primarily on the use of long term concentration-discharge relations to improve load estimates from low-frequency concentration data. However, in several comparison studies, none of the methods clearly outperformed the methods that were based on simple linear or stepwise interpolation (e.g. Preston et al., 1989; Smart et al., 1999). The main obstacle is the poorly understood non-stationary behavior of the concentration-discharge relationships. Especially in smaller catchments, event-scale concentrations-discharge relations are highly solute- and catchment-specific, show hysteresis, and change during the year (e.g. Jarvie et al., 2001; Jordan et al., 2007; Poor and McDonnell, 2007).

In recent studies, high-frequency measurements have increased understanding of short-scale variations of solute concentrations in surface water (Jordan et al., 2007; Harris and Heathwaite, 2005). For example, several researchers reported peaks in P-concentrations in

response to rainfall events (Stamm et al., 1998; Heathwaite and Dils, 2000). The NO_3 response to rainfall events depends on the hydrogeochemical properties of the catchment; some authors observed a lowering of concentrations (Borah et al., 2003; Chang and Carlson, 2004; Poor and McDonnell, 2007), while others detected concentration peaks in response to events (Rozemeijer and Broers, 2007; Wriedt et al., 2007; Tiemeyer et al., 2008). The new understanding of short-scale variations in water quality has not yet been applied for improved methodologies for estimating loads from low-frequency concentration data.

This study aimed at improving load estimates from low-frequency concentration measurements by reconstructing the responses of NO_3 and P concentrations to rainfall events using commonly available quantitative hydrological data. We present a unique year-round combined dataset of semi-continuous (15 minute interval) measurements of NO_3 and P concentrations, discharge, precipitation, and groundwater levels. Through a sequential multiple regression analysis, we related variables describing the water quality rainfall event responses to variables describing the hydrological responses. We applied these relations to reconstruct concentration patterns between low-frequency grab sample measurements, which significantly improved estimates of annual loads.

5.2 Methods

5.2.1 Study area and field measurements

We installed a multi-scale experimental setup in the Hupsel catchment (6.64 km²) in the eastern part of The Netherlands (Figure 5.7) (52°06' N; 6°65' E). This catchment was selected because of the dominance of agricultural land use, the dense artificial drainage network, and the absence of point sources and water inlet from outside the catchment. A detailed description of the Hupsel catchment and of all installations and measurements is given in Van der Velde et al. (2010). For this study, semi-continuous records of NO_3 and P concentrations and discharge were collected at the catchment outlet from June 2007 to July 2008. For the semi-continuous NO_3 concentration measurements we used a Hydrion-10 multi parameter probe (Hydrion BV, Wageningen, The Netherlands). Semi-continuous measurements of dissolved-P (ortho-P) and total-P concentrations were performed by a Sigmatax sampler and a Phosphax Sigma auto-analyzer (both Hach Lange GmbH, Düsseldorf, Germany). See the Supporting Information and Jordan et al. (2007) for a more detailed description of this equipment. The NO_3 concentration values in this paper are given in milligrams Nitrate per liter (mg NO_3 L⁻¹). For P, we focused our analyses on the total-P concentrations which are given in milligrams total-Phosphorus per liter (mg P-tot L⁻¹).

In addition to the automatic solute concentration measurements, we collected weekly grab samples from the catchment outlet. These weekly measurements were used to correct for the potential drift and offset of the continuous concentration measurements. The stream discharge at the catchment outlet was recorded every 15 minutes using a calibrated weir. Precipitation and groundwater levels were measured for the same period at an experimental

field within the catchment. More detailed information on our field measurements is given in the Supporting Information.

5.2.2 Event response characterization

The event responses of NO_3 and P concentrations, discharge, and groundwater levels were analyzed through a set of event response characteristics (Table 5.1), which will be discussed in this section. Firstly, we defined selection criteria for events, based on the continuous discharge records. We selected all events with a maximum discharge above 100 L s^{-1} (1.3 mm d^{-1}), a discharge increase of at least 20 L s^{-1} ($0.26 \text{ mm} \cdot \text{d}^{-1}$), and a discharge decrease after the maximum of at least 20 L s^{-1} . Less pronounced events generally did not significantly affect the load estimates, because the NO_3 and P concentrations did not respond. When varying rainfall intensities caused two discharge peaks to occur within 6 hours, these peaks were merged into one event. The start time of an event was defined as the first moment with a 5 % discharge increase within 2 hours, leading up to a discharge peak.

The events with uninterrupted records of precipitation, discharge, groundwater levels, and NO_3 or P concentrations were selected for further analysis. These rainfall events were characterized by the total rainfall amount (R_{tot}), the maximum rainfall intensity (RI_{max}), and the Antecedent Precipitation and Evaporation Index ($APEI$) (Table 5.1). The $APEI$ is a frequently used measure for the initial wetness of the catchment at the onset of the rainfall event. We derived the $APEI$ from precipitation and evaporation data, following the method described by Fedora and Beschta (1989). The Makkink relation (Makkink, 1957) was applied to estimate evapotranspiration using temperature and net incoming radiation data from the weather station within the Hupsel catchment.

The NO_3 and P concentration responses to the rainfall events were described by three event response characteristics: the maximum concentration change, the time to maximum concentration change, and the recovery time. A graphical explanation of these response characteristics is given in Figure 5.1. The maximum NO_3 concentration change during events (rdN) is described as a percentage of the starting concentration (N_s). For P, the starting concentrations (P_s) were very low relative to the peak concentrations (P_{max}). Therefore, absolute P concentration changes (dP) were more appropriate for characterizing the P concentration responses to events. The times to maximum change for NO_3 (TdN) and P (TdP) are defined as the time interval between the start of the event and the moment of maximum change. The concentration recovery time is determined by fitting an exponential recovery curve to the measured concentrations for the first 24 hours after the time of maximum concentration change. The concentration recovery is described by:

$$Rec(t) = e^{-\frac{t}{T_{rec}}} \quad [5.1]$$

where $Rec(t)$ [-] is the relative recovery of the concentration or discharge at time t when $t = 0$ represents the start of the recovery or the time of maximum change. The recovery time T_{rec} [T] for NO_3 is denoted by TN_{rec} and for P by TP_{rec} . The values for the total loads (LN

and LP) were calculated for the period between the start of the event until the time of 50% recovery of the discharge or until the start of the next event.

To characterize the discharge and groundwater level event responses, we derived the same response characteristics as described for the concentrations in the previous section (see also Table 5.1). In addition, we determined the average and the maximum discharge slope (SQ and SQ_{max}) as well as the time to the maximum discharge slope (TSQ_{max}). We also derived the average and the maximum slope of the groundwater levels (SG and SG_{max}).

Furthermore, we calculated a time series of the proportion of quick flow from the continuous discharge records. For this, we used the hydrograph separation method described by Hewlett and Hibbert (1963), with a constant separation slope of 0.2 Lh^{-2} . With this relatively low slope value, 100% base flow conditions only occur after extended dry periods and a uniform distribution of quick flow proportions over time was achieved. For each event, we determined the quick flow percentage at the start of the event (QF_s), the maximum quick flow percentage (QF_{max}), and the maximum change in quick flow percentage during the event (dQF).

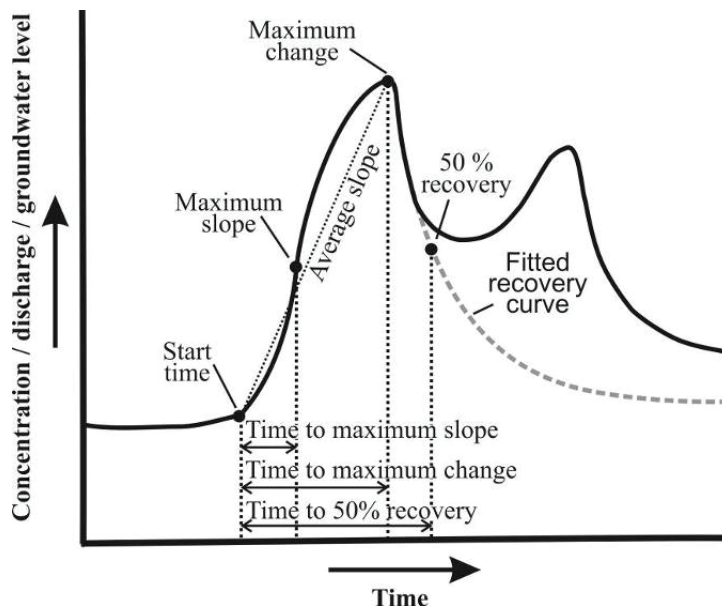


Figure 5.1. Graphical explanation of several rainfall event response characteristics. See main text for explanation.

Table 5.1. Summary of the event characteristics that were derived from the continuous measurements of the rainfall events that were analyzed in this study.

Rainfall characteristics	short	unit	Mean	Median	St. dev.
Total rainfall	<i>Rtot</i>	mm	10.1	9.3	5.4
Maximum rainfall intensity	<i>RImax</i>	mm h ⁻¹	3.3	2.8	2.4
Antecedent precipitation and evaporation index	<i>APEI</i>	-	17.4	15.1	10.1
NO ₃ characteristics	Short	Unit	Mean	Median	St. dev.
NO ₃ concentration at start of event	<i>Ns</i>	mg L ⁻¹	44.3	42.4	11.1
NO ₃ minimum concentration during event	<i>Nmin</i>	mg L ⁻¹	27.6	26.5	10.0
NO ₃ relative concentration change during event	<i>rdN</i>	%	37	37	18
Time to maximum NO ₃ concentration change	<i>TdN</i>	h	8.6	8.4	3.9
Recovery time NO ₃	<i>TNrec</i>	h	11.4	10.6	5.9
NO ₃ total load	<i>LN</i>	Kg	980	839	638
P characteristics	short	Unit	Mean	Median	St. dev.
P concentration at start of event	<i>Ps</i>	µg L ⁻¹	0.15	0.10	0.14
P maximum concentration during event	<i>Pmax</i>	µg L ⁻¹	0.94	0.77	0.89
P concentration change during event	<i>dP</i>	µg L ⁻¹	0.85	0.66	0.89
Time to maximum NO ₃ concentration change	<i>TdP</i>	h	6.8	5.0	5.4
Recovery time P	<i>TPrec</i>	h	6.1	5.5	4.0
P total load	<i>LP</i>	Kg	4.2	3.3	3.5
Discharge characteristics	short	Unit	Mean	Median	St. dev.
Discharge at start of event	<i>Qs</i>	L s ⁻¹	0.15	0.10	0.14
Maximum discharge during event	<i>Qmax</i>	L s ⁻¹	0.42	0.34	0.31
Discharge change during event	<i>dQ</i>	L s ⁻¹	0.27	0.21	0.24
Time to maximum discharge change	<i>TdQ</i>	h	11	10	6
Average slope rising discharge	<i>SQ</i>	L s ⁻¹ h ⁻¹	0.030	0.019	0.035
Maximum slope rising discharge	<i>SQmax</i>	L s ⁻¹ h ⁻¹	0.074	0.045	0.074
Time to maximum discharge slope	<i>TSQmax</i>	h	6	5	4
Recovery time discharge	<i>TQrec</i>	h	49	30	42
Total discharge	<i>Qtot</i>	m ³	8757	6963	5461
Quick flow percentage at start of event	<i>QFs</i>	%	36	42	31
Maximum quick flow percentage during event	<i>QFmax</i>	%	77	80	18
Quick flow percentage change during event	<i>dQF</i>	%	41	37	27
Groundwater level characteristics	short	unit	Mean	Median	St. dev.
Groundwater level at start of event	<i>Gs</i>	cm	-54	-57	22
Maximum groundwater level during event	<i>Gmax</i>	cm	-35	-33	17
Groundwater level change during event	<i>dG</i>	cm	20	18	12
Average slope rising groundwater level	<i>SG</i>	cm h ⁻¹	1.7	1.8	1.3
Maximum slope rising groundwater level	<i>SGmax</i>	cm h ⁻¹	5.7	5.8	3.5

5.2.3 Regression analysis

We firstly applied a singular linear regression analysis between all NO_3 and P concentration response characteristics and all quantitative hydrological event characteristics. This analysis gives an overview of the quantitative hydrological characteristics that can explain part of the variation in the NO_3 and P response characteristics to rainfall events.

Subsequently, a sequential multiple linear regression analysis was conducted. We excluded the data of 1 March to 3 April 2008 for this analysis, because we selected this period for the validation of the event response models. This period was chosen for validation because ten major and minor rainfall events affected the NO_3 and P concentrations and because our continuous time series were not interrupted by technical failures. The sequential regression analysis started with selecting the singular regressions with the highest coefficient of determination (R^2) for explaining the NO_3 and P response characteristics. Subsequently, we searched for the best regression with two explanatory variables. This regression was selected whenever the R^2 was at least 5% higher than the singular regression model. In the final step, we searched for the best regression model with three explanatory variables. Again, this model was only selected when the R^2 was 5% higher than the model with two explanatory variables. The selected event response models were validated using the data of the rainfall events during the validation period.

5.2.4 Load estimates

We first estimated the NO_3 and P loads for the validation period of 1 March to 3 April 2008. To reconstruct the NO_3 and P concentration patterns, we used our weekly samples for describing the base level concentrations and our event response models for describing the concentration changes during rainfall events. The base level concentrations were reconstructed by a LOWESS smooth interpolation (Cleveland, 1979) through our grab sample measurements during low flow conditions ($< 100 \text{ L s}^{-1}$ or 1.3 mm d^{-1}). The concentration changes during events were reconstructed by the event response models, using the quantitative hydrological event response characteristics from Table 5.1. We estimated the NO_3 and P loads from the reconstructed concentrations and the continuous discharge records. For comparison, we also calculated the ‘true’ loads based on our continuous concentration measurements. In addition, NO_3 and P loads were estimated from the interpolated concentrations without a concentration reconstruction during events. This represented a common load estimate from low-frequency grab sampling data.

As a next step, we applied the same concentration reconstruction procedure to estimate the total annual NO_3 and P loads. Again, we compared the load estimate from our reconstruction approach with a common load estimate without reconstruction and to the ‘true’ load estimate from the continuous concentration measurements. Note that our continuous concentration time series were interrupted for a few periods due to technical failures. For a fair comparison between the different load estimates, these missing data periods were excluded. However, we also made a best estimate of the total annual NO_3 and

P loads. This was achieved by using our concentration reconstruction approach to fill in the data gaps in our continuous time series of NO_3 and P concentrations.

5.3 Results

5.3.1 Field measurements and event characteristics

In total, 47 precipitation-discharge events occurred in the period from June 2007 until July 2008. Figure 5.2 shows the total time series of measured discharges and the NO_3 and P concentrations. We selected all events with complete continuous data records and excluded the events during the validation period from 1 March until 3 April. From the 47 events, 13 events were selected for NO_3 and 20 events for P. The selected events are indicated by dots in the NO_3 and P concentration graphs in Figure 5.2.

The responses of discharge, groundwater levels, and NO_3 and P concentrations to the selected rainfall events are shown in Figure 5.3. From this figure, the short term concentration responses to the events appear to be consistent throughout the year. The NO_3 concentrations repetitively show a temporal decrease in response to events. The total-P concentrations, which are generally very low, react to the events with a short and sudden increase. Our dissolved-P records showed the same temporal pattern as the total-P measurements. The dissolved-P/total-P ratio was rather constant at 40%. The event response characteristics for all rainfall events are tabulated in Table 5.3 in the Supporting Information. The summary statistics of the response characteristics are given in Table 5.1. The event characteristics show that our dataset covers a wide range of event properties and antecedent conditions.

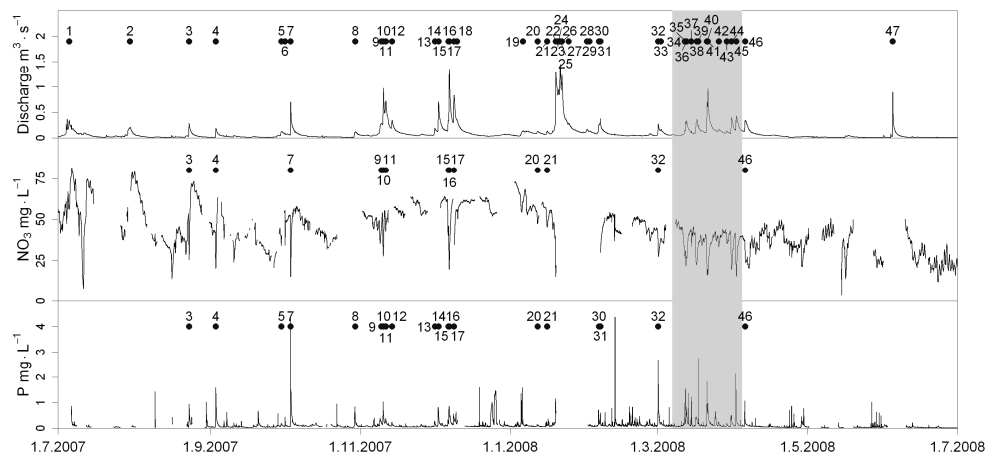


Figure 5.2. Graphs of the measured discharge and NO_3 and P concentrations from July 2007 until July 2008. The rainfall events marked in the NO_3 and P graphs were selected for further analysis; they occurred outside the validation period (indicated in grey) and have uninterrupted concentration time series.

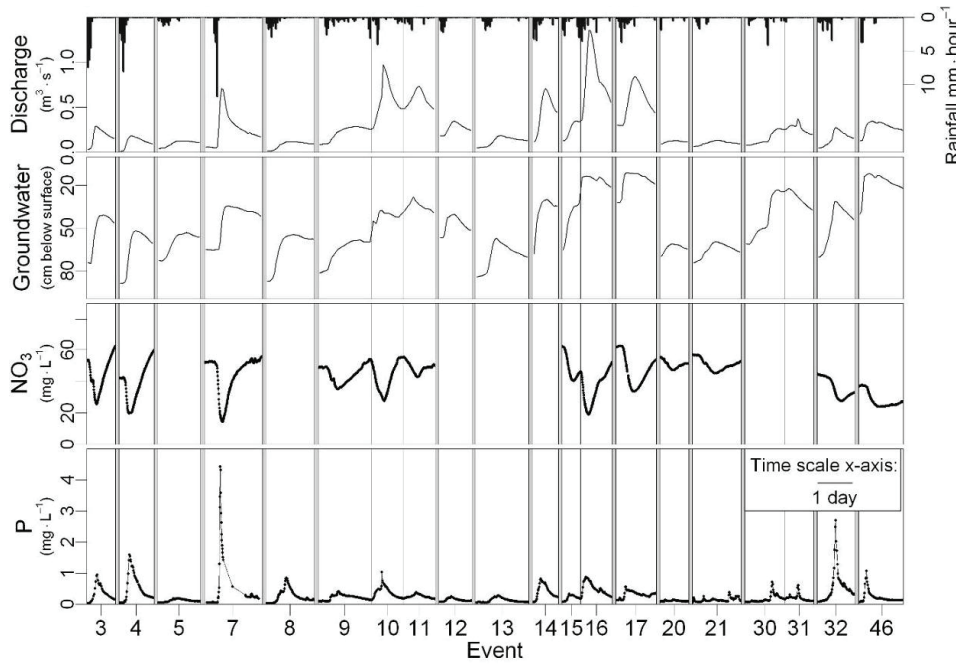


Figure 5.3. Responses of discharge, groundwater levels, and NO_3 and P concentrations to the selected rainfall events. The event numbers correspond to the numbers in Figure 5.2.

Table 5.2. Results of the sequential multiple regression analysis; the best event response models for explaining the NO_3 and P responses to rainfall events from quantitative hydrological event characteristics. The numbers between brackets are the parameter values belonging to the independent variable. For example, the response model for the relative changes in NO_3 concentrations in response to rainfall events: $rdN = 0.11 + 0.30 dQ + 0.084 SG$.

	Independent or explanatory variables				R^2
	Intercept	No. 1	No. 2	No. 3	
NO_3 event-response models					
rdN (%)	0.11	dQ (0.30)	SG (0.084)		0.95
TdN (h)	29.9	$TSQmax$ (1.14)	$\text{Log}(dQ)$ (2.84)	$QFmax$ (-29.2)	0.85
$TNrec$ (h)	29.2	$RImax$ (-1.63)	QFs (-4.6)	$Gmax$ (0.15)	0.86
P event-response models					
dP ($\text{mg}\cdot\text{L}^{-1}$)	-0.17	$RImax$ (0.24)	$APEI$ (-0.024)	$1/TQrec$ (17.0)	0.77
TdP (h)	10.82	$TQrec$ (-0.0042)	TdQ (0.87)	$QFmax$ (-14.2)	0.74
$TPrec$ (h)	1.89	$SQmax$ (-79.5)	$Rtot$ (0.45)	$Qmax$ (20.3)	0.82

5.3.2 Regression analysis

The results of the singular linear regression analysis between the NO_3 and P response characteristics and the quantitative hydrological characteristics are summarized in Figure 5.8. Table 5.2 gives the best event response models from the sequential multiple regression analysis. The coefficient of determination (R^2) for the NO_3 and P response characteristics varies from 74% for TdP up to 95% for rdN . Graphs with the measured versus the modeled NO_3 and P event response characteristics, both for the selected events as well as for the events in the validation period, are shown in Figure 5.9.

5.3.3 Load estimates

The event response models from Table 5.2 were applied to reconstruct the NO_3 and P concentration pattern for the validation period of 1 March to 3 April 2008. The reconstructed concentration patterns are shown in Figure 5.4b for NO_3 and 5.5b for P. These figures also present the actual, continuously measured concentrations and the LOWESS interpolation through our weekly grab sampling concentration measurements. The load estimates based on our reconstructed concentration patterns are shown in Figures 5.4c and 5.5c. Cumulative load estimates are given in Figures 5.4d and 5.5d. The total measured loads for 1 March to 3 April 2008 were 121 kg for P and $14.0 \cdot 10^3$ kg for NO_3 . The moving average interpolation through the low-frequency grab samples underestimated the measured P load by 63% and overestimated the measured NO_3 load by 20%. The event response reconstruction method underestimated the P load by 5% and overestimated the NO_3 load by 1%.

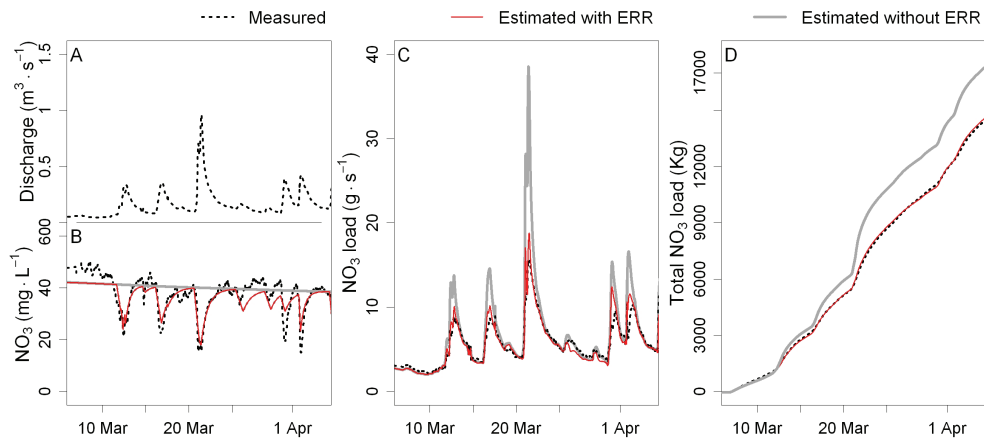


Figure 5.4. Results for NO_3 for the validation period from 1 March to 3 April 2008; the discharge records (A), the measured NO_3 concentrations, the moving average through the grab sampling measurements (without Event Response Reconstruction, ERR), and concentrations with event response reconstruction (ERR) (B), the measured and reconstructed NO_3 loads (C) and the cumulative measured and reconstructed NO_3 loads (D).

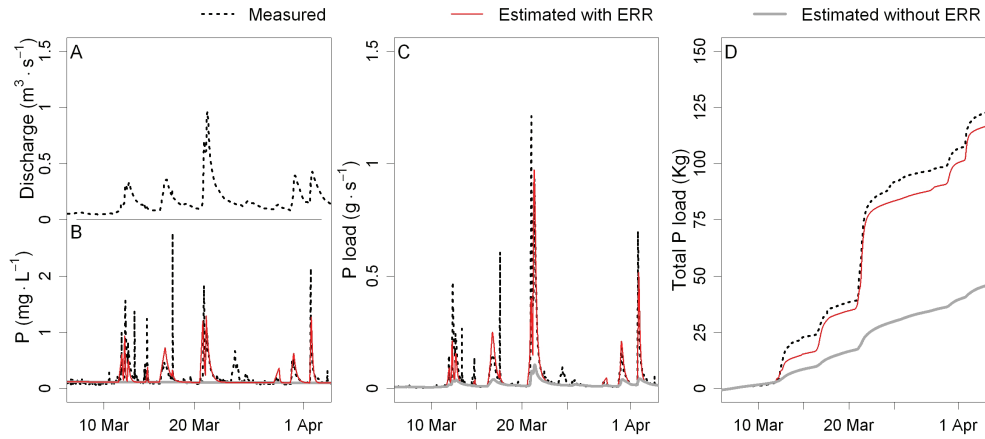


Figure 5.5. Results for P for the validation period from 1 March to 3 April 2008; the discharge records (A), the measured P concentrations, the moving average through the grab sampling measurements (without Event Response Reconstruction, ERR), and concentrations with event response reconstruction (ERR) (B), the measured and reconstructed P loads (C) and the cumulative measured and reconstructed P loads (D)

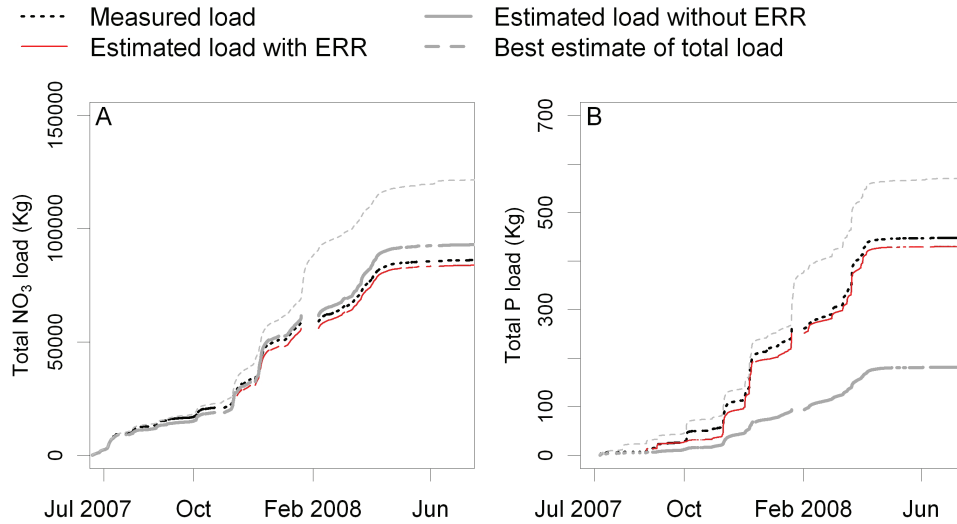


Figure 5.6. Measured and estimated annual NO_3 (A) and P (B) loads.

The results for the total annual load estimates for NO_3 and P are shown in Figure 5.6. The measured annual loads, without the missing data periods, were 448 kg for P and $86.1 \cdot 10^3$ kg for NO_3 . The LOWESS interpolation through the low-frequency grab samples

underestimated the P load by 60% and overestimated the measured NO₃ load by 8%. The event response reconstruction method underestimated the P load by 4% and underestimated the NO₃ load by 3%. The best estimates of the total annual loads for the Hupsel catchment, including the reconstructions for the missing data periods, came to 570 kg for P (0.27 kg·ha⁻¹) and 121 · 10³ kg for NO₃ (41 kg·ha⁻¹).

5.4 Discussion and conclusions

In this study, we successfully improved load estimates from low-frequency NO₃ and P concentration measurement using the explanatory strength of generally available and inexpensive quantitative hydrological data. Previously proposed methods to achieve this did not outperform standard interpolation methods (e.g. Preston et al., 1989; Smart et al., 1999). We related the rainfall event responses of NO₃ and P concentrations to precipitation records and to the responses of discharge and groundwater levels. These relations were used to improve the load estimates for our validation period from a 20% to a 1% bias for NO₃ and from a 63% to a 5% bias for P.

The foundation of this new approach to improve load estimates was a unique dataset of year-round continuous NO₃ and P measurements combined with continuous measurements of precipitation, discharge and groundwater levels. Another innovative key element was our quantification of the concentration responses to individual events, whereas previous studies primarily used long-term concentration-discharge relations for their attempts to improve load estimates (Preston et al., 1989; Smart et al., 1999). The short concentration changes during individual events are not captured by common low-frequency grab sampling, while they have a relatively large effect on total solute loads due to the simultaneous increase of the discharge.

In our research catchment, we found consistent and repetitive changes in NO₃ and P concentrations in response to rainfall events. The NO₃ concentrations dipped, while the P concentrations peaked during rainfall events throughout the year (Figure 5.3). For NO₃, similar responses to events were observed in comparable catchments by Borah et al. (2003); Chang and Carlson (2004); and Poor and McDonnell (2007). The lowering of the NO₃ concentrations during rainfall events is related to the dilution of NO₃-rich stream discharge by NO₃-poor precipitation water. The short peaks in the P concentrations in response to events are also in correspondence with previous work in comparable catchments (Stamm, 1998; Heathwaite and Dils, 2000; Jordan et al., 2007). These peaks were usually attributed to the flushing of particulate P during events. During dry periods, we observed large supplies of P-rich Fe- and Al-oxides accumulating at the ditch bottoms and inside tile drains in the Hupsel catchment. When the water flow velocities increased, this particulate P was detached and transported downstream (see also Stamm, 1998; Heathwaite and Dils, 2000; Jordan et al., 2007). In many catchments, spatial aspects influence the water quality response to rainfall events at the catchment outlet. While relevant, these within-catchment spatial variations were outside the scope of this paper. We

refer to Kirchner et al. (2000), Corwin et al. (2006), Lennartz et al. (2010), and references therein for work related to spatially varying processes.

The consistent concentration response to rainfall events implies a strong connection between the dynamics in solute concentrations and the variations in quantitative hydrological variables like precipitation, discharge and groundwater levels. This was confirmed by the results of our regression analyses. The singular regressions revealed many relations between the NO_3 and P event response characteristics and the quantitative hydrological response characteristics (Figure 5.8). Furthermore, the event response models from the sequential multiple linear regression analysis explained 74% up to 95% of the variance in the NO_3 and P response characteristics (see Table 5.2). These high coefficients of determination (R^2) supported our assumption that continuous quantitative hydrological data can be used for the prediction of the solute concentration response to rainfall events. The unexplained part of the variance in the NO_3 and P response characteristics can be attributed to uncertainties in the concentration measurements (Harmel et al., 2006), non-linearity of the relations, and possibly to seasonal changes in the concentration response to events. This seasonality in the hydrological conditions is covered by some of the explanatory variables (*APEI*, *Q_s*, *QF_s*, and *G_s*). Nevertheless, seasonality in temperature and land use also influences solute transport processes and might cause part of the unexplained variability in the NO_3 and P event response characteristics.

We applied the event response models to improve load estimates from low-frequency concentration data. Several previous studies reported on the effects of low sampling frequencies on load estimates (e.g. Kirchner et al., 2004; Johnes, 2007; Rozemeijer et al., 2010). In correspondence to this earlier work, our figures 5.4b and 5.5b clearly demonstrated the large deviations between the interpolated weekly concentrations and the actual concentrations during rainfall events. These deviations severely propagate into the load calculations, due to the simultaneous high discharges. For load estimates based on low-frequency concentration data, this results in overestimates of the NO_3 loads (Figures 5.4c and 5.4d) and underestimates of the P loads (Figures 5.5c and 5.5d). The reconstruction of the concentration patterns using the event response models produced much better load estimates, both for the validation period (Figures 5.4 and 5.5) and for the year-round measurements (Figure 5.6). In addition, we applied the response models to fill in the data gaps in the continuous water quality records. With this approach we produced the best estimates for the total yearly NO_3 and P loads of $121 \cdot 10^3$ kg ($41 \text{ kg} \cdot \text{ha}^{-1}$) and 570 kg ($0.27 \text{ kg} \cdot \text{ha}^{-1}$), respectively.

The results of this study demonstrate that using the explanatory strength of quantitative hydrological data can significantly improve load estimates. Our straightforward and transparent approach optimally combines the information about the concentration response to events from periods with frequent measurements with the information about long-term concentration patterns from low-frequency concentration data. Caution is required when extrapolating our event response models to other time periods, other catchments or other solutes. For extrapolation purposes, a process-based modeling approach would be a more

legitimate way to relate quantitative hydrological data to water quality dynamics. Nevertheless, adequate water quality modeling is complicated and often requires many input variables that are only marginally known.

The presented approach can be applied to improve load estimates for all monitoring locations with consistent relations between the dynamics in solute concentrations and the variation in quantitative hydrological variables. In some catchments, however, biochemical or human-induced variations might dominate concentration dynamics and should be accounted for. This may require different types of explanatory information, such as temperature data or loads from industrial spills. For the Hupsel Brook catchment, the high coefficients of determination (R^2) of our event response models indicated that the dynamics in NO_3 and P concentrations are primarily driven by weather-induced hydrological variations.

In this paper we showed that regional water quality monitoring would benefit from high frequent measurements during peak discharges obtained by in-situ analyzers or storm event samplers. It would be expensive and laborious to install on-site equipment for continuous measurements at all sampling locations of a regional monitoring network. However, collecting year-round continuous concentration datasets at representative locations during one year with a transportable field laboratory would be a valuable addition to a water quality monitoring network. The approach presented in this paper could then be applied to improve load estimates for periods without continuous measurements and for nearby monitoring locations in similar hydrological settings.

5.5 Supporting information

Map with the location of the Hupsel Brook research catchment (Figure 5.7). Detailed information on our field measurements. Event characteristics for the selected rainfall events between June 2007 and July 2008 (Table 5.3). Overview of the results of the singular linear regression analysis (Figure 5.8). Graphs with the measured versus the modeled NO_3 and P event response characteristics, both for the selected rainfall events as well as for the events in the validation period (Figure 5.9).

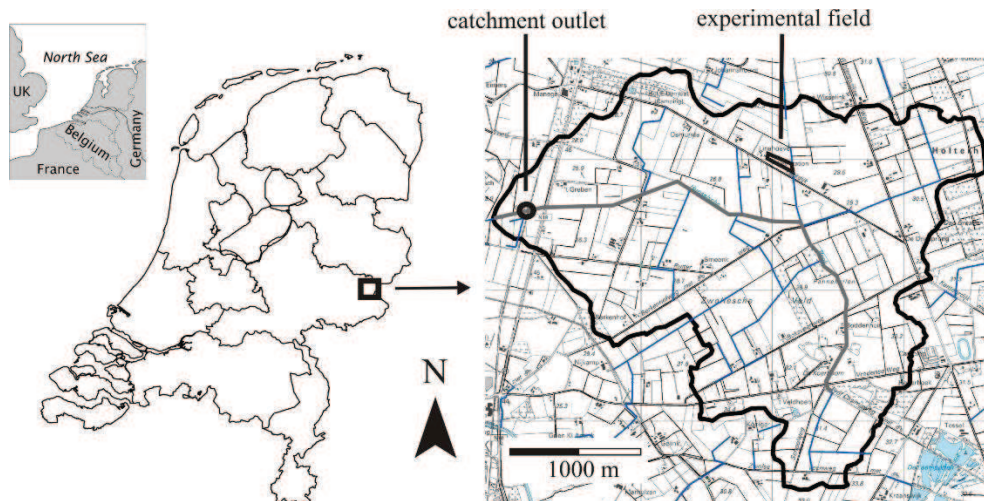


Figure 5.7. Location of the Hupsel catchment.

Measurement procedures

We used a Hydrion-10 multi parameter probe (Hydrion BV, Wageningen, the Netherlands) for continuous ion selective electrode measurements of NO_3 concentrations at the catchment outlet. The probe was placed in a flow-through cell which was continually supplied with stream water by a pump. Among other parameters, values of NO_3 , temperature, EC, and pH were stored every 10 minutes. All sensors and ion selective electrodes within the probe were cleaned and calibrated weekly.

For the P concentration measurements, we placed a Sigmatax sampler and a Phosphax Sigma auto-analyzer (both Hach Lange GmbH, Düsseldorf, Germany) at the catchment outlet. The total P concentrations were recorded every 30 minutes. The Phosphax Sigma was automatically cleaned and calibrated daily. The Sigmatax was installed for the automated stream water sample collection and the pretreatment (ultrasonic homogenization) of the 100 ml samples. The samples were not filtered and particulate P was included in the Phosphax total P measurements. A 10 ml sub-sample was delivered to the Phosphax Sigma auto-analyzer. This sample was digested using the sulphuric acid-persulphate method of Eisenreich et al. (1975). After mixing and quickly heating and

cooling down the sample, molybdate antimony and ascorbic acid were automatically added and mixed with the sample. The concentration of all P compounds, which have by now all been transformed to ortho-P, was determined by measuring the color change using a LED photometer.

In addition to the automatic water quality measurements, we collected weekly grab samples from the catchment outlet. These weekly measurements were used to correct for the potential drift and offset of the Hydrion-10 ion selective electrode NO_3 measurements. The samples were taken using a peristaltic pump and were filtered in situ ($0.45 \mu\text{m}$). Electrical conductivity and pH of the samples were measured directly in the field. The samplers were transported and stored at 4°C . Subsequently, they were analyzed within 48 hours, using IC (Ion Chromatography) and ICP-MS (Mass Spectrometry). Samples with deviating results for ions which were measured by more than one device and samples with an ionic unbalance were reanalyzed.

The stream discharge at the catchment outlet was recorded every 15 minutes using a calibrated V-shaped weir and a water level sensor. Precipitation records at 1 hour intervals were measured at a weather station of the Royal Netherlands Meteorological Institute (KNMI, De Bilt, The Netherlands), adjacent to the experimental field (Figure 5.7).

For the phreatic groundwater level measurements, we installed pressure sensors into 15 piezometers at the experimental field. The filters of the piezometers were placed 1-3 meters below the surface into the 3 meter thick sandy aquifer. The pressure sensors were installed in three transects at 1, 5, 20, 100 and 200 meters from the artificial ditch that drained the field. The phreatic groundwater levels were recorded every 10 minutes.

Table 5.3. Event characteristics for the selected rainfall events between June 2007 and July 2008. The longer names, the units, and the summary statistics of the characteristics are given in Table 5.1 in the main text.

Events	3	4	5	7	8	9	10	11	12	13	14	15	16	17	20	21	30	31	32	34	35	36	38	40	41	42	43	44	45	46	
Rainfall characteristics																															
Rtot	19.5	21.2	8.8	18.2	15.6	13.5	15.2	6.8	6.6	8.6	14.9	8.1	15.8	11.4	3.7	5.8	9.6	0.0	12.0	4.4	4.9	2.3	14.9	13.9	9	3.2	3.9	12.1	8.8	9.5	
Rlmax	7.4	8.0	1.3	11.7	2.9	2.6	4.0	1.9	2.2	1.9	3.4	2.7	3.6	3.7	1.9	1.7	4.1	0.0	3.4	1.8	3.7	1.4	1.7	3	3.4	1.1	1.7	2.4	6.1	3.7	
APEI	19	5	12	28	6	11	29	37	33	6	19	21	36	38	12	8	10	18	2	8	16	18	10	28	18	12	14	21	14		
NO₃ concentration characteristics																															
Ns	53	42	-	51	-	49	52	55	-	-	62	46	62	55	57	-	-	-	45	35	29	26	42	41	19	40	42	42	36	37	
Nmin	26	20	-	15	-	35	28	43	-	-	40	19	34	47	45	-	-	-	28	27	22	26	23	16	16	33	35	19	15	24	
rdN	52	53	-	71	-	29	47	23	-	-	35	58	46	15	21	-	-	-	38	21	30	4	46	61	18	17	17	55	58	37	
TdN	5.9	3.7	-	4.2	-	7.8	8.5	8.9	-	-	8.0	5.4	8.4	8.8	16.0	-	-	-	16.5	10.1	5.8	2.5	13.9	12.1	3.1	7.7	10.6	12.1	6.0	11.8	
TNrec	2.2	4.3	-	3.3	-	13.9	4.4	8.5	-	-	12.8	10.2	11.0	14.9	15.0	-	-	-	20.8	17.4	8.4	9.4	23.4	21.2	15.3	6.7	6.7	11.0	10.1	-	
LN	540	440	-	409	-	1286	1595	2639	-	-	554	1719	2302	1161	892	-	-	-	513	169	224	643	839	395	780	1458	679	968	1007	1329	
P concentration characteristics																															
Ps	0.05	0.05	0.06	0.07	0.04	0.10	0.15	0.20	0.09	0.07	0.08	0.09	0.20	0.14	0.10	0.07	0.050	0.205	0.08	0.18	0.22	0.57	0.09	0.10	0.62	0.10	0.09	0.08	0.14	0.08	
Pmax	0.95	1.59	0.20	4.41	0.85	0.42	1.02	0.39	0.25	0.29	0.82	0.34	0.88	0.57	0.15	0.38	0.72	0.61	2.70	1.00	1.55	0.84	0.46	1.82	0.98	0.24	0.21	0.52	2.12	1.05	
dP	0.90	1.54	0.11	4.33	0.77	0.34	0.94	0.30	0.17	0.22	0.74	0.26	0.79	0.49	0.05	0.28	0.60	0.49	2.57	0.88	1.44	0.72	0.34	1.71	0.87	0.13	0.11	0.41	2.02	0.96	
TdP	4.9	3.7	10.7	1.7	8.9	11.4	6.3	8.1	5.2	16.0	4.3	3.7	3.4	1.8	7.0	25.2	15.9	1.5	4.8	6.7	3.0	1.2	12.2	10.9	2.7	5.5	4.9	7.7	1.5	2.2	
TPrec	5.8	6.5	8.9	1.5	5.1	14.7	5.4	11.4	6.2	5.2	8.3	9.3	11.7	15.5	2.5	2.0	3.2	1.1	2.9	1.5	3.4	6.1	12.5	2.2	7.6	7.2	4.2	5.7	2.6	2.4	
LP	1.5	2.0	0.6	10.8	1.8	4.3	6.9	6.8	1.5	1.1	7.1	2.0	12.5	7.6	0.5	0.8	2.8	0.7	4.4	1.3	3.9	3.4	5.8	9.5	11.1	1.2	0.7	3.8	7.1	3.2	
Discharge characteristics																															
Qs	0.03	0.01	0.04	0.05	0.01	0.08	0.26	0.48	0.18	0.05	0.12	0.13	0.34	0.30	0.09	0.07	0.08	0.29	0.05	0.08	0.14	0.27	0.08	0.10	0.61	0.12	0.10	0.08	0.16	0.13	
Qmax	0.29	0.18	0.13	0.71	0.12	0.29	0.97	0.73	0.35	0.19	0.71	0.35	1.36	0.84	0.13	0.13	0.26	0.38	0.28	0.15	0.31	0.34	0.36	0.71	0.96	0.17	0.14	0.40	0.43	0.35	
dQ	0.26	0.17	0.08	0.66	0.10	0.20	0.72	0.25	0.17	0.14	0.59	0.22	1.02	0.54	0.04	0.07	0.19	0.09	0.23	0.08	0.13	0.07	0.28	0.61	0.36	0.05	0.04	0.31	0.27	0.22	
TdQ	7	8	15	4	17	24	8	11	8	20	9	10	6	9	10	17	24	2	13	10	6	5	19	12	5	12	11	12	7	9	
SQ	0.03	0.02	0.01	0.13	0.01	0.01	0.08	0.02	0.02	0.01	0.06	0.02	0.14	0.05	0.00	0.00	0.01	0.02	0.02	0.01	0.02	0.01	0.01	0.01	0.05	0.06	0.00	0.00	0.02	0.03	0.02
SQmax	0.10	0.05	0.01	0.26	0.02	0.03	0.21	0.04	0.03	0.02	0.14	0.05	0.26	0.10	0.01	0.01	0.04	0.05	0.06	0.02	0.07	0.02	0.03	0.20	0.17	0.01	0.01	0.06	0.09	0.07	
TSQmax	5	5	10	2	9	9	7	8	4	15	5	4	4	4	2	6	17	1	11	6	3	3	11	10	3	7	4	8	1	4	
TQrec	19	28	159	10	101	166	15	23	30	47	18	114	16	23	71	47	86	13	20	37	29	25	27	20	15	104	54	35	36	79	
Qtot	3200	2250	4276	4772	3907	16105	13763	23829	7776	6387	11726	8339	16867	18487	4107	5926	12127	2306	5479	3973	4730	5430	15859	11086	13758	6178	4693	9522	8324	7538	
QFs	42	0	47	16	54	43	78	88	60	0	52	42	76	70	24	0	70	3	23	57	77	6	0	83	0	0	0	0	42	13	
QFmax	93	93	79	94	92	81	94	92	79	72	92	77	94	89	45	49	69	77	83	61	80	81	77	86	89	27	27	78	78	68	
dQF	51	93	32	78	38	39	15	4	18	72	39	36	18	19	21	49	69	7	80	38	24	4	71	86	6	27	26	78	36	55	
Groundwater level characteristics																															
Gs	-74	-89	-73	-65	-88	-82	-55	-39	-57	-85	-70	-66	-24	-30	-70	-75	-62	-26	-71	-58	-44	-33	-58	-49	-12	-42	-46	-21	-28	-41	
Gmax	-46	-59	-55	-47	-55	-59	-39	-34	-41	-60	-30	-35	-14	-12	-62	-60	-24	-28	-31	-44	-30	-29	-20	-15	-9	-28	-36	-23	-10	-12	
dG	28	30	18	19	33	23	16	5	16	26	30	10	18	8	15	38	-2	40	14	14	4	37	35	14	10	-2	18	29			
SG	3.7	3.6	1.1	4.5	1.8	0.9	2.0	0.4	1.8	1.2	4.1	2.9	2.1	1.9	0.7	0.8	1.5	-1.2	2.9	1.3	1.9	0.5	1.8	2.7	0.5	1.1	0.8	-0.2	2.3	2.8	
SGmax	8.6	9.6	2.6	10.3	5.7	3.6	7.3	1.8	5.6	5.3	10.8	7.5	9.1	8.9	2.0	1.8	9.1	-1.1	6.8	3.7	5.9	2.1	6.3	8.6	0.8	3.2	3.9	0.1	9.6	12.0	

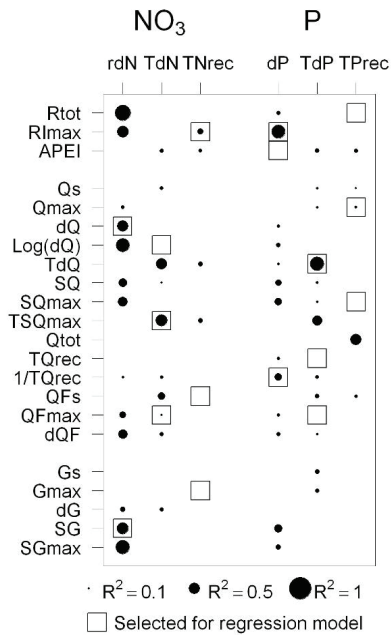


Figure 5.8. Overview of the coefficients of determination (R^2) of the singular linear regression analyses between the NO₃ and P event response characteristics and the characteristics of the discharge, groundwater levels and precipitation. No dot means that the R^2 was below 0.1. The squares indicate the variables that were selected in the sequential multiple regression analysis. The procedure of this sequential analysis (see main text) brings the possibility that the variables with the largest coefficients of determination in the singular regression are not necessarily selected in the event response models.

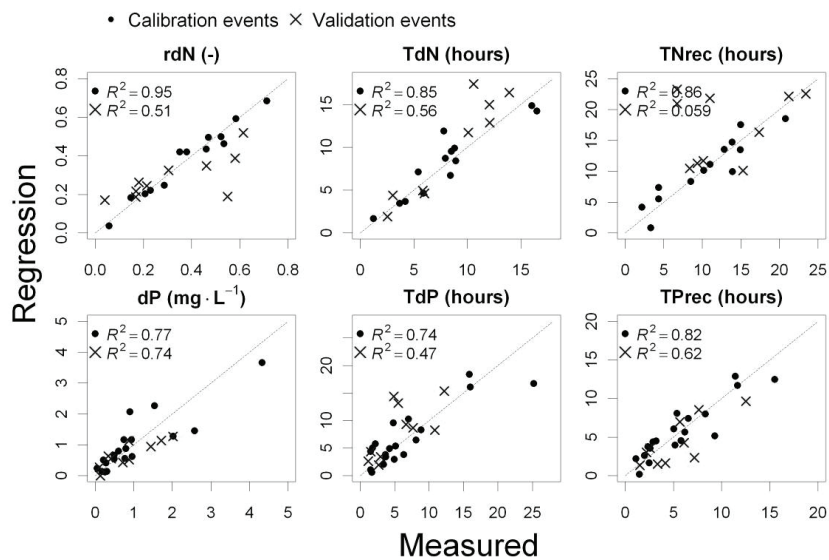


Figure 5.9. Graphs with the measured (x-axes) versus the modeled (y-axes) NO₃ and P event response characteristics, both for the selected rainfall events (dots) as well as for the events in the validation period (crosses).

The nitrate response of a lowland catchment: on the relation between stream concentration and travel time distribution dynamics

Abstract

Nitrate pollution of surface waters is widespread in lowland catchments with intensive agriculture. For identification of effective nitrate concentration reducing measures the nitrate fluxes within catchments need to be quantified. In this paper we applied a mass-transfer function approach to simulate catchment-scale nitrate transport. This approach was extended with time-varying travel time distributions and removal of nitrate along flow paths by denitrification to be applicable for lowland catchments. Numerical particle tracking simulations revealed that transient travel time distributions are highly irregular and rapidly changing, reflecting the dynamics of rainfall and evapotranspiration. The solute transport model was able to describe 26 years of frequently measured chloride and nitrate concentrations in the Hupsel Brook catchment (6.6 km² lowland catchment in the Netherlands) with an R^2 of 0.86. Most of the seasonal and daily variations in concentrations could be attributed to temporal changes of the travel time distributions. A full sensitivity analysis revealed that other measurements than just surface water nitrate and chloride concentrations are needed to constrain the uncertainty in denitrification, plant uptake, and mineralization of organic matter. Despite this large uncertainty our results revealed that denitrification removes more nitrate from the Hupsel Brook catchment than stream discharge. This study demonstrates that a catchment-scale lumped approach to model chloride and nitrate transport processes suffices to accurately capture the dynamics of catchment-scale surface water concentration as long as the model includes detailed transient travel time distributions.

This chapter is adapted from: Van der Velde, Y., G.H. de Rooij, J.C. Rozemeijer, F.C. van Geer and H.P. Broers (2010). The nitrate response of a lowland catchment: on the relation between stream concentration and travel time distribution dynamics. Water Resources Research, 46, W11534.

6.1 Introduction

Catchments without real hill-slopes, with an unconsolidated soil, a dense artificial drainage system, and with high inputs of nutrients due to intensive agriculture are found in deltas, river valleys, and plains worldwide. Polluted surface waters are an important environmental issue in all these catchments, with nutrient loads far exceeding loads in most mountainous catchments. Large-scale examples of relatively flat, densely drained agricultural plains causing nutrient pollution are the croplands in the Upper Mississippi River Basin implicated in the hypoxia in the Gulf of Mexico (Petrolia and Gowda, 2006) and the Pleistocene regions in the Netherlands whose discharge made shallow lakes turbid (Van der Molen et al., 1998).

In lowland catchments, local groundwater head gradients toward ditches and tube drains are the driving force for water flow and solute transport (Ernst, 1978; Raats, 1978). The dense artificial drainage systems create complicated dynamics in the spatial patterns of surface and subsurface fluxes of water and pollutants as they locally switch between active or passive depending on the ambient groundwater level (Van der Velde et al., 2009). The measurements of Wriedt et al. (2007) and their simulations with a simplified 2-dimensional flow model showed that temporal variations in groundwater heads and the resulting variations in groundwater flow route contributions can explain much of the observed dynamics in surface water nitrate concentrations. Thus, a hydrological model that accurately describes groundwater dynamics and the resulting fluxes of groundwater discharge, tube drain discharge, and overland flow is paramount to catchment-scale nitrate transport modeling. However, fully coupled water flow and solute transport models require many spatially distributed input parameters and are often tedious to operate at catchment scales for relevant spatial and temporal resolutions (Kollet et al., 2010).

A more conceptual approach is proposed by Seibert et al. (2009). Their Riparian Profile Flow-Concentration Integration Model (RIM-model) relates concentration-depth profiles in the riparian zone to surface water concentrations. However, to upscale this point-scale concept to an entire lowland catchment, the dynamics of the active drainage network should be taken into account. A travel time distribution (TTD) approach, as introduced by Rinaldo and Marani (1987) under the term Mass-transfer-functions, and later refined by Rinaldo et al. (1989 and 2006), relates flow routes to concentrations at basin scales. This approach is able to account for dynamic drainage networks if the TTD is allowed to change with time. The strengths of the TTD approach are that the approach is flow route-based rather than location-based, that it can be applied to large scales with only a few parameters, and that TTDs exist at any temporal and spatial scale (Sivapalan, 2003). However, the current implementations of the TTD approach at basin scales (Rinaldo et al., 2006, and Botter et al., 2005, 2008, 2009) have two major limitations. Firstly, these studies assumed a constant TTD (Rinaldo et al., 2006) or a combination of constant TTDs (Botter et al., 2008, 2009) to characterize the hydrology of a catchment. In a recent study Botter et al. (2010) showed that constant TTDs do not exist, because the travel path and travel time of a water droplet are affected by rainfall and drought events during its journey through the

catchment. Secondly, the TTD approach does not allow for spatial gradients of solutes. All previous catchment-scale transient studies using the TTD approach modeled a catchment as a completely mixed reservoir, which implies that all water droplets tend to the same equilibrium concentration independent of their location in the catchment. However, for nitrate, which is affected by denitrification, the groundwater concentration is often observed to decrease with depth or travel time (e.g. Rozemeijer and Broers, 2007; Visser et al., 2009; Zhang et al., 2009) and the TTD approach needs to be extended to include gradients along flow paths owing to denitrification.

An alternative approach to quantify catchment-scale solute transport is by studying how a signal of rainfall concentrations is converted to stream concentrations, i.e. how solute concentrations in rainfall are filtered to generate solute concentrations at the catchment outlet. It appeared that small catchments may act as fractal filters (Kirchner et al., 2000; Cardenas, 2007, 2008). These catchment filter properties are a useful tool to compare solute transport between catchments, but they only allow for the derivation of the distribution of reaction times. This reaction time distribution describes the times it takes the concentration of a stream to react on a precipitation event. It does not necessarily describe the actual contact times of water parcels with the lithosphere of a catchment. Consequently, reaction time distributions are not suited for concentration calculations in a TTD approach as proposed by Rinaldo et al. (2006). Kollet and Maxwell (2008) recognized the dynamic nature of TTDs. They used a particle tracking approach to calculate daily TTDs from a transient groundwater flow field and analyzed the resulting power spectra. However, they did not study the relation between transient TTDs and stream water quality dynamics.

Of the approaches reviewed above, transient TTDs describing the various flow routes to the stream combined with concentration profiles along the flow paths offer the best opportunity to model both the rapid and slow variations in surface water concentrations that have often been observed (e.g. Rozemeijer and Broers, 2007). The objectives of this paper are to extend the TTD approach for basin scales with transient TTDs and denitrification along flow paths, to quantify all nitrate fluxes and storages within a lowland catchment, and to assess to what extent temporal variations in TTDs can explain observed nitrate concentration changes.

A common problem in nitrate transport modeling is that the unknown nitrate flux by denitrification causes large model uncertainty (Haan and Skaggs, 2003). Visser et al. (2009) showed that this model uncertainty can partly be constrained by simultaneously solving the nitrate and chloride mass balances. If chloride (an inert, non-decaying tracer) and nitrate (a tracer with transport characteristics comparable to chloride but with denitrification) both mainly originate from agricultural inputs, the difference in behavior between chloride and nitrate can largely be attributed to denitrification. In this study we will adopt this approach of Visser et al. (2009) to partly constrain the uncertainty of the denitrification flux.

Firstly, we introduce a 26-year dataset of nitrate and chloride measurements at the outlet of the Hupsel Brook catchment (6.6 km²) during a period with declining agricultural inputs.

Secondly, we derive a catchment-scale solute transport model combining elements of the solute transport at basin scales model (Rinaldo et al., 2006, and Botter et al., 2005, 2008, 2009) and the RIM model (Seibert et al., 2009). This solute transport model is fed with transient travel time distributions derived by transient particle tracking and calibrated on measured surface water concentrations of nitrate and chloride. Thirdly, a parameter sensitivity analysis is performed and the added value of transient TTDs is evaluated.

6.2 Materials and methods

6.2.1 Study area

The Hupsel Brook catchment in The Netherlands has a long history as an experimental catchment and has been described extensively, for example by Wösten et al. (1985), Hopmans and Stricker (1989), Van Ommen et al. (1989), and Van der Velde et al. (2009, 2010). We offer a brief summary of the catchment characteristics and refer to the publications above for full details.

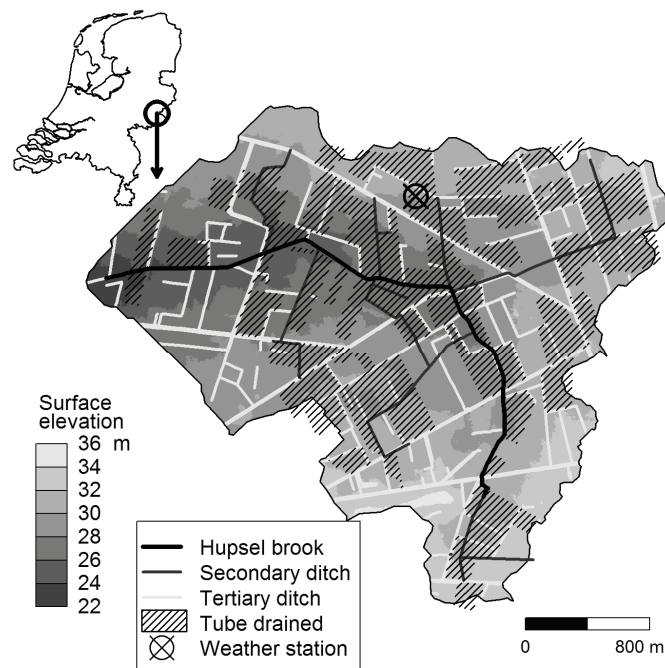


Figure 6.1. The Hupsel Brook catchment.

The Hupsel Brook catchment (Fig. 6.1) is situated in the eastern part of The Netherlands ($52^{\circ}06' N$; $6^{\circ}65' E$). The size of the catchment is 6.64 km^2 , with surface elevations ranging from 22 to 36 m above sea level. At depths ranging from 0.5 to 20 m a 20-30 m thick impermeable marine clay layer of Miocene age is found. This clay layer forms a natural

lower boundary for the unconfined groundwater flow (Van Ommen et al., 1989). The unconfined aquifer consists of Pleistocene aeolian sands with occasional layers of clay, peat, and gravel of which the spatial extent is only marginally known. The average thickness of this aquifer is around four meters, ranging from less than one to more than twenty meters. Wösten et al. (1985) classified the main soil type of the catchment as a sandy, siliceous, mesic Typic Haplaquad (See Wösten et al. (1985) for more details).

The Hupsel catchment is drained by a straightened and deepened main brook and by a dense artificial drainage network of ditches and tube drains. The spacing between the ditches averages 300 m (Fig. 6.1). Figure 6.1 also shows that tube drains were installed in approximately 50% of the agricultural fields in the catchment. The land use during the last decades has predominantly been agricultural with maize and grass land. A few small patches of forest are located in the catchment. Residential areas are absent, but individual houses and farms are scattered through the area. None of these houses is allowed to discharge waste water directly into the surface water network.

6.2.2 Collected data for period 1983-2008

6.2.2.1 Rainfall, evapotranspiration, and discharge

The meteorological station of the Royal Netherlands Meteorological Institute (KNMI) within the Hupsel Brook catchment has recorded hourly rainfall, incoming radiation, and temperature since 1993. For the period 1983 through 1992 we used data from a meteorological station located 28 km northeast of the catchment. The Makkink relation (Makkink, 1957), which requires incoming radiation and temperature, was applied to estimate daily potential evapotranspiration. Discharge records with an hourly resolution were available for the entire period.

6.2.2.2 Water quality measurements

Chloride and nitrate concentrations at the Hupsel Brook catchment outlet have been measured since 1985. The first part of the dataset was collected by an auto-sampler, taking average samples for every 5 mm of discharge (normalized by catchment area). This is the data-period with the highest temporal resolution. From 1994 through 2003 the local waterboard took grab samples with an irregular time spacing (weeks to months). Finally, we collected weekly grab samples for May 2007 till December 2008.

6.2.2.3 Chloride and nitrate input records

Nitrate and chloride inputs to the catchment are mainly agricultural inputs of manure and fertilizer. Estimates of these inputs were adopted from the work of *Van den Eerthwegh and Meinardi* (1999) for the period 1984 through 1993 and from *CBS-Statline* (<http://statline.cbs.nl>, 2009) for the period 1994 through 2007. All figures are regional estimates (260 km²) for the total input of nitrate and chloride. Deviations of 20% or more can be expected for small catchments such as the Hupsel Brook catchment. Atmospheric inputs of nitrate (2-3 mg L⁻¹) and chloride (1-2 mg L⁻¹) were small compared to the large uncertainty in agricultural inputs and were not considered.

6.2.3 Solute transport model

We developed a solute transport model for chloride and nitrate in lowland catchments. On the one hand, we wanted this model to cope with ephemeral active drainage systems which can be inferred from detailed topographic maps, soil type maps, and elevation data: properties that drive water transport (Van der Velde et al., 2009). On the other hand, the model should include catchment-scale lumped expressions for solute transport by sorption, diffusion, denitrification, mineralization, and plant uptake reflecting the lack of spatial data for solute input, chemical soil parameters, soil heterogeneity, and plant-solute interactions. For clarity, we subdivided the model into three parts: (1) Solute fluxes in the root zone, (2) catchment-scale flow route calculations within the saturated zone, and (3) solute transport with diffusion and denitrification along flow routes. The model is visualized in Fig. 6.2. The boxes in this figure represent the three parts. Definitions of the terms in this figure will be given in the corresponding paragraphs.

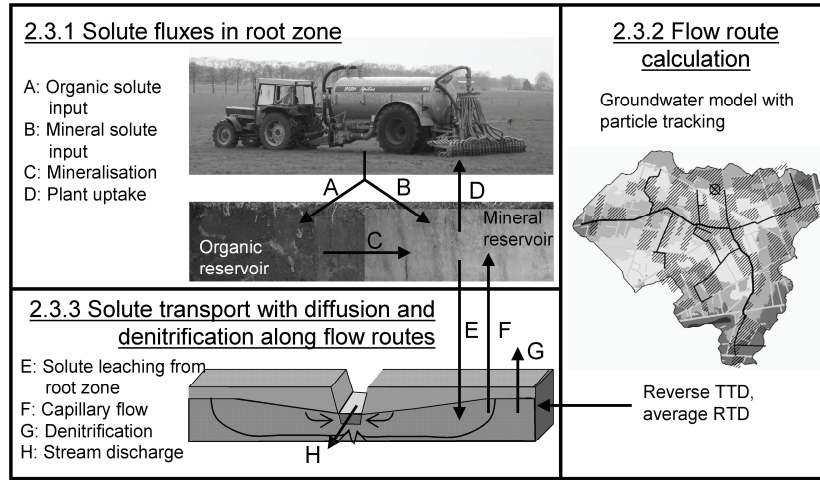


Figure 6.2. Schematic overview of the solute transport model. The headings indicate the sections of the main text detailing the model components.

6.2.3.1 Solute fluxes in the root zone

Within the root zone, mineralization of organic matter releases nitrate (Hassink et al., 1993) and plants take up large amounts of nitrate and chloride. We accounted for these processes by introducing an organic and mineral reservoir that both cover the entire catchment. We assumed that nitrate and chloride are only mobile in the mineral form: plant uptake, J_U [MT^{-1}], leaching from the root zone to the saturated zone, J_{leach} [MT^{-1}], and capillary flow from the saturated zone to the root zone, J_{cap} [MT^{-1}], can only occur with solutes in the mineral form (fluxes D, E and F in Fig 6.2.). The mass balances of the organic and mineral reservoirs are given by Equations [6.1] and [6.2], respectively:

$$\frac{dW_{org}(t)}{dt} = (1 - u_m) \cdot F(t) - r_m \cdot g_{temp}(t) \cdot W_{org}(t) \quad [6.1]$$

$$\frac{dW_{min}(t)}{dt} = r_m \cdot g_{temp}(t) \cdot W_{org}(t) + u_m \cdot F(t) - J_U(t) - J_{leach}(t) + J_{cap}(t) \quad [6.2]$$

with:

$$g_{temp}(t) = 0.1 \cdot Temp(t) \text{ for } Temp > 0 \text{ and } g_{temp}(t) = 0 \text{ for } Temp < 0 \quad [6.3]$$

The total solute mass stored in the organic reservoir is denoted by W_{org} [M], and in the mineral reservoir by W_{min} [M]. The fertilizer and manure rate is denoted by F [MT^{-1}] and u_m [-] is the fraction fertilizer in mineral form. Note that we assume that all chloride is applied in the mineral form ($u_{m\ Cl} = 1$). Consequently, chloride has no organic reservoir. The mineralization rate is denoted by r_m [T^{-1}] and is multiplied by a temperature coefficient g_{temp} [-] (Eq. [6.3]) to capture the seasonal dynamics of mineralization (Rodrigo et al., 1997). Although many studies also report considerable effects of soil moisture on mineralization (e.g. Herlihi, 1979), we did not explicitly include soil moisture. The large spatial heterogeneity of soil moisture, the correlation between soil moisture and temperature, and the lack of measured mineralization rates did not justify a more complex model that includes soil moisture. The fertilizer and manure input, $F(t)$, is derived by distributing the yearly estimated input of chloride and nitrate uniformly over the period March through October, in line with Dutch regulations on manure applications. From November through February no fertilizer is applied. Note that no spatial variation in nitrogen and chloride application was taken into account, since we described the entire catchment with a single root zone reservoir.

Plant uptake is considered proportional to the evapotranspiration flux, $E(t)$ [L^3T^{-1}]:

$$J_U(t) = \min(Cu E(t)\Delta t, W_{min}(t))\Delta t^{-1} \quad [6.4]$$

with Δt [T] the length of the calculation time step. Because plants can regulate their uptake of solutes to a large extent we defined a yearly average uptake concentration, Cu [ML^{-3}]. The minimum function (min) ensures that plants do not extract more than the available amount of solutes.

Leaching of solutes from the root zone into the saturated zone is approximated by:

$$J_{leach}(t) = \min\left(\max(P(t) - E(t), 0) \frac{W_{min}(t)}{\overline{S_{rz}}} \Delta t, W_{min}(t) - J_U(t)\Delta t\right)\Delta t^{-1} \quad [6.5]$$

with $P(t)$ [L^3T^{-1}] the rainfall flux over the entire catchment. The water flux that leaches through the root zone is assumed equal to the daily recharge: $\max(P(t) - E(t), 0)$. The term $\frac{W_{min}(t)}{\overline{S_{rz}}}$ is the average solute concentration in the root zone, with $\overline{S_{rz}}$ [L^3] the temporally averaged volume of water in the entire root zone of the catchment. The capillary flow of solutes from the saturated zone to the root zone, J_{cap} , is derived in section 6.2.3.3.

6.2.3.2 Catchment-scale flow route calculations within the saturated zone

Many studies used travel time distributions (TTDs) to describe catchment-scale flow routes (Rinaldo et al., 2006; Botter et al., 2008; Lindgren et al., 2004). TTDs can be constructed for the input as well as the output fluxes of a flow volume. Because our main interest is in the concentration of the catchment-scale discharge, we will consider TTDs for the output, from here on named the reverse TTD and denoted by f [T^{-1}]. The reverse TTD at a particular time describes for how long the water parcels that contribute to the discharge at that time have been inside the catchment. The reverse TTD is the basis for the reverse transfer function model:

$$q_{in}(t) = \int_0^{\infty} f(T, t+T) \cdot q_{out}(t+T) dT \quad [6.6]$$

where q_{in} is the influx and q_{out} the outflux of water [L^3T^{-1}]; $f(T, t)$ [T^{-1}] is the contribution of travel time T to the total reverse TTD (the distribution of travel times water parcels spent inside the catchment) of the water discharged at time t . Transfer functions can be constructed for soil volumes as well as entire catchments. Catchments, however, often have multiple exits for water as there is stream discharge, Q [L^3T^{-1}], evapotranspiration, E [L^3T^{-1}] and extraction by wells, O [L^3T^{-1}]. The reverse transfer function model for the catchment with multiple discharge routes is given by:

$$P(t) = \int_0^{\infty} f_q(T, t+T) \cdot Q(t+T) dT + \int_0^{\infty} f_e(T, t+T) \cdot E(t+T) dT + \int_t^{\infty} f_o(T, t+T) \cdot O(t+T) dT \quad [6.7]$$

where f_q [T^{-1}], f_e [T^{-1}], and f_o [T^{-1}] are the reverse TTDs of discharge via streams, evapotranspiration, and pumping.

Nitrate transforms through denitrification (bacterial decomposition of organic matter under anoxic conditions) into gaseous forms (Rivett et al., 2008). The age distribution of water stored inside the catchment describes how long nitrate has been subject to denitrification. The volume of water within the saturated zone of the catchment is denoted by $S(t)$ [L^3]. The age distribution of $S(t)$ is denoted by $h(\tau, t)$ [T^{-1}] and is from here on referred to as the Residence Time Distribution (RTD). It gives the fraction of $S(t)$ that entered at time $t-\tau$, with τ the residence time of a parcel of water inside the saturated zone of the catchment. The RTD can be expressed as a function of the out-flowing water by:

$$h(\tau, t) = \frac{1}{S(t)} \int_0^{\infty} f_q(\tau + \tau', t + \tau') \cdot Q(t + \tau') + f_e(\tau + \tau', t + \tau') \cdot E(t + \tau') + f_o(\tau + \tau', t + \tau') \cdot O(t + \tau') d\tau' \quad [6.8]$$

The deeper layers in the saturated zone have long travel times, while in the top of the saturated zone water moves fast and is constantly refreshed. This fast-flowing water,

however, is only a small portion of the total storage, and consequently has little influence on the RTD. In contrast, the out-flowing water is to a large extent influenced by these short travel times, particularly during high-discharge events. In summary, the RTD is expected to be relatively constant compared to the reverse TTD.

Transient reverse TTDs for discharge and evapotranspiration were calculated by tracking particles through a groundwater flux field generated by MODFLOW (McDonald and Harbough, 1988). The groundwater model, previously described in Van der Velde et al. (2009), was extended to include the period of 1983 through 2008. The main characteristics of the groundwater model were: a 5 by 5 meter horizontal grid resolution, daily time steps, a single layer, year-round fixed surface water levels, a fixed effective storage coefficient to describe unsaturated zone effects, and a depth-dependent evapotranspiration reduction function. Note that although year-round fixed surface water levels were used, the surface water network was only allowed to drain water, not to supply water. Drainage occurred only when groundwater levels exceeded the surface water levels, creating an ephemeral draining surface water network. Transmissivity and effective storage of the groundwater model were manually adjusted to improve the simulation results for discharge and one groundwater head measurement location for the years 1994 and 1995 (compared to the simulation results reported in Van der Velde et al., 2009). The model was validated for the years 1996 through 2001.

To calculate transient reverse TTDs, every four MODFLOW model cells received one particle for every 20 mm of rainfall. Each particle therefore represented 2000 liters of water. The average discharge of the brook is 50 L s^{-1} , which translates into a daily outflow via discharge of approximately 2000 particles on average. The effective porosity was kept at 0.35 throughout the model.

To simulate travel times longer than the runtime of the flow model, we used two modeled transient flux fields of 26 years consecutively, and performed the particle tracking over 52 years. Only the last 26 years were analyzed; the first 26 years were needed to fill the storage of the model with particles and estimates of their travel time.

6.2.3.3 Solute transport

On its journey through the subsurface, a parcel of water exchanges chloride and nitrate with neighboring parcels by diffusion. It is assumed that chloride and nitrate do not react with the soil (no sorption or desorption). In the interest of model simplicity, we only consider the end result of diffusion by relating the concentration at the time a parcel leaves the saturated zone (through capillary upward flow or the groundwater-surface water interface) to the travel time; the concentration in the discharge thus depends on discharge time t and travel time T . Botter et al. (2005) showed that for complex catchment systems, with large soil heterogeneity and dense drainage networks, surface water quality could effectively be described by travel times without knowing the exact locations of water parcel travel paths. The concentration of a single parcel of water is denoted by $c(\tau, t)$ [ML^{-3}]. The concentration change of a parcel of water along its flow route before discharging ($\tau < T$), is described by:

$$\frac{\partial c(\tau, t)}{\partial t} + \frac{\partial c(\tau, t)}{\partial \tau} = -r_n c(\tau, t) + r_d (C_{Eq}(\tau, t) - c(\tau, t)) \quad [6.9]$$

The first term on the right hand side of Eq. [6.9] describes decay of solutes (denitrification), with denitrification rate r_n [T^{-1}]. The second term describes the tendency of the parcel concentration to approach an equilibrium concentration, $C_{Eq}(\tau, t)$ [ML^{-3}] by diffusion and mixing. This process is controlled by the diffusion and mixing rate, r_d [T^{-1}]. Under complete mixing of the saturated zone, $C_{Eq}(\tau, t)$ has no spatial gradient along a travel path and is equal to the equilibrium concentration of the entire saturated zone $C_{Eq}(t)$. The spatial gradient of the water parcels concentration, $\frac{\partial c(\tau, t)}{\partial \tau}$, then is necessarily zero as well, and Eq. [6.9] reduces to:

$$\frac{\partial c(\tau, t)}{\partial t} = -r_n c(\tau, t) + r_d (C_{Eq}(t) - c(\tau, t)) \quad [6.10]$$

with:

$$C_{Eq}(t) = \frac{W_{sat}(t)}{S(t)} \quad [6.11]$$

with W_{sat} [M] the total solute mass in the saturated zone, which can be obtained by a catchment-scale solute mass balance, and S [L^3] the total water volume of the saturated zone. This approach was successfully applied for nitrate transport by Rinaldo et al. (2006) and Botter et al. (2008) for relatively short periods. However, long-term stream concentration records of nitrate in lowland catchments clearly show that lowland catchments are not completely mixed: during low discharge with long travel times, water parcels have low concentrations, while during average discharge with the associated average travel times, concentrations are much higher (e.g. Rozemeijer and Broers, 2007). This indicates that not all travel times tend to the same equilibrium concentration and that the assumption of complete mixing will not suffice to describe the seasonal dynamics of nitrate transport.

To accommodate a gradient in nitrate concentrations along a travel path caused by denitrification, we redefined the equilibrium concentration, $C_{Eq}(\tau, t)$, as the equilibrium concentration under average flow conditions after residence time τ . We also assumed that the equilibrium concentration as function of residence time can be described by instantaneously redistributing all solute mass in the saturated zone. However, the solutes are not redistributed evenly over the saturated zone, but the redistribution follows an exponential decrease in concentration with increasing travel time describing the effect of denitrification. Although physically unrealistic, this last assumption allowed us to rewrite $C_{Eq}(\tau, t)$ as:

$$C_{Eq}(\tau, t) = C_{Eq0}(t) e^{-r_n \tau} \quad [6.12]$$

with C_{Eq0} the equilibrium concentration for water parcels with zero travel time. Because $C_{Eq}(\tau, t)$ was defined as the equilibrium concentration of water parcels under average flow conditions (average storage \bar{S} and average residence time distribution $\bar{h}(\tau)$), $C_{Eq}(\tau, t)$ is also defined through:

$$W_{sat}(t) = \bar{S} \int_0^{\infty} C_{Eq}(\tau, t) \bar{h}(\tau) d\tau \quad [6.13]$$

Combined with Eq. [6.12] this gives:

$$C_{Eq}(\tau, t) = \frac{W_{sat}(t)}{\bar{S} \int_0^{\infty} \bar{h}(\tau') e^{-r_n \tau'} d\tau'} e^{-r_n \tau} \quad [6.14]$$

Note that for chloride without decay ($r_n = 0$) Eq. [6.14] is almost equal to Eq. [6.11] but with a temporally averaged storage instead of a transient storage.

The simplification of Eq. [6.9] into Eq. [6.10] is only allowed under complete mixing, $\frac{\partial c(\tau, t)}{\partial \tau} = 0$. By introducing Eq. [6.12], we violate this assumption. But as long as $r_n \ll r_d$ (which ensures that the concentration of a water parcel is largely determined by denitrification when the concentration gradients between the equilibrium concentration and the concentration of the water parcel are small), this set of equations adequately approximates Eq. [6.9].

Note that when the residence time is assumed a unique function of depth below surface (Raats, 1978; Broers, 2004; Broers and van Geer, 2005), Eq. [6.14] implies that the saturated zone concentration is depth-dependent. Similar concentration depth-profiles were used by Seibert et al. (2009) to relate surface water concentrations at the point scale to groundwater concentrations in the riparian zone. However, by making the equilibrium concentration a function of residence time instead of the depth below the soil surface, it is possible to simulate more complex systems that do not have a clear relation between depth and travel time, such as systems with ephemeral active drainage areas and tube drainage.

When we integrate Eq. [6.10] combined with Eq. [6.14] we obtain:

$$C(T, t) = C_o(t - T) e^{-(r_d + r_n)T} + \frac{e^{-(r_d + r_n)T}}{\bar{S} \int_0^{\infty} \bar{h}(\tau) e^{-r_n \tau} d\tau} \left(\int_0^T W_{sat}(t - T + \tau) e^{r_d \tau} d\tau \right) \quad [6.15]$$

with C [ML^{-3}] the concentration of water parcels leaving the catchment, and C_o [ML^{-3}] the starting concentration of a water parcel. This starting concentration is equal to the concentration of rainfall and is set to zero for both chloride and nitrate in this study. The catchment-scale mass balance of the solutes stored in the saturated zone is given by:

$$\frac{dW_{sat}(t)}{dt} = J_{leach}(t) - J_{cap}(t) - J_Q(t) - r_n \cdot W_{sat}(t) \quad [6.16]$$

with J_{cap} [MT^{-1}] and J_Q [MT^{-1}] the solute flux by capillary flow and stream discharge, respectively. The last term represents denitrification losses. The transfer function formulations of the solute fluxes leaving the saturated zone based on the reverse transfer function approach are:

$$J_Q(t) = Q(t) \int_0^{\infty} f_q(T, t) \cdot C(T, t) dT \quad [6.17]$$

$$J_{cap}(t) = \max[(E(t) - P(t), 0)] \int_0^{\infty} f_E(T, t) \cdot C(T, t) dT \quad [6.18]$$

Travel times within the surface water are not considered, which limits this approach to small catchments with surface water travel times far smaller than the travel times through the saturated zone.

6.2.4 Calibration and sensitivity analysis of the solute transport model

First, we optimized the model parameters with the parameter estimation code PEST (Doherty, 2002) on the entire nitrate and chloride stream concentrations data set. For this calibration with a single objective function we assumed no uncertainty in the parameters that resulted from the groundwater model (f_q , f_E , \bar{h} , and \bar{S}) and optimized the seven solute transport parameters (r_d , \bar{S}_{rz} , Cu_{Cl} , u_m , r_n , r_m , Cu_N). The rate of diffusion and mixing, r_d , and the average root zone water volume, \bar{S}_{rz} , were assumed equal for both nitrate and chloride. Via these two parameters the surface water chloride measurements could partly constrain the uncertainty in the nitrate mass balance. Plausible parameter ranges for all seven parameters were estimated from literature and field experience (Hassink, 1992; Schils and Kok, 2003; Haan and Skaggs, 2003) and are given in Table 6.1. Furthermore, the yearly inputs of chloride and nitrate were allowed to vary within ranges of 0.8 to 1.2 times the estimated inputs (which were regional estimates). Note that the calibration of the yearly inputs only helps to explain the observed yearly fluctuations in stream concentration, but does not describe travel time-related variations driven by seasonality and rainfall events (short-term concentration dynamics).

We subdivided the model period in eight time-intervals based on measurement type and frequency. For each of these intervals we not only calculated an average model error, $Er[-]$, but also calculated the $EAD[-]$; a measure that describes how well the model reproduces the temporal variations in surface water concentrations. The latter is derived from a plot showing the average difference between concentrations for 5 time-lag classes up to one month: 0-2 days, 2-5 days, 5-10 days, 10-20 days, and 20-30 days. We refer to this plot by Averaged Difference Plot, ADP (see Appendix A for a detailed derivation). For the calibration with PEST both error terms and an additional error term describing the difference between estimated and calibrated nitrate and chloride inputs were combined in

an objective function. We refer to Appendix B for a detailed description of the error terms and the objective function we minimized with PEST.

The uncertainty of the model results obtained by the optimized model, and the parameter sensitivity, were assessed by a global parameter sensitivity analysis of all parameters including the parameters that originated from the groundwater model. These parameters from the groundwater model (i.e. transient reverse TTD, the average RTD, and the average storage) were not recalculated because of excessive calculation times of the groundwater model. Instead, the sensitivity of the model to the calculated TTDs and RTD was evaluated by shifting the contributions of travel times within the distributions to larger contributions of younger or older water. The adjusted contribution of a certain travel or residence time was calculated by multiplying the original contribution with a shift factor, Um [-]:

$$Um(T, t) = \frac{\max \left[a \log \left(\frac{T}{\bar{T}(t)} \right) + 1, 0 \right]}{\int_0^{\infty} f(T, t) \cdot \max \left[a \log \left(\frac{T}{\bar{T}(t)} \right) + 1, 0 \right] dT} \quad [6.19]$$

with a [-] the shift parameter that shifts the mean of the distribution (a_f for the reverse TTD, a_h for the RTD), and $\bar{T}(t)$ the mean travel or residence time for time t . Positive a -values correspond to an increase and negative values to a decrease of the mean travel or residence time. The sensitivity of the model to the total average water storage in the saturated zone, \bar{S} , was evaluated by changing the soil porosity, por [-]. The sensitivity of the model to the inputs was evaluated by multiplying the calibrated inputs (PEST calibration) with a multiplication factor, Im . We randomly selected parameter sets from the ranges of Table 1 (uniform distributions). Models were designated “behavioral” when the average Er of the eight time intervals was less than 20%, the average EAD was less than 20%, and the R^2 was larger than 0.6. From 500 “behavioral” models the parameter correlations, the correlation between parameters and model output, and the model output uncertainty as a result of parameter equifinality were analyzed.

After calibration of the combined chloride and nitrate solute transport model with transient TTDs and evaluating the uncertainty of the calibrated solution caused by parameter equifinality (Beven and Freer, 2001), the optimal parameter set from the PEST calibration was used to run the same solute transport model with a time-averaged TTD. The time-averaged TTD is the flux-weighted average TTD for 26 years of calculated daily TTDs. This last calculation allowed us to assess the added value of transient TTDs over a single constant TTD.

Table 6.1 Calibrated parameter values and estimated parameter ranges used in the sensitivity analysis

Parameter		Parameter range	Calibrated value
r_d	Diffusion rate [d^{-1}]	0.01 – 0.5 [#]	0.20
$\overline{S_{rz}}$	Average water volume per area of the root zone [m]	0.05 – 0.15	0.093
Cu_{Cl}	Average chloride concentration of water taken up by plants [$mg L^{-1}$]	5 – 20	9.7
u_{mN}	Mineral fraction of nitrate input [-]	0.4 – 0.6	0.53
r_n	Denitrification rate [d^{-1}]	$1 \cdot 10^{-4} - 1 \cdot 10^{-2}$ [#]	0.0025
r_m	Mineralization rate [d^{-1}]	$1 \cdot 10^{-6} - 1 \cdot 10^{-4}$ [#]	$6.7 \cdot 10^{-5}$
Cu_N	Average nitrate concentration of water taken up by plants [$mg L^{-1}$]	150 – 350	261
a_f^*	TTD “shift parameter”	-0.1 – 0.3 ^S	0.0
a_h^*	RTD “shift parameter”	-0.1 – 0.3 ^{&}	0.0
Im_{Cl}^*	Fertilizer chloride input multiplier	0.8 – 1.2	1.0
Im_N^*	Fertilizer nitrate input multiplier	0.8 – 1.2	1.0
Por^*	Soil porosity \rightarrow total average storage	0.3 - 0.45	0.35

* parameter only used in the sensitivity analysis

[#] parameter values are drawn from log-transformed ranges

^S median travel time varies between 0.9 yr and 2.6 yr; $a_f = 0$ corresponds to a median travel time of 1.8 yr.

[&] median residence time varies between 2.1 yr and 4 yr; $a_h = 0$ corresponds to a median residence time of 3.1 yr.

6.3 Results and Discussion

6.3.1 Observed surface water concentrations and estimated agricultural inputs

The datasets of estimated chloride and nitrate inputs from agriculture and measured surface water concentrations of the Hupsel Brook catchment are shown in Fig. 6.3. The surface water concentrations of chloride and nitrate followed the decreasing trend in agricultural inputs. Both solutes also showed considerable seasonal and short-term fluctuations, the latter related to individual rain events. The seasonal fluctuations of nitrate concentrations were larger than those of chloride. The nitrate concentration approached zero during summers, while the chloride concentration remained relatively high. We infer that during low flows with long travel times, denitrification led to the observed low nitrate concentrations.

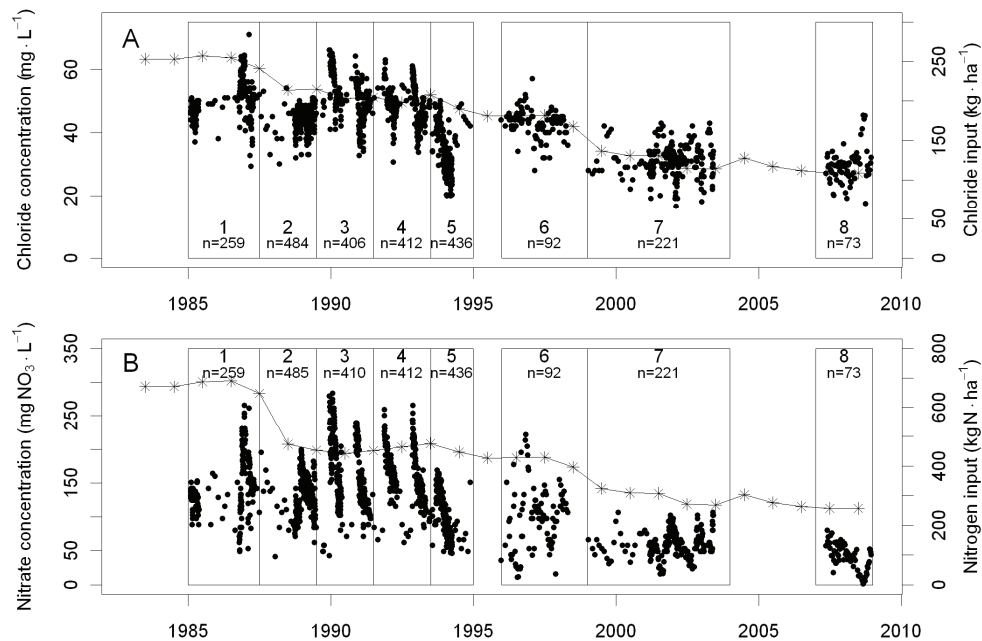


Figure 6.3. Chloride(A) and nitrate (B) concentrations in the Hupsel Brook (dots) and estimated chloride and nitrogen fertilizer inputs (line). The boxes 1 to 8 represent the eight intervals in which the dataset was subdivided during simulation and n denotes the number of measurements in each period.

6.3.2 Flow route calculation by groundwater model and particle tracking

Figure 6.4 shows the validation results of the groundwater model for the period 1996–2001. Good results were obtained for discharge as well as groundwater heads. The largest deviations between measured and predicted discharges between 500 and 5000 m³d⁻¹ are mainly caused by a few events that were either missed or falsely predicted by the groundwater model.

For every day during the model period of 26 years, a unique reverse TTD of the discharge was calculated by particle tracking through the transient flux field generated by the groundwater model. Figure 6.5 shows the results for an arbitrary chosen wet (high discharge) and a dry (low discharge) day. The logarithm of the travel time on the horizontal axis better reveals contributions of many different flow routes, each with characteristic time scales, than the travel time itself. Rainfall events in the past created the spiked shape of these outflow distributions: the reverse TTD will be zero for a travel time of j days if it did not rain j days ago. Particularly for relatively small travel times this produces pronounced spikes and ‘valleys’ in the reverse TTD. The spiked behavior for short travel times averages out for longer travel times because the averaging classes to derive the distribution cover larger time intervals (they are equidistant in log-time). With infinitely small classes

the entire distribution would be spiked reflecting contributions of all individual historical rainfall events.

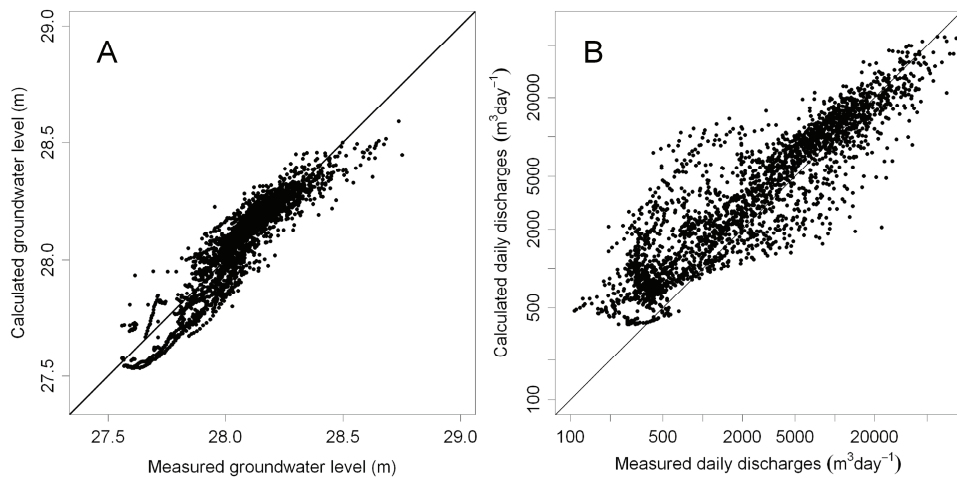


Figure 6.4. Validation results of the groundwater model for the period 1994-2001. Figure **A** shows the results for a groundwater level measured at the meteorological station; Figure **B** shows the results for the discharge at the catchment outlet.

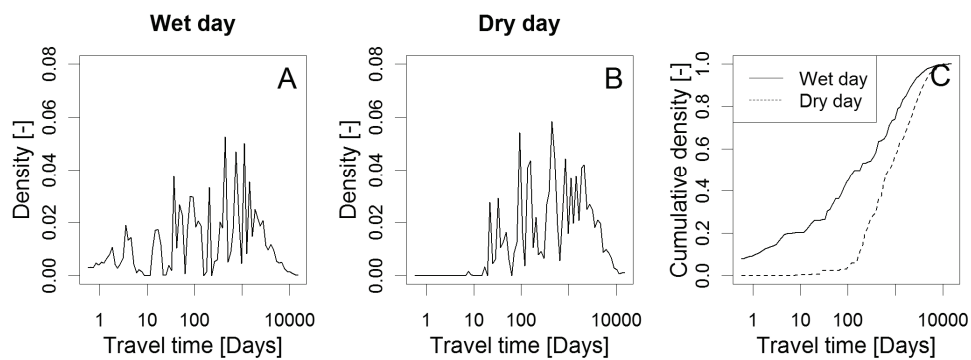


Figure 6.5. Reverse TTD for a wet day (**A**) and a dry day (**B**) and the cumulative reverse TTDs for both days (**C**).

Figure 6.6A shows the reverse TTDs for every day during the entire model period with the values of the vertical axis of figure 6.5A displayed in a color gradient. Vertical cross-sections in Fig. 6.6A give the reverse TTD of individual days as given in Figs. 6.5A and 6.5B. For any given day, Fig. 6.6A gives the contribution of all rainfall events in the past to the discharge of that day. The effect of individual rain showers and dry periods that appear as spikes in Fig. 6.5, appear in Fig 6.6A as bands that curve upward and to the right. Figure

6.6A shows that the individual spikes in Figs. 6.5A and 6.5B belong to a complex structure of time varying contributions of past rainfall events to the current discharge. The higher up in the graph, the longer ago the rainfall or drought event that caused the signal occurred. The curvature of the bands is caused by the logarithmic vertical scale. On a linear vertical scale the time-time space would create straight lines, but the detail for short travel times would be lost.

Figure 6.6B gives the average discharge-weighted reverse TTD with the 10% to 90% percentile. The average daily median travel time is 1.8 years, with the 0.1 quantile of daily median travel times at 0.72 years and the 0.9 quantile at 2.74 years. The hump for short travel times (<10 days) represents contributions of fast flow routes, such as overland flow and tube drainage. Especially during high flow periods the fast flow routes (<10 days) contribute significantly to the reverse TTD.

6.3.3 Solute transport model results

6.3.3.1 Calibration results

Simultaneous calibration of the chloride and nitrate transport model with PEST led to the optimal parameter set of Table 6.1. Figure 6.7 shows the simulation results for the eight selected time intervals, together with the observations. The behavior of both chloride and nitrate is captured well by the model. Chloride in Fig. 6.7 shows a slowly seasonally varying background concentration, with dilution during peak discharges. Nitrate shows more concentration variations than chloride. In many years, the nitrate concentration peaks in autumn during the first one or two discharge events. These peaks become less pronounced during the flushing season, during which most nitrates leached out of the catchment or were removed by denitrification.

The model performance was evaluated by the Er (relative absolute error), EAD (a dimensionless measure for temporal variation, Appendix B) and R^2 for each of the eight time intervals (Table 6.2). Overall satisfactory results for chloride and nitrate were obtained; an Er of around 8% for chloride and 12 % for nitrate; R^2 around 0.65 for chloride and 0.70 for nitrate. The best results are obtained for periods with large concentration variations such as periods 2, 3, and 4.

The Averaged Difference Plots (ADPs) of all intervals show good agreement between measurements and simulations (Fig. 6.8). This indicates that the nature of the observed temporal variations was well simulated by the model after calibration.

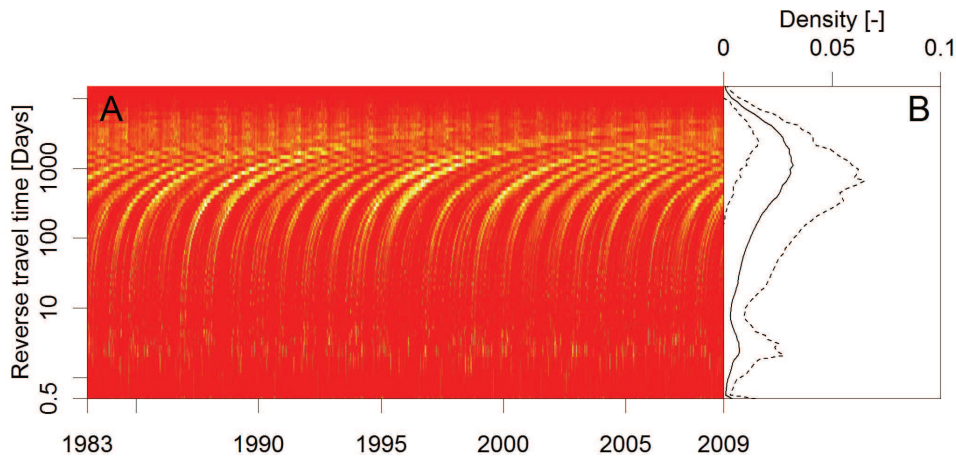
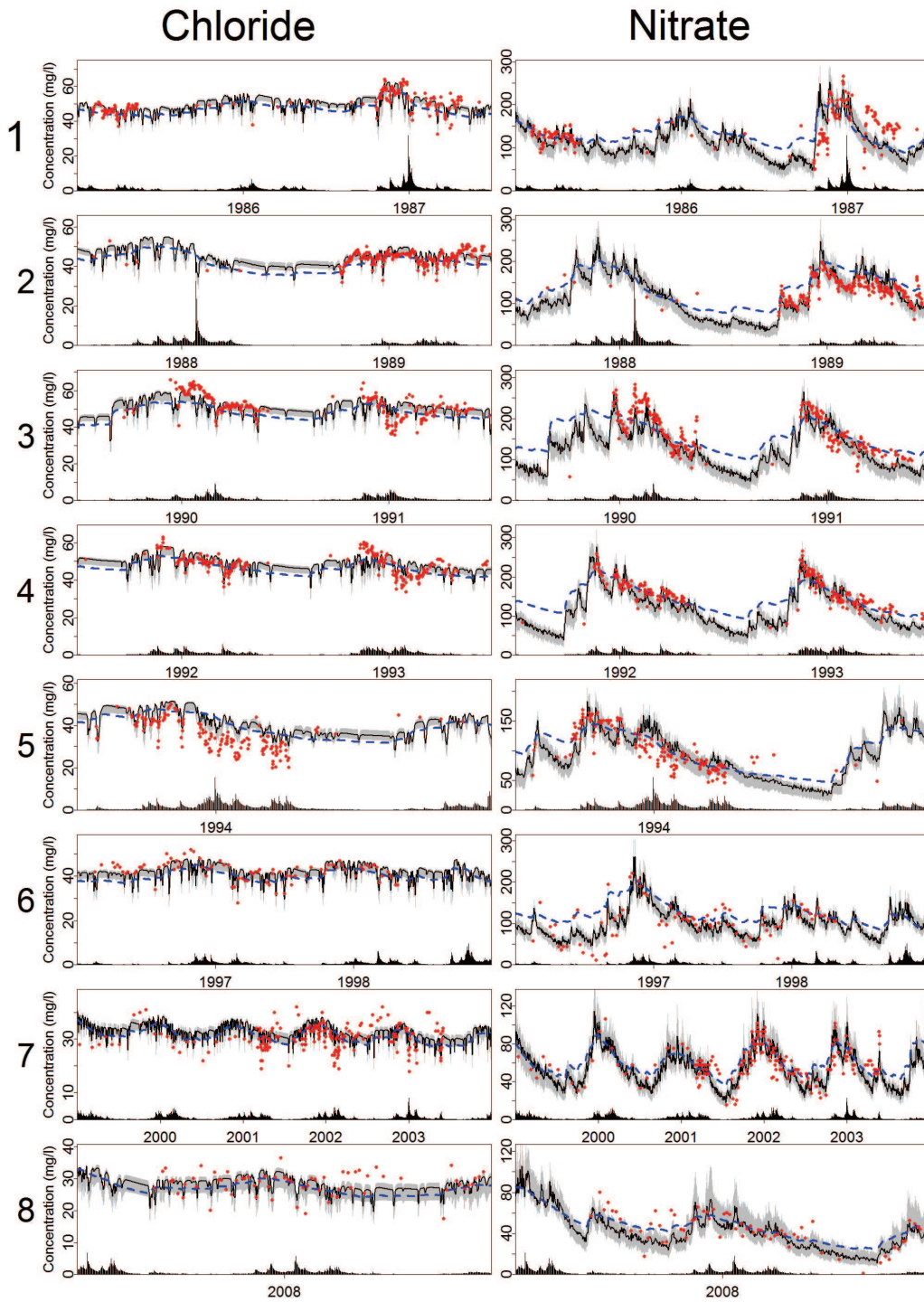


Figure 6.6. Daily reverse travel time distributions. The color gradient indicates the density of the distribution (values of 0 – 0.1, red to yellow) (A). Figure B gives the average (solid line) and 10 and 90 percentile of daily densities around the average (dotted lines).

Table 6.2 Model results after calibration by PEST. *Er* is the mean Error of the modeled concentration Relative to the measured concentration (i.e., if the absolute values of the difference between measured and modeled concentration within a time period are, on average, 4% of the measured concentration *Er* will be 0.04); *EAD* is the mean Error of the modeled Average Difference plot relative to the measured Average Difference Plot.

Period	Chloride			Nitrate		
	<i>Er</i> [-]	<i>EAD</i> [-]	<i>R</i> ² [-]	<i>Er</i> [-]	<i>EAD</i> [-]	<i>R</i> ² [-]
1 Jan 1983 – Jul 1987	0.04	0.06	0.71	0.17	0.25	0.43
2 Jul 1987 – Jul 1989	0.03	0.23	0.66	0.08	0.12	0.76
3 Jul 1989 – Jul 1991	0.05	0.17	0.62	0.11	0.14	0.77
4 Jul 1991 – Jul 1993	0.05	0.15	0.72	0.06	0.06	0.88
5 Jul 1993 – Jan 1996	0.15	0.27	0.65	0.13	0.22	0.69
6 Jan 1996 – Jan 1999	0.04	0.26	0.75	0.19	0.16	0.64
7 Jan 1999 – Jan 2007	0.08	0.29	0.49	0.11	0.14	0.70
8 Jan 2007 – Dec 2008	0.07	0.12	0.47	0.18	0.06	0.61
Jan 1983 – Dec 2008	0.06	0.05	0.86	0.11	0.19	0.86

Figure 6.7 (next page). Stream water chloride and nitrate concentrations for each of the eight time intervals of Fig. 6.3. The dots are the measurements. The solid line is the PEST simulation with transient reverse TTDs, the dashed line is the simulation with an average reverse TTD. The grey band envelopes the results of the “behavioral” runs from the sensitivity analysis. The bars at the bottom axis give an indication of the discharge at the catchment outlet (modeled).



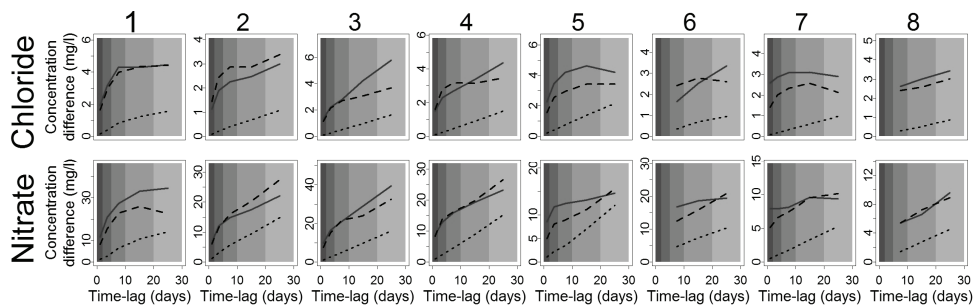


Figure 6.8. Average absolute Difference Plots (ADP, appendix A) for the eight modeled time intervals (Fig. 6.3) for chloride and nitrate. The five time-lag classes (0-2, 2-5, 5-10, 10-20, 20-30 days) of the ADP are indicated by the five shades of grey. The average concentration difference for each time-lag class is indicated by the value of the lines in the center of the time-lag class. The measurements are represented by the solid line, the model with transient reverse TTDs by the dashed line, and the model with constant reverse TTD by the dotted line.

6.3.3.2 Mass balance

Table 6.3 gives the solute mass balance for each of the time-intervals resulting from the PEST-calibration. The results show that the mineral chloride storage was around three times the yearly input during the entire model period. The chloride storage decreased with decreasing inputs from 620 to 280 kg ha⁻¹. Stream discharge removed around 80% of the yearly chloride input. Plants took up an increasing percentage of yearly input starting around 20% in 1985 to almost 40% in 2008. This relative increase was mainly caused by the decreasing input.

The model results show that nitrate storage in the organic reservoir of the root zone was very large (more than 20 times the yearly input). This is confirmed by a soil nitrogen survey on a 40 ha farm in the Hupsel Brook catchment in January 2006. An average soil nitrogen content of 2.3 gN kg⁻¹ dry soil was found. For an organic root zone of 35 cm this amounts roughly to 9·10³ kgN ha⁻¹. The decreasing N-inputs during the last time-intervals appeared to deplete the organic reservoir. Plant uptake remained relatively constant around 240 kgN ha⁻¹. Variations in plant uptake are primarily a function of evapotranspiration, but especially during the last time intervals this uptake was only possible by decreasing the mineral and organic storage. The total mineral nitrate storage was around one third of the yearly input, which is much less than the mineral storage for chloride. This difference is caused by denitrification of nitrate in the mineral phase. Between 25 to 40% of the yearly nitrogen input is removed by denitrification and another 20% leaves the catchment by discharge.

Table 6.3. Mass balances of chloride and nitrate for the eight simulated time-intervals calibrated by PEST. Indications of the uncertainty of the mass balance terms based on the sensitivity analyses are added in super-script.

		Time interval							
		1	2	3	4	5	6	7	8
Chloride	Yearly Input (kg ha ⁻¹ yr ⁻¹)	229 ¹	198 ¹	187 ¹	163 ¹	186 ¹	160 ¹	141 ¹	116 ¹
	Mineral storage (kg ha ⁻¹)	627 ²	575 ²	643 ²	611 ²	523 ²	528 ²	413 ²	355 ²
	Total storage change (kg ha ⁻¹ yr ⁻¹)	8	7	7	-24	-61	-18	-11	-26
	Removal by discharge (kg ha ⁻¹ yr ⁻¹)	182 ¹	159 ¹	146 ¹	154 ¹	209 ¹	139 ¹	112 ¹	99 ¹
	Removal by plant uptake (kg ha ⁻¹ yr ⁻¹)	39 ³	33 ³	34 ³	33 ³	36 ³	39 ³	40 ³	43 ³
Nitrogen	Yearly Input (kgN ha ⁻¹ yr ⁻¹)	639 ²	569 ²	518 ²	453 ²	412 ²	449 ²	276 ²	221 ²
	Organic storage (kgN ha ⁻¹)	9431 ¹	9603 ¹	9609 ¹	9608 ¹	9551 ¹	9496 ¹	9173 ²	8557 ²
	Mineral storage (kgN ha ⁻¹)	246 ³	277 ²	298 ²	269 ²	182 ³	234 ²	114 ³	82 ³
	Total storage change (kgN ha ⁻¹ yr ⁻¹)	100	59	-8	-53	-71	-55	-100	-147
	Removal by discharge (kgN ha ⁻¹ yr ⁻¹)	126 ²	132 ¹	109 ²	115 ²	136 ²	96 ²	53 ²	46 ²
	Removal by plant uptake (kgN ha ⁻¹ yr ⁻¹)	240 ³	201 ³	208 ³	201 ³	219 ³	240 ³	243 ²	261 ²
	Removal by denitrification (kgN ha ⁻¹ yr ⁻¹)	173 ³	177 ³	209 ³	189 ³	126 ³	168 ³	79 ³	61 ³

¹ Standard deviation “behavioral runs” less than 10% of mean value.

² Standard deviation “behavioral runs” less than 20% of mean value.

³ Standard deviation “behavioral runs” less than 40% of mean value.

6.3.3.3 Sensitivity analysis

The results of the sensitivity analysis are summarized in Fig. 6.9. Behavioral nitrate simulations are sensitive to travel time (a_f), diffusion rate (r_d), and denitrification rate (r_n), while the chloride simulations are more sensitive to the uptake concentration of plants and the fertilizer inputs. The correlation between errors in simulated chloride concentrations of the surface water and the denitrification rate shows that the coupled chloride and nitrate calculation partly constrained the uncertainty in the calculated denitrification flux. The correlations between parameters (Fig. 6.9B) reveal that travel time distributions are highly correlated with rate coefficients of diffusion and denitrification. This indicates that because both travel times and catchment-scale rate coefficients are uncertain and very difficult to measure, only the combination of travel time distributions with rate coefficients can be linked to measured concentrations. In Fig. 6.7 the results of the behavioral runs for the stream concentration are indicated by the grey band around the solution found by PEST. The bandwidth of the behavioral solutions seems to increase with time. This is probably caused by decreasing inputs that lead to a relative increase in the contribution of mineralization as a source for nitrate in discharge. The organic storage and mineralization, however, have not been measured and are relatively uncertain.

The high correlations between some parameters (Fig. 6.9B) indicate model over-parameterization, which resulted in relatively large uncertainties for those fluxes and storages that could not be measured. The chloride input and the chloride uptake by plants for example, have a strong negative correlation (Fig. 6.9B), which implies that when the uncertainty in at least one of these fluxes cannot be constrained by measurements, neither of them can be accurately determined.

An indication for mass-balance uncertainty is given in Table 6.3. In general the uncertainty for the nitrate mass balance is larger than that for the chloride mass balance. Figure 6.9A shows that the results for chloride are most sensitive to the inputs and to plant uptake. As a consequence, only small ranges of possible chloride inputs yield a usable (behavioral) model, which results in a small uncertainty for the chloride inputs (Table 6.3). The nitrate results, however, are most sensitive to the travel times and reaction rate parameters that can compensate for input uncertainty. Hence, wide ranges of nitrate inputs can yield good models (depending on travel time and reaction rate parameters), and the uncertainties in nitrate input therefore remained relatively large. These uncertainties propagated to all other mass balance terms. The denitrification flux is the most uncertain flux with a coefficient of variation of 20 to 40%. Evaluation of all behavioral runs showed that denitrification removed between 20 and 60% of the yearly input of nitrate and hence is a more dominant removal mechanism than surface water discharge (15-35%) in the Hupsel Brook catchment.

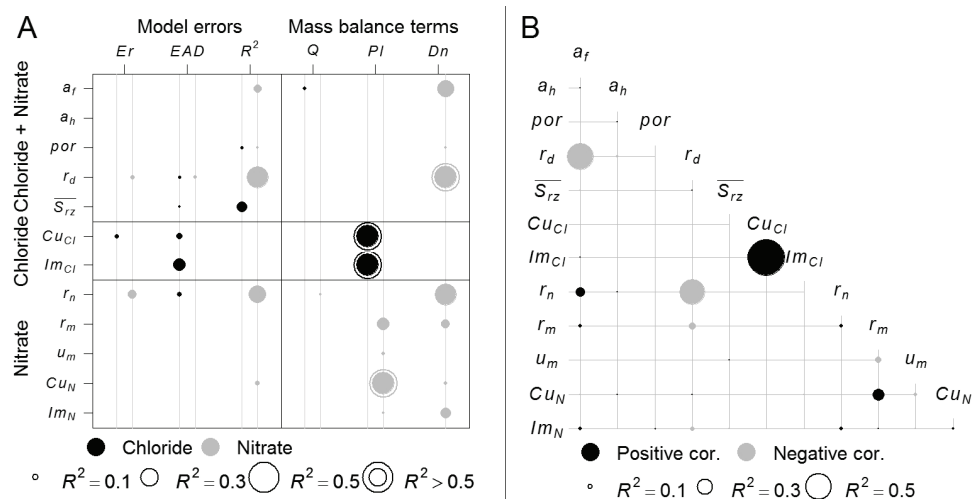


Figure 6.9. Sensitivity and correlation analysis of the 12 model parameters describing chloride and nitrate transport. Figure A shows the sensitivity of the model errors to the parameters and the correlations between parameters and three selected mass balance terms for both chloride and nitrate: Q = removal by discharge, PI = removal by plant uptake and Dn = removal by denitrification. Figure B shows the correlations between parameters. Only correlations larger than 5% are shown. A distinction is made between positive and negative correlations.

6.3.3.4 Transient TTD versus constant TTD

In Fig. 6.7 we compared a model with transient reverse TTDs to a model with constant average reverse TTD (the mean reverse TTD of Fig. 6.6B). It is clear that using transient instead of average reverse TTDs gives a much better representation of the dynamic nature of the solute concentrations.

The dilution of chloride concentrations during peak discharges is not grasped by the model with a constant reverse TTD. Because the mass balance needs to be maintained, this model compensates for this by lowering the chloride concentration during low flow periods. During summer, discharge is relatively old. Due to more denitrification of nitrate in older water, the calculated nitrate concentrations during summer of the transient reverse TTD model are considerably lower than of the constant reverse TTD model. The ADPs for chloride and nitrate in Fig. 6.8 also clearly demonstrate that the model with transient reverse TTDs much better describes observed surface water concentration changes.

6.3.4 Implications for travel time distributions

Hydrologists have often tried to find smooth analytical approximations for TTDs based on stationary flow fields that could also describe the reaction of a catchment to rainfall (Rinaldo et al., 2006; Botter et al., 2008; Lindgren et al., 2004). In Fig. 6.5 we show that travel time distributions are not smooth but spiked, reflecting rainfall and drought events during the journey of a water droplet. This spiked shape of transient reverse TTDs, in combination with significant contributions of long travel times in Fig. 6.5A shows that the Hupsel Brook catchment is able to discharge considerable amounts of old water during high discharge conditions (Kirchner, 2003) by rapidly increasing the active drainage area. Travel time distributions derived from unit hydrographs or from concentration input-output analysis describe the distribution of times it took the catchment to react to a rainfall event by discharge or stream concentration changes. These reaction time distributions do not describe the actual contact times and travel paths of water parcels through the soil, which are the important characteristics for solute transport. The spiked reverse TTDs presented in Fig. 6.5 do describe the distribution of contact times between rainwater and soil, while also being transfer functions to transfer discharge into historic rainfall (Eq. [6.7]). From the many spikes in the reverse TTDs of Fig. 6.5 it is clear that the transient reverse TTDs cannot simply be inverted from hydrographs or from concentration time series and more research is needed to unravel their controls.

The mixing of waters with different ages explains how a catchment is able to control the chemistry of discharge (Kirchner, 2003). The surface water concentration is a result of mixing of a large volume of old water with a relatively constant concentration with a discharge-dependent contribution of younger water with variable concentrations. This leads to clear relations between discharge and concentration. Consequently, for water quality purposes it is more relevant to know the contributions of relative young water to discharge than to know the average catchment travel time.

6.3.5 Catchment behavior and model limitations

The catchment-scale mineralization rate for nitrate resulting from the calibration (Table 6.1) is slightly lower than rates found by Hassink (1992). They found mineralization rates between $2 \cdot 10^{-4}$ to $5 \cdot 10^{-4} \text{ d}^{-1}$ for Dutch sandy soils in laboratory incubation tests at 25°C . Our rate, however, represents field conditions with an average yearly temperature of around 10°C (at 25°C our rate is multiplied by 2.5). Not many regional denitrification rates have been published. More importantly, we expect these rates to be highly dependent on local

aquifer properties such as dissolved organic carbon concentrations, pyrite concentrations, and thickness and heterogeneity of the top aquifer (Zhang et al., 2009). The mineral fraction of yearly applied N-fertilizer of 53% compares well to the ratios of applied manure in the study of Schils and Kok (2003).

The effect of the model parameters r_d and r_n on chloride and nitrate response is visualized in Fig. 6.10 for a solution of Eq. [6.15] with a constant equilibrium concentration in the saturated zone, $\overline{C_{Eq}}$. Chloride reaches its maximum concentration after a travel time in the saturated zone of around 20 days, while the nitrate concentration peaks after about 20 days and then gradually drops off as denitrification becomes more effective.

From Fig. 6.10 we conclude that the observed dilution of chloride concentrations during high discharge events (Fig. 6.7) stems from travel times shorter than 20 days, which is the contribution of fast flow routes. The hub during short travel times in Fig. 6.6B shows the average contribution of short travel times to the total reverse TTD. However, calculations of the contributions of short travel times to the discharge are very uncertain and sensitive to the chosen porosity and cell size.

According to Fig. 6.10, the nitrate concentration peaks for travel times around 20 days. The resulting temporal variation of surface water concentrations is much larger for nitrate than for chloride (Fig. 6.7). Figure 6.7 also warrants the conclusion that a constant travel time distribution is useful to evaluate the long term mass balance of a solute, but if we want to relate measured surface water concentrations to model simulations we need to incorporate the dynamic mixing of waters with different travel times via transient travel time distributions.

The sensitivity analysis showed that the calibrated optimal solution is a plausible solution, but that uncertainties are large, particularly in the denitrification flux and plant uptake of chloride and nitrate. Because the catchment-scale diffusion, denitrification, and mineralization rate parameters will always need calibration, stream concentration measurements can only constrain the uncertainty of the combined results for travel times and rate parameters, but not for the separate parameters. Additional measurements of organic nitrogen storage and plant uptake of nitrate would help to create a more reliable catchment-scale mass balance but will not necessarily lead to a better model for the stream concentrations.

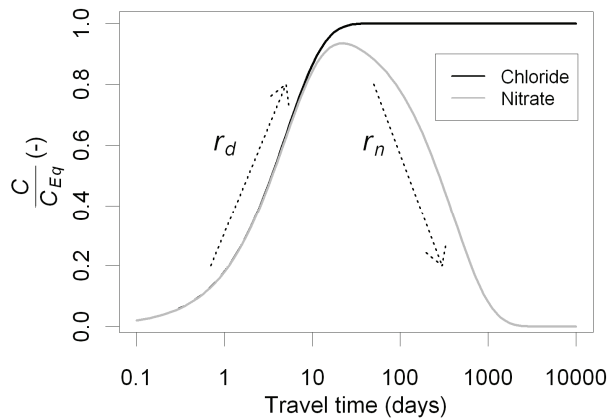


Figure 6.10. The concentration of chloride and nitrate relative to a constant equilibrium concentration, C_{Eq} , in a water parcel traveling through the subsurface as function of travel time. The diffusion rate r_d determines the influx of solutes in an initially solute-free water parcel, while r_n is the denitrification rate of the nitrate in a water parcel.

6.3.6 Model evaluation

We, intentionally, did not divide the measured dataset into a calibration and validation period. Our aim was to use the model to interpret the observed concentrations of nitrate and chloride, analyzing which part of the observed concentration variations can be attributed to overall mass balance changes and which part to travel time variations. Furthermore, the model was used to quantify the nitrate fluxes by plant uptake, denitrification, and stream discharge at the catchment scale and to evaluate to what extent the uncertainty in these fluxes could be constrained by simultaneously calculating the chloride and nitrate fluxes. Excluding part of the measurements for a separate model validation would not improve our understanding of the inner workings of the catchment and instead would increase the uncertainty of the model results.

The advantage of particle tracking combined with mass transfer functions over a fully coupled spatially distributed flow and transport model is the limited number of parameters that is needed to describe the solute transport by water parcels. The latter allowed us to create a very detailed groundwater flow model that focuses on the representation of tube drains and small ditches. This proved necessary to calculate the contributions of relatively short travel times that influence the surface water concentration most. The solute transport description by mass transfer functions allowed us to run the solute transport part of the model thousands of times so that catchment-scale solute transport parameters could be calibrated and sensitivity and uncertainty analyses could be performed. Furthermore, the proposed model setup reflected the available information: abundant information on topography and soil hydraulic properties and little information on the solute transport characteristics of soils and solute input.

6.4 Conclusions

We developed a model that describes daily chloride and nitrate concentrations with a single set of parameters for a period of 26 years. By assuming that the parameters that describe diffusive and convective transport are the same for chloride and nitrate, we were able to partly constrain the uncertainty in the unknown nitrate flux caused by denitrification. We estimated that denitrification removed between 20 and 60% of the yearly inputs, while stream discharge removed between 15 and 35%. These estimates take into account all parameter uncertainties and show that far more nitrate leaves the catchment by denitrification than by surface water discharge. The long-term trend of decreasing chloride and nitrate concentrations at the outlet of the 6.6 km² Hupsel Brook catchment originated from two decades of decreasing agricultural inputs. More rapid concentration fluctuations (seasonal and daily) were shown to arise from variations in groundwater travel times that were directly linked to temporal precipitation patterns.

Our results demonstrated that observed chloride and nitrate concentration dynamics cannot be solely explained from time series of discharge, rainfall, and solute inputs, but that the dynamics in contact times of water parcels with the soil, expressed by transient reverse Travel Time Distributions (TTDs), are essential for understanding observed concentration dynamics. To calculate transient reverse TTDs successfully, an adequate representation of the strongly ephemeral character of the surface water network was paramount. We showed that transient TTDs do not have the smooth shape they are often ascribed in the literature, but that they are spiked, reflecting precipitation and evapotranspiration periods. Especially for small catchments like the Hupsel Brook catchment with a relatively large proportion of fast flow routes and short travel times, large variances in travel time distributions can be expected. Therefore, hydrological models used for solute transport should not just describe the reaction of stream discharge or stream concentration on rainfall events. Instead, the models should focus on the dynamics of travel times and travel path of water parcels within a catchment.

Appendix 6A: Average absolute Difference Plot (ADP)

We characterized the temporal variation of stream water concentrations by an Average absolute Difference Plot (ADP). We defined 5 time-lag classes up to one month: 0-2 days, 2-5 days, 5-10 days, 10-20 days, and 20-30 days, and calculated a mean absolute concentration change for pairs of concentrations within each time-lag class. The resulting averaged differences can be plotted for the different lag classes in an ADP. The ADP is calculated by

$$AD(l) = \frac{1}{\|N(l)\|} \sum_{(t_1, t_2) \in N(l)} |C(t_2) - C(t_1)| \quad [\text{A6.1}]$$

where $AD(l)$ is the average absolute concentration difference within time-lag class l . $N(l)$ is the set of data pairs within class l and $\|N(l)\|$ is the number of data pairs. The measured or modeled concentration is denoted by C . We chose the ADP method over the more commonly used correlogram, because the ADP deals more easily with uneven sampling intervals of concentration measurements and because the unit of the ADP (concentration) compares better to the mean absolute concentration error in the calibration objective function.

Appendix 6B: Calibration specifications

We calibrated the solute transport model by minimizing the sum of three error terms. The first error term, ER , describes the mean absolute error. The second error term, EAD , describes the deviation between the ADP of the measurements and the model, and the last error term describes the deviation of the calibrated nitrate and chloride inputs from the estimated inputs.

The relative mean absolute error between model and measurements is calculated by:

$$Er_{i,p} = \frac{\sum_{t=1}^{n_p} |C_{q,i}(t) - C_{m,i}(t)|}{\sum_{t=1}^{n_p} C_{m,i}(t)} \quad [\text{B6.1}]$$

where subscript i denotes chloride ($i = \text{Cl}$) or nitrate ($i = \text{N}$), and p denotes the time interval. The modeled concentration is denoted by C_q and the measured concentration by C_m . The number of measurements within an interval is given by n_p .

We compared the ADP of the measurements with that of the model at all measurement times. For perfect measurements and a perfect model, both ADPs should be equal. However, to account for measurement errors (due to the sampling strategy, laboratory analyses and sample transportation and handling) an estimate of the measurement error is subtracted from the ADP of the measurements. We arbitrarily defined the measurement error as 25% of the mean absolute difference of the first time-lag class (lag times up to 2

days when available, otherwise the first lag class available). The ADP differences between measurements and model are valued by:

$$EAD_{i,p} = \frac{1}{5} \sum_{l=1}^5 \left(\frac{AD_{mod,i,p}(l) - (AD_{meas,i,p}(l) - 0.25AD_{meas,i,p}(1))}{AD_{meas,i,p}(l) - 0.25AD_{meas,i,p}(1)} \right) \quad [B6.2]$$

where $AD_{mod}(l)$ is the average difference of the modeled concentrations with time lags within class l while $AD_{meas}(l)$ is the corresponding averaged difference of the observed concentrations. An estimate for the measurement error is given by $0.25AD_{meas}(l)$ as indicated above.

Because we also calibrated the yearly fertilizer input, the number of calibration parameters was rather large. We reduced the consequent risk of non-uniqueness by introducing an extra error term, EF . This term allows for deviations from the estimated input, but also guides the calibration toward an input value as close as possible to the estimated input:

$$EF_{i,p} = \left(1 - \frac{Fcal_{i,p}}{Fest_{i,p}} \right)^2 \quad [B6.3]$$

with $Fcal$ [MT^{-1}] the calibrated and $Fest$ the regional estimated fertilizer rate. The objective function that was minimized to find an optimal solution is given by:

$$Obj = w_1 \left(\sum_{p=1}^8 Er_{Cl,p} + \sum_{p=1}^8 Er_{N,p} \right) + w_2 \left(\sum_{p=1}^8 EAD_{Cl,p} + \sum_{p=1}^8 EAD_{N,p} \right) + w_3 \left(\sum_{p=1}^8 EF_{Cl,p} + \sum_{p=1}^8 EF_{N,p} \right) \quad [B6.4]$$

where $w_{1..3}$ are the weighting factors for the individual error terms. These weighting factors were determined by performing several calibration runs that minimize Eq. [B6.4], until the individual error terms contributed 5:2:1 to the Obj reflecting the importance of each of the error terms. We further improved this calibration by two data corrections: excluding concentration measurements taken during the 10% lowest flows and excluding the 2% largest deviations between measured and modeled solute concentrations. The first correction excluded measurements during periods with long surface water residence times. Plant uptake and stream bed denitrification at those times are important extra loss-terms that blur the comparison between measurements and model results. Furthermore, during dry conditions only a small part of the main brook drains water that reaches the catchment outlet. The transport characteristics of this part of the catchment deviate from those of the catchment as a whole (caused by a locally sandier and thicker aquifer). For these reasons we considered it undesirable to calibrate a solute transport model for the entire catchment on measurements taken during low flows. The second correction reduces the impact of any large measurement errors or of discharge peaks that were wrongly predicted by the groundwater model.

Synthesis and discussion

7.1 Questions and answers

This thesis addresses five fundamental questions on the origin of surface water quality dynamics of lowland catchments. The answer to each of these questions is presented in a synthesis of the corresponding chapter and discussed from a scientific and a water management perspective.

What are the dominant flow routes that contribute to the surface water discharge at both the field scale and the catchment scale of the Hupsel Brook catchment and how do these flow routes affect surface water nitrate concentrations? (Chapter 2)

In the Hupsel Brook catchment we installed a nested scale discharge and nutrient concentration monitoring experiment. For a single pasture field, we measured fluxes of groundwater flow, overland flow, and tube drain flow during a winter period of November through May. Approximately 80% of the discharge originated from tube drains, while the remaining 20% was overland flow and groundwater flow. This field is just one field among many fields within the catchment, all with different drainage patterns, soil properties, and surface topography, and it is unlikely to be representative for all the other fields. Therefore, we hypothesized that the measured volumes for each of the flow routes are location-specific but that the typical reaction of a certain flow route to rainfall events is flow-route specific and can be used to upscale the field-scale measurements to the catchment scale. This assumption allowed us to link the flow routes at the field scale to the hydrographs of two larger nested catchment scales (40 ha and 650 ha). By deploying linear combinations of the hydrographs of the individual flow routes at the field site, we reconstructed the hydrographs of the two nested catchment scales. We found that the contribution of tube drain flow decreased with increasing scale (80% at the field scale, 67% for the sub-catchment and 59% for the entire catchment) and that the contribution of overland flow and

groundwater flow increased at larger scales. This scaling effect was attributed to increasing stream and ditch densities and a decreasing percentage of tube drain fields with increasing scale.

The highest nitrate concentrations within the catchment were measured in tube drain effluent. We found that the average nitrate concentration of tube drains was approximately eight times higher than the concentration of overland flow and groundwater flow. Tube drain effluent is by far the most important source for nitrate within the catchment. The lower nitrate concentration of overland flow causes dilution of the nitrate concentration at the catchment outlet during peak discharges.

Scientific contribution

In catchment hydrology, the partitioning of rainfall into flow routes that contribute to surface water discharge is recognized as a major source of uncertainty (Weiler et al., 2003; McDonnell 2003). As it became clear that subsurface drainage is a major contributor to surface water pollution with nitrates, many studies measured tube drain fluxes of water and nitrate (e.g. Nangia et al., 2010; Tiemeijer et al., 2008; De Vos et al., 2000). However, none of these studies measured all the flow routes that contribute to surface water discharge and consequently the partitioning of rainfall into flow routes has never fully been quantified experimentally. This thesis describes the first scientific study in a lowland catchment that measures the separate contributions of tube drain flow, overland flow, and groundwater flow to discharge. In combination with two nested-scale catchments with continuous discharge records, our dataset gives new opportunities for research on the scaling behavior of water fluxes and solute transport.

Contribution to water management

A nested-scale measurement setup as presented in Chapter 2 is paramount for understanding the observed discharge and water quality dynamics at catchment scales. Only by understanding the processes at the field site, we were able to relate the observed nitrate concentration dilution during discharge events at the catchment outlet to overland flow. Overland flow turned out to be a far more important discharge mechanism in poorly drained lowland catchments than is commonly assumed (Rozemeijer and Van der Velde, 2008). Because these measurements are very labor intensive, the results of single studies have to be extrapolated to other time periods and other catchments. However, in contrast with our study, several other catchment and field-site studies reported increasing nitrate concentrations during discharge peaks (Tiemeyer et al., 2008; Rozemeijer and Broers, 2007, and Wriedt et al., 2007). These examples show that nitrate concentration dynamics are catchment-specific. Hence, a single field site does not yield enough information to extrapolate the contribution of flow routes to locations with clearly different soil types, drainage densities or aquifers thicknesses. Therefore, to characterize catchments where nutrient management is desirable, targeted measurement campaigns with nested-scale discharge and concentration measurements, including detailed flow route measurements at field sites, are needed. Luckily, a single campaign probably provides enough information for many years of operational management.

Subsurface drainage was found to be the main source of nitrate in surface waters of the Hupsel Brook catchment. Reducing the surface water nitrate concentration, therefore, should focus on reducing nitrate loads in the effluent of subsurface drainage. Especially, reducing the nitrate loads of a few tube drains with extremely high nutrient loads will significantly reduce surface water concentrations.

How can the dominant hydrological mechanisms that drive the individual flow route fluxes be captured in catchment-scale model concepts? (Chapter 3)

In Chapter 3, we identified three main hydrological mechanisms that determine the flux of individual flow routes in freely draining lowland catchments:

- The dynamic area of active drainage network (streams, ditches, and tube drains). Under wet conditions all tube drains and soil surface depressions generate discharge, while under dry conditions almost all streams, ditches, and tube drains dry up.
- Interaction between the unsaturated and the saturated zone. Water stored in the unsaturated zone acts as an amplifier, converting the precipitation signal to an increase of the groundwater level. The amplification factor varies with the soil water content.
- Ponding and a varying surface water level inside streams and ditches. Ponding and high surface water levels reduce groundwater level gradients towards the surface water network and hence reduce fluxes from groundwater to surface water.

Groundwater level measurements at the field site and detailed groundwater level model simulations revealed that the spatial distribution of groundwater depths can be approximated by a normal distribution. The mean and variance of this distribution were found to be unique functions of the amount of water stored in the saturated zone of the catchment. Based on these findings, we formulated a catchment-scale process model that accounts for the three dominant hydrological mechanisms. All terms of the water balance at any given time were considered functions of the distribution of groundwater depths at that time. Separate discharges for tube drain flow, overland flow, and groundwater flow were calculated by dividing the interface between saturated groundwater and the actively draining surface water network in three separate interfaces: the interface between the saturated groundwater and tube drains, between the saturated groundwater and soil surface, and between the saturated groundwater and the surface water network. We showed that these new model concepts can accurately describe observed discharge and groundwater levels.

Scientific contribution

The presented model concepts contribute to the ongoing discussion how to include spatially variable processes in lumped hydrological models (Tetzlaff et al, 2008, McDonnell et al., 2007; Kirchner, 2006; Sivapalan, 2003; Regianni et al, 1998). New in our model approach is the use of dynamics in the spatial structure of the groundwater table (characterized by the mean and standard deviation of the groundwater depth distribution) to calculate time series of discharge. This relation between dynamics in the spatial structure of the groundwater

table and the shape of hydrographs has not been established before and has considerable potential to advance catchment-scale process models.

This thesis shows that the dynamics in the interface between the saturated zone and the soil surface is the major driver for catchment-scale discharge. In the literature many conceptual models incorporated comparable “variable source area”-concepts (e.g. TOPMODEL by Kirkby and Beven, 1979, PDM by Moore, 2007). However, none of these studies explicitly accounted for a dynamic surface water network resulting in dynamic groundwater exfiltration areas as proposed in this study. The idea of a dynamic active draining surface water network is strongly related to the concepts of dynamics in connectivity between upstream and downstream areas (Ocampo et al., 2006; Molenat et al., 2008) or the Fill-and-Spill hypothesis proposed by Tromp-van Meerveld and McDonnell (2007). A certain amount of subsurface water storage is required before a ditch or a stream starts draining the groundwater. This can be seen as a threshold process at the point or field scale. As a catchment becomes wet enough for even the smallest headwaters (Bishop et al., 2008) to start draining water, the upstream areas are connected to the downstream areas and solutes can move rapidly through a catchment. Under these conditions the local groundwater head gradients are large and the travel paths towards the nearest streams are short. Therefore, accounting for a dynamic surface water network is essential in conceptualizing catchment-scale solute transport and discharge dynamics in lowland catchments. A dynamical active draining surface water network is likely to be important in many types of moderately sloped catchments. The presented ideas to conceptualize this dynamical behavior may also provide opportunities for modeling subsurface connectivity through fractures in hillslopes (an idea generated in discussions with M.C. Westhoff and H.H.G. Savenije, 2010).

Another innovation is the integration of saturated, unsaturated, and surface flow into a single mass balance. Especially, explicitly accounting for the effects of unsaturated zone storage is crucial for describing the highly dynamic interaction between groundwater and surface water (see also Seibert et al, 2003).

Contribution to water management

The proposed concepts show that a groundwater monitoring network designed to quantify the groundwater-surface water interaction should capture both the spatial structure of the groundwater table and its dynamics. Such a groundwater level monitoring network should not only measure groundwater levels in the center of agricultural fields but also next to or inside streams. This focus on the spatial structure of local groundwater gradients is mostly lacking in current groundwater monitoring networks that try to characterize regional groundwater level gradients. Hence the interaction between groundwater and surface waters cannot be fully quantified from these monitoring networks. Groundwater depth surveys for a range of dry to wet conditions throughout a catchment may also provide the relation between storage and the spatial structure of the groundwater table (GDD-curve).

Furthermore, the results show that measured groundwater levels contain a wealth of information on discharge and the potential risk for flooding, especially when several groundwater level time series are available. An effective strategy to improve flood

forecasting in lowland catchments seems to be to include real time measurements of groundwater levels. The presented model approach gives footholds on how to include the spatial and temporal dynamics of groundwater tables in catchment-scale discharge models.

How can the information derived from a nested-scale experimental setup be utilized to constrain uncertainty in catchment-scale flow route contributions to discharge? (Chapter 4)

In Chapter 4 we assessed the value of nested-scale discharge and groundwater level monitoring for estimating contributions of flow routes at the catchment-scale. We used the scaling concepts for lowland hydrology developed in Chapter 3 to upscale field-site measurements (Chapter 2) to the catchment scale. The presented upscaling method is the model-equivalent of the measurement-based upscaling approach introduced in Chapter 2. In Chapter 2 we argued that not the actual volumes (of groundwater, surface water, soil water, etc.) measured at the field site, but the typical reaction of flow routes on rainfall events can be used to upscale flow route discharges from the field site to the catchment scale. In Chapter 4 we quantified these typical reactions of flow routes to rainfall events by quantifying the process-specific parameters of the LGSI-model, which were assumed scale invariant. The spatial structure of the groundwater table, which was assumed scale-specific, determines the interface between saturated groundwater and the surface water system and hence the discharge of a certain flow route at a certain scale. We showed that using this scaling method scale-invariant information (ensembles of process-specific parameters) can be derived from field-site measurements and that this information can effectively be used to constrain flow route discharge uncertainty at the catchment scale.

We identified three ways by which nested-scale monitoring contributes to improved flow route predictions at catchment-scale. First of all, the detailed storage and flux measurements at the field site allowed us to formulate model concepts that accurately describe the field-scale flow routes. Secondly, a combination of nested-scale measurements and nested-scale models constrains parameter uncertainty and hence flow route discharge uncertainty. Finally, a LGSI-model of which the parameters are conditioned on nested-scale measurements much better predicted extreme discharges and nutrient loads than a LGSI-model that is constrained on catchment-discharge only.

Scientific contribution

Many studies showed that upscaling field-site measurements to catchment scales can easily lead to wrong conclusions as field-sites can prove non-representative of the patterns and processes that emerge at larger scales (Sivapalan, 2003; Soulsby et al., 2006; Didszun and Uhlenbrook 2008). In our upscaling approach the focus is not on defining scale-representative process parameters, but on quantifying the spatial structure of the groundwater table for each scale (i.e. the relation between storage and the distribution of groundwater depths). This idea, that scale effects in lowland hydrology can be attributed to scale differences in the spatial structure of the groundwater table, offers new opportunities to link groundwater level measurements to discharge across nested scales as demonstrated in Chapter 4. The advantage of the presented approach over many approaches reported in

literature is that we do not try to calculate the shape of groundwater table from physical principles and hence do not have to try to upscale these physical principles. By simply quantifying the spatial structure of the groundwater table at a certain scale from measurements, we account for the dominant scaling mechanism.

Contribution to water management

We showed that combined nested-scale monitoring of groundwater levels and discharges allowed us to create more accurate predictions of both nitrate loads and peak discharges. In the current monitoring programs in The Netherlands surface water discharge, groundwater levels and their water quality are monitored independently and often even by different governmental agencies. As the primary focus of hydrological monitoring often lies with safety during peak discharges and on water quality of large downstream surface water bodies, (periods of) nested-scale monitoring of groundwater levels, discharges and their water quality would be an effective improvement of the current monitoring networks.

How do rainfall-induced dynamics in nitrate and phosphorus concentrations affect load estimates for the Hupsel Brook catchment? (Chapter 5)

Continuous concentration measurements of nitrate and phosphate at the catchment outlet revealed large short-term concentration dynamics in response to discharge events for both solutes and a seasonal pattern in the nitrate concentration. Nitrate concentrations during discharge events were observed to dilute, while phosphate concentrations peaked. We showed that these concentration responses could be deconstructed into three response characteristics: maximum concentration change, time to maximum concentration change, and the recovery time. We related these concentration response characteristics to observed discharge, rainfall, and groundwater time series, and found that we could accurately predict the concentration responses of both nitrate and phosphate to rainfall events. This result confirmed our hypothesis that short-term concentration variability is mainly weather-induced and can be predicted from commonly available or cheap-to-measure hydrological variables. We applied the relations between hydrological variables and the concentration response characteristics to significantly improve yearly load estimates based on a weekly grab-sample water quality dataset. Using this event based correction we achieved a much stronger improvement than previous studies that tried to use relations between discharge and concentrations (e.g. Preston et al., 1989; Smart et al., 1999). Linear interpolation between concentration measurements would have overestimated nitrate loads and underestimated phosphate loads.

Scientific contribution

We presented a new dataset of continuous nitrate and phosphate concentrations. This dataset contributes to a growing collection of continuous water quality datasets reported in literature (e.g. Jordan et al, 2007; Kirchner 2004). Collecting such datasets at many different locations around the world and identifying the entire spectrum of possible water quality behaviors is essential for the development of new model concepts that can account for water quality dynamics. Especially because this dataset is part of a nested-scale experimental setup, in which also discharge, groundwater levels, and field-scale fluxes of

different flow routes were measured, this dataset can be used to develop and test new water quality model concepts.

The clear relationships between the concentration response to rainfall events and hydrological parameters indicate that the short-term dynamics in surface water concentrations are primarily driven by hydrologic processes. Therefore, efforts to improve water quality models of lowland catchments should focus on improving the description of the local hydrology, with special attention paid to fast flow routes such as overland flow and preferential flow phenomena (see also Rode et al., 2010 and Beven, 2010).

Contribution to water management

We showed that short periods with continuous concentration measurements can characterize the concentration response during discharge events. A method is provided to use the information of short periods with continuous concentration records to reconstruct the dynamics of nitrate and phosphate concentrations in datasets obtained by infrequent grab-sample monitoring. This method significantly improves load estimates of both nitrate and phosphate.

To what extent can surface water quality dynamics be explained from dynamics in contact times between water parcels and the soil matrix within the catchment? (Chapter 6)

Numerical simulations of the contact times between water parcels and soil, expressed in travel time distributions, revealed that travel time distributions are irregularly shaped and change rapidly, reflecting individual rainfall events and evapotranspiration. We hypothesize that dynamics in travel time distributions can be used to describe water quality dynamics. To test this hypothesis, the mass-response function approach (Rinaldo and Marani, 1987) was extended by including denitrification, incomplete mixing of the saturated zone, dynamic travel time distributions, mineralization of organic matter, and plant uptake of solutes. This solute transport model was used to simulate both chloride and nitrate transport in the Hupsel Brook catchment. Nitrate was simulated because of its negative impact on surface water ecosystems. Chloride was assumed to behave similarly as nitrate within the saturated groundwater, but without losses due to denitrification. Therefore, chloride was simulated to identify the effects of denitrification on nitrate concentration dynamics at the catchment outlet. The model was able to describe 26 years of frequently measured chloride and nitrate concentrations both with an R^2 of 0.86. From these model results we concluded that most of the seasonal and daily variations in concentrations could be attributed to temporal changes of the travel time distributions. Despite a large uncertainty, our results show that denitrification removes more nitrate from the Hupsel Brook catchment than stream discharge does. Denitrification can also explain the difference in chloride and nitrate concentration dynamics. This study demonstrates that a catchment-scale lumped approach to chloride and nitrate transport processes suffices to accurately model the dynamics of catchment-scale surface water concentration as long as the model includes detailed transient travel time distributions.

Scientific contribution

This is the first study that successfully relates the dynamics in travel time distributions to observed dynamics in chloride and nitrate concentrations. So far, the only other studies that addressed non-stationary travel time distributions were theoretical studies (Botter et al., 2010; McDonnell et al., 2010) or studies that tried to measure travel times and found dynamic mean travel times (e.g. Morgenstern et al., 2010).

Many studies treated the travel time distribution as a catchment characteristic that is constant with time (Rinaldo et al., 2006, Botter et al, 2008, Kirchner et al, 2001). Our simulation results show that travel time distributions change rapidly under the forcing by rainfall and evapotranspiration to a degree that renders it impossible to characterize the Hupsel Brook catchment by its mean or median travel time only. For quantifying solute transport dynamics at the catchment scale it may even be more relevant to know the contribution of young water (< 100 days) than the mean or median travel time, as it is the contribution of young water that most strongly affects the surface water quality dynamics.

Niemi (1977) proposed to simplify transient travel time distributions with travel times expressed in time [T] to a stationary travel time distribution with travel times expressed in cumulative flow leaving the catchment [L^3]. This approach was successfully applied by Van Ommen et al. (1988) and Rodhe et al. (1996) and discussed by McDonnell et al. (2010) and Rinaldo and Kircher during the conference “30 years of stochastic subsurface hydrology” (2010). Niemi (1977) formulated three conditions under which this assumption is valid:

- Storage should be relatively constant.
- The ratios of flow routes contributing to the discharge remain constant.
- All discharge mechanisms of a catchment have the same travel time distribution.

Especially the last two assumptions are hard to justify for the Hupsel Brook catchment. In Chapter 2 we observed large fluctuations of flow route ratios contributing to discharge. Secondly, in the Hupsel Brook catchment the cumulative evapotranspiration (a second discharge mechanism) approximately equals the cumulative surface water discharge. It has recently been shown that because of completely different flow paths, the travel time distribution of evapotranspiration significantly differs from the travel time distribution of discharge (Brooks et al, 2010). Therefore, we conclude that the dynamic nature of catchment-scale travel time distributions can not be simplified through Niemi’s approximation.

Another innovation of Chapter 6 is the simultaneous calculation of chloride and nitrate. We could partly constrain the uncertainty in the catchment-scale nitrate mass balance by assuming that chloride and nitrate are both non-sorbing solutes with the same transport characteristics in the saturated zone. Nitrate removal by denitrification thus was the only difference in transport through the saturated zone between both ions. This example shows that parameter equifinality (Beven and Freer, 2001) can significantly be reduced when a model is forced to describe a combination of nitrate and chloride concentration datasets.

The chance that a model produces “the right results for the right reasons” (Kirchner, 2006) increases with each additional dataset the model is able to describe.

Contribution to water management

We demonstrated reasonably accurate modeling of nitrate and chloride mass balances of a lowland catchment. A methodology is provided to link the results of detailed groundwater models -used by many water boards in The Netherlands- to catchment-scale solute transport models that describe surface water concentrations and solutes masses stored within a catchment. A long term surface water quality dataset, combined with continuous discharge measurements at the catchment outlet are prerequisites for successfully applying this approach.

We found large amounts of organic nitrogen storage in the root zone originating from historic high nitrogen inputs, possibly as large as 10 to 20 times the current yearly inputs. This large nitrogen pool provides a major source of nitrate leaching to the groundwater. The uncertainty in the organic nitrogen storage in the root zone and the evolution of this storage dominate the uncertainty in predicted future surface water concentrations. Mineralization of organic material in the root zone will continue to release nitrate for many years and reduce the effects of agricultural input reducing measures, as demonstrated in this study. We recommend measuring the organic nitrogen content of the root zone in any monitoring program of the nitrogen balance of a catchment.

7.2. Outlook

New measurements

During the past decade, ideas derived from new datasets have driven advances and falsification of model concepts (e.g. Tromp-van Meerveld et al., 2007; Brooks et al., 2010; Kirchner et al., 2003, Kirchner et al., 2001, Westhoff et al., 2007; Van der Ploeg, 2008; Bloem, 2009). In this thesis too, the innovative experimental setup provided the data on flow route discharges across scales that allowed us to formulate new concepts for catchment scale interactions between groundwater and surface water. New types of measurements will continue to provide the new information on the travel paths and travel times of water and solutes needed to advance model concepts. Examples of water and soil properties that can be measured and may lead to new insights are water temperature, water age, soil moisture distributions, and simultaneous behavior of concentrations of multiple solutes in both subsurface and surface waters.

In this thesis we described the relatively fast response of surface water quality to rainfall and evapotranspiration. However, catchments are also subject to continuous but mostly slow changes in e.g. land use, agricultural inputs, and climate. Only long term discharge and water quality datasets can reveal relations between climate, land use, and water quality. Because of the current lack of long term water quality datasets the validation of model concepts that try to describe these relations is hardly possible. Therefore, it is crucial that recent measurement campaigns that provided datasets of discharge and water quality of streams (for example the Hupsel Brook catchment) are transformed to (semi-)permanent

monitoring programs and new observation campaigns and monitoring programs are initiated.

Water quality models and travel time distributions

In catchment hydrology most models focus on discharge. In order to use catchment-scale hydrological models for describing and predicting water quality, we need to understand the flow paths and travel times of water within catchments (McDonnell, 2003; McDonnell et al., 2010; Kirchner, 2006). In this thesis the first steps towards discharge models that also describe the flow routes of discharge within a catchment are made. We introduced models that define discharge by a composite of flow routes and models in which discharge is treated as a composite of travel times. From the flow route approach we learned that most short-term (hours to days) water quality variations can be described by dynamic mixing of flow route contributions. However, modeling flow routes alone is not enough to fully understand the water quality dynamics, as the water quality of flow routes is not constant with time but changes with the subsurface flow paths and travel times of the water parcels contributing to a certain flow route. The travel time approach yielded very good results for describing daily, seasonally and yearly nitrate concentrations dynamics. This approach showed that major advances in conceptualizing solute transport at the catchment scale can be achieved by developing a stochastic model of the movement of water parcels within a catchment. Such a model would simultaneously describe the transient distributions of travel times and discharge, without the need for time consuming spatially distributed hydrologic simulations (see also Botter et al., 2010).

Comparing catchments

Advances in catchment-scale solute transport concepts can also be made by comparing catchments that have different characteristics. In particular, new insights can be gained by comparing lowland catchments, where water and solute fluxes are driven by local and highly dynamic groundwater gradients, and sloping catchments, where the bedrock determines the groundwater gradient.

In lowland catchments past research focused mainly on Darcian groundwater flows, while in hillslope hydrology the focus was on direct runoff generated on the steep slopes. These mindsets have led to extensive use of groundwater-driven concepts in lowland hydrology and unit-hydrograph concepts in hillslope hydrology. However, in both lowland and hillslope hydrology a mismatch between surface water quality measurements and the prevailing hydrological theories gave rise to shifts in hypotheses on water flow. The recognition of large contributions of pre-event water to the discharge in hillslope hydrology (the “old water paradox”; Kirchner, 2003) created the awareness of the importance of subsurface storage and subsurface flow paths. In contrast, the rapid reactions of concentrations in surface waters of lowland catchments (this thesis) points to the importance of preferential flow phenomena that cause accelerated runoff and significant contributions of short travel times.

Similarities between hillslope and lowland hydrology also manifest themselves in the dynamic surface water network of ditches and tube drains in lowland catchments and the

hillslope connectivity through fractures. In both lowland and sloped catchments it has been observed that first a threshold in subsurface storage has to be exceeded before surface waters start generating discharge.

Integration of subsurface and in-stream processes

In this thesis, novel catchment-scale concepts that predict surface water quality were developed by integrating soil physics, groundwater hydrology, and water chemistry. In-stream processes that add or remove nutrients from surface waters were not considered as the travel times of water inside the surface water network of the Hupsel Brook catchment are short (< day). Many studies, however, showed that these processes may dominate surface water quality dynamics in large catchments or in catchments with long residence times inside the surface water network (e.g. De Klein, 2008; Lindgren and Destouni, 2004; Krause et al, 2009; Rode et al, 2010). Therefore, applying the concepts developed in this thesis to basins larger than the Hupsel Brook catchment or to basins with longer surface water residence times requires expanding the concepts with in-stream processes and connectivity within the surface water network.

References

- Alexander, R.B., R.A. Smith, and G.E. Schwarz, 2000. Effect of stream channel size on the delivery of nitrogen to the Gulf of Mexico. *Nature*, 403, 758-761.
- Behrendt, H., and A. Bachor, 1998. Point and diffuse load of nutrients to the Baltic Sea by river basins of north east Germany (Mecklenburg-Vorpommern). *Water Science and Technology*, 38, 147-155.
- Bentley, W.J., and R.W. Skaggs, 1993. Changes in entrance resistance of subsurface drains. *Journal of Irrigation and Drainage Engineering* 119, 584-598.
- Beven, K.J., and M.J. Kirkby, 1979. Physically based, variable contributing area model of basin hydrology, *Hydrological Science Bulletin* 24, 43-69.
- Beven, K.J., 2001. How far can we go in distributed hydrological modelling?, *Hydrol. and Earth System Sc.* 5, 1-12.
- Beven, K.J., 2010. Preface: Preferential flows and travel time distributions: defining adequate hypothesis tests for hydrological process models. *Hydrol. Process.* 24, 1537–1547.
- Beven, K.J., and J. Freer, 2001. Equifinality, data assimilation, and uncertainty estimation in mechanistic modelling of complex environmental systems using the GLUE methodology. *J. of Hydrol.* 249, 11– 29
- Bierkens, M.F.P., 1998. Modeling water table fluctuations by means of a stochastic differential equation, *Water Resour. Res.* 34, 2485-2499.
- Bishop, K., I. Buffam, M. Erlandsson, J. Fölster, H. Laudon, J. Seibert, and J. Temnerud, 2008. *Aqua Incognita: the unknown headwaters*. *Hydrol. Process.* 22, 1239–1242.
- Bjerg, P.L., and T.H. Christensen, 1992. Spatial and temporal small-scale variation in groundwater quality of a shallow sandy aquifer. *Journal of Hydrology* 131, 133-149.
- Bloem, E., 2008. Variation in space and time of water flow and solute transport in heterogeneous soils and aquifers. A new multi-compartment percolation sampler and a new parameterization of the spatio-temporal solute distribution. PhD thesis, Wageningen University, Wageningen.
- Borah, D.K., M. Bera, and S. Shaw, 2003. Water, Sediment, Nutrient and Pesticide Measurements in an Agricultural Watershed in Illinois During Storm Events. *Transactions of the ASAE*, 46, 657-674.
- Botter, G., E. Bertuzzo, and A. Rinaldo, 2010. Transport in the hydrologic response: Travel time distributions, soil moisture dynamics, and the old water paradox. *Water Resour. Res.* 46, doi:10.1029/2009WR008371

- Botter, G., E. Milan, E. Bertuzzo, S. Zanardo, and A. Rinaldo, 2009. Inference from catchment-scale tracer circulation experiments. *J. Hydrol.*, 369, 368-380.
- Botter, G., E. Peratoner, M. Putti, A. Zuliani, R. Zonta, A. Rinaldo, and M. Marani, 2008. Observation and modeling of catchment-scale solute transport in the hydrologic response: A tracer study. *Water Resour. Res.*, 44, doi: 10.1029/2007WR006611
- Botter, G., E. Bertuzzo, A. Bellin, and A. Rinaldo, 2005. On the Lagrangian formulations of reactive solute transport in the hydrologic response. *Water Resour. Res.*, 41, doi: 10.1029/2004WR003544
- Boumans, L.J.M., D. Fraters, and G. van Drecht, 2005. Nitrate leaching in agriculture to upper groundwater in the sandy regions of the Netherlands during the 1992-1995 period. *Environmental Monitoring and Assessment* 102, 225-241.
- Broers, H.P., 2002. Strategies for regional groundwater quality monitoring. PhD thesis, Faculty of Geosciences, Utrecht University, Utrecht,
- Broers, H.P., and F.C. van Geer, 2005. Monitoring strategies at phreatic wellfields: A 3D travel time approach. *Ground Water*, 43, 850-862.
- Broers, H.P., 2004. The spatial distribution of groundwater age for different geohydrological situations in the Netherlands: implications for groundwater quality monitoring at the regional scale. *J. Hydrol.*, 299, 84-106.
- Brooks, J.R., H.R. Barnard, R. Coulombe, and J.J. McDonnell, 2010. Ecohydrologic separation of water between trees and streams in a Mediterranean climate. *Nature Geoscience*, 3, 100-104.
- Cardenas, M.B., 2007. Potential contribution of topography-driven regional groundwater flow to fractal stream chemistry: Residence time distribution analysis of Tóth flow. *Geophysical Research Letters*, 34, L05403.
- Cardenas, M.B., 2008. Surface water-groundwater interface geomorphology leads to scaling of residence times. *Geophysical Research Letters*, 35, L08402.
- Carlier, N., and G. De Marsily, 2004. Assessment and modeling of the influence of man-made networks on the hydrology of a small watershed: Implications for fast flow components, water quality and landscape management. *J. Hydrol.* 285, 76-95.
- Chang, H., and T.N. Carlson, 2004. Patterns of phosphorus and nitrate concentrations in small central Pennsylvania streams. *The Pennsylvania Geographer*, 42, 61 -74.
- Cherry, K.A., M. Shepherd, P.J.A. Withers, and S.J. Mooney, 2008. Assessing the effectiveness of actions to mitigate nutrient loss from agriculture: A review of methods. *Science of the Total Environment*, 406, 1 – 23.
- Clark, M.P., D.E. Rupp, R.A. Woods, H.J. Tromp-van Meerveld, N.E. Peters, and J. E. Freer, 2009. Consistency between hydrological models and field observations: linking processes at the hillslope scale to hydrological responses at the watershed scale. *Hydrol. Process.*, 23, 311-319.
- Cleveland, W.S., 1979. Robust locally weighted regression and smoothing scatterplots. *J. Am. Stat. Ass.*, 74, 829-836.
- Conley, D.J., S. Björck, E. Bonsdorff, J. Carstensen, G. Destouni, B.G. Gustafsson, S. Hietanen, M. Kortekaas, H. Kuosa, H.E.M. Meier, B. Müller-Karulis, K. Nordberg, A. Norkko, G. Nürnberg, H. Pitkänen, N.N. Rabalais, R. Rosenberg, O.P. Savchuk, C.P. Slomp, M. Voss, F. Wulff, and L. Zillén, 2009. Hypoxia-related processes in the Baltic Sea. *Environmental Science & Technology*, 43, 3412-3420.
- Corwin, D.L., J. Hopmans, and G.H. De Rooij, 2006. From Field- to Landscape-Scale Vadose Zone Processes: Scale Issues, Modeling, and Monitoring. *Vadose Zone J.*, 5, 129-139.

- De Jonge, H., and G. Rothenberg, 2005. New device and method for flux-proportional sampling of mobile solutes in soil and groundwater. *Environmental Science & Technology* 39, 274-282.
- De Klein, J.J.M., 2008. From Ditch to Delta, Nutrient retention in running waters. PhD thesis, Wageningen University, Wageningen.
- De Louw, P., G. H. P. Oude Essink, P. J. Stuyfzand, and S. E. A. T. M. van der Zee, 2010. Upward groundwater flow in boils as the dominant mechanism of salinization in deep polders, The Netherlands. Submitted to *Journal of Hydrology*.
- De Vos, J.A., 2001. Monitoring nitrate leaching from submerged drains. *Journal of Environmental Quality*, 30, 1092-1096.
- De Vos, J.A., D. Hesterberg, and P.A.C. Raats, 2000. Nitrate leaching in a tile-drained silt loam soil. *Soil Science Society of America Journal*, 64, 517-527.
- De Vries, J.J., 1995. Seasonal expansion and contraction of stream networks in shallow groundwater systems. *J. Hydrol.*, 170, 15-26.
- De Vries, J.J., 1994. Dynamics of the interface between streams and groundwater systems in lowland areas, with reference to stream net evolution. *J. Hydrol.*, 155, 39-56.
- De Zeeuw, J.W., and F. Hellinga, 1958. Neerslag en afvoer. *Landbouwkundig Tijdschrift* 70, 405-422 (in Dutch with English summary).
- Didszun, J., and S. Uhlenbrook, 2008. Scaling of dominant runoff generation processes: Nested catchments approach using multiple tracers. *Water Resour. Res.*, 44, doi:10.1029/2006WR005242.
- Doherty, J., 2002. PEST Model-Independent Parameter Estimation, <http://www.sspa.com/pest/download/pestman.pdf>.
- Ernst, L.F., 1978. Drainage of undulating sandy soils with high groundwater tables. *J. hydrol.*, 39, 1-30.
- EU, 2000. Council Directive of 23 October 2000 establishing a framework for Community action in the field of water policy. Directive number 2000/60/EC. Brussels.
- Fedora, M.A., and R.I. Beschta, 1989. Storm runoff simulation using an antecedent precipitation index (API) model. *J. Hydrol.*, 112, 121-133.
- Feller, W, 1971. *An Introduction to Probability Theory and Its Applications*, Vol. 2, 2nd ed. Wiley, New York.
- Gächter, R., S.M. Steingruber, M. Reinhardt, and B. Wehrli, 2004. Nutrient transfer from soil to surface waters: Differences between nitrate and phosphate. *Aquatic Sciences*, 66, 117-122.
- Gallart, F., J. Latron, P. Llorens, and K. Beven, 2007. Using internal catchment information to reduce the uncertainty of discharge and baseflow predictions. *Advances in Water Resources* 30, 808-823.
- Haan, P.K., and R.W. Skaggs, 2003. Effect of parameter uncertainty on DRAINMOD predictions: II Nitrogen loss. *Am. Soc. of Agricultural Engineers*, 46, 1069-1075.
- Harmel, R.D., R.J. Cooper, R.M. Shade, R.L. Haney, and J.G. Arnold, 2006. Cumulative uncertainty in measured streamflow and water quality data for small watersheds. *T. ASABE*, 49, 689-701.
- Harris, G., and A.L. Heathwaite, 2005. Inadmissible evidence: knowledge and prediction in land and riverscapes. *J. Hydrol.*, 304, 3-19.
- Hassink, J., 1992. Effects of soil texture and structure on carbon and nitrogen mineralization in grassland soils. *Biol. Fertil. Soils*, 14, 126-134.

- Hassink, J., L.A. Bouwman, K.B. Zwart, J. Bloem, and L. Brussaard, 1993. Relationships between soil texture, physical protection of organic matter, soil biota, and C and N mineralization in grassland soils. *Geoderma*, 57, 105-128.
- Heathwaite, A.L., and R.M. Dils, 2000. Characterising phosphorus loss in surface and subsurface hydrological pathways. *Science of the Total Environment*, 251, 523-538.
- Herlihy, M., 1979. Nitrogen mineralization in soils of varying texture, moisture and organic matter. I. Potential and experimental values in fallow soils. *Plant and Soil*, 53, 255-267.
- Hewlett, J.D., and A.R. Hibbert, 1963. Moisture and energy conditions within a sloping soil mass during drainage. *J. Geophys. Res.*, 68, 1081-1087.
- Hirt, U., B.C. Meyer, and T. Hammann, 2005. Proportions of subsurface drainages in large areas – Methodological study in the Middle Mulde catchment (Germany). *Journal of Soil Science and Plant Nutrition*, 168, 375-385.
- Hopmans, J.W., and J.N.M. Stricker, 1989. Stochastic analysis of soil water regime in a watershed. *J. Hydrol.*, 105, 57-84.
- Jarvie, H.P., C. Neal, R. Smart, R. Owen, D. Fraser, I. Forbes, and A. Wade, 2001. Use of continuous water quality records for hydrograph separation and to assess short-term variability and extremes in acidity and dissolved carbon dioxide for the River Dee, Scotland. *Science of the Total Environment*, 265, 85-98.
- Jaynes, D.B., S.I. Ahmed, K.J.S. Kung, and R.S. Kanwar, 2001. Temporal dynamics of preferential flow to a subsurface drain. *Soil Science Society of America Journal* 65, 1368-1376.
- Jencso, K.G., B.L. McGlynn, M.N. Gooseff, S.M. Wondzell, K.E. Bencala, and L.A. Marshall, 2009. Hydrologic connectivity between landscapes and streams: Transferring reach- and plot-scale understanding to the catchment scale. *Water Resour. Res.*, 45, doi:10.1029/2008WR007225.
- Johnes, P.J., 2007. Uncertainties in annual riverine phosphorus load estimation: Impact of load estimation methodology, sampling frequency, baseflow index and catchment population density. *J. Hydrol.*, 332, 241-258.
- Jordan, P., A., Arnscheidt, H. McGrogan, S. McCormick, 2007. Characterizing phosphorus transfers in rural catchments using a continuous bank-side analyser. *Hydrol. Earth Syst. Sc.*, 11, 372-381.
- Jury, W.A., and K. Roth, 1990. *Transfer functions and solute movement through soil*. Birkhauser Verlag, Basel, 226 pp.
- Kamra, S.K., J. Michaelsen, W. Wichtmann, and P. Widmoser, 1999. Preferential solute movement along the interface of soil horizons. *Water Science and Technology*, 40, 61-68.
- Kim, C.P., J.N.M. Stricker, and P.J.J.F. Torfs, 1996. An analytical framework for the water budget of the unsaturated zone. *Water Resour. Res.* 32, 3475-3484.
- Kirchner, J.W., 2003. A double paradox in catchment hydrology and geochemistry. *Hydrol. Process.*, 17, 871-874.
- Kirchner, J.W., 2006. Getting the right answers for the right reasons: Linking measurements, analyses, and models to advance the science of hydrology. *Water Resour. Res.*, 42, W03S04, doi:10.1029/2005WR004362.
- Kirchner, J.W., X. Feng, and C. Neal, 2000. Fractal stream chemistry and its implications for contaminant transport in catchments. *Nature*, 403, 524-527.
- Kirchner, J.W., X. Feng, C. Neal, and A.J. Robson, 2004. The fine structure of water-quality dynamics: the (high-frequency) wave of the future. *Hydrol. Process.*, 18, 1353-1359.

- Kollet, S.J., and R.M. Maxwell, 2008. Demonstrating fractal scaling of baseflow residence time distributions using a fully-coupled groundwater and land surface model. *Geophysical Research Letters*, 35, L07402.
- Kollet, S.J., R.M. Maxwell, C.S. Woodward, S. Smith, J. Vanderborght, H. Vereecken, and C. Simmer, 2010. Proof of concept of regional scale hydrologic simulations at hydrologic resolution utilizing massively parallel computer resources. *Water Resour. Res.*, 46, doi:10.1029/2009WR008730.
- Kraijenhoff van de Leur, D.A., 1958. A study of non-steady groundwater flow with special reference to a reservoir-coefficient. I. *De Ingenieur* 70, B87-94
- Kraijenhoff van de Leur, D.A., 1962. A study of non-steady groundwater flow.II. *De Ingenieur* 74, 285-292
- Ladouche, B., A. Probst, D. Viville, S. Idir, D. Baque, M. Loubet, J.L. Probst, and T. Bariac, 2001. Hydrograph separation using isotopic, chemical and hydrological approaches (Strengbach catchment, France). *Journal of Hydrology* 242, 255-274.
- Langlois, J.L., and G.R. Mehuys, 2003. Intra-storm study of solute chemical composition of overland flow water in two agricultural fields. *Journal of Environmental Quality* 32, 2301-2310.
- Lazzarotto, P., C. Stamm, V. Prasuhn, and H. Flüßler, 2006. A parsimonious soil-type based rainfall-runoff model simultaneously tested in four small agricultural catchments, *J. Hydrol.* 321, 21-38.
- Lennartz, B., B. Tiemeyer, G.H. Rooij, and F. Doležal, 2010. Artificially drained catchments-from monitoring studies towards management approaches. *Vadose Zone J.*, 9, 1-3.
- Lindgren, G.A., G. Destouni, and A. V. Miller, 2004. Solute transport through the integrated groundwater-stream system of a catchment. *Water Resour. Res.*, 40., doi:10.1029/2003WR002765.
- Lindström, G., B.J. Johansson, M. Persson, M. Gardelin, and S. Bergström, 1997. Development and test of the distributed HBV-96 hydrological model, *J. Hydrol.*, 201, 272-288.
- Makkink, G.F., 1957. Testing the Penman formula by means of lysimeters. *Journ. Int. of Water Eng.*, 11, 277-288.
- McDonald, M.G., and Harbaugh, A.W., 1988. A modular three dimensional finite-difference groundwater flow model, US Geological Survey, *Techniques of Water Resources Investigations*, Book 6, chap. A1.
- McDonnell, J.J., M. Sivapalan, K. Vaché, S. Dunn, G. Grant, R. Haggerty, C. Hinz, R. Hooper, J. Kirchner, M. L. Roderick, J. Selker, and M. Weiler, 2007. Moving beyond heterogeneity and process complexity: A new vision for watershed hydrology. *Water Resour. Res.*, 43, doi:10.1029/2006WR005467.
- McDonnell, J.J., 2003. Where does water go when it rains? Moving beyond the variable source area concept of rainfall-runoff response, *Hydrological Processes* 17, 1869–1875.
- McDonnell, J.J., K.J. McGuire, P. Aggarwal, K. J. Beven, D. Biondi, G. Destouni, S. Dunn, A. James, J. Kirchner, P. Kraft, S. Lyon, P. Maloszewski, B. Newman, L. Pfister, A. Rinaldo, A. Rodhe, T. Sayama, J. Seibert, K. Solomon, C. Soulsby, M. Stewart, D. Tetzlaff, C. Tobin, P. Troch, M. Weiler, A. Western, A. Wörman, and S. Wrede, 2010. How old is streamwater? Open questions in catchment transit time conceptualization, modelling and analysis. *Hydrol. Process.*, 24, 1745–1754.
- McGuire, K.J., and J.J. McDonnell, 2006. A review and evaluation of catchment transit time modeling. *J. Hydrol.*, 330, 543–563

- Molénat, J., C. Gascuel-Oudou, L. Ruiz, and G. Gruau, 2008. Role of water table dynamics on stream nitrate export and concentration in agricultural headwater catchment (France), *J. Hydrol.*, 348, 363-378.
- Moore, R.J., 1985. The probability-distributed principle and runoff production at point and basin scales, *Hydrological Sciences Journal* 30, 273-297.
- Moore, R.J., 2007. De PDM rainfall-runoff model, *Hydrol. Earth Syst. Sci.*, 11, 483-499.
- Morgenstern, U., M. K. Stewart, and R. Stenger, 2010. Dating of streamwater using tritium in a post-bomb world: continuous variation of mean transit time with streamflow. *Hydrol. Earth Syst. Sci. Discuss.*, 7, 4731-4760.
- Mulla, D.J., P.H. Gowda, A.S. Birr, and B.L. Dalzell, 2003. Estimating nitrate-N losses at different spatial scales in agricultural water sheds. In: Y. Pachepsky, D.E. Radcliffe, and H.M. Selim (eds.) *Scaling methods in soil physics*, pp. 295-307. CRC Press, Boca Raton, Florida, U.S.A.
- Nangia, V., P. H. Gowda, D. J. Mulla, and G. R. San, 2010. Modeling impacts of tile drain spacing and depth on nitrate-nitrogen losses. *Vadose zone J.*, 3, 61-72.
- Nash, J.E., and J.V. Sutcliffe, 1970. River Flow Forecasting through Conceptual Models. Part I-A, Discussion of Principles. *J. Hydrol.*, 10, 282-290.
- Niemi, A.J., 1977. Residence time distributions of variable flow processes, *Int. J. of Applied Radiation and Isotopes*, 28, 855-860.
- Ocampo, C.J., M. Sivapalan, and C. Oldham, 2006. Hydrological connectivity of upland-riparian zones in agricultural catchments: Implications for runoff generation and nitrate transport, *J. hydrol.* 331, 643-658.
- Oenema, O., D. Oudendag, and G.L. Velthof, 2007. Nutrient losses from manure management in the European Union. *Livest. Sci.* 112, 261-272.
- Petrolia, D.R., and P.H. Gowda, 2006. Missing the boat: Midwest farm drainage and Gulf of Mexico hypoxia. *Review of Agricultural Economics*, 28, 240-253.
- Poor, C.J., and J.J. McDonnell, 2007. The effects of land use on stream nitrate dynamics. *J. Hydrol.*, 332, 54-68.
- Preston, S.D., V.J. Bierman, and S.E. Silliman, 1989. An evaluation of Methods for the Estimation of Tributary Mass Loads. *Water Resour. Res.*, 25, 1379-1389.
- Raats, P.A.C., 1978. Convective transport of solutes by steady flows I. General theory. *Agric. Water Managem.*, 1, 201-218
- Reggiani, P., M. Sivapalan, and M. S. Hassanizadeh, 1998. A unifying framework for watershed thermodynamics: Balance equations for mass, momentum, energy and entropy, and the second law of thermodynamics. *Adv. Water Res.* 22, 367-398.
- Rinaldo, A., and M. Marani, 1987. Basin Scale Model of Solute Transport. *Water Resour. Res.*, 23, 2107-2118.
- Rinaldo, A., A. Bellin, and M. Marani, 1989. A study on solute NO₃-N transport in the hydrologic response by an MRF model. *Ecol. Modelling*, 48, 159-191.
- Rinaldo, A., G. Botter, E. Bertuzzo, A. Ucelli, T. Settin, and M. Marani, 2006. Transport at basin scales: 1. Theoretical framework. *Hydrol. Earth Syst. Sci.*, 10, 19-29.
- Rivett, M.O., S. R. Buss, P. Morgan, J.W.N. Smith, and C. D. Bemment, 2008. Nitrate attenuation in groundwater: A review of biogeochemical controlling processes. *Water Research*, 42, 4215 - 4232.

- Rode, M., G. Arhonditsis, D. Balin, T. Kebede, V. Krysanova, A. van Griensven, and S.E.A.T.M. van der Zee, 2010. New challenges in integrated water quality modeling. *Hydrol. Process.* doi: 10.1002/hyp.7766.
- Rodgers, P., C. Soulsby, S. Waldron, and D. Tetzlaff, 2005. Using stable isotope tracers to assess hydrological flow paths, residence times and landscape influences in a nested mesoscale catchment. *Hydrol. Earth Syst. Sci.*, 9, 139–155
- Rodrigo, A., S. Recous, C. Neel, and B. Mary, 1997. Modelling temperature and moisture effects on C-N transformations in soils: comparison of nine models. *Ecological Modelling*, 102, 325-339.
- Rozemeijer, J.C., and Y. van der Velde, 2008. Oppervlakkige afstroming ook van belang in het vlakke Nederland (Dutch). *H₂O*, 19, 92-94.
- Rozemeijer, J.C., and H.P. Broers, 2007. The groundwater contribution to surface water contamination in a region with intensive agricultural land use (Noord-Brabant, The Netherlands). *Environmental Pollution* 148, 695-706
- Rozemeijer, J.C., 2010. Dynamics in ground- and surface water quality. From field-scale processes to catchment-scale monitoring. PhD thesis, Faculty of Geosciences, Utrecht University, Utrecht.
- Rozemeijer, J.C., Y. Van der Velde, F.C. Van Geer, G.H. De Rooij, P.J.J.F. Torfs, and H.P. Broers, 2010a. Improving load estimates for NO₃ and P in surface waters by characterizing the concentration response to rainfall events. *Environ. Sci. Technol.*, 44, 6305-6312.
- Rozemeijer, J.C., Y. Van der Velde, H. De Jonge, F.C. Van Geer, H.P. Broers, M.P.F. Bierkens, 2010b. Application and evaluation of a new passive sampler for measuring average solute concentrations in a catchment-scale water quality monitoring study. *Environ. Sci. Technol.*, 44, 1353-1359.
- Rozemeijer, J.C., Y. van der Velde, R.G. McLaren, F.C. van Geer, H.P. Broers, and M.F.P. Bierkens, 2010c. Using field scale measurements of flow route contributions to improve integrated model representations of dynamic groundwater-surface water interactions. *Water Resour. Res.*, 46, W11537, doi:10.1029/2010WR009155.
- Rozemeijer, J.C., Y. van der Velde, F.C. van Geer, H.P. Broers, and M.F.P. Bierkens, 2010d. Direct quantification of the tile drain and groundwater flow route contributions to surface water contamination: from field-scale concentration patterns in groundwater to catchment-scale surface water quality. *Environmental Pollution*, 158, 3571-3579.
- Schils, R.L.M., and I. Kok, 2003. Effects of cattle slurry manure management on grass yield, *Netherlands Journal of Agricultural Sciences*, 51-1/2, 41-66.
- Seibert, J., A. Rodhe, and K. Bishop, 2003. Simulating interactions between saturated and unsaturated storage in a conceptual runoff model, *Hydrol. Process.*, 17, 379–390.
- Seibert, J., T. Grabs, S. Köhler, H. Laudon, M. Winterdahl, and K. Bishop, 2009. Linking soil- and stream-water chemistry based on a Riparian Flow-Concentration Integraton Model, *Hydrol. Earth Syst. Sci.*, 13, 2287–2297.
- Shaman, J., M. Stieglitz, and D. Burns, 2004. Are big basins just the sum of small catchments? *Hydrol. Process.*, 18, 3195–3206.
- Šimunek, J., M.Th. Van Genuchten, and M. Sejna, 1998. HYDRUS-1D, version 2.01, code for simulating the one-dimensional movement of water, heat and multiple solutes in variably saturated porous media. US Salinity Laboratory, USA.
- Sivapalan, M., 2003. Process complexity at hillslope scale, process simplicity at the watershed scale: is there a connection?, *Hydrol. Process.*, 17, 1037–1041.

- Sivapalan, M., G. Blöschl, L.Zhang, and R. Vertessy, 2003. Downward approach to hydrological prediction. *Hydrol. Process.* 17, 2101–2111.
- Skaggs, A., M.A. Brevé, and J.W. Gilliam, 1994. Hydrologic and water quality impacts of agricultural drainage. *Critical Reviews in Environmental Science and Techn.*, 24, 1-32.
- Smart, T.S., D.J. Hirst, and D.A. Elston, 1999. Methods for estimating loads transported by rivers. *Hydrol. Earth Syst. Sc.*, 3 (2), 295-303.
- Soulsby, C., C. Neal, H. Laudon, D. A. Burns, P. Merot, M. Bonell, S. M. Dunn, and D. Tetzlaff, 2008. Catchment data for process conceptualization: simply not enough? *Hydrol. Process.* 22, 2057–2061.
- Soulsby, C., D. Tetzlaff, S.M. Dunn, and S. Waldron, 2006. Scaling up and out in runoff process understanding: insights from nested experimental catchment studies. *Hydrol. Process.*, 20, 2461–2465
- Soulsby, C., J. Petry, M.J. Brewer, S.M. Dunn, B. Ott, and I.A. Malcolm, 2003. Identifying and assessing uncertainty in hydrological pathways: A novel approach to end member mixing in a Scottish agricultural catchment. *J. Hydrol.*, 274, 109-128.
- Stamm, C., H. Flühler, R. Gächter, J. Leuenberger, and H. Wunderli, 1998. Preferential transport of phosphorus in drained grassland soils. *Journal of Environmental Quality*, 27, 515-522.
- Stamm, C., R. Sermet, J. Leuenberger, H. Wunderli, H. Wydler, H. Flühler, and M. Gehre, 2002. Multiple tracing of fast solute transport in a drained grassland soil. *Geoderma*, 109, 245-268.
- Stuyt, L.C.P.M., and W. Dierickx, 2006. Design and performance of materials for subsurface drainage systems in agriculture. *Agricultural water management*, 86, 50-59.
- Tetzlaff D, J.J. McDonnell, S. Uhlenbrook, K.J. McGuire, P. Bogaart, F. Naef, A. Baird, S.M. Dunn, and C. Soulsby, 2008. Conceptualizing catchment processes: simply complex? *Hydrol. Process.*, 22, 1727–1730.
- Tetzlaff, D., S. Waldron, M.J. Brewer, and C. Soulsby, 2007. Assessing nested hydrological and hydrochemical behaviour of a mesoscale catchment using continuous tracer data. *J. of Hydrol.*, 336, 430–443.
- Therrien, R., R.G. McLaren, E.A. Sudicky, and S.M. Panday, 2009. *HydroGeoSphere, A Three-dimensional Numerical Model Describing Fully-integrated Subsurface and Surface Flow and Solute Transport (Draft)*, Groundwater Simulations Group, University of Waterloo, Waterloo, Canada.
- Tiemeyer, B, P. Kahle, and B. Lennartz, 2006. Nutrient losses from artificially drained catchments in North-Eastern Germany at different scales. *Agricultural water management*, 85, 47-57.
- Tiemeyer, B., B. Lennartz, and P. Kahle, 2008. Analyzing nitrate losses from an artificially drained lowland catchment (North-Eastern Germany) with a mixing model. *Agriculture, Ecosystems and Environment*, 123, 125-136.
- Tiemeyer, B., R. Moussa, B. Lennartz, and M. Voltz, 2007. MHYDAS-DRAIN: A spatially distributed model for small, artificially drained lowland catchments, *Ecological Modelling*, 209, 2-20.
- Tiemeyer, B., P. Kahle, and B. Lennartz, 2010. Designing monitoring programs for artificially drained catchments. *Vadose Zone J.*, 9, 14-24.
- Todini, E., 1996. The ARNO rainfall-runoff model, *J. Hydrol.* 175, 339-382.
- Tomer, M.D., D.W. Meek, D.B. Jaynes, and J.L. Hatfield, 2003. Evaluation of Nitrate Nitrogen Fluxes from a Tile-Drained Watershed in Central Iowa. *Journal of Environmental Quality*, 32, 642–653.

- Tromp-van Meerveld, H.J., and J.J. McDonnell, 2006. Threshold relations in subsurface stormflow: 2. The fill and spill hypothesis. *Water Resour. Res.*, 42, W02411, doi:10.1029/2004WR003800.
- Uchida., T. Y. Asano, Y. Onda, and S. Miyata, 2005. Are headwaters just the sum of hillslopes? *Hydrol. Process.*, 19, 3251–3261.
- Van de Griend, A.A., J.J. De Vries, and E. Seyhan, 2002. Groundwater discharge from areas with a variable specific drainage resistance, *J. Hydrol.*, 259, 203-220
- Van den Eerthwegh, G.A.P.H., and C.R. Meinardi, 1999. Water- en nutriëntenhuishouding van het stroomgebied van de Hupselse beek (in Dutch). Wageningen Universiteit, Wageningen.
- Van den Eertwegh, G.A.P.H., J.L. Nieber, P.G.B. De Louw, H.A. Van Hardeveld, and R. Bakkum, 2006. Impacts of drainage activities for clay soils on hydrology and solute loads to surface water. *Irrigation and Drainage*, 55, 235-245.
- Van der Molen, D.T., R. Portielje, W.T. de Nobel, and P.C.M. Boers, 1998. Nitrogen in Dutch freshwater lakes: trends and targets. *Environmental Pollution*, 102, 553-557.
- Van der Ploeg, M.J., 2008. Polymer tensiometers to characterize unsaturated zone processes in dry soils. PhD thesis, Wageningen University, Wageningen.
- Van der Velde, Y., G.H. De Rooij, and P.J.J.F. Torfs, 2009. Catchment-scale non-linear groundwater-surface water interactions in densely drained lowland catchments. *Hydrol. Earth Syst. Sci.*, 13, 1867-1885.
- Van der Velde, Y., J.C. Rozemeijer, G.H. De Rooij, F.C. Van Geer, and H.P. Broers, 2010a. Field-scale measurements for separation of catchment discharge into flow route contributions. *Vadose Zone J.*, 9, 25-35.
- Van der Velde, Y., G.H. de Rooij, J.C. Rozemeijer, F.C. van Geer, and H.P. Broers, 2010b. The nitrate response of a lowland catchment: on the relation between stream concentration and travel time distribution dynamics. *Water Resour. Res.*, 46, W11534, doi:10.1029/2010WR009105.
- Van der Velde, Y., J.C. Rozemeijer, G.H. de Rooij, F.C. van Geer, P.J.J.F. Torfs, and P.G.B. de Louw, 2010c. Nested-scale discharge and groundwater level monitoring to improve predictions of flow route discharges and nitrate loads. *Hydrol. Earth Syst. Sci.*, Submitted.
- Van Genuchten, M. Th., 1980. A closed-form equation for predicting the hydraulic conductivity of unsaturated soils, *Soil Sci. Soc. Am. J.*, 44, 892–898.
- Van Ommen, H.C., R. Dijkma, J.M.H. Hendrickx, L.W. Dekker, J. Hulshof and M. Van Den Heuvel, 1989. Experimental assessment of preferential flow paths in a field soil. *Journal of Hydrology* 105, 253-262.
- Van Schaik, N.L.M.B., 2010. The role of macropore flow from plot to catchment scale. A study in a semi-arid area. PhD thesis. Faculty of Geosciences, Utrecht University, Utrecht.
- Visser, A., 2009. Trends in groundwater quality in relation to groundwater age. PhD thesis, Faculty of Geosciences, Utrecht University, Utrecht.
- Visser, A., H.P. Broers, R. Heerdink, M.F.P. Bierkens, 2009. Trends in pollutant concentrations in relation to time of recharge and reactive transport at the groundwater body scale. *J. Hydrol.*, 369, 427–439
- Vitousek, P.M., R. Naylor, T. Crews, M. B. David, L. E. Drinkwater, E. Holland, P. J. Johnes, J. Katzenberger, L. A. Martinelli, P. A. Matson, G. Nziguheba, D. Ojima, C. A. Palm, G. P. Robertson, P. A. Sanchez, A. R. Townsend, F. S. Zhang, 2009. Nutrient Imbalances in Agricultural Development. *Science*, 324, 1519-1520.
- Ward, R.C., and M. Robinson, 1990. Principles of hydrology, 3th edition. McGraw-Hill. Cambridge, UK.

- Weiler, M., B.L. McGlynn, K.J. McGuire, and J.J. McDonnell, 2003. How does rainfall become runoff? A combined tracer and runoff transfer function approach. *Water Resour. Res.*, 39, doi:10.1029/2003WR002331.
- Westhoff, M.C. H.H.G. Savenije, W.M.J. Luxemburg, G.S. Stelling, N.C. van de Giesen, J.S. Selker, L. Pfister, and S. Uhlenbrook, 2007. A distributed stream temperature model using high resolution temperature observations. *Hydrol. Earth Syst. Sci.*, 11, 1469–1480.
- Wösten, J.H.M., G.J. Veerman, W.J.M. De Groot, and J. Stolte, 2001. Waterretentie- en doorlatendheidskarakteristieken van boven- en ondergronden in Nederland: de Staringreeks. Vernieuwde uitgave, 86 pp, <http://www2.alterra.wur.nl/Webdocs/PDFFiles/AlterraRapporten/AlterraRapport153.pdf>.
- Wösten, J.H.M., J. Bouma, and G.H. Stoffelsen, 1985. Use of soil survey data for regional soil water simulation models. *Soil Science Society of America Journal*, 49, 1238-1244.
- Wriedt, G., J. Spindler, T. Neef, R., and M. Rode, 2007. Groundwater dynamics and channel activity as major controls of in-stream nitrate concentrations in a lowland catchment system? *J. of Hydrol.*, 343, 154-168.
- Zhang Y.-C., C.P. Slomp, H.P. Broers, H.F. Passier, and P. van Cappellen, 2009. Denitrification coupled to pyrite oxidation and changes in groundwater quality in a shallow sandy aquifer. *Geochimica et Cosmochimica Acta*, 73, 6716–6726.
- Zhang, G.P., H.H.G. Savenije, F. Fenicia, and L. Pfister, 2006. Modelling subsurface storm flow with the Representative Elementary Watershed (REW) approach: Application to the Alzette River Basin, *Hydrol. Earth Syst. Sc.*, 10, 937-955.

Summary

Introduction

High nutrient loads of surface waters are a widespread environmental issue in lowland catchments with intensive agriculture. High nutrient concentrations stimulate plant and algal growth that reduce the ecological and recreational functioning of small headwaters. In turn the high nutrient loads of small headwaters cause algal blooms and hypoxia in downstream rivers and lakes, and, if the problem is widespread, even in coastal water bodies such as the Gulf of Mexico and the Baltic Sea. In order to identify effective abatement measures, we need to better understand the processes that drive nutrient transport towards surface waters from the moment of application at the soil surface. This thesis describes the movement of water and nutrients within lowland catchments and hence contributes to the knowledge needed for sustainable management of the groundwater and surface water resources of lowland catchments.

Materials and methods

We chose the Hupsel Brook catchment (6.5 km², the Netherlands) as an example catchment for freely draining lowland catchments. The Hupsel Brook has a long history as an experimental catchment with 30 years of frequent data on water quality, discharge, groundwater levels, and weather available. Within this catchment we installed an elaborate nested-scale discharge and nutrient monitoring network. At a field-site (0.9 ha) we separated tube drain discharge from groundwater flow and overland flow towards the surface water network. All fluxes were measured every five minutes from November 2007 through December 2008. Furthermore, the groundwater storage within this field was measured continuously. At two larger scales (0.4 and 6.5 km²) we measured discharge continuously and took weekly grab samples to measure water quality. At the catchment outlet we also measured nitrate and phosphate concentrations every 15 minutes. To complement this setup, average monthly nitrate and phosphate concentrations of tube drains and surface waters were measured throughout the catchment using passive samplers.

Many different model concepts ranging from spatially distributed process models to catchment-scale transfer function models were applied to identify processes that can explain the observed behavior of discharge and water quality. Furthermore, these models were used to extrapolate the observed behavior of discharge and water quality to other time periods, locations and scales.

Results

At the field site we measured that approximately 80% of surface water discharge originated from tube drains, while the other 20% was the combined flux of overland and groundwater flow. Based on the detailed measurements of both groundwater storage and flow route fluxes, a novel hypothesis on the relation between spatial scale and discharge was formulated: at any scale from the field scale upward, discharge of lowland catchments is primarily driven by the dynamics in the shape of the groundwater table at that scale (characterized by a mean and standard deviation of groundwater depths). This hypothesis was tested by demonstrating that scale effects in observed discharge between our nested scales could be explained entirely by scale differences in the dynamics of the shape of the groundwater table. These findings were further validated by showing that combining nested-scale monitoring of discharge and groundwater levels with nested-scale models in which only the shape of the groundwater table was allowed to vary, improved predictions of peak discharges and nitrate loads. This model setup also allowed us to calculate separate contributions of flow routes to the total discharge across scales. Although tube drain effluent was the dominant flow route at the field site, the contribution of tube drain rapidly decreased with increasing scale to an estimated 25-50% at the catchment outlet.

The strong relations we found between surface water quality dynamics during rainfall events (nitrate and phosphate concentrations) and hydrologic variables confirm the crucial role of flow route contributions for surface water quality. However, long term water quality variations spanning seasons and years are not understood by quantifying just the solute concentration response to rainfall events. Therefore we applied transient travel time distributions in combination with a mass response function approach to link the solute concentration in surface water to the contact time of water parcels with the soil matrix. We showed that this approach could successfully describe both short term and long term concentration dynamics during 26 years of chloride and nitrate concentrations measurements at the catchment outlet.

Conclusions and outlook

In this thesis we describe how innovative nested-scale discharge and water quality measurements lead to the formulation of novel concepts for catchment-scale interactions between groundwater and surface water. We showed that parsimonious models that describe solute transport at the catchment scale are feasible and are currently the most effective way to relate both the observed high frequency natural dynamics and the long term changes in water quality to field-scale processes. However, these models should focus on the flow paths and travel times of water parcels inside a catchment, rather than on reproducing the correct discharge at the catchment outlet. In this thesis, we successfully developed and tested model concepts that define discharge by a composite of flow routes and concepts in which discharge is treated as a composite of travel times. To validate and improve these concepts, more datasets of flow route discharges, corresponding water quality, and subsurface storage of other catchments are needed. Important advances in these model concepts can be achieved by comparing solute transport in catchments with contrasting topographies and climates. Further developing the 'multimethodological' approach introduced in this thesis, in particularly a stronger integration of subsurface and in-stream processes, will yield basin-scale models of surface water quality that can facilitate a more sustainable management of groundwater and surface water resources; even under the multitude of stresses imposed by intensive land use in densely populated lowland areas.

Samenvatting

Introductie

Uitspoeling van nutriënten naar het oppervlaktewater is een veel voorkomend probleem in laaglandstroomgebieden met intensieve landbouw. Hoge nutriëntconcentraties in bovenstroomse sloten en beken stimuleren plant- en algengroei waardoor de ecologische- en recreatiewaarde van dit water achteruit gaat. Op hun beurt veroorzaken de grote nutriëntvrachten vanuit de bovenstroomse beken algenbloei en zuurstofloosheid in benedenstroomse rivieren en meren. Als het probleem zeer uitgebreid is kan zuurstofloosheid zelfs optreden in kustwateren zoals is waargenomen in de Golf van Mexico en de Baltische Zee. Om effectieve maatregelen te kunnen treffen die het uitspoelen van nutriënten tegengaan, is een beter begrip van transport van nutriënten vanaf het moment van aanbrengen op het maaiveld naar het oppervlaktewater noodzakelijk. Dit proefschrift heeft tot doel ons inzicht in de water- en nutriëntstromen van laaglandstroomgebieden te vergroten en hierdoor bij te dragen aan de kennis die nodig is voor een duurzaam beheer van grond- en oppervlaktewater in laagland stroomgebieden.

Materiaal en methoden

Het stroomgebied van de Hupselse Beek (6.5 km², Achterhoek) is gekozen als een voorbeeld stroomgebied voor vrijafwaterende laagland stroomgebieden. Dit stroomgebied heeft een lange geschiedenis als experimenteel stroomgebied met 30-jarige meetreeksen van waterkwaliteit, afvoer, grondwaterstanden en neerslag. In het stroomgebied van de Hupselse Beek hebben we een genest meetnet voor afvoeren en nutriëntconcentraties opgezet. Voor één perceel (0.9 ha) hebben we elke 5 minuten afzonderlijk de afvoer via buisdrainage en de gecombineerde afvoer via oppervlakkige afstroming en grondwaterstroming gemeten vanaf november 2007 tot december 2008. Verder werden in deze periode continu de grondwaterstanden in het perceel gemeten. Op twee grotere schalen (0.4 en 6.5 km²) hebben we continu afvoeren gemeten en wekelijks hebben we watermonsters geanalyseerd om de waterkwaliteit te bepalen. Bij het uitstroompunt van het gehele stroomgebied hebben we automatisch elk kwartier de fosfaat en nitraat concentraties geanalyseerd. Deze opzet werd aangevuld met “passive samplers” die maandgemiddelde concentraties meten van nitraat en fosfaat in buisdrains en oppervlaktewater op verspreide locaties in het stroomgebied.

Om de geobserveerde afvoeren en waterkwaliteitsmetingen te interpreteren en hun gedrag te extrapoleren naar andere locaties en andere tijdsperioden hebben we vele typen modellen toegepast variërend van gedetailleerde ruimtelijk gedistribueerde procesmodellen tot eenvoudige “transferfunctie” modellen op stroomgebiedschaal.

Resultaten

Op onze veldlocatie hebben we gemeten dat ongeveer 80% van alle afvoer afkomstig is van buisdrainage. De andere 20% is een combinatie van grondwaterstroming en oppervlakkige afvoer. Gebaseerd op deze metingen en op de gemeten grondwaterstanden hebben we een nieuwe hypothese geformuleerd over de relatie tussen grondwaterberging en afvoer: voor schalen groter dan de perceelschaal wordt afvoer van laaglandstroomgebieden voornamelijk gestuurd door de vorm van de grondwaterspiegel gekarakteriseerd door de ruimtelijk gemiddelde en variatie van de grondwaterstandsdiepte. Deze hypothese hebben we getest door te demonstreren dat schaaffecten in geobserveerde afvoer volledig kunnen worden verklaard door schaalverschillen in de dynamiek van de grondwaterspiegel. Dit resultaat hebben we gevalideerd door te laten zien dat een model waarin deze hypothese is toegepast betere resultaten geeft voor afvoer- en nitraatvrachtvoorspellingen dan een model waarin deze hypothese niet is toegepast. Met dit modelconcept hebben we de bijdragen van individuele stroomroutes aan de totale stroomgebiedsafvoer geschat. Hoewel buisdrainage ook op stroomgebiedschaal een belangrijke afvoercomponent was, nam de bijdrage van buisdrainage sterk af met een toenemende schaal. Op stroomgebiedschaal hebben we de bijdrage van buisdrainage geschat op 25-50% van de totale afvoer.

De sterke relaties tussen de dynamiek in oppervlaktewaterkwaliteit en hydrologische variabelen tijdens buien bevestigen de cruciale rol van stroomroutes voor waterkwaliteit. Echter de seizoens- en jaarlijkse variaties in waterkwaliteit kunnen niet worden verklaard met alleen het kwantificeren van de bijdragen van verschillende stroomroutes. Daarom hebben we niet-stationaire reistijdverdelingen in combinatie met “mass-response” functies toegepast om de oppervlaktewaterkwaliteit te relateren aan de contacttijd tussen water en de bodem. We hebben laten zien dat deze benadering zowel de korte- als de langetermijn dynamiek van nitraat en chloride concentraties bij het uitstroompunt goed kan beschrijven.

Conclusie en vooruitblik

In dit proefschrift wordt beschreven hoe innovatieve metingen van afvoer en waterkwaliteit leiden tot de formulering van nieuwe concepten over interacties tussen grondwater en oppervlaktewater op stroomgebiedsschaal. We laten zien dat simpele modellen met weinig parameters in staat zijn nutriënttransport op stroomgebiedschaal nauwkeurig te beschrijven. Deze modellen blijken momenteel het meest effectief in het beschrijven van de geobserveerde korte- en langetermijn dynamiek van waterkwaliteit vanuit perceelschaalprocessen. Deze modellen moeten zich dan wel richten op een correcte beschrijving van de routes en reistijden van water binnen het stroomgebied in plaats van zich alleen te concentreren op een correcte reproductie van de afvoer. In dit proefschrift hebben we op een succesvolle manier modelconcepten ontwikkeld en getest die afvoer beschrijven als een samengestelde afvoer van diverse stroomroutes of als mix van waterdeeltjes met verschillende reistijden. Om deze modellen te kunnen verbeteren en valideren zijn nieuwe vergelijkbare datasets nodig van andere stroomgebieden. Ook kunnen de hier geïntroduceerde concepten verder worden ontwikkeld door stroomgebieden met verschillende topografie en klimaten met elkaar te vergelijken. Het doorontwikkelen van de geïntegreerde benadering zoals uitgevoerd in dit onderzoek, met een nadruk op een sterkere integratie van de processen die zich afspelen in waterlopen, zullen stroomgebiedschaal modellen opleveren die een meer duurzaam beheer van grondwater en oppervlaktewater mogelijk maken.

Dankwoord

Na 4 jaar van inhoudelijke vrijheid, schitterend veldwerk en zwoegen op het schrijven van artikelen is mijn proefschrift eindelijk af. Deze vrijheid was niet vanzelfsprekend en ik ben Chris te Stroet, Frans van Geer en Gerrit de Rooij die mij deze vrijheid gaven dank verschuldigd. Allereerst gaf Chris mij de mogelijkheid om vanuit TNO te gaan promoveren. Frans zorgde ervoor dat Joachim en ik onze grootse plannen konden uitvoeren, organiseerde een prachtig zeilweekend op de Waddenzee en gaf inspirerende begeleiding. Ger stimuleerde mij met meeslepende verhalen, een indrukwekkend internationaal netwerk en een strenge rode pen, mijn ideeën uit te werken tot volwaardige artikelen en dit proefschrift.

Joachim, onze intensieve samenwerking gaf ons de motivatie om wekelijks en vaak meerdere keren per week naar Hupsel te rijden. We waren namelijk niet alleen verantwoordelijk voor ons eigen veldwerk, maar ook voor het slagen van elkaars proefschrift. Vooral jouw positieve instelling en doorzettingsvermogen zorgden ervoor dat we de inwoners van Hupsel voor ons wisten te winnen, een enorme opstelling bouwden en natuurlijk twee keer per jaar een geweldige DYNAQUAL-nieuwsbrief uitbrachten. Ook heb ik kunnen profiteren van jouw schrijverstalent resulterend in twee volledig gezamenlijke publicaties (hoofdstukken 2 en 5). Ik heb met heel veel plezier met je samengewerkt en enorm veel geleerd, bedankt!

Onze ambitieuze veldwerkideeën werden mogelijk door de hulp van vele specialisten: Pieter Hazenberg heeft de opstelling van pompen en fluxmeters ontworpen die nu vier jaar later nog steeds draait. Harm Gooren heeft, toen het veldwerk ons belemmerde artikelen te schrijven, het onderhoud en de reparaties op zich genomen. Ydo Hoogkamp en Lex van Loon verzorgden de Hydrions. Samen met Hubert de Jonge hebben we de SorbiSense zodanig doorontwikkeld dat het bruikbare resultaten geeft voor typisch Nederlandse slootjes, buisdrainage en grondwater. Verder zijn we zeer tevreden over de fosfaat-analyzers van Hach-Lange en zijn we het laboratorium van TNO/Deltares en Universiteit Utrecht dankbaar voor de duizenden waterkwaliteitsanalyses die zij voor ons hebben uitgevoerd.

Wim Kimmels is de sympathieke boer die zijn land openstelde voor twee destructieve onderzoekers. Bij de familie Kimmels konden we altijd binnen lopen voor een kopje koffie en hun verhalen over de boerderij en het weer waren voor ons zeer informatief. Met hulp van vele vrienden en collega's hebben we meer dan honderd boringen in dit ene perceel gezet en hebben we enkele honderden meters aan sleuven gegraven om alle meetinstrumenten te installeren. Iedereen erg bedankt voor de geleverde inspanning!

Naast de directe begeleiding van Ger en Frans hebben een groot aantal mensen meegedacht, meegeschreven en meetdata aangeleverd. Marc Bierkens, Piet Groenendijk en Johan Valstar waren vooral in de beginfase betrokken bij het opzetten van het DYNAQUAL-veldwerk en het sturen van de eerste theoretische analyses. Paul Torfs heeft uitgebreid meegeschreven aan hoofdstukken 3, 4 en 5 en is een grote *R*-inspiratiebron. Vooral gedurende de laatste 2 jaren heb ik veel hulp gekregen van Hans-Peter Broers. Jouw enthousiasme voor de dynamische reistijdverdelingen werkte aanstekelijk en ik hoop dat we hier samen nog een vervolg aan kunnen geven. Vanaf het begin dat ik bij TNO kwam werken in 2003, werkte ik samen met Perry de Louw. Daarom was het erg leuk en leerzaam dat we in het laatste jaar weer samen aan twee artikelen konden schrijven. Nu maar hopen dat ze ook gepubliceerd gaan worden! Waardevol voor ons onderzoek waren de vele meetreeksen van afvoer, neerslag en waterkwaliteit van de Hupsel die we kregen van Piet Warmerdam, Jacques Kole, Gé van den Eertwegh, Gert van den Houten van het waterschap Rijn en IJssel en het KNMI.

Nu ik besloten heb niet bij Deltares terug te keren, maar ga proberen mijn carrière in de wetenschap voort te zetten, denk ik met veel plezier terug aan de jaren bij TNO/Deltares. Eerst wil ik mijn kamergenoten Marijn, Dimmie, Wiebe, Perry, Jacco en Gerrit bedanken voor de gezellige sfeer op onze kamer en natuurlijk ook alle andere Deltarianen en TNOers voor de koffieverhalen, interesse in mijn onderzoek en de vele spannende avonturen in Brabant, Friesland, Noord-Holland en India.

Toen de nadruk meer kwam te liggen op het schrijven van artikelen was ik steeds vaker te vinden in Wageningen bij de vakgroepen SEG en HWM. Hier genoot ik van het gezamenlijk koffiedrinken en de discussies met kamergenoten Bram, Anton en Tessa en de andere AIO's van SEG en HWM (vaak met bier en tot laat in de avond). Ik ben dan ook zeer blij dat Sjoerd van der Zee en Remko Uijlenhoet mij de mogelijkheid hebben gegeven nog enkele maanden te mogen werken aan het opzetten van een vervolgstudie.

Goede vriendschappen met Jan, Tjibbe en André, Arnaut, Bert, Chris en Peter, Bart en Daphne en de oud-huisgenoten van de Nobelweg hebben gezorgd voor mooie momenten van afleiding. Speciale herinneringen koester ik aan de (te) ambitieuze plannen die we maakten tijdens lange avonden in het café zoals het opknappen van een oude Peugeot 404, voetbalwedstrijden winnen met SKV-8 en verre reizen naar Zuid-Afrika en India. Ook het beklimmen van de Pico de Aneto afgelopen jaar was en bleef een mooie uitdaging.

Rust en ontspanning kan ik altijd vinden bij mijn ouders, broer en zus in De Wilp. De mooie wandelingen en de gezellige ochtenden aan de koffietafel waren de weinige momenten dat ik mijn proefschrift kon vergeten en volledig kon opgaan in de verhalen over gevangen of verspeelde snoekbaarzen, de groentetuin, de oppaskinderen, de stapavonden van Minke en de voetbalwedstrijden van Willem.

Lieve Ruth, ik heb je leren kennen toen ik met mijn AIO-schap begon. Tijdens de afgelopen vier jaar hebben we prachtige fietsvakanties gemaakt, zijn we gaan samenwonen en zijn we onafscheidelijk geworden. Nu zijn we sinds kort met zijn drieën en ik heb heel veel zin in de komende jaren om samen met jou en Jinke nog veel avonturen te gaan beleven.

Ype van der Velde

Wageningen, november 2010.

Curriculum Vitae

Ype van der Velde, 26 September, 1979, Grijpskerk.

- | | |
|--------------|---|
| 1991-1997 | Drachtster Lyceum, pre-university education (VWO), Drachten. |
| 1997-2003 | Wageningen University, MSc. in Soil, Water and Atmosphere (with distinction). Specializations: Hydrology and Soil physics. |
| 2001 | MSc. Thesis at TNO and Wageningen University. |
| 2001-2002 | Traineeship at Deakin University, School of Ecology and the Environment, Warrnambool, Australia. |
| 2002-2003 | MSc. Thesis at the Institute of Terrestrial Ecology (ITÖ), ETH, Zurich, Switzerland. |
| 2003-2006 | Researcher Geohydrology at TNO. |
| 2006-2010 | PhD-candidate at Wageningen University, Soil physics, Ecohydrology and Groundwater Management group and TNO/Deltares. |
| 2010-present | Post-doc at Wageningen University, Soil physics, Ecohydrology and Groundwater Management group, and the Hydrology and Quantitative Water Management group |

Publications related to this thesis:

- Van der Velde, Y.*, J.C. Rozemeijer*, G.H. De Rooij, F.C. Van Geer, and H.P. Broers (2010), Field-scale measurements for separation of catchment discharge into flow route contributions, *Vadosezone Journal* 9, 25-35.
- Van der Velde, Y., G.H. De Rooij and P.J.J.F. Torfs (2009), Catchment-scale non-linear groundwater-surface water interactions in densely drained lowland catchments, *Hydrol. Earth Syst. Sci.* 13, 1867-1885.
- Van der Velde, Y., G.H. de Rooij, J.C. Rozemeijer, F.C. van Geer and H.P. Broers (2010), The nitrate response of a lowland catchment: on the relation between stream concentration and travel time distribution dynamics, *Water Resources Research* 46, W11534, doi:10.1029/2010WR009105.
- Van der Velde, Y., J.C. Rozemeijer, G.H. de Rooij, F.C. van Geer and P.J.J.F. Torfs, and P.G.B. de Louw (submitted), Nested-scale discharge and groundwater level monitoring to improve predictions of flow route discharges and nitrate loads. *Hydrol. Earth Syst. Sci.*
- Rozemeijer*, J.C., Y. van der Velde*, F.C. Van Geer, G.H. De Rooij, P.J.J.F. Torfs, and H.P. Broers (2010), Improving load estimates for NO₃ and P in surface waters by characterizing the concentration response to rainfall events, *Environ. Sci. Technol.* 44, 6305-6312.
- Rozemeijer, J.C., Y. Van der Velde, H. De Jonge, F.C. Van Geer, H.P. Broers, M.P.F. Bierkens (2010), Application and evaluation of a new passive sampler for measuring average solute concentrations in a catchment-scale water quality monitoring study, *Environ. Sci. Technol.* 44, 1353-1359.
- Rozemeijer, J.C., Y. van der Velde, R.G. McLaren, F.C. van Geer, H.P. Broers, and M.F.P. Bierkens (2010), Using field scale measurements of flow route contributions to improve integrated model representations of dynamic groundwater-surface water interactions, *Water Resources Research* 46, W11537, doi:10.1029/2010WR009155.
- Rozemeijer, J.C., Y. van der Velde, F.C. van Geer, H.P. Broers, and M.F.P. Bierkens (2010), Direct quantification of the tile drain and groundwater flow route contributions to surface water contamination: from field-scale concentration patterns in groundwater to catchment-scale surface water quality, *Environmental Pollution* 158, 3571-3579.
- Rozemeijer, J.C., and Y. van der Velde (2008), Oppervlakkige afstroming ook van belang in het vlakke Nederland (Dutch), *H2O*, 19, 92-94.

*Both authors can be considered first author

Notes

This thesis was made possible by financial support from Deltares, TNO, RIVM and Alterra.

On the cover is a picture taken by Joachim Rozemeijer. It shows our field site during conditions with extensive ponding.

This thesis is printed by “GVO drukkers & vormgevers B.V. | Ponsen & Looijen”.

